DEVELOPMENT AND CHARACTERIZATION OF NOVEL BIOMATERIALS FOR FABRICATION OF MULTILAYERED VASCULAR GRAFTS

A Dissertation

by

DAVID KANDELL DEMPSEY

Submitted to the Office of Graduate and Professional Studies of
Texas A&M University
in partial fulfillment of the requirements for the degree of

DOCTOR OF PHILOSOPHY

Chair of Committee,	Elizabeth Cosgriff-Hernàndez
Committee Members,	Melissa Grunlan
	Duncan Maitland
	Mariah Hahn
Head of Department,	Gerard Coté

December 2013

Major Subject: Biomedical Engineering

ABSTRACT

Current synthetic alternatives to autologous grafts have often failed in small diameter applications (<6 mm) due to their thrombogenicity and compliance mismatch of native vasculature. No known synthetic material is capable of providing a non-thrombogenic inner layer that promotes endothelial cell (EC) interactions while also providing sufficient compliance and burst pressure for long term success *in vivo*. We have developed a multilayer design with an inner thromboresistant poly(ethylene glycol) (PEG) hydrogel based on Scl2-2 proteins designed to promote rapid *in situ* endothelialization. The bioactive component is reinforced with an electrospun segmented polyurethane (SPU) layer with tunable mechanical properties to withstand physiological loading conditions. The modulating of electrospun parameters to influence graft architecture coupled with the tunability of SPU mechanical performance is expected to give rise to improved graft biomechanical properties. Unfortunately, this advantage was found to be limited to only one property at a time. To this end, we have developed a novel semi-IPN approach to expand the range of possible graft compliance and burst pressures in order to simultaneously achieve biomechanical properties that exceed autologous veins.

In addition to matching biomechanical properties, probability of long term success is also dependent on the grafts retention of perfomance despite cell-mediated attack. Typically, in the case poly(ether urethanes) (PEUs) and poly(carbonate urethanes) (PCUs), oxidative stability is the primary focus in the development of biostable SPUs. We have characterized the biostability of several commercially available

polyurethanes while simultaneously evaluating the predictive capabilities of two main *in vitro* test methods to optimize our graft's design.

Despite ensured long term performance through optimizing biostability, a permanent scaffold prevents vasoactivity, a key function of vasculature. We have taken a tissue engineering approach to restorate vasoactivity by evaluating a novel aromatic biodegradable poly(ester urethane) (PEsU) for the reinforcing layer of a tissue engineering vascular graft (TEVG). This PEsU was expected to degrade into safe byproducts given its design based on glycolic acid and ethylene glycol. Following characterization, the PEsU was determined to be a strong potential reinforcing layer of a potential TEVG design.

In summary, we have improved small diameter grafts through a multilayer design approach. Our graft demonstrated favorable initial fabrication feasibility, promising *in vivo* testing, biomechanical properties exceeding autologous veins, and strong oxidative stability. Overall, we have optimized the reinforcing layer through improvement of biomechanical properties via modulated material chemistry, optimized biostability, and identification of a biodegradable component expected to allow for restored vasoactivity.

DEDICATION

To my family, who always taught me to appreciate what I have, but never settle when you have a chance to be better.

ACKNOWLEDGEMENTS

This experience has certainly been the most demanding, trying, and stressful time of my life. To say I could not have done it alone would be nothing short of a huge understatement. There are so many people that deserve to be recognized, starting with my advisor, Dr. Elizabeth Cosgriff-Hernandez. The tremendously challenging expectations that she puts on her students has forced me to strive to a higher level of knowledge I could not have imagined I would ever reach before working in her lab. I also want to acknowledge the amount of extra detail and attention she gives her students to make sure their well-being is always as positive as possible. I am forever grateful for the unique opportunities she has provided for me and proud of what has been set up for my future.

I also would like to thank my committee members Dr. Melissa Grunlan, Dr. Duncan Maitland, and Dr. Mariah Hahn for providing their unique perspectives in my research. Their input provided me the opportunity to be more well-rounded and better suited for the complex new problems I face ahead of me. Finally, I want to also thank the chair of my Master's committee, Dr. Christian Schwartz. Without the initial opportunities he provided me, I may have never had the chance to even embark on the challenges I am facing today.

The research and development team at DSM Biomedical have not only provided the funding for my research throughout my entire PhD program but also the opportunity to expand my skills outside of the academic scene. All of the projects conducted at Texas

A&M and on site in Berkeley, California have allowed me to evolve into a valuable resource in the industrial arena. Bob Ward, Chander Chawla, Jerry Parmer, Patrick Gray, James Parakka, Ananth Iyer, Shanger Wang, John Zupancich, Natthárika Aumsuwan, and anyone else I have met along the way certainly deserve my extensive gratitude.

I could not even begin to envision being able to complete this work without the tremendous support I have been given throughout my time here. Starting with Kevin Plumlee and Matt Darden, who constantly taught me the importance of having a life outside of school and that working in a research lab should have just as much fun as work. I also would like to acknowledge Hugh Benhardt and Thomas Wilems, for not only being great friends to me during my time here but also setting the hard work ethic standards I still pride myself on living up to. I of course have to thank all of my labmates: Bobby Moglia, Nick Sears, Mary Beth Browning, Jenny Robinson, Roya Nezarati, Pauline Luong, Tyler Touchet, Joon Eoh, Calvin Mackey, and Stacy Cereceres for not only offering up their expertise but also willing to provide support whenever I needed it.

I also need to extend my deepest gratitude to those in the Bryan/College Station and San Francisco Bay Area communities who have been there for me throughout my journey. I want to start off by acknowledging David Weiser and his family for being so supportive and always willing to welcome me into their home. I also need to thank the Lazaroff family in College Station for providing a welcoming home away from home while I was trying to adjust to the new area. As for the bay area, I want to graciously thank my two new very close friends, Carlos Perez and Julian Delfino, who despite

knowing me for only a few short months have been an unimaginable source of support and constant reminder of the life waiting for me after I finish my graduate work.

Finally, I want to thank my family for always being there throughout my entire graduate school journey. It is no less than an understatement to say that these past 6 years apart have been very difficult on us but I am eternally grateful that we could persevere through it and emerged with stronger bonds. I am so happy to have family such as my Aunt Linda and Uncle Neil Beckerman, who were always willing to make time for me during the rare opportunities I was home to see them. My sister Sarah, despite having her own obstacles, has always been there for me when all I needed was someone to listen. Last, but certainly not least, I have to thank my mother Susan for always being supportive in spite of any choices I have made in my life. She is the source of my strength and inspiration to always work hard and make time for others no matter what the cost or benefit. Everything I have in my life is owed to her and she deserves all the credit.

NOMENCLATURE

ATR	Attenuated total reflectance
BDI	Butane diisocyanate
BDO	Butane diol
BPO	Benzoyl peroxide
CAD	Coronary artery disease
$CdCl_3$	Deuterated chloroform
$CHCl_3$	Chloroform
$CoCl_2$	Cobalt (II) chloride
DA	Diacrylate
DMA	Dimethacrylate
DMAC	N,N'-dimethylacetamide
DMEM	Dulbecco's Modified Eagle Medium
DMF	N,N'-dimethylformamide
DSC	Differential scanning calorimetry
EC	Endothelial cell
e-PTFE	Expanded polytetrafluoroethylene
ESC	Environmental stress cracking
FBGC	Foreign body giant cell
FBS	Fetal bovine serum
FTIR	Fourier transform infrared

G-E-G-G	Glycolide-ethylene glycol-glycolide
GPC	Gel permeation chromatography
ΔH	Change in enthalpy
H_2O_2	Hydrogen peroxide
H_2SO_4	Sulfuric acid
HDI	Hexane diisocyanate
HMDI	Hexamethylene diisocyanate
ID	Inner diameter
IPDI	Isophorone diisocyanate
IPN	Interpenetrating network
KBr	Potassium bromide
KI	Potassium iodide
LDI	Lysine diisocyanate
LDL	Low density lipoprotein
LiBr	Lithium bromide
MDI	Methylene di (p-phenyl isocyanate)
MIO	Metal ion induced oxidation
M_w	Weight average molecular weight
NaOH	Sodium hydroxide
$Na_2S_2O_3$	Sodium thiosulfate
$(NH_4)_6Mo_7O_{24}$	Ammonium heptamolybdate
NH_4NO_3	Ammonium nitrate

NH_4OH	Ammonium hydroxide
NMR	Nuclear magnetic resonance
OD	Outer diameter
PBS	Phosphate buffered saline
PCL	Poly(ε-caprolactone)
PC-PU	Polycarbonate-polyurethane
PCU	Poly(carbonate urethane)
PDI	Polydispersity index
PDMS	Polydimethylsiloxane
PEG	Poly(ethylene glycol)
PEGDA	Poly(ethylene glycol)-diacrylate
PEsU	Poly(ester urethane)
PEU	Poly(ether urethane)
PEUU	Poly(ether urethane urea)
PET	Poly(ethylene terephthalate)
PMN	Polymorphonuclear leukocyte
PPO	Poly(propylene oxide)
PTFE	Polytetrafluoroethylene
ROI	Reactive oxygen intermediate
SEM	Scanning electron microscopy
Semi-IPN	Semi-interpenetrating network
SMC	Smooth muscle cell

SPU	Segmented polyurethane
TCPS	Tissue culture polystyrene
TE	Tissue engineering
TEVG	Tissue engineering vascular graft
T_g	Glass transition temperature
T_m	Melting temperature
TSPCU	Silicone modified thermoplastic poly(carbonate urethane)

TABLE OF CONTENTS

Page

Page

LIST OF FIGURES

FIGURE Page

FIGURE Page

FIGURE Page

LIST OF TABLES

CHAPTER I

INTRODUCTION

1.1 Coronary Artery Disease

Coronary artery disease (CAD) accounts for close to the majority of all cardiovascular disease related deaths in the United States[1] with annual costs exceeding close to $150 billion.[2] In addition, CAD is estimated to become the leading cause of death in the world by 2020.[3] Patients experience CAD as a result of atherosclerosis, a multifocal inflammatory buildup of low density lipoproteins (LDLs) which form fatty streaks, **Figure 1.1**. Depending on physiological location, LDL buildup can cause localized turbulent flow patterns within the artery resulting in tissue injury with subsequent monocyte recruitment and macrophage differentiation.[4] Macrophages oxidize the LDLs on the vessel wall and encompass them along with smooth muscle cells (SMCs) to form foam cells. The foam cells then build up behind the endothelial wall by combining with collagen matrix synthesized by SMCs. The atheroma continues to expand as a result and over time can produce localized turbulent flow within the vessel damaging the endothelial layer. The body recognizes the site of injury and sends platelets which aggregate and eventually lead to occlusion. In addition, atheromas could potentially rupture causing the contents to form an occlusive thrombus[5] or flow downstream and occlude smaller diameter vessels. In the most severe of these cases, invasive surgical approaches including coronary artery bypass or arterial replacement procedures are used prior to atheroma rupture.

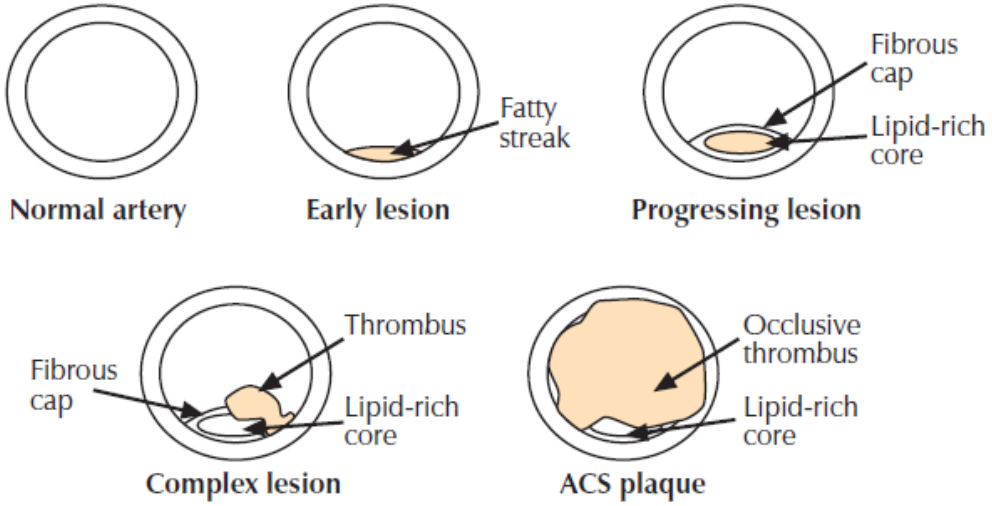

Figure 1.1. Atheroma formation. Starting at infancy, fatty streak forms which progresses into additional complex plaque formation covered by a fibrous cap. The cap eventually weakens and ruptures allowing for an occlusive thrombus to aggregate or flow downstream (Figure taken from Reference 4)

Autologous grafts harvested from the saphenous vein or internal mammary artery have been the gold standard but are not available in approximately 20% of patients due to disease, trauma, or anatomic abnormalities.[6,7] Allografts derived from cadaveric saphenous veins are a more readily available alternative to autologous grafts but are often met with complications typically involving damage to the intimal layer due to pre-implantation processing and immunological risks.[8-12] Synthetic grafts such as the Dacron graft, composed of poly(ethylene terephthalate) (PET), and the Gore-Tex graft, made of expanded polytetrafluoroethylene (e-PTFE) have also been used as alternatives to autologous grafts. These options have been successful in large diameter applications, but in smaller applications ($d < 6$ mm), grafts typically occlude due to thrombosis and intimal hyperplasia derived from compliance mismatch at the anastomosis site. Large diameter grafts have been successful in particular due to antithrombotic treatments. The

same treatments have been unsuccessful in preventing occlusion in small grafts leading scientists to believe compliance mismatch is the dominant cause of occlusive failure.

Studies have shown a direct correlation between compliance and long-term patency of vascular grafts ranging from saphenous veins to synthetic grafts,[13] **Figure 1.2.** In an end-to-end anastomosis model, the difference in stiffness causes a convergence of flow at the proximal end and a divergence of flow at the distal end of the graft due to dilation. The discontinuity of flow results in stagnation points at the distal end forming eddies, which increase shear stresses on the walls of the native tissue. These stresses can often damage the endothelial layer and induce platelet aggregation at the injury site which blocks flow.[14] Alternatively, the platelets may migrate downstream also resulting in graft occlusion. The stagnation points can provide a lack of blood flow in localized areas distal to the anastomosis. As a result the wall shear stress or rate is reduced causing the artery to reduce its inner diameter to increase the applied forces via intimal hyperplasia. The inner diameter of the artery is ultimately expected to decrease until occlusion.[15,16] Alternatively, the increased platelet residential time allows for prolonged release of growth factors from the platelets inducing further smooth muscle cell proliferation.[16] Finally, intimal hyperplasia can arise from the stress concentrations applied along the suture line of the distal anastomosis as a result of the artery increasing the proliferation of smooth muscle cells to accommodate the enhanced radial stresses applied.[17]

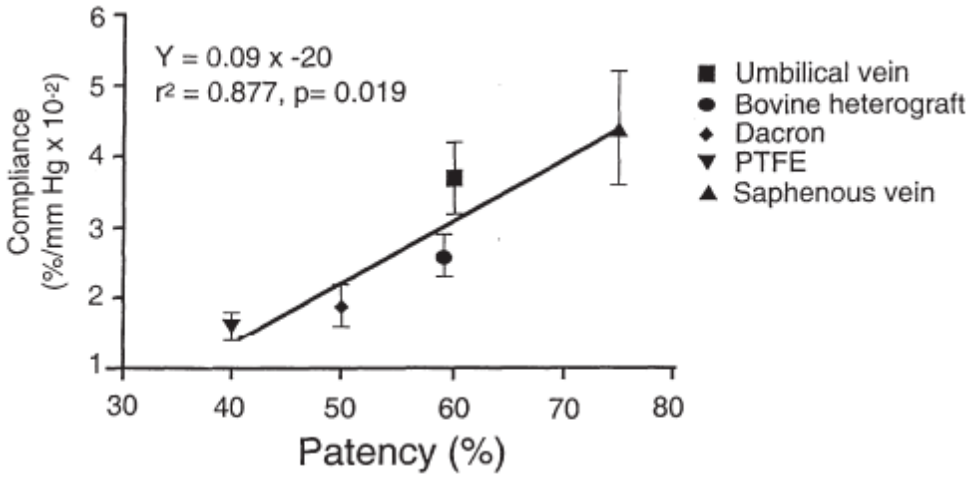

Figure 1.2. Direct correlation of graft compliance and 5 year patency rates. (Figure taken from Reference 13)

1.2 Vascular Graft Materials

Materials developed for vascular grafts can be categorized into two main groups: natural and synthetic materials. The former typically involves either collagen or a combination of collagen and gelatin. Scaffolds have been fabricated before by dissolving collagen and mixing in smooth muscle cells before combining it with a Dacron® graft and an additional collagen-fibroblast solution. Endothelial cells were then seeded on the inside to form a non-thrombogenic intimal layer. While the approach showed promise in fabricating vascular grafts *ex vivo* the resultant grafts had poor burst pressure due to lack of SMC alignment.[18] SMCs were later aligned by culturing them under stressed conditions though mechanical properties were still well below that of an autologous artery.[19-22] Electrospun collagen and elastin fibers have been used to form composite grafts/cell hybrids. Collagen I was electrospun and showed a three dimensional architecture for an ideal tissue engineered scaffold,[23] though burst pressure and

compliance values were not reported. In addition, the feasibility of the use of electrospun collagen I in blood contacting applications has yet to be determined.[24] Ratios of collagen and elastin have been electrospun in a blend to better mimic each layer of the lumen separately.[25] The challenge of matching native vessel structure and mechanical properties still exists with no current studies addressing the issue using purely natural materials.[26]

Synthetic materials are advantageous over natural materials in that burst pressure has been achieved in traditional synthetic grafts as well as the risk of batch-to-batch variability is greatly reduced. Woven or knitted Dacron® grafts were the first to be fabricated with various porosities to optimize the rate of cellular ingrowth however pre-clotting procedures using fibrin layers were required to prevent leakage. Numerous coatings have been applied to Dacron grafts to ultimately improve its success rate including: fluoropolymer for thromboresistance,[27] collagen and heparin for tissue incorporation without clotting,[28] fibrin for cultivation of endothelial cells,[29] silicone elastomer to make more bioinert,[30] and gelatin to improve neointima formation.[31] While these techniques have shown improvement in acute tissue ingrowth, scientists have determined the main cause of failure in the long term (>6 months) to be compliance.

Expanded-polytetrafluoroethylene (e-PTFE) is the preferred graft of the two traditional synthetic grafts. E-PTFE grafts mechanically are less stiff (3-6 MPa[32,33]) than Dacron grafts (12 MPa) in the circumferential direction but still have much greater stiffness than native arteries and veins (600, 900 kPa respectively). The mechanical difference of both synthetic options compared to autologous grafts is further highlighted

with their results in patency. While e-PTFE and Dacron® graft patency rates were found to be statistically similar after 5 years, the patency of autologous grafts was still far greater.[26] For endothelialization, increased porosity going from 30-90 μm in a canine[34] model was found to be effective but a smaller increase of 30-60 μm showed no difference in canines[35] or humans.[36] Furthermore, e-PTFE grafts are believed to be more thromboresistant than other vascular grafts due to the electronegativity of the material. This feature has been further enhanced with carbon coating or impregnation which was found to decrease platelet adhesion even more.[35,37-39] Finally, fibrin glue incorporated with growth factors has been utilized to increase thromboresistance.[40,41] Though these techniques have been very successful in preventing acute occlusion by combating thrombosis, ultimately patency was not found to improve with any of them again leaving scientists to believe compliance is the key cause. Thus, a new material is needed that can address the issues with mechanical properties so that compliance does not remain an issue.

1.3 Polyurethane Grafts with Improved Compliance

Synthetic grafts can occlude via numerous pathways related to compliance mismatch between native tissue and the graft at the anastomosis; therefore it is important to develop vascular grafts with better compliance despite the inverse relationship with burst pressure. Segmented polyurethanes (SPUs) have been used frequently in biomedical devices since the 1960s[42] due to their established mechanical properties, high tunability, and biocompatibility.[43,44] This subclass of polyurethanes consists of a soft segment,

typically a high molecular weight polyol, and hard segment composed of a low molecular weight aromatic or aliphatic isocyanate compound and chain extender with hydroxyl or amine end groups.[45,46]

SPUs provide a favorable option for meeting requisite mechanical properties, including compliance,[47] as their tunability allows for excellent mechanical strength and good fatigue life while also providing the needed flexibility. More importantly, their microphase morphology provides the added polymer chain interactions to achieve elastomeric mechanical properties superior to traditional graft materials. SPUs are made of a hard segment consisting of a low molecular weight isocyanate-terminated molecule and an alcohol or amine terminated chain extender. The soft segment is typically made of a high molecular weight polyol or polyamine. SPU polymer chains form hard domains dispersed within a soft segment matrix as unstrained conditions.[48] The hard segment provides strength and rigidity while the soft segment adds flexibility.

At initial strains (< 100%) the soft segment matrix chains respond to axial forces by stretching parallel to the force direction. Hard segments are then expected to break up at approximately 100% strain. Following hard segment breaking, the smaller domains orient themselves in the direction of the strain. During this section, also known as the rubbery plateau, little to no additional stress is applied to the material. At the onset of strain hardening (~200-300%), soft segment crystallization is initialized and there is a stronger dependence between soft and hard segment orientation.[48] The same stress vs. strain behavior has been seen in mechanical testing of carotid artery tissue including strain hardening.[49] The key difference between SPU mechanical response and native

tissue response lies in the onset of strain hardening. The deformation point in SPUs' curves is around 200-300% strain but in carotid tissue, the sharp increase in tensile stress is seen as early as 100%.[49] Thus, inducing an earlier strain hardening effect on SPUs could provide could provide the opportunity to meet the compliance of native tissue without sacrificing burst pressure.

Silicones have also long been used in medical devices because of their known biostability, anti-adhesive properties and, most importantly, low modulus due to low glass transition temperature.[50-53] Applications of silicones have been limited to devices not requiring useful engineering properties because the elastomers have been generalized as relatively weak when it comes to load bearing applications.[54] Tensile strength has been enhanced previously by covalently incorporating stronger chemical groups within the backbone[55] or polar side groups.[56,57] Mechanical fatigue life has also been improved with the inclusion of a urethane component in the silicone backbone for use in a commercially available material, Avcothane 51.[58] It is evident that these approaches to increasing the tensile strength and fatigue life of silicone elastomers are effective. However, the mechanical properties of the additive/copolymer component are often compromised as a result. Thus a new approach is needed that allows the designer to retain the characteristic properties of each component in a combination without sacrificing the other.

Interpenetrating polymer networks (IPNs) are distinguishable from most blends or copolymers in that they can provide the ability to retain the major characteristics of one network component without sacrificing any properties of the other. Briefly, traditional

IPNs incorporate two or more covalently crosslinked polymer networks that are not covalently bonded together but cannot be separated without breaking chemical bonds. Semi-interpenetrating polymer networks (semi-IPNs) differ from standard IPNs in that the components can potentially be separated without the need for breaking covalent bonds. SPUs have often been used as one of the components in semi-IPNs for various biomedical applications[59-64] to contribute to the overall mechanical properties of the network. These applications can include wound dressings,[65-67] uretral[68] and blood contacting materials.[69-71] Poly(dimethyl siloxane) (PDMS)-based materials have also been utilized as components in both IPNs,[72-76] and semi-IPNs[77,78] for various biomedical applications. Finally, a scarce amount of SPU/PDMS[79-81] semi-IPNs have been synthesized though, to the best of our knowledge, none have focused on optimizing compliance and burst pressure vascular grafts. Based on the previous work presented, semi-IPNs are a strong approach in achieving overall favorable *in vivo* performances, but the strict materials approach only accounts for a portion of the control over graft biomechanical properties. Exploration into the fabrication of grafts has the potential for even further enhancement vascular graft performance through control over graft architecture.

1.4 Fabrication of Polyurethane Grafts

The growing prevalence of polyurethanes in medical devices is due to the previously reviewed performance properties and tunability, therefore it should be of no surprise that this class of materials has been frequently explored in prior vascular graft

designs. Early polyurethane graft designs utilized a phase separation technique[82] which typically earned a compliant description however burst strength was most likely insufficient given the need for reinforcing materials such as polyesters[83] or silicones.[84] Thus, new designs still need to address the compliance match requirement but also look to retain burst pressure eliminating the need for a reinforcing layer.

Electrospinning has recently gained significant attention in the design of various biomedical devices because it provides a facile and tunable method to produce porous scaffolds and devices, **Table 1.1**. In addition, specific electrospun fibers have previously been demonstrated to retain strength well beyond fibers produced via alternative methods but with similar architectures;[85] however, their porous morphology still allows for a highly compliant material.[86] Briefly, a polymer is dissolved in a conductive solvent and dispensed through a charged needle positioned at a specific distance from a grounded/oppositely charged collector at a controlled rate. The electrical force applied on the polymer solution stretches the droplet emerging from the needle until a critical voltage causes a jet to spring towards the collector.[87] The solution jet experiences whipping paths and splaying prior to reaching the target which dries any remaining solvent leaving fibers with diameters on the order of nanometers to low microns.

Table 1.1. Electrospun polyurethane medical devices

Electrospun Polyurethane Medical Devices	
General Tissue Engineering (TE)[88-118]	Wound Dressing[119-127]
Musculoskeletal TE[128-134]	Drug Delivery[135-139]
Neurological TE[140,141]	Additional Devices[142-151]
Cardiovascular TE[136,152-180]	

A typical electrospinning setup allows the user to manipulate several variables to tailor the resulting fiber mesh to meet the specific needs of their application. Fiber alignment and patterning has been of interest especially in vascular grafts because control over fiber orientation and morphology can have an added effect on the construct's overall mechanical properties better mimicking of graft properties. More common attempts at controlling fiber alignment include setups that replace a stationary target with a rotating mandrel to help spool the fibers forcing them to align in the direction of rotation.[181-186] While the technique is highly proficient in providing the small diameter tubular overall construct needed for synthetic vascular grafts, tissue anisotropy is still not fully captured with the rotating mandrel setup alone.

Recently, it was found that polyurethanes could be patterned on the micro scale using substrates fabricated from soft lithography.[95] When electrospun on the PDMS substrates with specific grid patterns, the removed PEsU fibers were found to mimic the same grid pattern. The fibers showed a bimodal distribution of diameter with smaller fibers inside the grids and larger fused ones along the raised pattern features. Commercially available BioSpan®, a poly(ether urethane urea) (PEUU), was also electrospun on the same grid patterns and showed no fusing or orientation along the topography features. When both SPUs were electrospun on flat PDMS substrates both sets of fibers had randomized fiber orientations though the PEsU fibers still showed a bimodal diameter distribution with the same fiber fusion effect. The study concluded that the ester linkages within the PEsU fibers showed greater sensitivity to changes in the electric field due to surface topography differences because of their greater dipole

moments[187] than the ether groups in PEUU. In addition, the fibers were attracted to each other as the polar carbonyl groups of the linkage are presumed to align themselves in the direction of the electric field[188] leaving oppositely charged ends facing incoming fibers. With this new phenomena on select electrospun polyurethane chemistries, the unique patterned and bimodal distribution of fiber morphologies is expected to give a more complex improved control over graft biomechanical properties.

Though fabrication of the electrospun graft, coupled with modulation of material chemistry is a promising approach for achieving both compliance and burst pressure simultaneously, it does not guarantee the success of the graft in the long term. The mechanical performance of the graft must be maintained. Thus a key component not yet addressed in this review important in retaining graft properties is determining the biostability of the vascular graft.

1.5 Understanding Polyurethane Biostability for Retention of Graft Properties

Maintaining biostability has been a functional requirement in designing traditional vascular grafts due to the expected exposure to water and macrophage mediated biodegradation.[189] Following implantation, the body's inflammatory response begins with an initial appearance by polymorphonuclear leukocytes (PMNs), a neutrophil, but are known to disappear within 24-48 hours.[190] Monocytes then migrate to the site and differentiate into macrophages which eventually fuse together to form foreign body giant cells (FBGCs), which create a closed compartment where they secrete reactive oxygen intermediates, acids, and enzymes.[190-192]

Before the effects of the cell-biomaterial interactions can be studied, it is important to understand that the general degradation process typically followed by polymers. The degradation medium (i.e., water, salts, peroxides, enzymes) is first adsorbed on the polymer surface. Next, the medium diffuses into the bulk of the polymer and begins to chemically react with the unstable or labile bonds in the polymer chains. The reactions often result in polymer chain cleavage reducing the polymer chain length or molecular weight. When the length is reduced enough the degradation medium is able to dissolve portions of the degraded polymer and transport them out of the bulk polymer.[46]

The first generation of polyurethanes, poly(ester urethanes) (PEsUs), were known to degrade quickly in the body due to their hydrolytically labile aliphatic soft segments.[193,194] Water molecules infiltrate the polymer matrix and attack the bond connecting the backbone oxygen and carbon of the carbonyl within the ester linkage leaving alcohol and carboxylic acid end groups,[46] **Figure 1.3**.

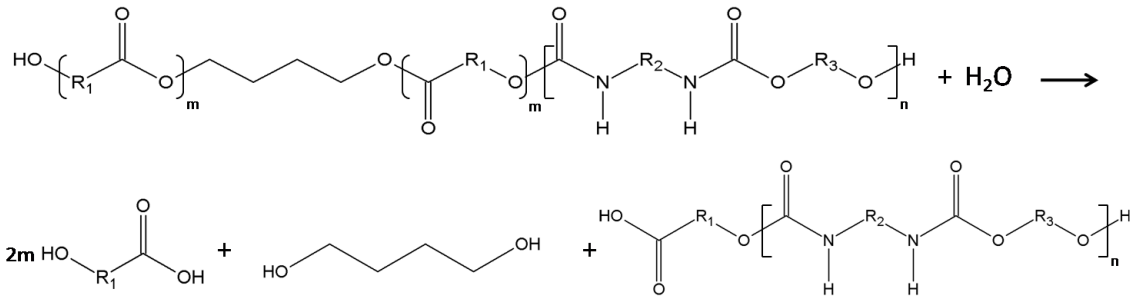

Figure 1.3. Hydrolysis reaction of general segmented PEsU.

The degradation behaviors of polyurethanes are most often characterized with *in vitro* degradation studies.[195-210] Depending on the hydrophilicity of the polyurethane in

question, degradation behavior can fall into two distinct categories: bulk degradation[202,209], and surface erosion.[202,211] Polymers known to be highly hydrophilic will exhibit a diffusion rate that is faster than the rate of hydrolytic degradation allowing water molecules to penetrate before cleaving the ester linkages. Evidence of degradation will be spread throughout the bulk of the polymer as a result. This behavior is commonly referred to as bulk degradation. For more hydrophobic polymers, the opposite is true where the rate of hydrolysis is faster than that of diffusion leaving degradation evidence only on the surface of the polymer. These materials are undergoing surface erosion.

Enzymatic hydrolytic degradation is a more specific form of hydrolysis than the general reaction because it is dependent on location of the implant as well as ability of the enzyme to be adsorbed, **Table 1.2**.[212] Following restructuring of the polymer for adsorption and desorption, the adsorbed enzyme reacts with and cleaves labile bonds before releasing them into the solution.[212,213] Unlike non-specific hydrolysis, which can undergo surface erosion or bulk degradation depending on reactivity and diffusion variables, enzymatic degradation is only limited to the surface of the material. Enzymes typically have molecular sizes that are significantly larger than water molecules which limit their diffusion.

Table 1.2. List of enzymes

Enzymes	
Chymotrypsin[209,211,214-221]	Urease[222]
Cholesterol Esterase[223-229]	Papain[218,220,222,230-235]
Bromelain[218,220,221]	Elastase[110,236-240]
Protease K[218,219]	Ficin[218,220,221]
Collagenase[110,224,241-243]	Carboxyl Esterase[244-246]
Cathepsin B[163,224,247]	Plasmin[248,249]
Cathepsin C[220]	Lipase[202,250-257]

Poly(ether urethanes) (PEUs) were developed to resist hydrolysis with more biostable ether grou0ps in their soft segments. However, research found these soft segments to be subject to oxidative degradation including metal ion oxidation and environmental stress cracking.[194,258-260] These included medical devices such as pacemaker lead coatings and breast implants. Briefly, an oxygen radical abstracts an α-methylene from the ether soft segment. The newly formed radical then combines with an additional oxygen radical forming a hemiacetal which oxidizes into an ester linkage. The ester hydrolyzes forming an acid or aldehyde with or without the presence of another oxygen radical. The radical formed during the initiation of oxidation can also combine with a nearby formed radical creating a crosslinked network at the surface of the material leading to surface embrittlement,[261] **Figure 1.4.**

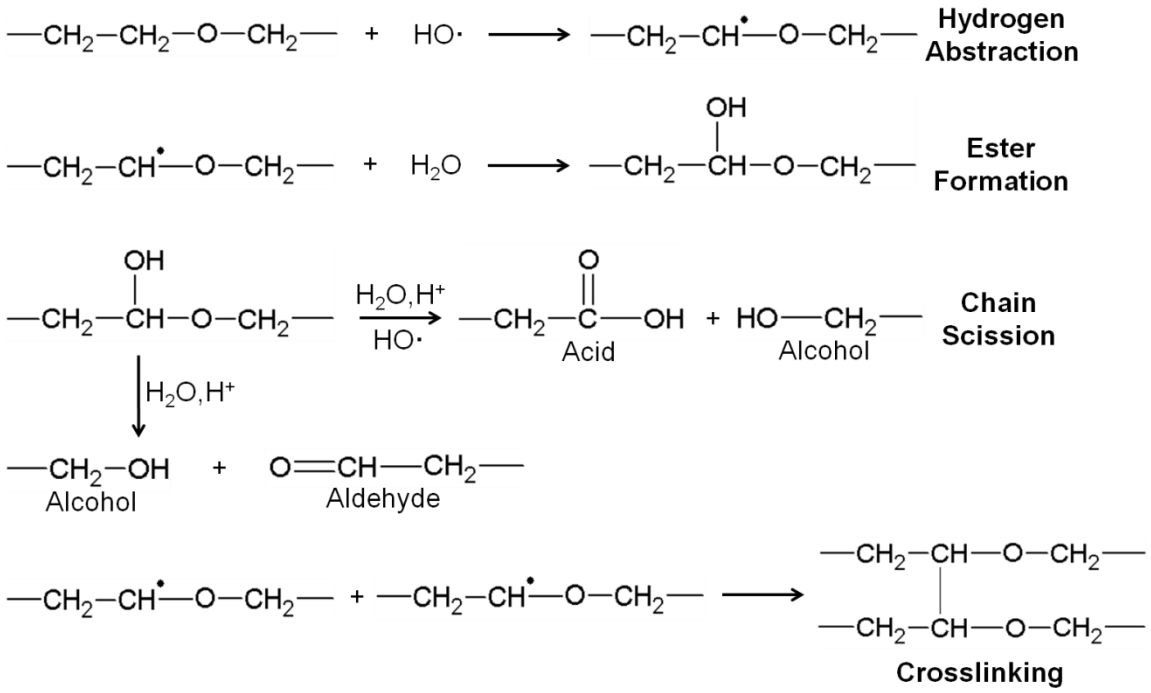

Figure 1.4. Ether soft segment oxidative degradation[262]

Oxidative degradation, like enzymatic hydrolysis, is also limited to the surface of the polymer but diffusion of the oxygen radicals is not limited due to their size but rather their high reactivity. It is expected that initiation of the oxidation process will occur before radicals can infiltrate the polymer matrix, though research has shown the possibility of radical chain transfer allowing migration into the material.[263]

Several attempts have been made to expand on the biostability of PEUs to help also resist oxidative degradation. For example, incorporating other known biostable components into the SPU chain including polyisobutylenes,[264-270] and polytetrafluoroethylene[270] has proven to be effective. Silicones, mainly PDMS, have been used in biomedical devices because of their elastomeric properties and excellent resistance to both hydrolytic and oxidative degradation.[264,271,272] However, their

mechanical properties again are typically insufficient in applications where the device has to withstand physiological forces. Others incorporated antioxidants on the surface of PEU elastomers to maintain their favorable mechanical properties. Synthetic antioxidants such as Santowhite®[273,274] and Irganox® are potential candidates[273,274] as well as natural antioxidants such as vitamin E[275,276] due to its safe release products.[277,278] However, these surface treatments are not permanent.

Recently, SPU synthesis chemists have developed a new generation of polyurethanes which incorporate carbonate groups within the soft segment known to be more biostable than polyether formulations of the same compositional ratios.[44,279-281] Poly (carbonate urethanes) (PCUs) are expected to undergo oxidative degradation similar to PEUs, **Figure 1.5.**, but the lower nucleophilicity of the carbonate group significantly slows down the degradation rate.

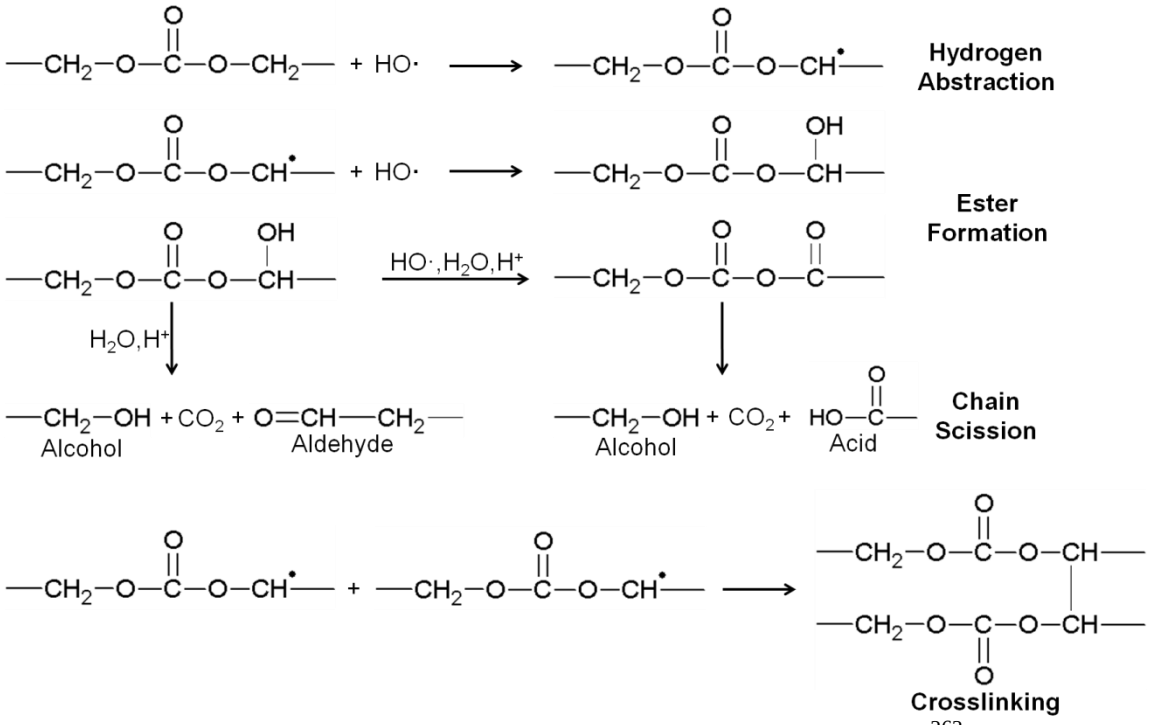

Figure 1.5. Carbonate soft segment oxidative degradation.[262]

Thermoplastic PCU elastomers exhibit the same mechanical properties as PEU formulations of similar hard segment compositions; however, PCUs are expected to retain most properties due to the electrophilic nature of the soft segment carbonate groups. The enhanced biostability demonstrated by accelerated oxidation tests in the literature makes PCUs very strong candidates for biostable applications, especially the reinforcing layer of a biostable multilayer graft.[194,282-285] While the multilayer approach is promising to provide the requisite properties for successful *in vivo* deployment, there will always be some concern over foreign material remaining in the body. Furthermore, the full function of an artery or vein cannot be replicated without also enabling vasoactivity, a highly advantageous feature of autologous grafts. Therefore a tissue

engineering approach needs to be employed to not only replace the function of native tissue but to ultimately restore it.

1.6 Biodegradable Polyurethanes for Tissue Engineering Vascular Grafts (TEVGs)

The field of tissue engineering employs a multidisciplinary approach that combines the knowledge and technology of cells, biomaterials and bioactive factors to fabricate organs.[286] The overall goal of tissue engineered organs is to not just replace the function of natural tissue but to also restore it over time.[287] Therefore a TE approach to fabricating a vascular graft could not only mimic graft biomechanical properties but also allow for the restoration of graft vasoactivity. However; the function of vascular tissue is greatly dependent on its structure and vice versa,[288] therefore it is crucial for the tissue engineering vascular grafts (TEVGs) to initially function similarly to natural vessels.

Two main approaches have been used in designing an optimal scaffold for a TEVG: scaffolds composed of biodegradable and resorbable materials, and permanent scaffolds made from decellularised blood vessels.[289-291] As the focus of this work is to develop and characterize biomaterials for a multilayered vascular graft, only the former of the two categories will be covered in this review. SPUs are highly tunable which allows for flexibility in designing biomedical applications as it relates to degradation as well as mechanical properties. Thus with the abundance of polyurethane component choices, SPUs have been utilized for various TE scaffolds including several cardiovascular scaffolds, **Table 1.3.**

Table 1.3. Polyurethane Tissue Engineering Scaffolds

Polyurethane Tissue Engineering Scaffolds	
General TE Scaffolds[110,142,160,292-310]	Bone TE Scaffolds[129,292,311-401]
Muscle TE Scaffolds[129,130,170,402-404]	Cartilage TE Scaffolds[329,331,332,358,375,378,396,405-426]
Neurological TE Scaffolds[140,351,410,427]	Ligament TE Scaffolds[89,128]
Skin TE Scaffolds[351,375,410,428-432]	Liver TE Scaffolds[433-438]
Cardiovascular TE Scaffolds[109,115,129,155,157,160-162,164,165,173,174,176,177,180,296,298,299,344,439-494]	

A key functional requirement in the design of TE scaffolds yet to be addressed in this review is the rate of degradation needed to ensure proper integration of neotissue within the scaffold. It has been shown that components of polyurethane structure can have specific effects on degradation.[495] Several studies have been conducted to help understand the effects on degradation specifically caused by the hard segment. Tang et al. observed in separate studies the effects of hard segment chemistry and hard segment content on the enzymatic degradation of polycarbonate-polyurethanes (PC-PU)s.[225,226] The study on hard segment chemistry specifically looked at differences in the polycarbonate-polyurethanes synthesized from hexane diisocyanate (HDI), methylene di (p-phenyl diisocyanate) (MDI), and hexamethylene diisocyanate (HMDI). Ultimately it was concluded that MDI and HMDI degraded at a much slower rate than HDI likely due to less hydrogen bonding among the carbonate and urethane linkages in the PC-PU synthesized from the latter isocyanate.[225] Though it was also found that PC-PUs with MDI and HMDI were found to initially degrade similarly, at later time points HMDI-based polyurethanes degraded more.[225] The same degradation patterns were observed by Kim et al. in poly(ester urethane urea)s synthesized with the same choice of isocyanates

for acceleration hydrolysis and enzymatic degradation.[496] Though Tang and colleagues concluded that hydrogen bonding could be a parameter to consider for biostable polyurethanes,[225] the same can also be applied for resorbable polyurethanes intended to degrade.

While the choice of isocyanate can affect the degree of hydrogen bonding and ultimately the degradation rate of resorbable polyurethanes, the aforementioned isocyanates are not hydrolytically labile. To make the hard segment increasingly labile, lysine diisocyanate (LDI) is a common choice due to its known lack of cytotoxic degradation byproducts.[310,497-499] The use of LDI allows urethane linkages to be hydrolyzed into lysine products.[310,497] The effects of the isocyanate following degradation have also shown to contribute to further degradation. Bruin et al. have hypothesized that when LDI is cleaved, it forms carboxylic acid groups which can further catalyze hydrolytic degradation.[500] Others such as Elliot and colleagues conclude that urethanes and ureas can only degrade enzymatically therefore the effects of carboxylic acids in the degradation medium are not significant.[214]

Though the effects of choice and amount of isocyanate in the hard segment of polyurethanes have been found to affect the degradation behavior of polyurethanes, the chain extender has been shown to contribute as well. For enzymatic degradation, it was found by Skarja et al. that the use of an amino acid-peptide based chain extender including ester linkages could increase the enzymatic lability of the PUs significantly though they were not susceptible to hydrolysis.[209] Though they did not observe degradation behavior, Dahiyat et al. synthesized a series of putrescine based

poly(phosphoester urethane)s with chain extenders containing phosphoester linkages likely to be hydrolytically labile. In a more recent study by Tatai and colleagues, the rate of hard segment hydrolytic degradation was accelerated with the use of a hydrolysable chain extender based on poly(DL-lactide) and ethylene glycol. Ultimately, results indicated the hard segment's rate of degradation to be higher than that of the basic poly(ε-caprolactone) (PCL) soft segment.[501] It can be seen from the aforementioned studies that chain extender chemistry is an additional item to consider in designing resorbable polyurethanes.

Despite the observations discussed previously, the composition of the ester-based soft segment most often controls the polyurethane's degradation rate *in vitro*.[502-506] With regards to these soft segments, ultimately degradation rate is dependent on the rate of medium diffusion through the polymer. One major property associated with medium uptake is hydrophilicity known to have a clear effect on the degradation rates of various polyesters.[507] Several studies have synthesized polyurethanes with soft segments comprised of hydrophilic and/or hydrophobic components.[208,215,508-511] A prime example of this approach is the use of the poly(ethylene glycol)-poly(propylene oxide)-poly(ethylene glycol) (PEG-PPO-PEG) triblock, better known as Pluronics®. By varying the molar ratios of PEG and PPO the hydrophilicity of the polyurethane can be affected. In a study by Gorna and Gogolewski, the triblock was included to make the polyurethane more hydrophilic was PCL was also included to add hydrophobicity to the polymer as well as hydrolytic lability. As expected, evidence of degradation was most prevalent in specimens with the highest amount of Pluronics®.[208]

Controlling hydrophilicity may be an effective method to tailor degradation rate but it is not the only pathway to control water uptake. The crystalline morphology of the polyurethane structure can also affect the diffusion rate of degradation mediums. Skarja et al. found that polyurethanes with amorphous soft segments increases the rate of hydrolysis[511] while an increase in crystallinity would decrease the degradation speed.[215,511] Despite the differences found in these studies it was concluded that hydrophilicity is the more dominant effect in soft segments.[215,511]

1.7 Summary

Segmented polyurethanes show great promise in developing multilayered vascular grafts by providing greater control over graft biomechanical properties which ensures long term success *in vivo*. Using the thermoplastic polymer in a semi-interpenetrating polymer network further enhances its ability to match the requisite mechanical properties needed for successful *in vivo* deployment of the vascular grafts. Silicone networks will help modify the mechanical behavior of the vascular graft to better mimic that of native carotid artery tissue. The use of carbonate-based polyols in the soft segment of the SPUs will further enhance the overall biostability of the vascular graft and ensure better retention of mechanical properties in the long-term. Electrospinning will allow for the further tuning of the vascular graft with optimal fiber diameter and orientation giving it the best morphology needed to incorporate a bioactive non-thrombogenic intimal layer. Finally, it is believed that the incorporation of a

biodegradable component in the vascular graft design coupled with controlled electrospun fiber morphology, would allow for restoration of graft vasoactivity.

CHAPTER II

FABRICATION AND INITIAL TESTING OF MULTILAYER VASCULAR GRAFTS*

2.1 Introduction

Traditional synthetic options typically used as small diameter vascular grafts in bypass and arterial replacement surgery result in acute and long term re-occlusion rates. Early flow obstruction can be attributed to the inherent thrombogenicity of most commercially available synthetic materials often causing substantial platelet adhesion and aggregation. Long term decreases in patency of distal arterial vasculature can be attributed to the synthetic graft's lack of requisite mechanical properties to match the compliance of native tissue without sacrificing burst pressure. Past options have provided burst pressures that exceed the properties of autologous veins but the lack of compliance has been directly correlated to decreases in rate of 5 year patency.[512] Thus matching compliance with the reinforcing layer has been proven to be just as crucial as providing a thromboresistant inner layer. Research has previously addressed these gaps by developing new designs that better mimic the properties of native blood vessels,[19,513-515] but these attempts have typically resulted in impractical fabrication requirements.[18,516-518] Thus, a novel and inexpensive synthetic design needs to be

*Excerpts and select figures reprinted with permission from "Multilayer Vascular Grafts Based on Collagen-Mimetic Proteins," by MB Browning, D Dempsey, V. Guiza, S. Becerrea, J. Rivera, B. Russell, M. Höök, F. Clubb, M. Miller, T. Fossum, J-F Dong, A.L. Bergeron, M. Hahn, and E. Cosgriff-Hernandez, Acta Biomaterialia 2012, 8 (3), 1010-1021. Copyright (2012) Elsevier.

developed that incorporates both the biological and mechanical properties of autologous grafts but also allows for the availability provided by current synthetic options.

Our multilayer graft is expected to successfully provide a thromboresistant inner layer that also promotes rapid endothelialization through a Scl2-2 protein based PEG hydrogel coating. The bioactive hydrogel has been previously reported to provide integrin binding sites known to only allow the binding of endothelial cells;[519] however the hydrogel is not expected to withstand physiological loading.[520-523] Therefore, our reinforcing layer of the multilayer graft must provide the necessary material strength to withstand physiological loads, but also retain the requisite mechanical properties needed for long term patency. SPUs were selected because of their established biocompatibility, durability, and fatigue resistance.[46] In addition the reinforcing layer of the graft was fabricated using electrospinning to provide a porous fibrous architecture expected to yield even greater compliance values. Furthermore, the high tunability of SPUs along with the modulation of electrospun graft architecture is expected to improve graft biomechanical properties beyond reported values from autologous veins.

The current study focuses on the feasibility of fabricating the composite vascular graft. In addition to the well documented complications arising from thrombosis and intimal hyperplasia, the graft's ability to withstand processing effects and surgical deployment must also be evaluated. To this end we have electrospun the reinforcing layer and characterized its resultant architecture prior to composite fabrication. The fibrous sleeve was subject to biomechanical testing to obtain initial trends from graft architecture. While it is important to optimize the layers for their separate applications,

the overall feasibility of the graft could be the cause of initial device failure prior to known complications. Therefore, it is crucial to the overall success of the multilayer vascular graft design for the graft to be evaluated for initial performance prior to long term studies.

2.2 Materials and Methods

2.2.1 Materials All chemicals were used as received and purchased from Sigma Aldrich (St. Louis, MO) unless otherwise noted.

2.2.2 SPU Electrospinning BioSpan® (DSM-Polymer Technology Group; Berkeley, CA, USA) and Carbothane® (Lubrizol; Wikliffe, Ohio, USA) were dissolved at 15 wt% in dimethylacetamide (DMAC) for electrospinning. A 4 mm diameter copper rod collector was dipped in a 5 wt% PEG solution in chloroform. After drying, it was grounded and positioned 35 cm away from the tip of a blunted 20 gauge syringe needle. The SPU solutions were dispensed at a rate of 1.0 mL per hour with a syringe pump (KDS 100, KDS Scientific) as a voltage of approximately 14 kV was applied to the needle tip using a high voltage source (Gamma High Voltage, Ormond Beach, FL, USA) for 2 to 8 hours.[524] After the designated time period, the copper rod with the mesh was placed in water overnight to dissolve the inner PEG layer, and the mesh was removed from the rod while submerged. High resolution images of electrospun fiber mats were captured using a field emission – scanning electron microscope (JSM-7500F, JEOL) operated at 2 kV to confirm fibrous morphology. Fiber diameter was quantified using a pixel-to-length ratio approximation on 25 randomly selected fibers in the micrographs.

2.2.3 Multilayer Graft Fabrication Mesh sleeves were taken through a graded ethanol/water soak (70%, 50%, 30%, and 0%; 30 minutes each) to ensure hydration and penetration of the aqueous hydrogel precursor solutions into the mesh prior to polymerization. The pre-wetted meshes were placed in a cylindrical mold with an inner glass mandrel (3 mm OD). Hydrogel solutions were pipetted between the mandrel and the hydrated mesh (4 mm ID) and crosslinked as described in Section 2.3, **Figure 2.1.** Given that the inner diameters of the mesh and the multilayer graft (i.e. the hydrogel layer) were held constant, the outer diameter of the multilayer graft was dependent on the thickness of the electrospun mesh. In these studies, the electrospun mesh thickness was modulated from approximately 0.2 to 1.2 mm, resulting in graft wall thickness between 0.7 and 1.7 mm and corollary graft outer diameters between 4.4 and 6.4 mm.

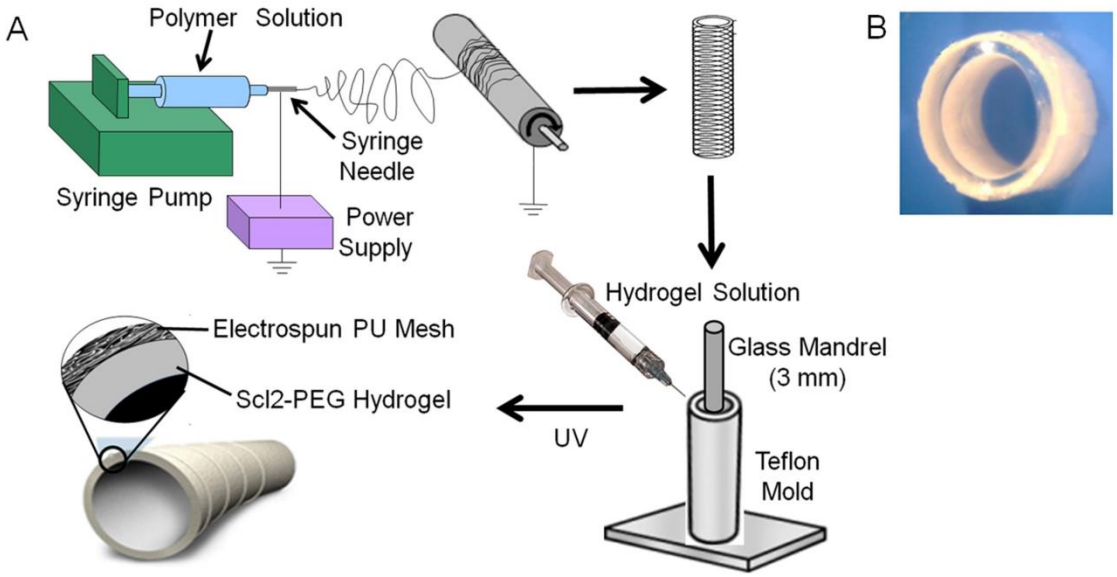

Figure 2.1. Multilayer graft fabrication. (A) Fabrication process of multilayer grafts. (B) Multilayer graft.

2.2.4 Multilayer Graft Biomechanical Properties To determine the dependence of multilayer graft suture retention strength, burst pressure and compliance on the thickness of the electrospun mesh layer, BioSpan® was electrospun for 2 to 8 hours to form reinforcing meshes with varied thicknesses. Electrospun meshes were then combined with 20 wt% poly(ethylene glycol)-diacrylate (PEGDA) (6 kDa) hydrogels for testing. Graft suture retention strength was determined in accordance with the straight across procedure described in the American National Standard Institute – Association for the Advancement of Medical Instruments VP20-1994. Briefly, 18 mm long tubular samples were cut lengthwise to obtain rectangular strips (approximately 12 mm wide). A 5.0 commercial PDS II monofilament suture (Ethicon, Inc) was inserted 2 mm from the short edge of the sample, looped, and tied. The lower end of the sample and the suture loop were secured in the grips of a uniaxial load test machine (Instron 3342) and extended at a rate of 100 mm/min until the suture pulled through the sample wall. Suture retention strength was considered to be the maximum force recorded prior to sample failure.

For burst pressure and compliance assessment, a nonporous latex tube lining was inserted into multilayer grafts (35 mm long). Burst pressure was determined from a method adapted from Sarkar et al.[525] Deionized water was pumped into the latex tubes at a rate of 140 mL/min using a syringe pump (KD Scientific), and the pressure was measured using a high pressure gauge (0 to 60 psi pressure range, NoShok) connected downstream of the graft. The ends of the grafts were firmly secured and sealed to

prevent leaking. The maximum pressure prior to construct failure was recorded as the burst pressure.

The static compliance of separate latex-lined grafts was measured as previously described.[526] Briefly, a syringe pump (Harvard Apparatus) was used to subject the multilayer grafts to a pressure ramp (0-150 mmHg). Intraluminal pressure was monitored using standard in-line strain gauge pressure transducers (Merit Medical, South Jordan, UT), and the outer diameter was measured with a He-Ne laser micrometer (BenchMIke, Lasermike). Compliance (C) was calculated from the recorded pressure, P, and diameter, D, according to the following equation:

$$C=\frac{\Delta D}{D_0 \cdot \Delta P}=\frac{D_{120}-D_{80}}{D_{80} \cdot 40}$$

2.2.5 In Vivo Acute Thromboresistance All procedures were approved by the Institutional Animal Care and Use Committee. Multilayer grafts (3 cm in length, 4 mm inner diameter) were implanted in a 6 month old Yucatan miniature pig (30-40 kg) using a previously described technique.[527] Briefly, anesthesia was induced by intramuscular injection of Telazol (5 mg/kg) and buprenorphine (0.01-0.05 mg/kg) followed by intubation and administration of isoflurane (2-4% MAC) in 100% oxygen for maintenance of a surgical plane of general anesthesia. Using sterile technique, an 8-12 cm incision was made in the ventral midline of the neck. The carotid arteries were sequentially exposed and vascular clamps placed at each end of the area of interest on the artery to provide temporary vessel occlusion. An end-to-end anastomosis was performed using a continuous pattern of 7-0 prolene sutures. A multilayer graft with PEG-Scl2-2 (10% 3.4 kDa, 12 mg protein mL^{-1}) was implanted on the left side, and a

PEGDA (10% 3.4 kDa) control graft was implanted on the right side. After confirming patency and hemostasis, subcutaneous tissues and skin were closed routinely. Digital subtraction and 3-D angiography were performed via the transfemoral technique with systemic anticoagulation using heparin after placement of the sheath and maintenance of activated clotting lines of 2-3x baseline in order to prevent thromboembolic complications related to the procedure itself. After removal of the catheter and sheath, the animal was maintained under anesthesia for 5 hours. The patency and anatomy of the grafts were assessed using vascular Doppler and two dimensional ultrasound imaging techniques. The study subject was then heparinized and humanely euthanized while still under general anesthesia. The carotid arteries were carefully removed for further evaluations.

2.3 Results and Discussion

2.3.1 Electrospun architecture Prior to biomechanical property evaluation of the electrospun reinforcing layer, the fiber morphology was first characterized to ensure consistent reliable fiber deposition. The macroscopic view of a harvested electrospun SPU mesh tube, **Figure 2.2a,** illustrates an apparent consistent graft size and mechanical integrity throughout full length which suggests fibers are deposited evenly throughout the process. Resultant fiber morphology observed on the microscopic scale, **Figure 2.2b**, exhibited minimal variation in fiber diameter (1.6 ± 0.1 μm) as well as minimal fiber fusions expected to favorably affect graft compliance. In addition, consistent increases in graft thicknesses ranging from 0.21 ± 0.06 mm up to 1.19 ± 0.17 mm were measured

from the scanning electron micrographs. These changes in wall thickness, assuming no effect on fiber morphology with increased deposition time, are expected to influence graft biomechanical properties.

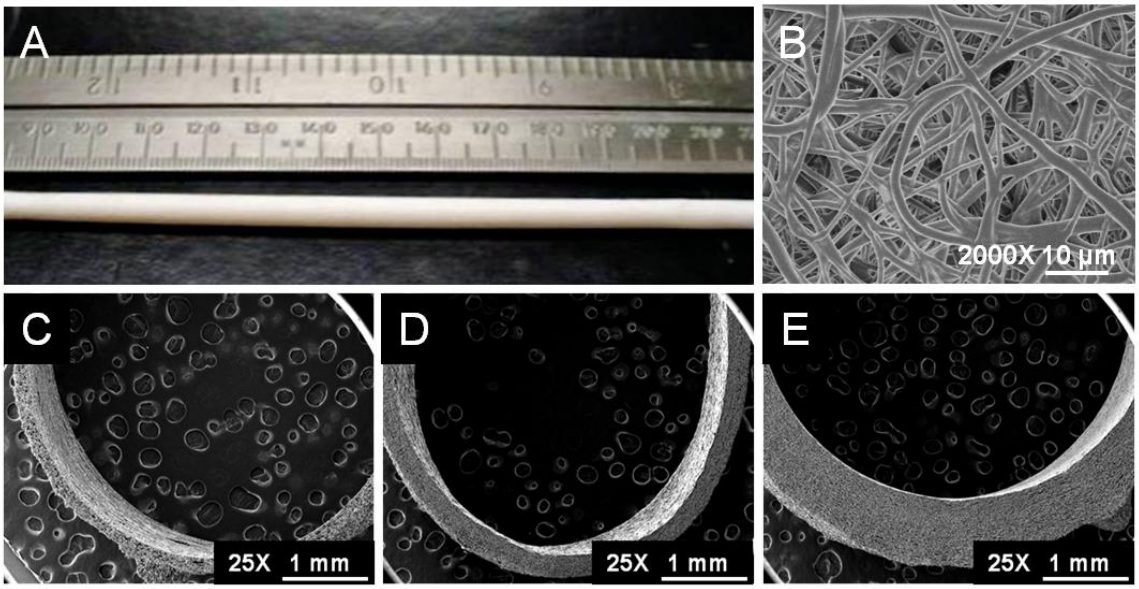

Figure 2.2. Reinforcing electrospun mesh tube. (A) Electrospun SPU mesh tube. (B) Representative SEM image of fibrous SPU mesh tube. Cross-sectional views of (C) low thickness tube (wall thickness ≈ 0.17 mm), (D) medium thickness tube (wall thickness ≈ 0.36 mm), and (E) high thickness tube (wall thickness ≈ 0.78 mm).

2.3.2 Multilayer Graft Biomechanical Properties The long term *in vivo* success of our multilayer graft design is highly dependent on the resultant biomechanical properties of the electrospun reinforcing layer. The grafts are expected to provide the requisite suture retention strength needed for implantation as well as burst pressure and compliance values comparable to reported autologous vein properties. While burst pressure and suture retention strengths have already been replicated in current synthetic options,[512] compliance values are substantially lower than autologous veins which resulted in poor patency after 5 years. Stewart et al. hypothesized that low compliance

grafts do not distend as wide as distal arteries creating a disruption in flow patterns downstream of the graft.[16] Consequently, stagnation points are created along the walls of the native vasculature which the arterial wall attempts to eliminate via intimal hyperplasia to reach original mean shear stress values. Graft wall thickness was changed by modulating electrospinning time in an attempt to control graft biomechanics, **Table 2.1**

Effects on graft biomechanical properties with increasing mesh thickness were monitored. A distinct positive correlation was found between graft thickness and burst pressure as well as suture retention strength. Burst pressure was found to increase from 534 ± 84 mmHg up to 1404 ± 40 mmHg which translated to 163% increase over the full range of graft thicknesses. The effect of thickness on burst pressure was attributed to a materials known dependence on construct dimensions, where the increase in graft thickness can be related to an increase in cross-sectional area. As a result the material, whose finite stress limit is not expected to change, can withstand more force with a given increase in cross-sectional area.[528]

Table 2.1. Biomechanical properties of multilayer vascular grafts.

Thickness (mm)	Burst Pressure (mmHg)	Suture Retention Strength (gf)	Compliance (%/mmHg x 10^{-4})
0.21 ± 0.06	534 ± 84	406 ± 124	5.9 ± 1.4
0.39 ± 0.06	665 ± 113 (↑ 25%)	764 ± 234 (↑ 88%)	3.6 ± 1.0 (↓ 39%)
0.72 ± 0.06	905 ± 186 (↑ 69%)	1390 ± 316 (↑ 242%)	2.7 ± 0.2 (↓ 54%)
1.19 ± 0.17	1404 ± 40 (↑ 163%)	1734 ± 33 (↑ 327%)	1.8 ± 0.1 (↓ 69%)
Saphenous Vein[512]	*1680 ± 307*	*196 ± 2*	*4.4 ± 0.8*

(average ± standard deviation; n=16 for compliance, n=4 for burst pressure)

As for graft compliance, only the thinnest graft provided a compliance higher than reported autologous values which unfortunately could only withstand a burst pressure of less than a third of the vein's property. The inverse effect of thickness on compliance can be related to the definition of elastic modulus where, the increased stress response of a graft due to increased wall thickness, is then expected to increase the modulus as well and thus decrease compliance. This negative correlation has been demonstrated previously in the literature with current synthetic grafts.[512]

With regards to suture retention strength, the lowest thickness reached strengths of 406 ± 124 gf which already match autologous properties. Increased thickness up to highest value was found to further increase the suture retention strength more than threefold. This suggests that all multilayer vascular grafts can provide the suture retention sufficient for implantation.

While compliance values exceeded autologous graft properties in the samples with the lowest thickness, the burst pressure loss limited grafts to only achieving one property at a time while autologous graft anisotropy allows for simultaneous properties. This limitation indicates that the tunability of the current SPUs along with architectural tailoring using electrospinning are both insufficient to achieve simultaneous improvements in burst pressure and compliance. A novel approach involving changes to electrospun SPU chemistry and processing effects was then explored and will be discussed in the next chapter.

2.3.3 In Vivo Acute Thromboresistance Multilayered grafts were implanted into a miniature Yucatan pig for 5 hours. During the implantation surgery, grafts were found to hold sutures and retain physiological blood flow, **Figure 2.3a**, suggesting that graft biomechanical properties were sufficient for use *in vivo*. Furthermore, the examination through intravital imaging exhibited excellent patency on the inner layer with no effects on blood flow or arterial narrowing observed. In addition, evidence of thromboresistance was characterized via angiography, gross pathology, and micro tomography, **Figure 2.3b-d**, which was then corroborated with acute *in vitro* testing.[528] Overall the multilayer graft was found to perform very favorably *in vivo* for an acute time frame (5 hours). While effects of compliance could not be examined *in vivo,* longer implantation testing is planned which would allow for that evaluation.

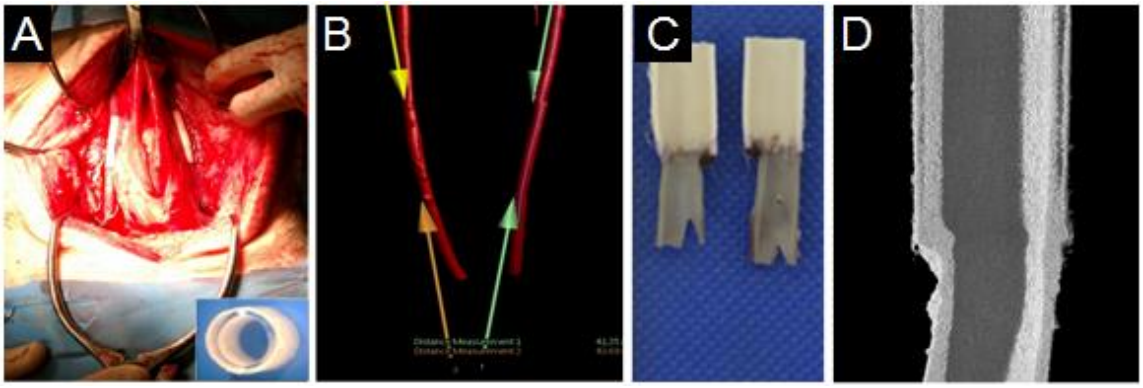

Figure 2.3. Multilayer vascular graft implantation. (A) Implantation into porcine carotid artery. In vivo acute thromboresistance was established via (B) angiography, (C) gross pathology, and (D) micro tomography.

2.4 Conclusions

In this chapter, the feasibility of our multilayered vascular graft design was evaluated for potential use in small-diameter applications. Consistent fibrous morphology of the electrospun graft was demonstrated with minimal fusions. The resultant meshes were then coated with the PEG hydrogel layer and testing for compliance and burst pressure, which revealed a strong correlation between mesh thickness and compliance/burst pressure. Despite achieving favorable compliance levels with the thinnest electrospun grafts, the inverse relationship between burst pressure and compliance brought the grafts burst strength down well below reported autologous vein properties. In addition to promising initial biomechanics data, the multilayer graft's suturability and burst pressure were found to be sufficient *in vivo* along with evidence of acute thromboresistance after 5 hours of implantation. It should be noted, that only the graft design *feasibility* was tested in this chapter. The favorable *in vitro* biomechanical testing and acute *in vivo* implantation results have provided the justification for further optimization of the reinforcing layer's biomechanical properties through more complex approaches presented in the next chapter.

CHAPTER III

SYNTHESIS OF A PCU/PDMS SEMI-INTERPENETRATING NETWORK THAT MATCHES THE MECHANICAL BEHAVIOR OF NATIVE ARTERIES

3.1 Introduction

A compliance mismatch between the graft and artery has been previously reported to cause flow separation and stagnation zones in vasculature downstream from synthetic grafts.[16] This decrease in mean shear stress experienced along the vascular wall induces a physiological response to increase the arterial wall thickness via intimal hyperplasia in an attempt to restore the target wall shear stress.[14] Given the known correlation between graft compliance and patency of autologous and synthetic small diameter vascular grafts,[512] this biomechanical property has become one of the key design requirements in the development of improved arterial prostheses. Along with the initial testing results of our preliminary multilayer graft design, no known homopolymer has been shown to provide the appropriate compliance without sacrificing suture retention strength and/or burst pressure.

We have selected SPUs for our multilayer design due to their high tunability which provides multiple mechanisms to tailor graft mechanical properties to enhance clinical performance. Early polyurethane grafts such as the Corvita, Thoratec, and PulseTec vascular grafts were developed as an alternative to the standard Dacron and GoreTex grafts with modest improvements in compliance. However, compliance values were still well below autologous standards.[84] Newer commercial SPU grafts such as the

UCL-Nano™ and Myolink grafts, now available in Europe, have exhibited improved compliance values well over traditional homopolymer options.[529,530] Unfortunately, no record of the burst pressure of these grafts is available indicating that it meets minimum standards for implantation. SPU materials have been previously explored in our laboratory as an option for an electrospun reinforcing layer of a multilayered vascular graft.[528] Despite outperforming current polyurethane grafts in achieving high compliance values by modulating graft architecture with electrospinning parameters, the graft did not retain burst pressure comparable to current grafts.[529] Furthermore, an inverse correlation between burst pressure and compliance was still observed making it difficult to match the high burst pressure and high compliance of native arteries.

Although polyurethanes are similar to arteries in their high elastic recovery at low strains and high tensile strength, arteries typically display an earlier and more robust strain hardening region.[49] Arterial tissue is composed of alternating layers of elastin and collagen with elastin serving as the key contributor at low strains and collagen becoming more dominant at high strains.[531] The similarity in the SPU stress response may be attributed to the microphase-separated morphology with elastomeric stretching of the soft segment matrix dominant at low strains followed by hard domain rotation/shear and strain-induced crystallization of the soft segment as strain is increased.[532] To reduce modulus in a polyurethane to improve compliance, a lower hard segment content is typically chosen; however, this also results in reduced tensile strength which has been correlated with lower burst pressures.[533] Therefore, a new strategy must be employed beyond typical segmental chemistry modifications to better match arterial properties

without sacrificing the desirable high elastic recovery and tensile strength of the polyurethane.

Interpenetrating polymer networks (IPNs) have been explored in biomedical devices due to their ability to maintain the desirable properties of multiple materials.[534-538] Similarly, semi-interpenetrating polymer networks (semi-IPNs) replace one of the covalently crosslinked networks with a linear component which allows for separation without change in chemical composition and ease of processing. For this work, semi-IPNs based on a linear SPU was selected to allow for full use of their attractive characteristics without sacrificing key mechanical properties. A crosslinked silicone network was selected as the second component of the semi-IPN given the prevalence of the material class in biomedical devices[539-541] and demonstrated biostability.[542] Previous research has explored employing an SPU coupled with a poly(dimethylsiloxane) (PDMS)-based macromer to improve the compliance of a vascular graft.[81] The authors attributed the increase in compliance to the proposed plasticization of the physically crosslinked SPU network by the siloxane molecules.

In the present study, we propose to implement this PDMS-SPU semi-IPN design in an electrospun graft to improve compliance while maintaining burst pressure. The effect of semi-IPN chemistry on compliance and burst pressure of electrospun grafts with similar thickness and fiber morphology was determined. Dynamic mechanical analysis (DMA), differential scanning calorimetry (DSC), and attenuated total reflectance (ATR)-FTIR were used to assess microphase morphology and correlate with observed biomechanical properties to identify key structure-property relationships.

Finally, the biomechanical properties of these electrospun SIPN grafts were then compared to reported values of current autologous grafts to assess their potential as arterial prostheses.

3.2 Materials and Methods

3.2.1 Materials Poly(carbonate urethane) (PCU) Carbothane® PC3575A was purchased from Lubrizol (Boston, MA) and used as received. Methacryloxypropyl terminated PDMS and (3-Acryloxy-2-hydroxypropoxypropyl) terminated PDMS, **Figure 3.1**, were purchased from Gelest, Inc. (Morrisville, PA) and used as received. The PDMS-dimethacrylate (PDMS-DMA) macromer had a reported weight average molecular weight (M_W) range of 380-550 Da and the PDMS-diacrylate (PDMS-DA) macromer had a reported M_W range of 600-900 Da. Poly(ethylene glycol) (PEG) with M_W of 35 kDa, N,N'-dimethylacetamide (DMAC), chloroform, and benzoyl peroxide (BPO) were purchased from Sigma Aldrich (Milwaukee, WI) and used as received.

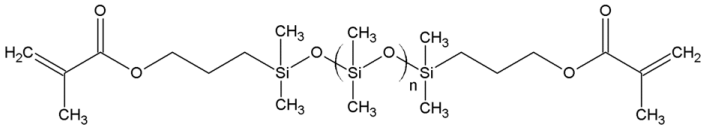

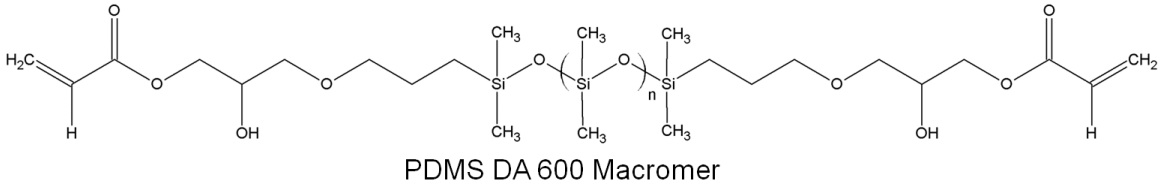

Figure 3.1. Chemical structures of PDMS macromers

3.2.2 Electrospun Graft Fabrication

3.2.2.1 Solution Preparation PCU pellets were subject to a minimum of 24 hours vacuum drying at ambient temperature prior to use. DMAC and chloroform were stored over molecular sieves prior to solution preparation to avoid minimize water content. PCU solutions were prepared by dissolving the SPU pellets at 18 wt% in DMAC and purged with nitrogen. SIPN solutions were made by first mixing DMAC and chloroform at a 3:1 ratio followed by the addition of 1 wt% thermal initiator, BPO. The PDMS-DMA macromer was then added at 5, 10, or 20 wt% concentrations of the original 18 wt% solute and allowed to dissolve before adding the remaining PCU component, **Table 3.1**. Solution viscosities were adjusted as needed to maintain a viscosity of 10 Pa·s to avoid variation in electrospun architecture. [543] A 25 wt% solution of PEG 35 kDa in chloroform was also prepared for use as a sacrificial inner layer to aid in graft harvesting.

Table 3.1. Electrospun semi-IPN compositions

	Percentage Carbothane® 3575A	Percentage PDMS Macromer	Solvent	BPO Initiator Content
Pure PCU	100%	0%	DMAC	0%
5/95 DMA 380	95%	5% DMA 380	3:1 DMAC:$CHCl_3$	1%
10/90 DMA 380	90%	10% DMA 380	3:1 DMAC:$CHCl_3$	1%
20/80 DMA 380	80%	20% DMA 380	3:1 DMAC:$CHCl_3$	1%
10/90 DA 600	90%	10% DA 600	3:1 DMAC:$CHCl_3$	1%

(DMAC = N,N'-dimethylacetamide, $CHCl_3$ = Chloroform, BPO = Benzoyl Peroxide)

3.2.2.2 Electrospinning Process All electrospinning runs were performed inside an enclosed acrylic box to maintain consistent levels of approximately 50% relative humidity and 21°C temperature. Prior to electrospinning PCU or SIPN solutions, a sacrificial layer of PEG was electrospun onto 5 mm mandrels to maintain fibrous morphology on layer while also providing separation between the PCU and mandrel. Briefly, the 25 wt% PEG 35 kDa solution was poured into a 10 mL glass syringe equipped with a blunted 20 gauge needle. The solution was dispensed out of the needle at 0.5 mL/hr using a KDS 100 syringe pump (KD Scientific, Holliston MA) with a distance to collector (DTC) of 52 cm onto the stainless steel mandrel rotating at 500 rpm. A positively charged voltage of 14 kV was applied to the tip of the 20 gauge needle and a negatively charged 2 kV was applied to the mandrel using high voltage sources

purchased and used as received from Gamma High Voltage (Ormond Beach, FL). The PEG 35 kDa solution was allowed to spin for 5 minutes before the syringe was replaced with one loaded with Carbothane® or a semi-IPN solution. The PCU and SIPN solutions were subject to the same parameters except the positive voltage was increased to approximately 20 kV and the negative to 5 kV. All PCU/SIPN solutions were electrospun for 2 hours and 15 minutes to achieve a graft thickness of approximately 0.2 mm. Solutions were electrospun for 4-6 hours for mesh thicknesses of 0.4 mm.

3.2.2.3 Heat Treatment Electrospun meshes were soaked overnight in deionized water to dissolve the inner electrospun PEG layer and facilitate the removal of the electrospun grafts from the mandrel. The grafts were then dried under vacuum overnight to remove excess water. Finally, the electrospun SIPN grafts were subject to a 12 or 24 hour heat treatment on 5 mm diameter PTFE rods to covalently crosslink the siloxane network. A set of Carbothane® electrospun grafts were also heat treated to isolate the effects of the curing conditions on the electrospun PCU material properties.

3.2.3 Graft Characterization Grafts were cut into 4 cm long pieces for all materials testing. Characterization was performed on both as-spun and heat-treated grafts to observed effects of the curing cycle on electrospun fiber architecture and properties. Fiber morphology of electrospun grafts were observed using scanning electron microscopy (SEM). Changes in viscoelastic response were monitored using dynamic mechanical analysis (DMA). Microphase morphology was then further investigated with differential scanning calorimetry (DSC) and ATR-FTIR spectroscopy. Crosslinking of covalent PDMS networks was confirmed with NMR spectroscopy.

3.2.3.1 Scanning Electron Microscopy (SEM) Fiber morphology was examined using SEM with a JEOL NeoScope JCM-5000 (Tokyo, Japan) at a 5 kV acceleration voltage. Specimens were coated with approximately 4 nm of gold using a Cressington Sputter Coater 108 (Watford, England) prior to imaging. Similar fiber diameter and junction quality of as-spun grafts were confirmed prior to heat treatment and microphase morphology/biomechanical analysis.

3.2.3.2 Microphase Morphology Analysis Effects of electrospinning and heat treatment on the material properties of the Carbothane® and semi-IPN grafts were examined using DMA, DSC, and ATR-FTIR analysis. DMA was conducted with a TA RSA3 on grafts cut into strips of approximately 5 cm in width. Specimens were subject to a temperature ramp from -90°C to 100°C at a rate of 5°C/min while under a 0.1% cyclic strain at 1 Hz frequency. DSC thermograms (n=3) were collected on specimens of approximately 10-15 mg which were subjected to a temperature ramp of -90°C to 100°C with the same rate under nitrogen gas using a TA DSC Q100 (Houston, TX). For DSC, all analysis was performed on the first scan to examine processing effects from electrospinning and/or heat treatment. Finally, proposed effects on microphase morphology were corroborated by using ATR-FTIR to examine changes in hydrogen bonding within the hard domains of the electrospun PCU. Briefly, 32 spectral scans of as spun and heat treated electrospun grafts were taken and averaged over the wavenumber range of 4000 to 700 cm^{-1} using a Bruker ALPHA equipped with a Germanium ATR single reflectance module. The carbonyl wavenumber region (1800 to 1600 cm^{-1}) of segmented polyurethanes was monitored to examine changes in the hydrogen bonding of

the urethane carbonyl as an indicator of microphase morphology.[544] Specifically, the free urethane carbonyl absorbance near 1730 cm^{-1} was expected to be reduced while the hydrogen bound carbonyl absorbance at 1700 cm^{-1} would increase with evidence of microphase separation.

3.2.3.3 Biomechanical Testing Static compliance of each graft was measured using a method described previously.[526] Briefly, a nonporous latex tube was inserted inside each graft prior to testing. The grafts were subject to a pressure ramp from 0 to 150 mmHg using deionized water dispensed via a syringe pump connected to the latex tube. A standard in line strain gauge pressure transducer from Merit Medical (South Jordan, UT) was used to measure intraluminal pressure while the outer diameter of the graft was measured with a Lasermike He-Ne laser micrometer. Compliance (C) was calculated using the following equation:

$$C = \frac{\Delta D}{D_0 \cdot \Delta P} = \frac{D_{120} - D_{80}}{D_{80} \cdot 40}, \qquad (1)$$

where ΔP is change in pressure and D_{120} and D_{80} are the graft outer diameters at 120 and 80 mmHg intraluminal pressure, respectively. Compliance values were recorded 5 times on each graft and values from each graft were averaged to obtain the reported value (n=15 total). Burst pressure testing was then performed on the same graft by pumping deionized water into the graft at 100 mL/min until the electrospun mesh failed (n=3).[525] The maximum pressure upon failure was measured and recorded using a NoShok high pressure gauge ranging from 0 to 60 psi (Berea, OH), which was then converted to mmHg. Both burst pressure and compliance were performed under standard laboratory conditions (25°C) and simulated physiological conditions (37°C, high relative humidity).

Prior to testing at simulated physiological conditions, grafts were equilibrated in water at 37ºC overnight.

3.2.3.4 Confirmation of Silicon Network Formation Nuclear magnetic resonance (NMR) spectroscopy was utilized to determine the extent of silicone network formation in the semi-IPNs after heat treatment. Briefly, as-spun and heat-treated grafts were dissolved in deuterated chloroform ($CdCl_3$) at a concentration of 10 mg/mL. Solutions were allowed to settle in order to identify gel fractions, if any, formed by the crosslinked network. Small 1 mL samples were then extracted from the solute fraction and analyzed with H NMR (300 MHz, $CDCl_3$): PDMS DMA 380 δ 0.08 (s, 3H, -CH3), 0.52-0.57 (m, 2H, -CH2-), 1.62-1.73 (m, 2H, -CH2-), 1.95 (s, 3H, -CH3), 4.07-4.12 (m, 2H, -CH2-), 5.54 (s, 1H, =CH2), 6.10 (s, 1H, =CH2), PDMS DA 600 δ 0.03-0.12 (m, 3H, -CH3), 0.47-0.58 (m, 2H, -CH2-), 1.52-1.68 (m, 2H, -CH2-), 3.39-3.55 (m, 2H, -CH2-), 3.85-3.90 (m, 1H, -CH-), 4.18-4.29 (m, 2H, -CH2-), 5.80-5.97 (m, 1H, =CH2), 6.07-6.22 (m, 1H, -CH), 6.38-6.53 (m, 1H, =CH2). Following initial characterization, changes in spectral peaks of the semi-IPNs characteristic only of the silicone component were monitored for potential crosslinking of the PDMS macromer.

3.2.4 Statistical Analysis A student's T-test was performed to determine statistical significance between groups of data. All comparisons were made with a 95% confidence interval. (α=0.05)

3.3 Results and Discussion

3.3.1 Initial Graft Characterization Synthetic vascular grafts were fabricated by electrospinning 18 wt% solutions of Carbothane® dissolved in DMAc or varied blends of Carbothane® and up to 20% silicone macromer DMA 380 or DA 600 dissolved in 3:1 DMAc:$CHCl_3$. All solutions were electrospun for approximately 2-3 hours to produce grafts of approximately 0.2 mm thickness. Similar fiber morphologies of each electrospun fiber mesh were then confirmed with SEM to isolate material composition changes from architectural effects. Following morphology comparison, all 0.2 mm thick electrospun PCU/PDMS blends were subjected to a 12 hour 50°C heat treatment to facilitate silicone network formation for the overall semi-IPN. Electrospun PCU grafts were also subject to the same heating cycle to observe the effects of heat treatment on PCU grafts.

All as-spun fiber meshes had similar fiber morphologies in both PCU and all PCU/PDMS compositions, **Figure 3.2** which indicates the morphology was unaffected by PDMS macromer content. Heat treatment of all grafts produced fiber junctions with higher percent fusion within the mesh than their as-spun counterparts. The increase in fusion at fiber junctions was attributed to the softening of the fibers during the 12 hours at 50°C. These decreases in fiber interbond arc length[545] has been cited as a direct source of increases in modulus and ultimate elongation in the circumferential direction of a tubular graft.[545-547] Furthermore, this softening was enhanced with higher concentrations of the PDMS DMA 380 macromer and to a greater extent in the 10/90 DA 600 system. Given our recent report on the effect of increased fusion on graft biomechanical

properties, compliance was expected to decrease and burst pressure was expected to increase with this change in fiber architecture.[533]

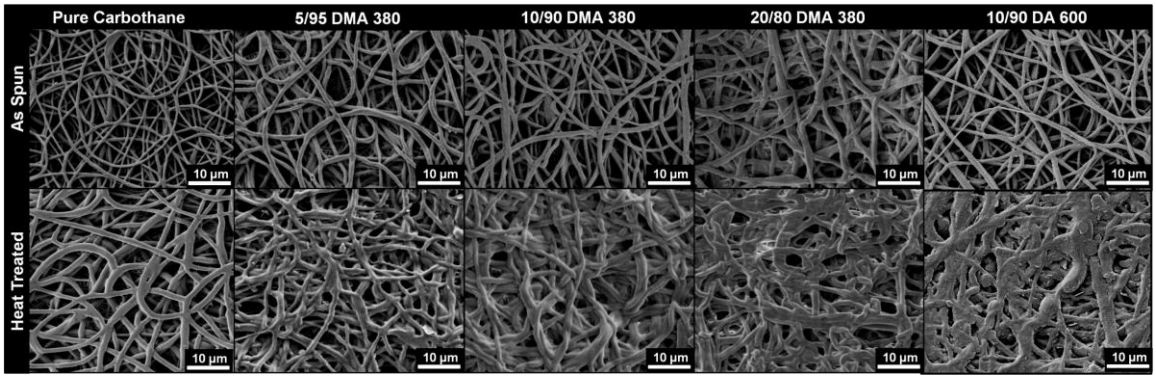

Figure 3.2. Scanning electron micrographs of 0.2 mm thick electrospun grafts comparing fiber morphology before and after heat treatment (50°C, 12 hours)

3.3.2 Graft Biomechanical Properties Compliance and burst pressure measurements were conducted on 0.2 mm thick electrospun Carbothane® grafts and semi-IPN grafts with varied levels of PDMS DMA 380 or PDMS DA 600 macromer. Prior to heat treatment to crosslink the silicone macromers, compliance of as-spun grafts increased and burst pressure decreased with the presence of the silicone macromer, **Table 3.2**. This was attributed to the low glass transition temperature (T_g) of the silicone macromer[548] and the disruption of soft segment crystallinity and hydrogen bonding in the polyurethane.[81] An exception to this trend was observed in the 10/90 PDMS DA 600 grafts which exhibited an increase in compliance and an increase in burst pressure over as-spun Carbothane® grafts. This unexpected phenomenon was attributed to premature initiation of PDMS DA 600 crosslinking during the electrospinning process. A low level of crosslinking prior to heat treatment was confirmed by the loss of the acrylate peaks in

the NMR spectra of the as-spun graft as compared to the polymer solution. This effect was likely not observed by the methacrylate components due to the lower reactivity of methacrylate groups compared to acrylates,[549,550] which limited the possibility of radical initiation in the PDMS DMA grafts. A 12 hour heating cycle at 50°C was then applied to grafts to covalently crosslink the unreacted silicone macromers. Carbothane® grafts were subjected to the same treatment to monitor changes to the polyurethane component of the semi-IPN meshes.

Table 3.2. Initial biomechanical properties of as spun and heat treated electrospun grafts

		Carbothane	5/95 DMA 380	10/90 DMA 380	20/80 DMA 380	10/90 DA 600
As Spun	Compliance	3.8 ± 1.0	6.7 ± 1.2	4.2 ± 0.5	5.0 ± 1.2	4.7 ± 0.4
	Burst Pressure	1188 ± 101	1103 ± 39	991 ± 220	901 ± 130	2069 ± 22
Heat Treated	Compliance	4.7 ± 0.8	5.9 ± 0.7	7.4 ± 0.8	3.7 ± 0.5	6.5 ± 1.9
	Burst Pressure	1470 ± 73	1246 ± 151	905 ± 101	1036 ± 136	2322 ± 150

(average ± standard deviation; n=15 for compliance, n=3 for burst pressure; graft thickness = 0.2 mm, 50°C, 12 hours)

3.3.2.1 Effect of Heat Treatment on Carbothane® Grafts Interestingly, both compliance and burst pressure of Carbothane® grafts increased following heat treatment. Compliance increased from 3.8 ± 1.0 to 4.7 ± 0.8 %/mmHg x 10^{-4} and

burst pressure increased from 1190 ± 100 to 1470 ± 70 mm Hg. Changes in chemical structure, fiber architecture, and polyurethane microphase morphology after heat treatment of the Carbothane® grafts were investigated to determine the cause of the observed improvements in biomechanical properties. No changes in structure were observed in proton NMR spectra and SEM analysis of the fiber morphology displayed minimal effects of heat treatment, **Figure 3.2**. Microphase morphology before and after heat treatment was then examined using DMA. The storage modulus plot of the as-spun Carbothane® exhibited a broad T_g of the polycarbonate soft segment at approximately -9°C and an additional melting transition temperature (T_m) at 39°C, **Figure 3.3a**. In comparison to the storage modulus plot of a cast Carbothane® film, the electrospun graft displayed a much broader Tg with a strong melting peak at a lower melting temperature (39ºC vs 63ºC). Eceiza et al. reported a similar transition at 45ºC in the storage modulus plot of a poly(carbonate urethane) and assigned it to melting of crystalline soft domains.[551] Therefore, it was hypothesized that alignment of soft segment chains during electrospinning enhanced crystallization and limited phase separation, as evidenced by the increased breadth of the Tg. Similar behavior was observed in electrospun polycaprolactone-based polyurethanes as compared to the cast film.[552]

3.3.2.1 Effect of Heat Treatment on Carbothane® Grafts Interestingly, both compliance and burst pressure of Carbothane® grafts increased following heat treatment. Compliance increased from 3.8 ± 1.0 to 4.7 ± 0.8 %/mmHg x 10^{-4} and burst pressure increased from 1190 ± 100 to 1470 ± 70 mm Hg. Changes in chemical structure, fiber architecture, and polyurethane microphase morphology after heat treatment of the Carbothane® grafts were investigated to determine the cause of the observed improvements in biomechanical properties. No changes in structure were observed in proton NMR spectra and SEM analysis of the fiber morphology displayed minimal effects of heat treatment, **Figure 3.2**. Microphase morphology before and after heat treatment was then examined using DMA. The storage modulus plot of the as-spun Carbothane® exhibited a broad T_g of the polycarbonate soft segment at approximately -9°C and an additional melting transition temperature (T_m) at 39°C, **Figure 3.3a**. In comparison to the storage modulus plot of a cast Carbothane® film, the electrospun graft displayed a much broader Tg with a strong melting peak at a lower melting temperature (39ºC vs 63ºC). Eceiza et al. reported a similar transition at 45ºC in the storage modulus plot of a poly(carbonate urethane) and assigned it to melting of crystalline soft domains.[551] Therefore, it was hypothesized that alignment of soft segment chains during electrospinning enhanced crystallization and limited phase separation, as evidenced by the increased breadth of the Tg. Similar behavior was observed in electrospun polycaprolactone-based polyurethanes as compared to the cast film.[552]

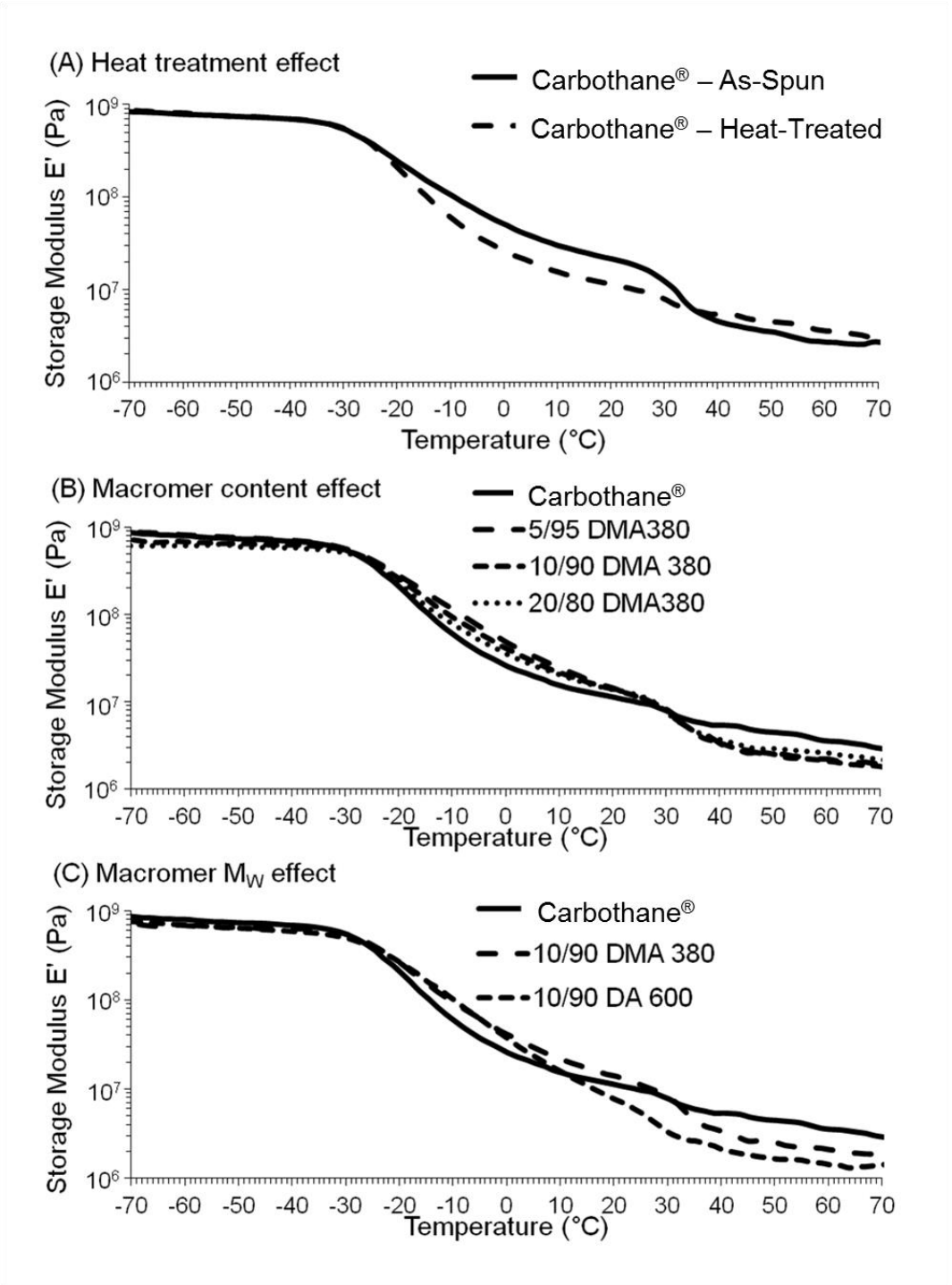

Figure 3.3. DMA storage modulus plots of 0.2 mm thick electrospun grafts comparing effects of (A) heat treatment (12 hours at 50°C) on Carbothane®, (B) PDMS macromer content on heat treated specimens, and (C) PDMS macromer M_w on heat treated specimens

Following heat treatment, a reduction in soft segment crystallization ($\Delta H = 18 \pm 2$ vs $\Delta H = 12 \pm 3$) in the Carbothane® DSC thermogram **Figure 3.4** was accompanied by reduced breadth of the soft segment T_g in the storage modulus plot indicative of improved phase separation, **Figure 3.3a**.[553,554] Infrared spectroscopy has previously been used to assess phase separation from an analysis of the extent of hard segment hydrogen bonding.[555] However, this assessment was inconclusive in the PCU given the convolution of the urethane carbonyl region with the carbonyls of the polycarbonate-based soft segment. Nevertheless, the DSC and DMA analyses provides strong evidence that the improvement in biomechanical properties of the Carbothane® grafts was due to reduced soft segment crystallinity and enhanced microphase separation after heat treatment. Specifically, reduced crystallinity was expected to enhance the flexibility of the soft segment matrix and reduce modulus which has been linked to compliance.[533] The enhanced burst pressure was attributed to the increase in phase separation and order of the hard domains. Similar annealing effects have resulted in increased polyurethane tensile strength[556] which has been correlated with increased burst pressure.[533]

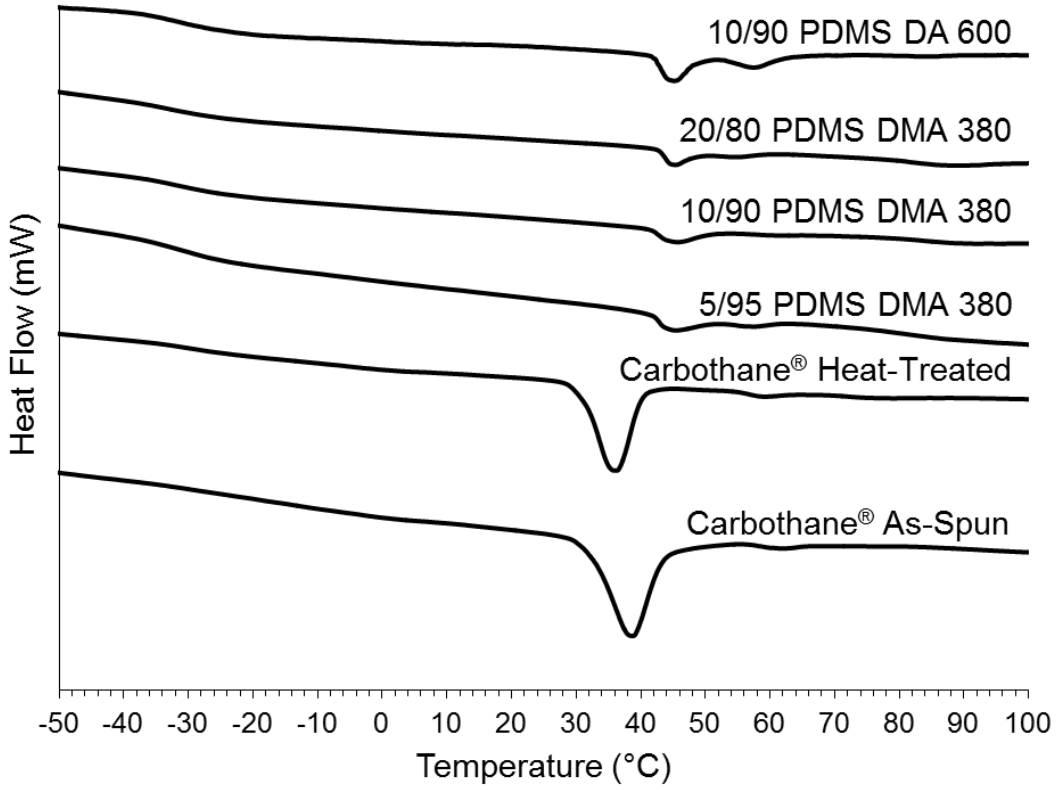

Figure 3.4. DSC thermograms of 0.2 mm thick electrospun Carbothane® and heat treated PCU/PDMS macromer blends (12 hours, 50°C)

3.3.2.2 Effect of Heat Treatment on Semi-IPN Grafts The effect of heat treatment on the compliance and burst pressure of semi-IPN grafts varied based on the macromer chemistry and macromer concentration. Biomechanical properties of 5/95 PDMS DMA 380 grafts were unchanged after heat treatment. The enhanced phase separation observed in the Carbothane® control grafts upon heat treatment was not observed, **Figure 3.3b**. In contrast, heat treatment of the 10/90 PDMS DMA 380 graft

resulted in a substantial increase in compliance beyond previously reported saphenous vein values[512] but no effect on burst pressure. Finally, the 20/80 PDMS DMA 380 graft exhibited a small increase in burst pressure and a substantial decrease in compliance. The observed differences in biomechanical properties as a function of macromer content and chemistry were hypothesized to be a result of differences in fiber architecture, silicone network formation and polyurethane phase morphology. Fiber architecture changes were assessed with SEM, as described above, with particular attention given to the extent of fiber fusion. Silicone network formation was assessed using proton NMR of the silicone sol fraction present in semi-IPNs after heat treatment. Finally, the effect of silicone macromer on phase morphology and soft segment crystallinity was assessed using DMA and DSC, respectively.

An increase in fiber fusion was observed with increasing DMA 380 concentration, **Figure 3.2**. We have previously demonstrated that increasing fusion can result in enhanced burst pressure and decreased compliance. Although not statistically significant, there is an overall trend of increasing burst pressure with increasing concentration of the DMA 380, **Table 3.2**. There was little improvement observed in burst pressure with heat treatment for any of the DMA 380 semi-IPN grafts. The degree of crosslinking assessed by the silicone present in the NMR spectra of the sol fraction was low for both the 5/95 and 10/90 semi-IPNs. It was hypothesized that this low level of crosslinking was insufficient for mechanical reinforcement. The 20/80 PDMS DMA 380 graft did exhibit more crosslinking; however, the network formation remained insufficient to cause a significant increase in burst pressure. In contrast, minimal silicone

in the sol fraction of the heat treated 10/90 600 DA semi-iPN graft indicated excellent crosslinking and a corollary increase in burst pressure. The improved network formation and burst pressure of the DA 600 semi-IPN graft is likely due to the increased reactivity of the acrylate and higher molecular weight of the silicone macromer. Following heat treatment, the 10/90 DA 600 semi-IPN graft also exhibited the lowest storage modulus drop of all the thin grafts, **Figure 3.3c,** as well as most significant microphase separation and highest ordered soft segment crystallinity in its DSC thermogram, **Figure 3.4**. Finally, the degree of fiber fusion of the 10/90 PDMS DA 600 grafts following heat treatment appeared to be more similar to Carbothane® which had minimal effects on biomechanical properties, **Figure 3.2**. As a result, the graft exhibited improved biomechanical properties as compared to its as-spun counterpart and the Carbothane® control. Overall, the increased compliance of the semi-IPN grafts was attributed to the silicone macromer disrupting soft segment crystallinity of the polyurethane, as described above. Indeed, a substantial decrease in soft segment crystallinity was observed for all semi-IPN grafts, **Figure 3.4**.

3.3.2.3 Effect of Thickness on Carbothane® Grafts In order to increase the burst pressure of the Carbothane® grafts to match saphenous vein values, the graft thickness was increased from 0.2 to 0.4 mm. Our laboratory has previously demonstrated that increasing graft thickness via longer electrospinning times can be effectively used to enhance burst pressure.[528] Increased thickness of the Carbothane® grafts resulted in a modest increase in burst pressure from 1190 ± 100 to 1330 ± 70 mm Hg and decrease in compliance from 3.8 ± 1.0 to 3.2 ± 0.1 %/mmHg x 10^{-4}. Initial 12 hour heat treatment of

0.4 mm thick Carbothane® specimens produced no changes in graft properties or DMA plots (results not shown) indicating longer heat treatment times were needed. Increasing the duration of heat treatment to 24 hours increased the compliance (5.1 ± 0.5 %/mmHg x 10^{-4}) and burst pressure (2260 ± 160 mm Hg) of Carbothane® grafts to values that exceeded reported autologous vein properties (saphenous vein compliance: 4.4 ± 0.8 %/mmHg x 10^{-4} [557] and burst pressure: 1680 ± 307 mmHg [558]). Additional heat treatment times (48 and 72 hours) did not result in additional improvements in graft biomechanical properties (data not shown).

3.3.2.4 Graft Performance under Physiological Conditions The DMA storage modulus plots of the grafts displayed thermal transitions between 30ºC and 40ºC. Therefore, it is reasonable to assume that the performance of the grafts under standard testing temperature of 25ºC would differ from physiological conditions (37ºC). To address this issue, the biomechanical properties of the most promising grafts, Carbothane® (0.4 mm thickness) and 10/90 PDMS DA 600 (0.2 mm thickness), were equilibrated in water at 37ºC overnight and then tested in a warm room that was held at a constant 37°C and 100% relative humidity. The results were then compared with previous results obtained under standard laboratory conditions (20°C, ~50% humidity).

As-spun grafts of both materials were found to exhibit substantial increases in compliance, **Figure 3.5**, after equilibration in water and testing at 37ºC. The increase in compliance was attributed to partial melting of the crystalline soft segment, as described above with heat treatment. Interestingly, this almost doubling of compliance at 37ºC was not accompanied by a significant change in burst pressure as observed with grafts after

heat treatment. Both sets of heat-treated grafts displayed large decreases in burst pressure at physiological conditions with more modest increases in compliance. The large increase in burst pressure of heat-treated grafts observed at 20ºC (Carbothane®: 2260 vs 1330 mm Hg; semi-IPN: 2360 vs 2070 mm Hg) is likely due to a combination of polymer morphology and increased fusions. Given that testing under physiological conditions did not significantly alter fiber architecture, the decrease in heat-treated graft burst pressures at 37°C was attributed to changes in polymer morphology. Specifically, we hypothesized that a further reduction of the soft segment crystallinity (T_m = 36 ± 1°C) occurred during incubation at 37º which caused the observed decrease in graft burst pressures. The less substantial decrease in the semi-IPN could then be attributed to the added reinforcement of the silicone network and the increased melting temperature of the soft segment in the semi-IPN (45 ± 1, 56 ± 2°C). Overall, the improved compliance of both grafts under the more physiological conditions while maintaining acceptable bust pressures suggests favorable performance during implantation may be expected. Based on the established correlation with compliance and 5 year patency rates from previous in vivo studies, these Carbothane® and 10/90 PDMS DMA 380 grafts are expected to exceed previous graft options, **Figure 3.6**.[512]

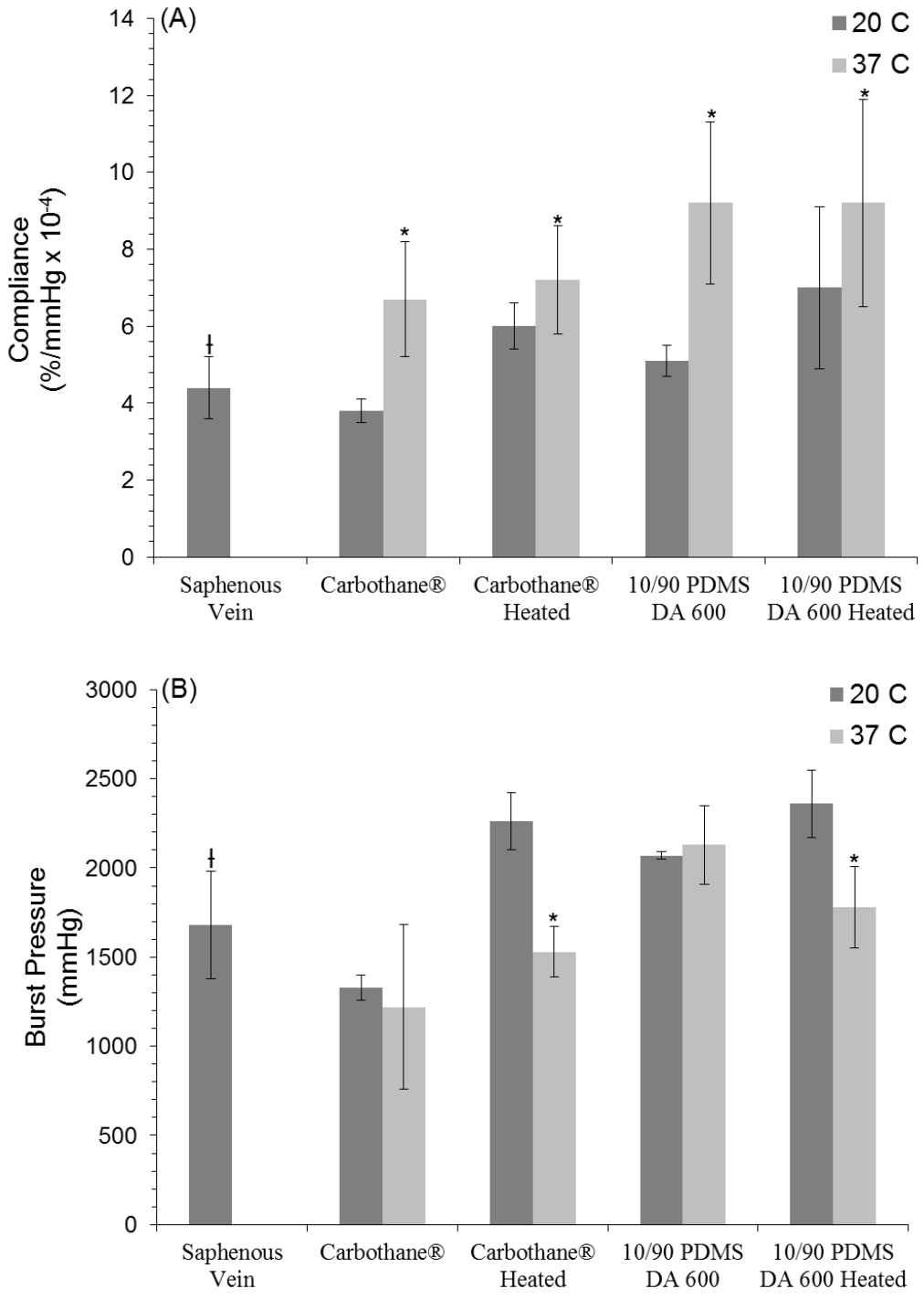

Figure 3.5. (A) Compliance and (B) burst pressures of 0.4 mm Carbothane® and 0.2 mm 10/90 PDMS DA 600 grafts testing at 20°C (room temperature) and 37°C (body temperature); [I]data taken from previous *in vivo* saphenous vein data from literature; *p<0.05 from 20°C.

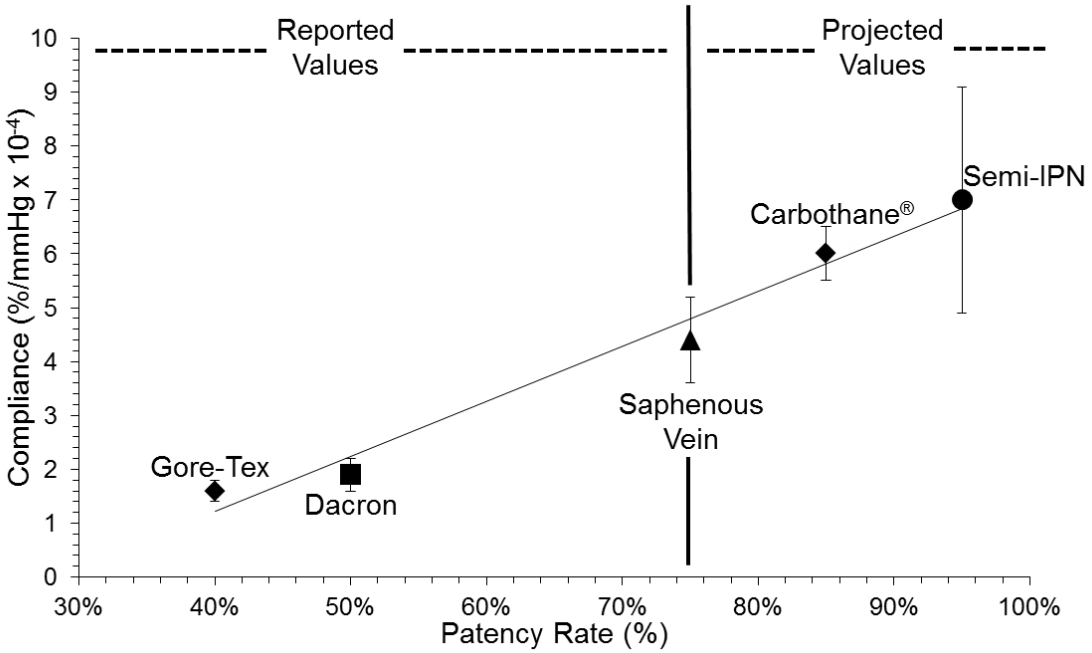

Figure 3.6. Projected patency rates of heat treated 0.4 mm thick Carbothane® and 0.2 mm 10/90 PDMS DA600 semi-IPN grafts based on past linear relationship observed in previous *in vivo* data.[512] The patency data for the different grafting materials used in the femoro-popliteal position used in this study were obtained from several recent large studies.

3.3.4 Confirmation of Crosslinking in Semi-IPN Grafts It can be expected that the presence of the silicone macromers in the as-spun grafts could potentially increase graft compliance but never improve burst pressure over pure Carbothane grafts due to hydrogen bond disruption. Initial testing had demonstrated this effect to be true with all grafts containing the PDMS DMA 380 macromer but the DA 600 macromer showed only improvements. Further investigation into the effects on the microphase morphology within the as-spun graft indicated higher order crystalline domains existed in the as-spun PDMS DA 600 system than Carbothane® despite the lack of heat

treatment to crosslink the macromers, **Figure 3.7**. It is expected that the additional energy provided by the fiber jet stretching during the electrospinning process allows for premature radical initiation of the acrylate group. As a result, the PDMS DA macromer crosslinks while still in solution and in transit to collection on the rotating mandrel. This allows for formation of crystalline domains of sizes similar to the methacrylate based semi-IPNs but on a higher order. Results correlate with the improved biomechanical properties of PDMS DA 600 reported earlier. Heat treatment of the PDMS DA 600 then shows a sharper T_g around -30°C than the as spun graft as well as an additional endotherm at close to 60°C which suggests further crystallization of the soft segment is permitted. The effect on microphase morphology of the heat treated semi-IPN graft was then translated again to even better biomechanical properties.

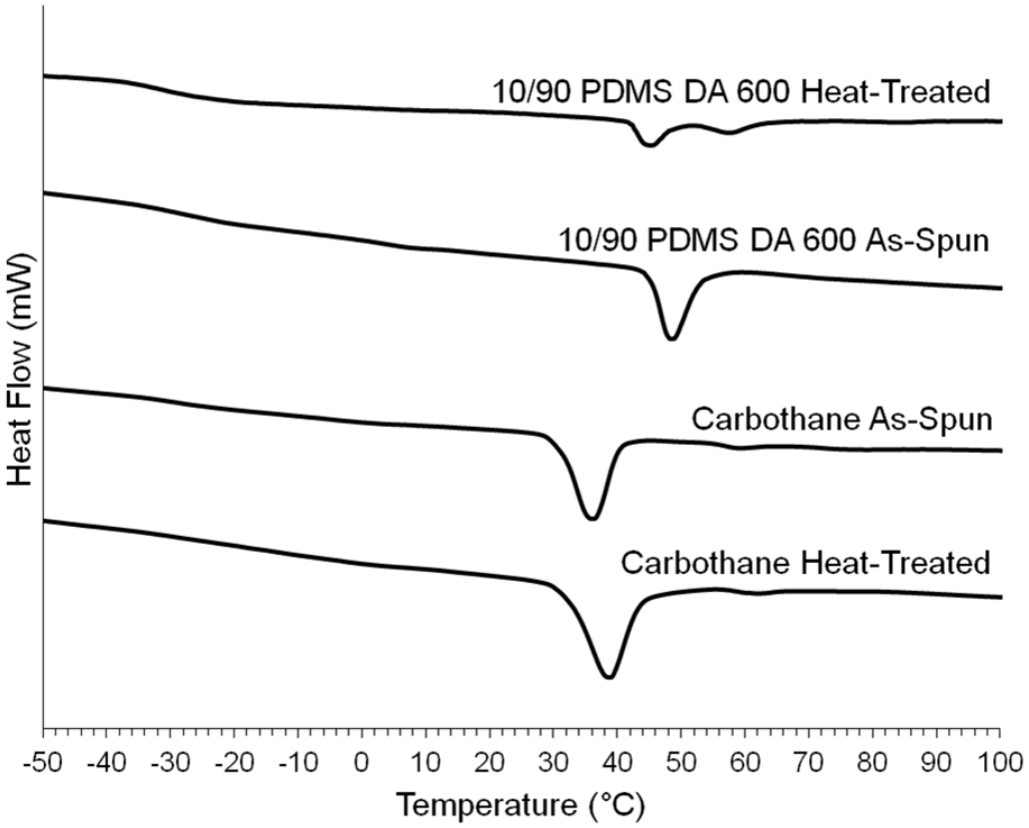

Figure 3.7. DSC thermograms (first scan) of 0.2 mm thick electrospun Carbothane® and 10/90 PDMS DA 600 grafts before and after heat treatment (12 hours, 50°C)

NMR spectroscopy was then utilized to confirm crosslinking of the PDMS macromers. Peaks characteristic of the silicone groups within both macromers were identified in their respective spectra as well as peaks specifically assigned to methacrylate and acrylate end groups for the PDMS DMA and DA macromers respectively, **Figure 3.8**. Spectra from Carbothane® grafts identified peaks characteristic of the poly(carbonate urethane) (PCU) that go unchanged following heat treatment, **Figure 3.9.**

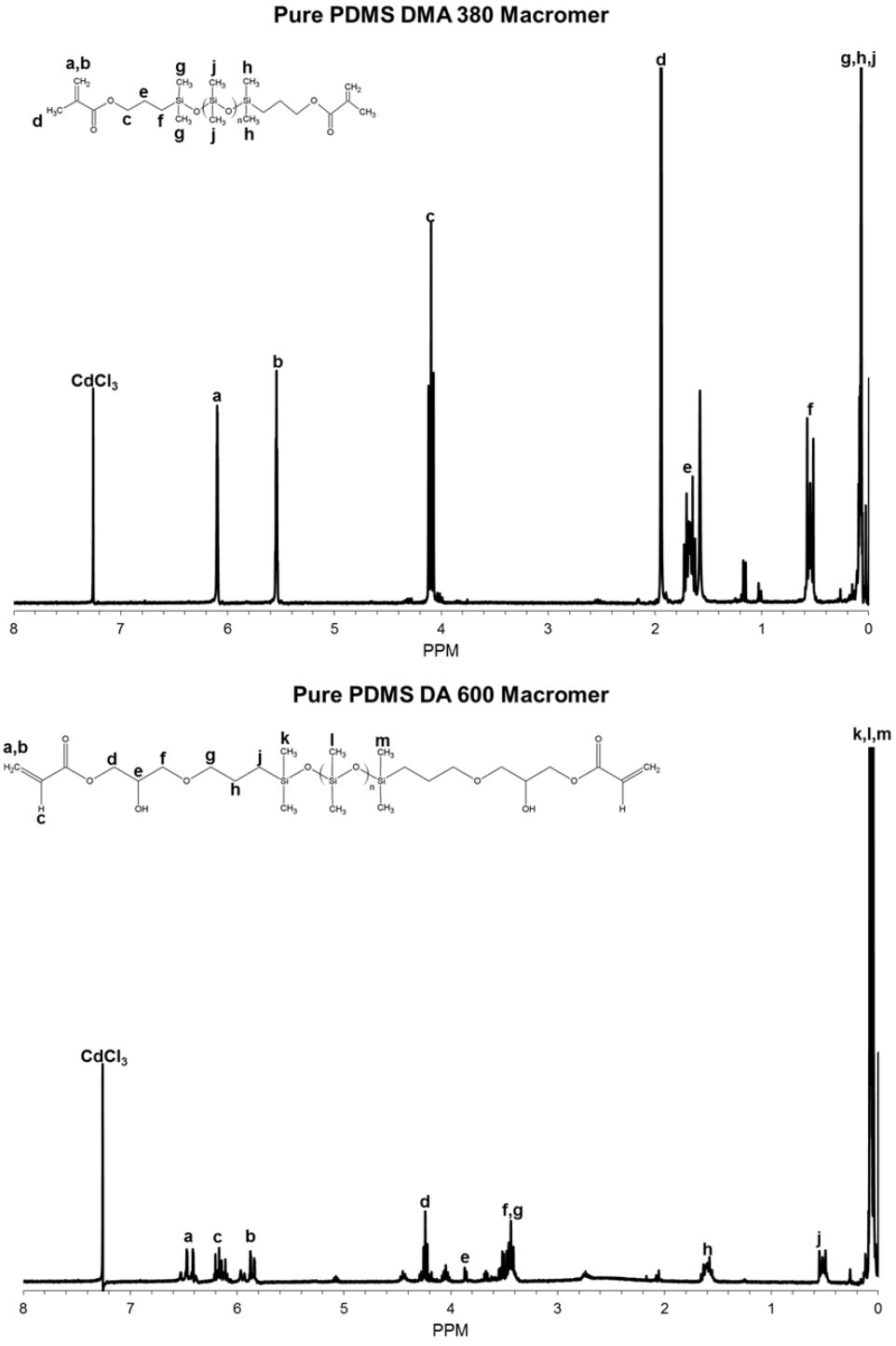

Figure 3.8. ^{H}NMR spectra of PDMS DMA 380 and PDMS DA 600 macromers

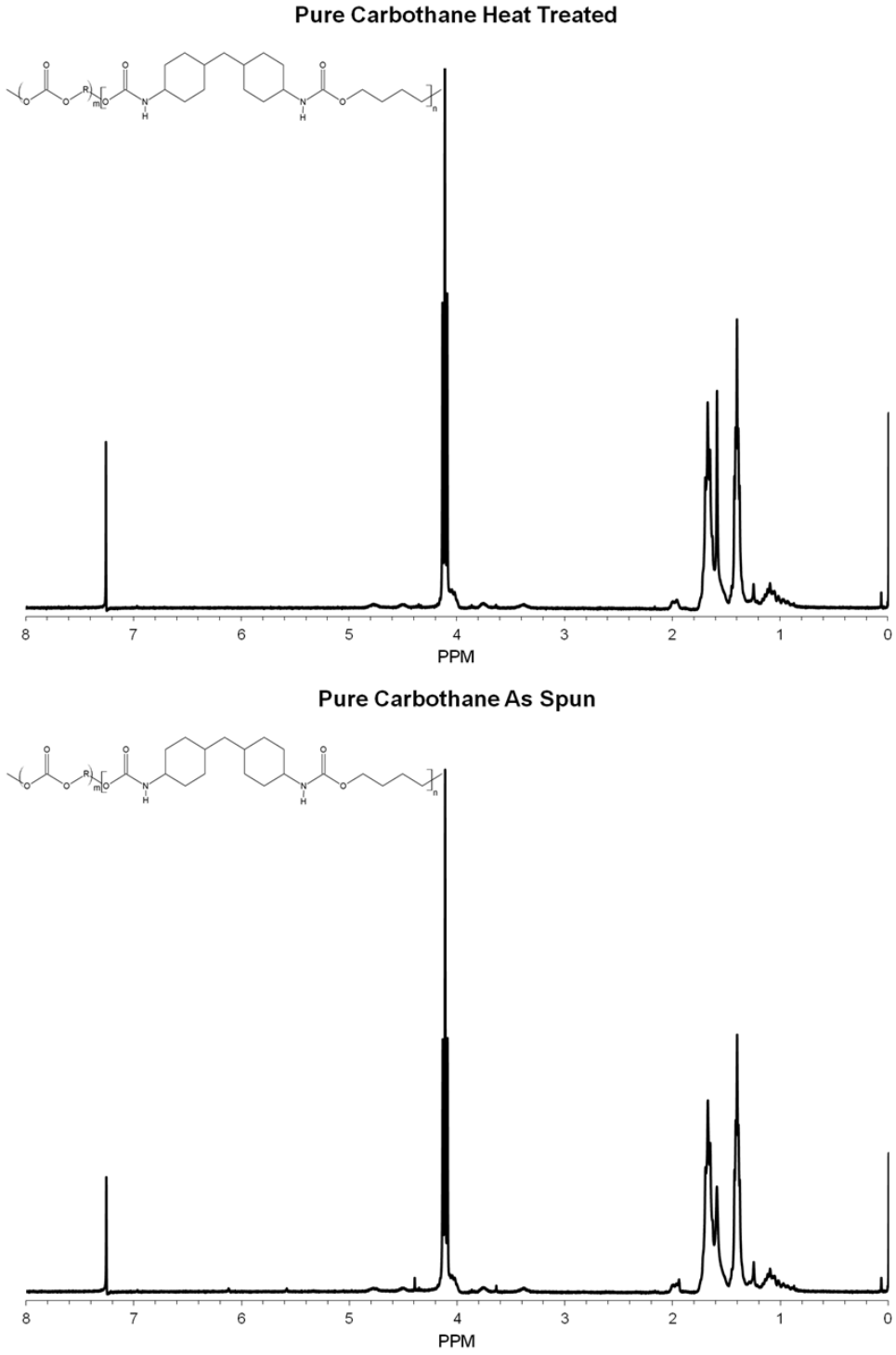

Figure 3.9 ^{H}NMR spectra of Carbothane® grafts before and after heat treatment

The 10/90 PDMS DMA 380 grafts compared to 20/80 grafts show a clear distinction in their NMR spectra following heat treatment due to differences in degree of crosslinking of the macromers with increases in concentration, **Figure 3.10-3.11.** While the 20/80 grafts exhibit full crosslinking with losses of the silicone and end group peaks, the 10/90 spectra still contained soluble unreacted macromers which are present after heat treatment.

Despite lack of heat treatment on the 10/90 PDMS DA 600 grafts, their biomechanical properties still exhibited enhanced biomechanical properties over Carbothane® grafts suggesting the macromer is behaving differently during the electrospinning process. The NMR spectra of the as spun grafts, in addition to the expected effect on the heat treated samples, shows no evidence of the acrylate end groups but still a minor presence of the silicone groups from the macromer, **Figure 3.12**. The results suggest that the PDMS DA 600 macromer could potentially be forming a crosslinked network prior to electrospun fiber collection which affects biomechanical properties. The silicone peak could potentially be attributed to remaining unreacted macromer and/or silicone impurities which remains soluble for NMR spectroscopic analysis.

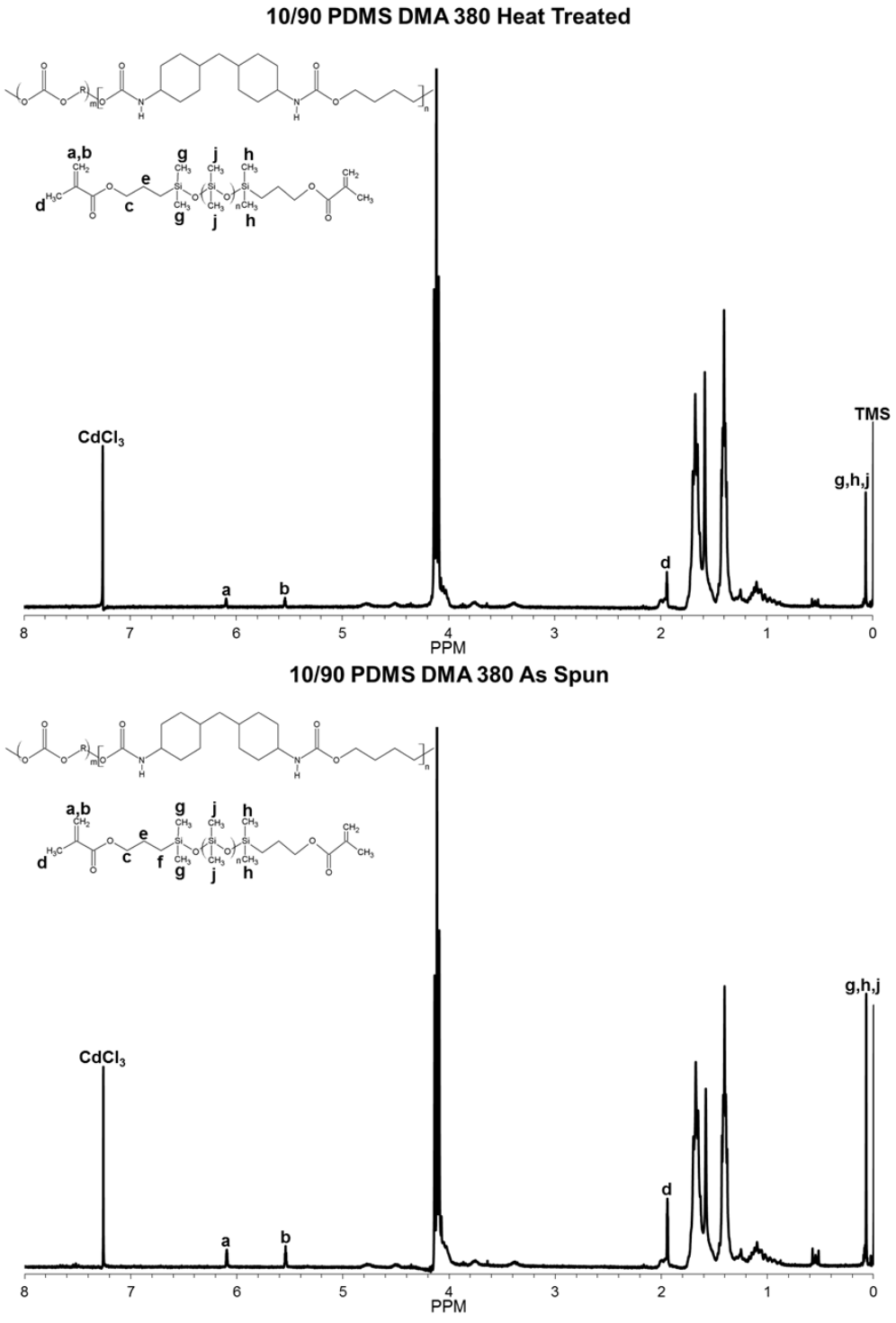

Figure 3.10. ^{H}NMR spectra of electrospun 10/90 PDMS DMA 380 grafts before and after heat treatment (12 hours, 50°C)

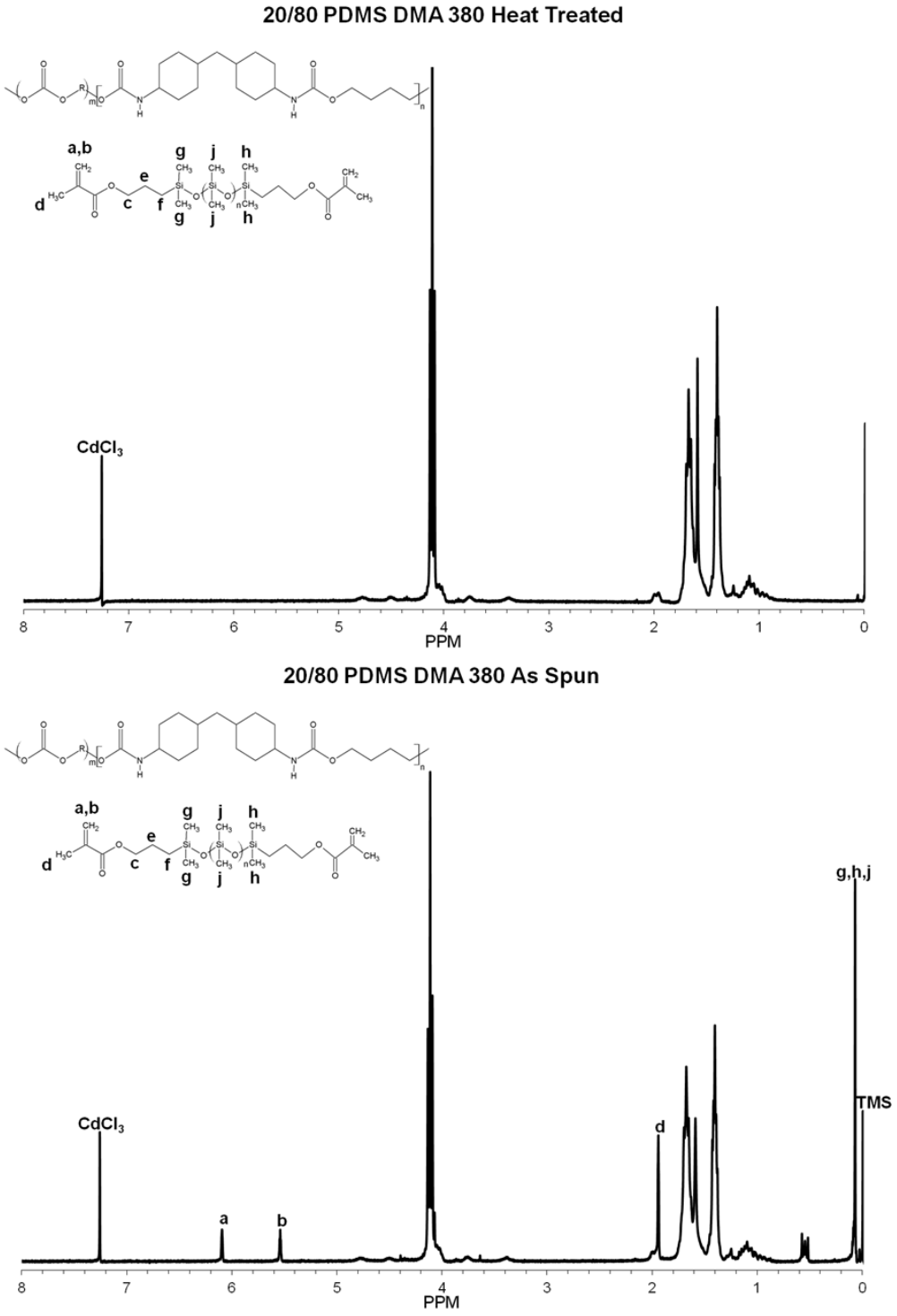

Figure 3.11. ^{H}NMR spectra of electrospun 20/80 PDMS DMA 380 grafts before and after heat treatment (12 hours, 50°C)

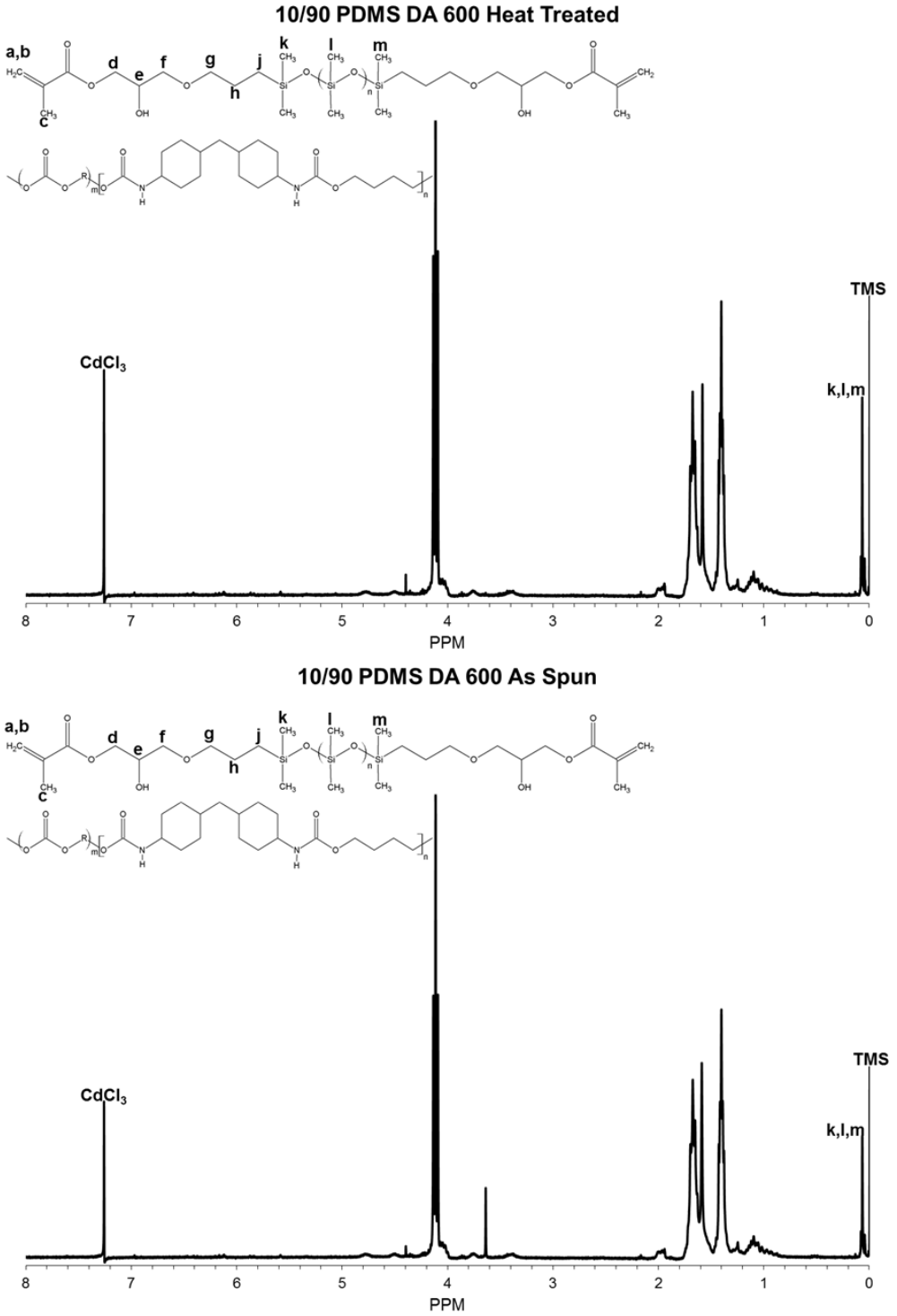

Figure 3.12. ^{H}NMR spectra of electrospun 10/90 PDMS DA 600 grafts before and after heat treatment (12 hours, 50°C)

3.4 Conclusions

Carbothane® electrospun grafts displayed morphological changes after heat treatment that improved graft compliance and burst pressure values beyond previously reported autologous vein properties. The range of biomechanical properties of the PCU grafts was then expanded with the incorporation of a silicone network. Biomechanical properties of the most promising grafts were then assessed under physiological conditions. Although the graft burst pressure dropped significantly due to disruption of soft segment crystallization, the values remained comparable to autologous veins. Compliance values for both grafts showed additional improvements at 37ºC. Given the known correlation of graft compliance and patency, the improved compliance of both the heat-treated Carbothane® and the 10/90 PDMS semi-IPN grafts provide promising alternatives to current synthetic grafts and autologous veins as arterial replacements.

CHAPTER IV

INVESTIGATION OF EFFECT OF POLYURETHANE CHEMISTRY ON BIOSTABILITY OF COMPOSITE VASCULAR GRAFTS

4.1 Introduction

When considering the need for long term implantation success, graft biomechanical properties make up only half of the functional requirements in a vascular graft design. The other is the ability to maintain the graft's performance over time, specifically in regard to predicting and optimizing the biostability of the SPU(s) selected. SPUs have been modified over time to meet design requirements including the need for more biostable formulations. The first generation of polyurethanes incorporated a polyester based soft segment which was later found to be susceptible to rapid hydrolysis.[42,559] PEUs, expected to be more resistant to hydrolytic degradation,[194] were then developed to provide superior biostability; however these materials showed substantial surface and full thickness cracking as a result of soft segment chain scission and crosslinking.[258] The failure mechanism of these devices was attributed to metal ion-induced accelerated oxidative (MIO) degradation,[560] which makes them more likely to fail via environmental stress cracking (ESC).[261,561]

In addition to MIO degradation, the immunological response to foreign body materials has been cited as a pathway for polyurethane degradation,[562] where polyurethane materials are still shown to degrade *in vivo* without the presence of metals.[563] A rigorous investigation by Henson suggests macrophages and foreign body

giant cells release a multitude of enzymes, acids, and reactive oxygen intermediates (ROIs) during phagocytosis.[564,565] Previous *in vivo* and *in vitro* work has demonstrated oxidative attack to be the more dominant mechanism[261,273] over enzymatic degradation.[566] PCUs based on polycarbonate diols were synthesized as a new option for biostable SPUs that still result in favorable microphase separation and mechanical properties.[567,568] These PCUs have been evaluated as an alternative to PEUs with increased biostability and supported by initial *in vitro* and *in vivo* studies demonstrating improved resistance to oxidative attack.[2,9,27,36-38] In addition, this new line of SPUs are less susceptible to ESC given an observed reduction in the depth of degradation[16,30,39] that was attributed to the lower permeability of polycarbonate to oxygen, water, and hydrogen peroxide.[569] Despite initial successes indicating enhanced biostability of PCUs, the materials are still susceptible to oxidative degradation. Thus additional attempts have been made to further improve PCU's resistance to oxidation.

New PCU formulations were created to further enhance oxidative stability, specifically by reducing the probability of chain scission via two methods, silicone modification and/or reduction of soft segment. Both of these strategies are well supported by similar attempts to improve PEU biostability. Previous studies have shown that covalently bonding silicone to polyurethanes has improved the resistance of SPUs to both in vitro and in vivo biodegradation as well as reducing the effect of MIO and ESC.[25,42,43] Reduction of soft segment ether content in the harder Pellethane® and Elasthane™ grades also resulted in improved oxidative resistance.[570] The increase in

oxidative resistance is attributed to the decrease in available α-methylene carbons adjacent to the ether linkage.[568]

Validation of the increase biostability of these new formulations remains challenging given the length of time necessary to show statistically significant degradation using animal models. Accelerated *in vitro* testing remains a valuable asset in predicting long-term biostability of SPUs using relatively short term experiments with the caveat that the *in vitro* testing accurately reproduces the clinical findings. *In vitro-in vivo* correlations of polyurethane degradation suggests that oxidative degradation is the dominant mechanisms leading to device failure. Numerous studies predicting the oxidative stability of SPUs have been conducted with a variety of methods trying to simulate or provide correlations to physiological degradation rates *in vivo*. The quantity of potential hydrogen peroxide molecules, hydroxyl radicals, and superoxide anions released during phagocytosis has been previously approximated with *in vitro* testing.[571] Various concentrations of hydrogen peroxide have been explored with some or no metal ions to provide an accelerated *in vitro* environment.[282,572-574] The most common of these compositions includes a 0.1 M concentration of cobalt (II) chloride ($CoCl_2$) and 20% hydrogen peroxide (H_2O_2) held at 37°C.[261,276,575] The accelerated system has also been reported to provide a strong correlation between the *in vitro* treatment and *in vivo* results, where 24 days in the $CoCl_2/H_2O_2$ medium approximated 1 year of implantation for select polyurethane compositions.[273] Alternatively, the ISO 10993-13 (1998) standard for the evaluation of medical devices suggests the incubation of materials in a 3% H_2O_2 solution at 37°C as a method to simulate real time oxidative degradation of biomaterials. To the

best of our knowledge, the oxidative stability testing of commercially available segmented SPUs through the strict use of 3% H_2O_2 without metal ions has been very limited within the literature.[563] Previous studies look to maintain approximate physiological levels but also incorporate the metal ion to simulate the effects of different pacemaker lead metals.[576-579] Despite individual representation within the literature, a more comprehensive comparative study between the proposed physiological rate and accelerated *in vitro* treatments is needed to evaluate the methods for predictability of performance *in vivo*.

The present study compares the accelerated *in vitro* cobalt (II) chloride and concentrated hydrogen peroxide system with the 3% H_2O_2 *in vitro* system. Effects on the oxidative stability from silicone modification of PCUs and soft segment content reduction were examined in both the accelerated and 3% H_2O_2 systems. Changes in the surface chemistry and morphology of the PCUs were monitored using ATR-FTIR spectroscopy and SEM respectively. Effects on the bulk of the material were examined by tracking molecular weight and uniaxial tensile property changes using gel permeation chromatography (GPC) and tensile testing. Results from the present study were then compared with previous *in vivo* studies to predict the oxidative degradation profile of each material. Relative percent changes in levels of hydrogen peroxide content in the degradation media were calculated using Iodometric titration to determine ROI production. Finally, the predictive capabilities of each test based on changes in peroxide content and comparison to *in vivo* degradation results were evaluated for use in future oxidative stability studies.

4.2 Materials and Methods

4.2.1 Materials Commercially available poly(carbonate urethanes) PCUs Bionate® 80A PCU, Bionate® 75D PCU, Bionate® II 80A PCU, Bionate® II 75D PCU, CarboSil® 20 80A silicone-modified thermoplastic poly(carbonate urethane) (TSPCU), and CarboSil® 20 55D TSPCU were synthesized by DSM Biomedical (Berkeley, CA). Resins were dried for approximately 4 hours at 100ºC prior to melt extrusion into films 200-300 μm thick by DSM Biomedical. Films were cut into 1.5 cm x 4 cm rectangular specimens and dog bones according to ASTM standard 1708D with the gauge length parallel to the direction of film extrusion. Rectangular and dog bone specimens were annealed in sealed vials at 90°C for 24 hours followed by slow cooling prior to *in vitro* biodegradation. Cobalt (II) chloride hexahydrate ($CoCl_2$), N,N'-dimethylformamide (DMF), lithium bromide (LiBr), potassium iodide (KI), sulfuric acid (H_2SO_4), sodium thiosulfate ($Na_2S_2O_3$), ammonium hydroxide (NH_4OH), ammonium nitrate (NH_4NO_3), and ammonium heptamolybdate ($(NH_4)_6Mo_7O_{24}$), and starch solution were purchased and used as received from Sigma Aldrich (Milwaukee, WI). H_2O_2 at concentrations of 3% and 30% (w/v) were purchased and used as received from VWR International.

4.2.2 In Vitro Biodegradation All *in vitro* experiments were conducted at 37°C on unstrained films (n=5) in two different oxidative solutions: accelerated oxidative and physiological approximated treatment based on the ISO 10993-13 standard. An oxidative solution of 0.1 M $CoCl_2$ and 20% H_2O_2 was used to treat the PCUs at an accelerated rate for 36 days with solution changes every 3 days to maintain a relatively constant concentration of radicals. PCUs treated according to ISO standard 10993-13

were subject to a 3% H_2O_2 solution with weekly media changes for 12 months. The 3% method did not include any concentration of metal ions to catalyze hydrogen peroxide decomposition. The films were rinsed with reverse osmosis water and vacuum dried overnight at ambient temperatures before characterization.

4.2.3 Characterization

4.2.3.1 Attenuated Total Reflectance-Fourier Transform Infrared Spectroscopy (ATR-FTIR) Changes in surface chemistry were observed using ATR-FTIR spectroscopy. Spectra were recorded with a Bruker ALPHA FTIR spectrometer equipped with a 45° germanium crystal (Billerica, MA). All spectra were normalized to the 1600 cm^{-1} peak corresponding to the C=C bond stretch of the aromatic ring in the PCU hard segment. Changes in soft segment content were quantified by monitoring differences in the 1256 cm^{-1} peak height (C-O of soft segment carbonate) relative to the internal reference peak using the equation below:

$$\%\, Soft\ segment\ change = \frac{I - I_{untr}}{I_{untr}} x100\%,$$

where I = 1256 cm^{-1} peak height relative to the 1600 cm^{-1} peak height.

4.2.3.2 Uniaxial Tensile Testing Following cleaning and drying, dog bone specimens were strained at a rate of 100%/min to failure using an Instron 3345 equipped with air pneumatic grips (Norwood, MA). Tensile stress was calculated and plotted versus percent elongation. Initial 2% secant modulus, tensile strength, and ultimate elongation were all calculated from the resultant stress vs. strain plots.

4.2.3.3 Gel Permeation Chromatography (GPC) Changes in molecular weight and molecular weight distribution were monitored using GPC. Briefly, specimens were

dissolved in a 0.1 M LiBr solution of DMF at approximately 5 mg/mL concentrations. GPC solutions were incubated at 70°C for 6 hours with mild periodic agitation to ensure full specimen dissolution and elimination of hydrogen bonding. Specimens were eluted through a GPC Max (Viscotek, Malvern, PA) equipped with two Phenomenex columns with pores of 10^3 and 10^5 Å in diameter. DMF with 0.05 M LiBr at a flow rate of 1.0 mL/min at 80°C was used as an eluent and refractive index response was used as detection. OmniSEC software was calibrated using a set of conventional narrow polystyrene standards with molecular weights of 10, 50, 100, 300, 500, 800, 1000 kDa (Agilent Technologies, Santa Clara, CA). Weight average molecular weight ($\overline{M_W}$) and polydispersity index (PDI) were calculated from chromatograms of annealed untreated and degraded specimens from accelerated and 3% H_2O_2 *in vitro* treatments. $\overline{M_W}$ and PDI values were reported as average ± standard deviation.

4.2.3.4 Scanning Electron Microscopy (SEM) SEM was used to examine the surfaces of unstrained and strained to failure PCUs before and after *in vitro* treatment. Surface morphology of unstrained and strained to failure specimens were observed using a JEOL JCM-5000 NeoScope scanning electron microscope (SEM). An acceleration voltage of 5 kV and working distance of 8 mm were used. A gold layer of approximately 200-300 Å was deposited on all specimens prior to imaging to increase conductivity. Unstrained specimens were harvested from annealed untreated and degraded rectangular films. Strained to failure specimens were taken from fractured tensile testing specimens. Images were taken at magnitudes of 500X and 2000X to highlight both low and high resolution surface topography features.

4.2.4 Monitoring Peroxide Levels Percent hydrogen peroxide was calculated using a basic iodometric titration process performed in a previous oxidation study to confirm changes in peroxide content.[574] KI solution was prepared in 1% (w/v) concentration with deionized water. Ammonium molybdate solution was prepared by dissolving 9 grams of $(NH_4)_6Mo_7O_{24}$ and 24 grams of NH_4NO_3 in 10 mL of 6 N NH_4OH and 100 mL of deionized water. H_2SO_4 solution was prepared in a 20% (v/v) concentration with deionized water. Finally 0.2 N sodium thiosulfate solution was prepared by dissolving 25 g $Na_2S_2O_3$ in 1 L of deionized water.

Approximately 1 mL of each *in vitro* treatment solution was taken prior to a scheduled solution change and weighed to the nearest 0.1 mg. The samples were added to a solution of $Na_2S_2O_3$, KI, and DI water of 10, 10, and 50 mL respectively. Two drops of ammonium molybdate solution were then added. The solution was titrated with 0.2 N $Na_2S_4O_6$ until the liquid appeared to be a faint yellow color, followed by an addition of 2 mL of starch solution before the final exact titration with 0.2 N $Na_2S_4O_6$ solution was performed. The process was repeated with water for each sample. Percent hydrogen peroxide content was calculated using the following equation:

$$\%H_2O_2 = \frac{0.34\ x\ \left(V_{H_2O_2} - V_{water}\right)}{solution\ sample\ weight}$$

The procedure was conducted on oxidative medium with 3, 10, and 20% H_2O_2 concentration combined with 0, 0.05, 0.1 and 0.2 M $CoCl_2$ to decompose the peroxide into radicals. Levels of peroxide were calculated at 0, 3 and 7 days.

4.2.5 Statistical Analysis A two-tailed student's T-test was performed to determine statistical significance between groups of data. All comparisons were made with a 95% confidence interval. (α=0.05)

4.3 Results and Discussion

4.3.1 Initial Characterization All three PCU products were expected to include a polycarbonate glycol and similar hard segment chemistries with CarboSil® TSPCU products also containing silicone at approximately 20% of the soft segment content, **Table 4.1**. Structural features of all of the PCUs were examined with infrared spectroscopy. Characteristic ATR-FTIR spectra of each PCU film prior to treatment are shown in **Figures 4.1-4.6.** The materials all exhibited the same peaks characteristic of thermoplastic PCU with the exception of CarboSil® 20 80A TSPCU and CarboSil® 20 55D TSPCU samples, which also included peaks assigned to groups within the silicone segment, **Table 4.2**. Soft segment indices were calculated from the ATR-FTIR spectra of the PCUs to determine changes in soft segment content. The 1600 cm^{-1} peak of all PCUs was assigned to the C=C stretch of the aromatic ring within the hard segment based on previous studies observing MDI-based polyurethanes.[544] The aromatic ring band also served as the internal reference peak, which all spectra peak heights of interest were normalized.

Table 4.1. Characterization of polyurethanes

Material	Hard Segment	Soft Segment	Hardness Grade
Bionate® PCU	MDI/BDO	Polycarbonate Glycol	80A 75D
Bionate® II PCU	MDI/BDO	Polycarbonate Glycol	80A 75D
CarboSil® TSPCU	MDI/BDO	Polycarbonate Glycol/Silicone Diol	20 80A 20 55D

MDI = methylene di(p-phenyl isocyanate); BDO = butane diol

Table 4.2. ATR-FTIR spectral assignments

Wavenumber (cm^{-1})	Spectral Assignment
1742	C=O Carbonate Nonbonded
1724	C=O Carbonate H-bonded
1705	C=O Urethane H-bonded
1600	C=C Benzene Ring
1534	C-N + N-H Amide
1415	C-C Benzene Ring
1313	C-N + N-H
1256	C-O-C of Carbonate
1232	C-N
1115	C-O
803	Si-CH_3 of Silicone

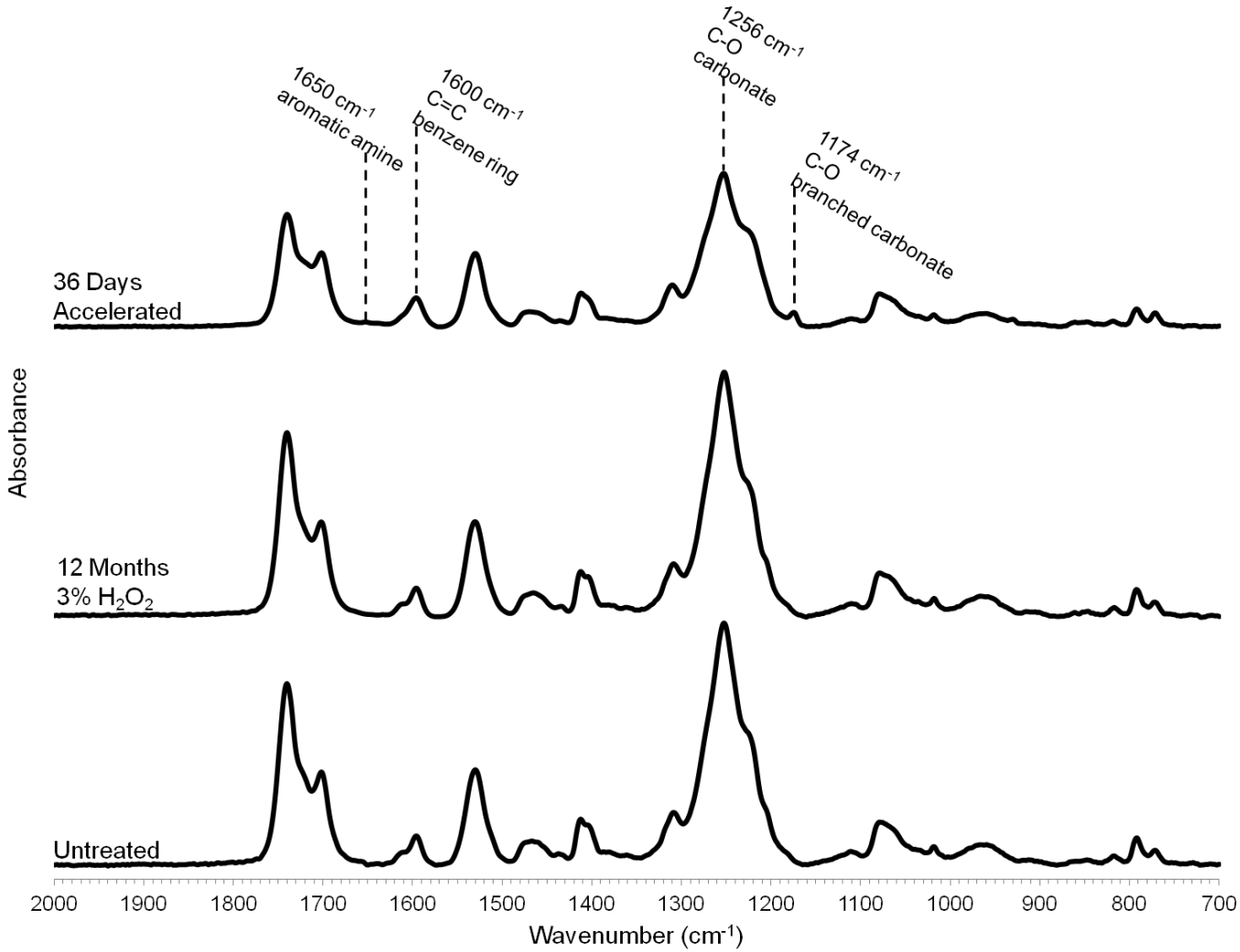

Figure 4.1. ATR-FTIR spectra of untreated Bionate® 80A specimens compared to specimens after 12 months *in vitro* treatment (3% H_2O_2 at 37°C) and 36 days accelerated *in vitro* treatment (0.1M $CoCl_2$/20% H_2O_2 at 37°C)

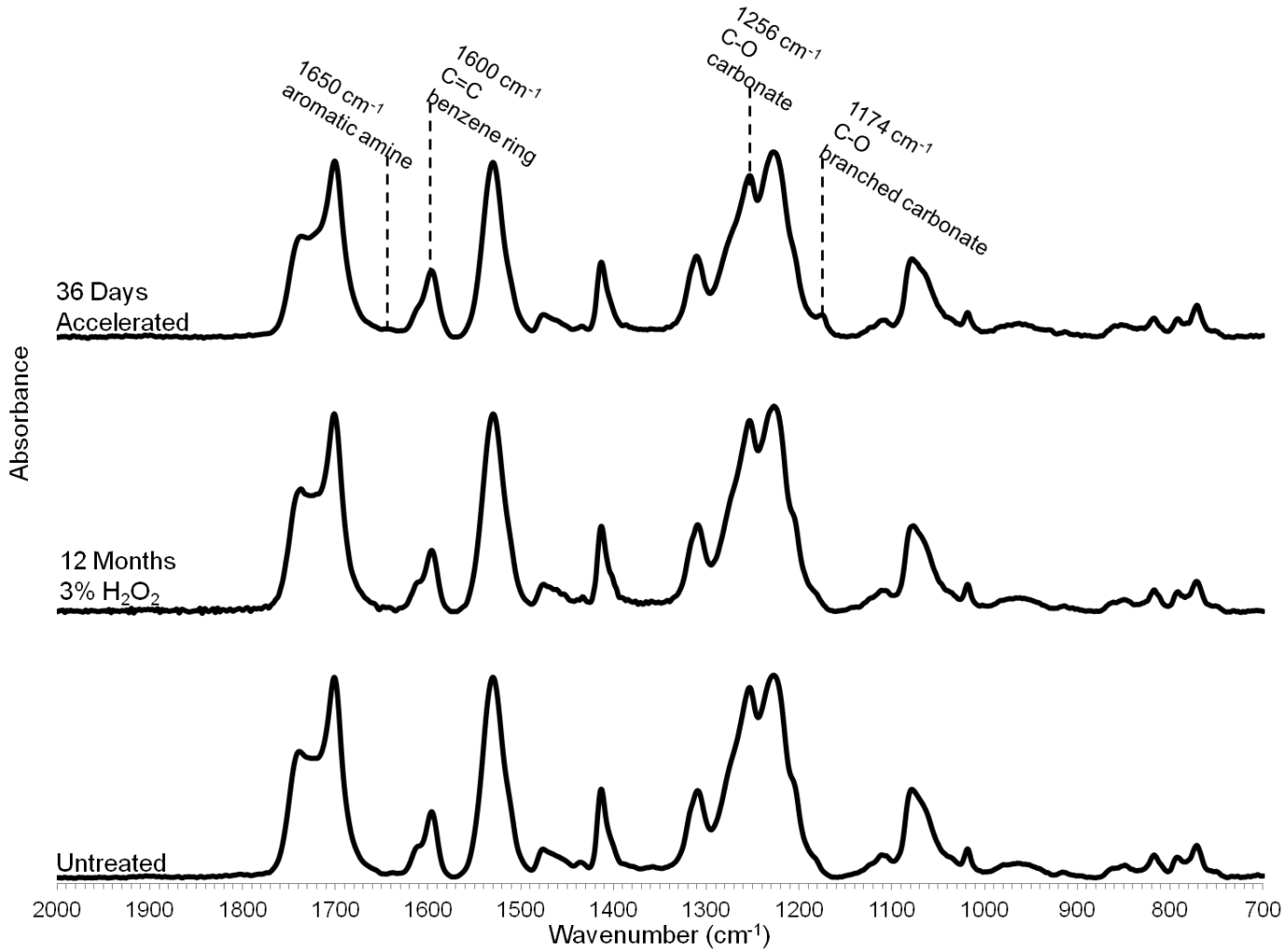

Figure 4.2. ATR-FTIR spectra of untreated Bionate® 75D specimens compared to specimens after 12 months *in vitro* treatment (3% H_2O_2 at 37°C) and 36 days accelerated *in vitro* treatment (0.1 M $CoCl_2$/20% H_2O_2 at 37°C)

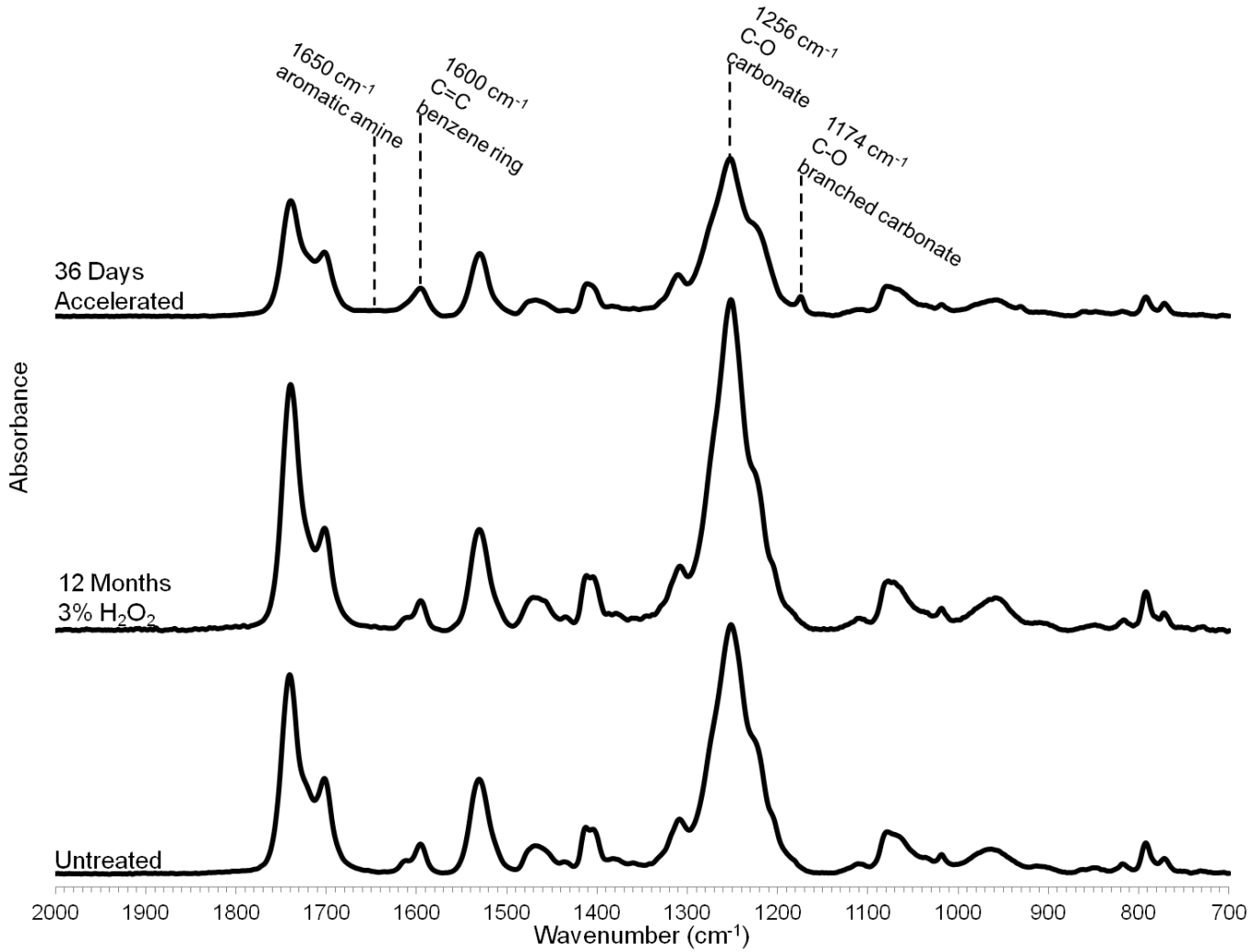

Figure 4.3. ATR-FTIR spectra of untreated Bionate® II 80A specimens compared to specimens after 12 months *in vitro* treatment (3% H_2O_2 at 37°C) and 36 days accelerated *in vitro* treatment (0.1 M $CoCl_2$/20% H_2O_2 at 37°C)

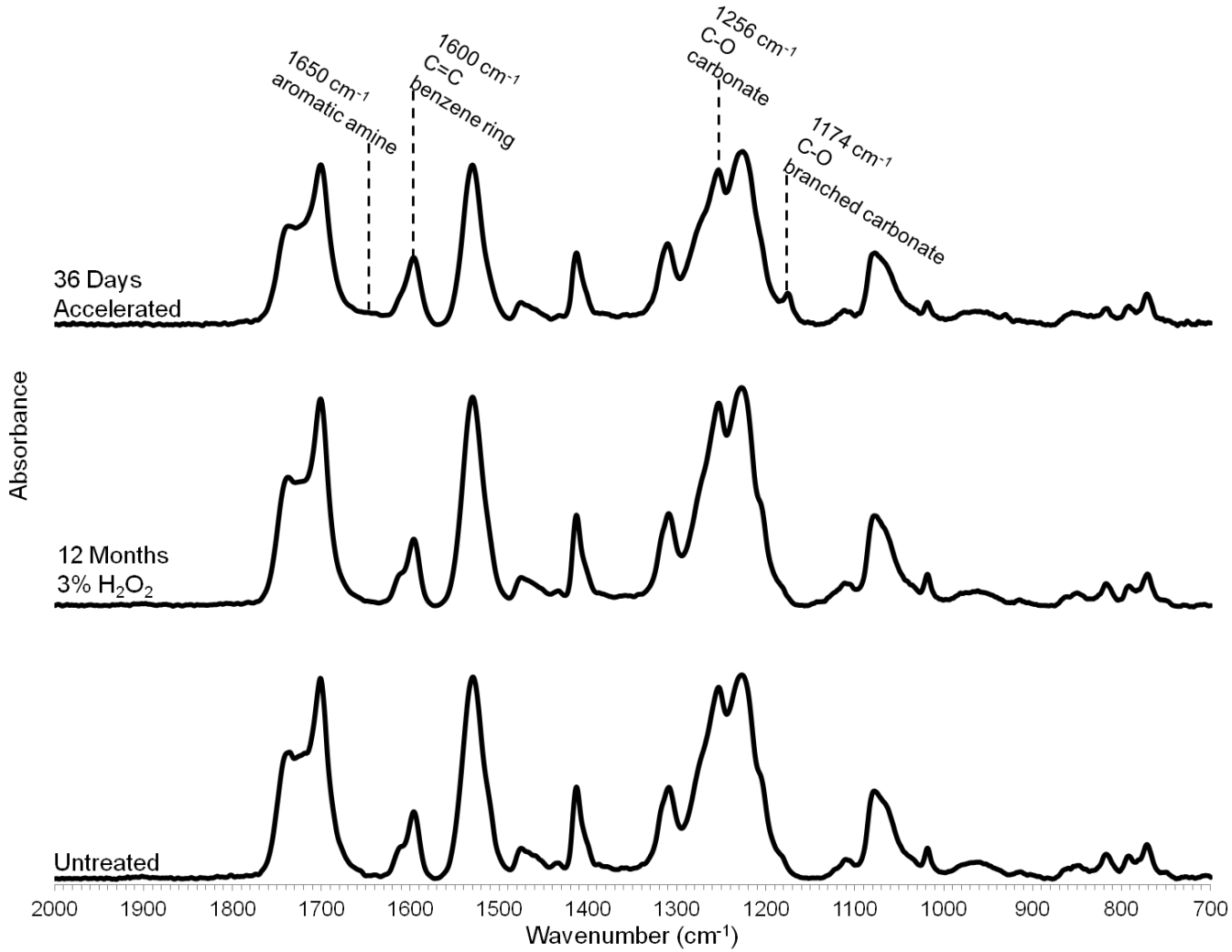

Figure 4.4. ATR-FTIR spectra of untreated Bionate® II 75D specimens compared to specimens after 12 months *in vitro* treatment (3% H_2O_2 at 37°C) and 36 days accelerated *in vitro* treatment (0.1 M $CoCl_2$/20% H_2O_2 at 37°C)

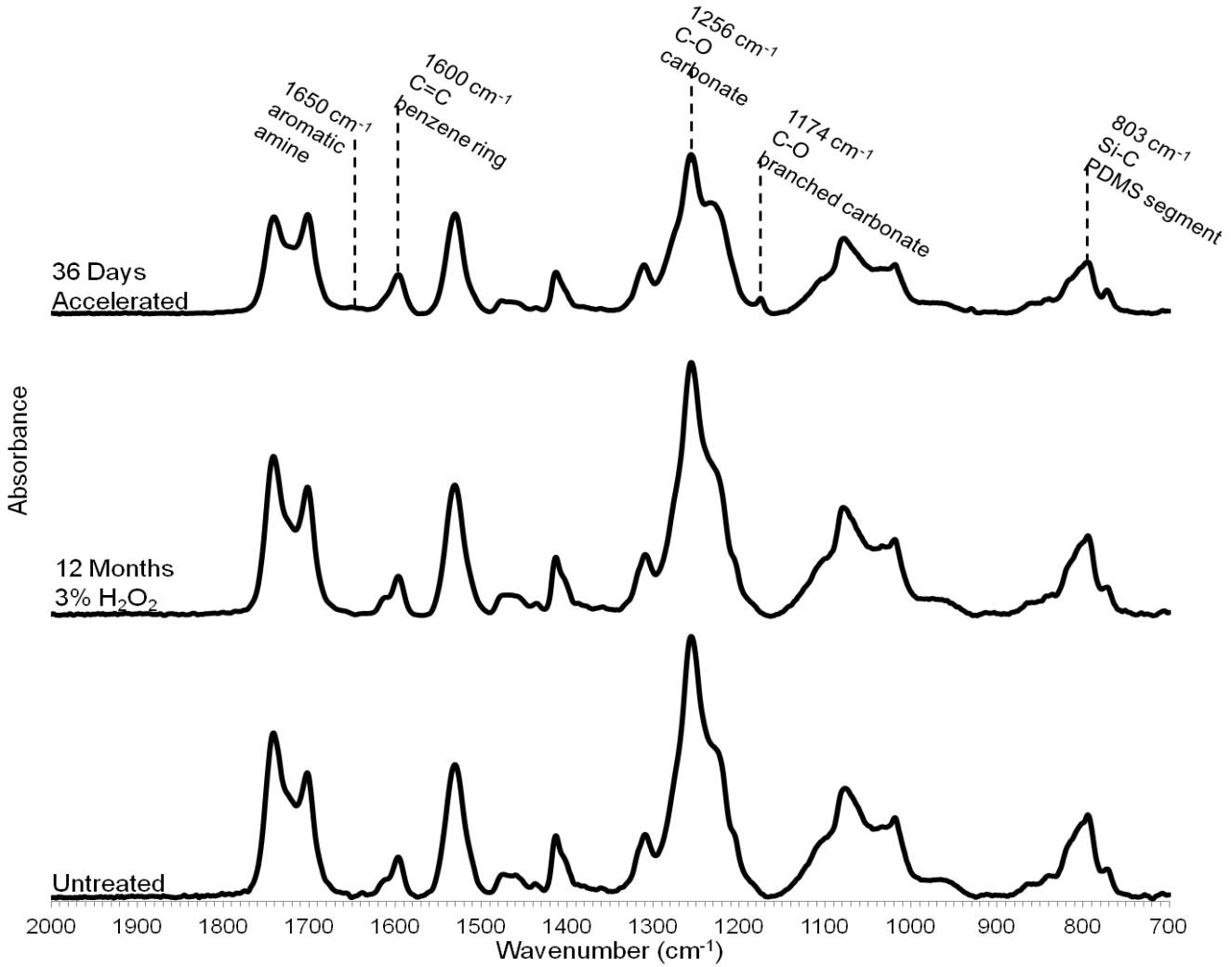

Figure 4.5. ATR-FTIR spectra of untreated CarboSil® 20 80A specimens compared to specimens after 12 months *in vitro* treatment (3% H_2O_2 at 37°C) and 36 days accelerated *in vitro* treatment (0.1 M $CoCl_2$/20% H_2O_2 at 37°C)

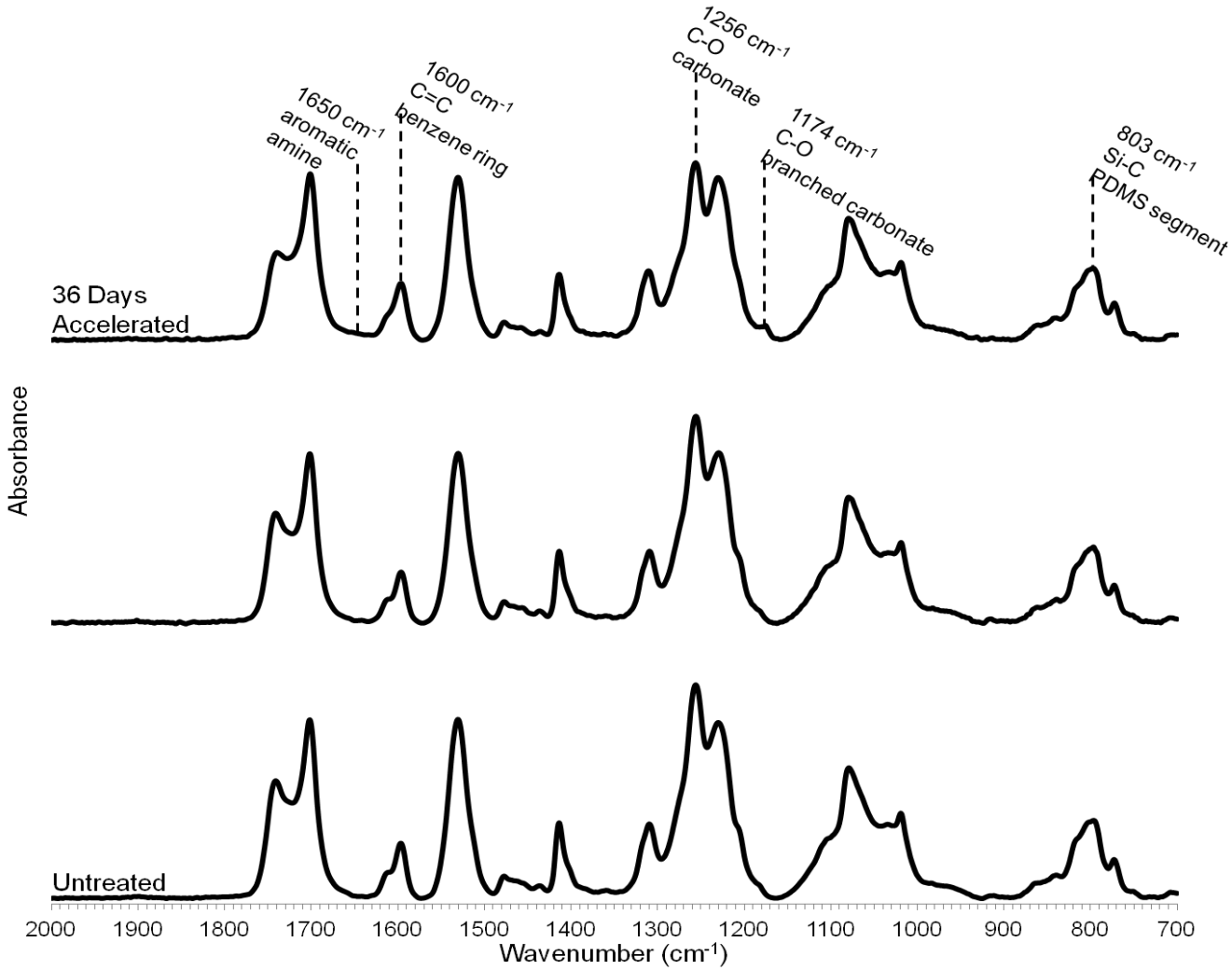

Figure 4.6. ATR-FTIR spectra of untreated CarboSil® 20 55D specimens compared to specimens after 12 months *in vitro* treatment (3% H_2O_2 at 37°C) and 36 days accelerated *in vitro* treatment (0.1 M $CoCl_2$/20% H_2O_2 at 37°C)

As expected, the soft segment indices of all soft 80A hardness grade materials were found to be significantly higher than their harder grade components, **Table 4.3**. This indicated an increased presence of soft segment carbonate linkages on the surface of the annealed extruded films. Bionate® II 80A PCU has a polycarbonate diol different from the standard macroglycol used in Bionate® 80A PCU. While no additional peaks were visible in Bionate® II 80A PCU, the soft segment carbonate index was found to be higher in the new PCU compared to Bionate® 80A PCU. The difference in chemistry is presumed to allow for greater enrichment of the soft segment in Bionate® II 80A PCU following melt extrusion processing. While the result is highly pronounced in the soft grade material, no significant difference is reported between the hard grade PCUs. CarboSil® 20 80A TSPCU exhibited a lower soft segment carbonate index likely due to the introduction of silicone glycol to the soft segment.

Table 4.3. Soft segment loss of PCUs after 12 months *in vitro* treatment (3% H_2O_2 at 37°C) and accelerated *in vitro* treatment (0.1 M $CoCl_2$/20% H_2O_2 at 37°C)

		Untreated	12 Months 3% H_2O_2		36 Days Accelerated	
		1256/ 1600 cm^{-1}	1256/ 1600 cm^{-1}	Percent Change	1256/ 1600 cm^{-1}	Percent Change
Bionate® PCU	80A	9.1 ± 0.2	8.5 ± 0.2[a]	-7 ± 2%	5.2 ± 0.7[a]	-27 ± 10%
	75D	3.1 ± 0.1	3.0 ± 0.1	-1 ± 1%	2.4 ± 0.1[a]	-16 ± 1%
Bionate® II PCU	80A	9.3 ± 0.3	11.0 ± 0.5[a]	+18 ± 5%	5.7 ± 0.2[a]	-34 ± 3%
	75D	3.0 ± 0.1	2.9 ± 0.1[a]	-2 ± 1%	2.3 ± 0.1[a]	-21 ± 2%
CarboSil® TSPCU	20 80A	6.5 ± 0.1	6.6 ± 0.2	+1 ± 3%	4.1 ± 0.3[a]	-27 ± 9%
	20 55D	4.0 ± 0.1	4.0 ± 0.1[a]	+2 ± 1%	3.1 ± 0.2[a]	-20 ± 6%

(average ± standard deviation; n=10; [a]$p<0.05$ from untreated)

Molecular weights calculated with GPC were found to be fairly similar between the hard soft grade material with the exception of Bionate® II 80A PCU. Bionate® II 80A

material had a substantially higher molecular weight than its 75D counterpart as well as all of the other PCU materials. The polydispersity index (PDI) was similar indicating that the differences in soft segment content and chemistry did not influence the molecular weight distribution. No significant differences were observed between the untreated Bionate® 80A and Bionate® II 80A PCUs despite the differences in soft segment composition and molecular weights. However; tensile testing of untreated dog bones yielded substantially higher initial secant moduli and lower percent elongation in the harder grade materials as expected given the lower soft segment content, **Table 4.4**. The CarboSil® products were found to exhibit lower ultimate tensile strengths and ultimate elongations given the presence of the silicone groups within the soft segment. Previous research has shown linear silicones to have weaker ultimate tensile strengths than TPUs, but remain highly flexible allowing for greater ultimate elongation.[580]

Table 4.4. Uniaxial tensile properties of PCUs before and after 12 months *in vitro* treatment (3% H_2O_2 at 37°C) and accelerated *in vitro* treatment (0.1 M $CoCl_2$/20% H_2O_2 at 37°C)

		2% Secant Modulus (MPa)			Ultimate Tensile Strength (MPa)			Percent Elongation		
		Untreated	12 Months	36 Days Accelerated	Untreated	12 Months	36 Days Accelerated	Untreated	12 Months	36 Days Accelerated
Bionate®	80A	20 ± 1	19 ± 2	19 ± 1	68 ± 6	55 ± 7[a]	54 ± 2[a]	364 ± 8%	392 ± 25%[a]	367 ± 10%
PCU	75D	670 ± 25	950 ± 79[a]	750 ± 21[a]	47 ± 2	48 ± 4	39 ± 5[a]	184 ± 14%	183 ± 14%	163 ± 30%
Bionate® II	80A	17 ± 1	19 ± 1	19 ± 1[a]	65 ± 10	64 ± 1	80 ± 5[a]	415 ± 43%	423 ± 18%	417 ± 10%
PCU	75D	1106 ± 68	1291 ± 24[a]	1049 ± 41	50 ± 6	52 ± 7	43 ± 7	213 ± 26%	169 ± 10%[a]	181 ± 20%
CarboSil®	20 80A	21 ± 1	22 ± 1	23 ± 2[a]	46 ± 3	41 ± 3[a]	49 ± 4	359 ± 25%	393 ± 19%	391 ± 20%[a]
TSPCU	20 55D	135 ± 6	125 ± 6[a]	137 ± 2	40 ± 3	38 ± 1	39 ± 3	302 ± 17%	304 ± 9%	275 ± 20%

(average ± standard deviation; n=5; [a]$p<0.05$ from untreated)

4.3.2 In Vitro Biodegradation

4.3.2.1 Accelerated In Vitro Treatment A 0.1 M $CoCl_2$/20% H_2O_2 solution was used to accelerate oxidative degradation of the PCUs by generating higher concentrations of ROIs. The cobalt ions are expected to rapidly decompose the hydrogen peroxide molecules via the Haber-Weiss reaction. [190] The increased concentration of ROIs within the degradation medium was expected to help simulate a longer degradation period *in vivo*. Results after 24 days have been projected to resemble approximately 12 months of *in vivo* implantation, as indicated by previous correlation studies of similar materials.[273] The current study's endpoint of 36 days of *in vitro* treatment is therefore expected to simulate even longer implantation periods.

Greater soft segment loss was observed in all of the softer grade materials in the accelerated medium due to the higher probability of soft segment chain scission at the more prevalent carbonate linkages, **Table 4.3**. Briefly, ROIs abstract the α-methylene carbon within the soft segment leaving an open radical along with the backbone. The radical then reacts with a hydroxyl to form a hemiacetal which can oxidize into an ester. Chain scission results from acid hydrolysis of the ester and soft segment loss can be attributed to solubilization of low $\overline{M_W}$ soft segment species.[190] In the accelerated medium, Bionate® 80A PCU displayed approximately 27.5% soft segment loss at the surface following 36 days accelerated *in vitro* treatment. The PCU soft segment losses were found to be lower than expected values given previous 12 month *in vivo* data which showed a 32% soft segment loss using the same peak height analysis method.[273] Previous *in vivo* results did show the silicone modified PCU to exhibit a greater

oxidative biostability under real physiological conditions but those were not seen with the accelerated treatment, **Figure 4.5, Table 4.3**. Bionate® II 80A PCU exhibited a slightly greater soft segment carbonate loss in the accelerated medium though results were not statistically significant, **Figure 4.1, Figure 4.3, Table 4.3.** All hard grade PCUs also displayed soft segment loss but less than their softer grade counterparts in the accelerated medium. No significant difference was found between the three PCUs themselves, **Table 4.3.** The lack of separation between the three materials is likely due to the decreased soft segment content acting as the dominant variable.

All materials exhibited evidence of surface crosslinking with emergence of the 1174 cm^{-1} peak following 36 days accelerated *in vitro* treatment, **Figures 4.1-4.6,** indicating the presence of branched ethers.[575] Similar results were observed in previous in vivo studies where both Bionate® 80A PCU and CarboSil® 20 80A TSPCU exhibited ATR-FTIR spectra with the presence of the 1174 cm^{-1} peak.[273,581] The result has previously been attributed to the attraction of two free radicals on the soft segment chain resulting in crosslinking of the soft segment before progression into hydrolysis chain scission.

In addition to soft segment changes, the presence of the aromatic amine group in all the materials, as shown by the emerging 1650 cm^{-1} peak, indicates that the PCUs also experienced hard segment degradation, **Figures 4.1-4.6**.[261] Briefly, the α-methylene carbon next to the urethane group in the PCUs is again abstracted from the hard segment and the same proposed progression into chain scission is expected to occur, leaving free aromatic amines.[261] Previous *in vivo* studies also confirmed hard segment degradation in

both Bionate® 80A PCU and CarboSil® 20 80A TSPCU which again is in agreement with the accelerated treatment.

In the accelerated medium, all 80A specimens exhibited greater $\overline{M_W}$ loss than their harder grade counterparts with the greatest separation occurring between the two CarboSil® materials, **Table 4.5**. However; the percent molecular weight losses were minimal compared to surface soft segment content losses indicating that the bulk of all the materials were retained following 36 days of accelerated treatment.

Table 4.5. Molecular weight changes of PCUs after 12 months *in vitro* treatment (3% H_2O_2 at 37°C) and accelerated *in vitro* treatment (0.1 M $CoCl_2$/20% H_2O_2 at 37°C)

		12 Months 3% H_2O_2 % $\overline{M_W}$ Change	36 Days Accelerated % $\overline{M_W}$ Change
Bionate® PCU	80A	-9 ± 3%[a]	-12 ± 6%[a]
	75D	-2 ± 2%	-8 ± 3%[a]
Bionate® II PCU	80A	-2 ± 3%	-9 ± 6%[a]
	75D	-19 ± 4%[a]	-5 ± 5%
CarboSil® TSPCU	20 80A	-8 ± 3%[a]	-15 ± 5%[a]
	20 55D	-11 ± 3%[a]	-6 ± 6%

(average ± standard deviation; n=10; [a]$p<0.05$ from untreated)

All materials retained their uniaxial tensile properties following 36 days accelerated *in vitro* treatment. Bionate® 80A and 75D PCU grades, exhibited a small loss in ultimate tensile strength, and Bionate® II 80A PCU exhibited increases in both initial secant modulus and ultimate tensile strength, **Table 4.4**. These increases in tensile properties

were attributed to possible reorganization of the hard domains as a result of prolonged incubation in solution.

Bionate® 80A PCU exhibited the highest density of pitting among all 6 materials despite its spectral changes, while all other Bionate® materials showed similar densities, **Figures 4.7-4.12.** The differences in results for Bionate® 80A PCU could be attributed to the limited depth of the ATR-FTIR instrument when monitoring affected SPU depth. CarboSil® products exhibited a reduced pitting density likely due to the presence of silicone on the surface. Decreases in pit density of the TSPCU have also been previously demonstrated *in vivo*.[273] Despite evidence of surface degradation in the form of pitting, there was no evidence of environmental stress cracking even on the strained-to-failure specimens of any of the PCUs in the study. This is in contrast to PEUs that are subject to ESC after accelerated oxidative treatment[261] and *in vivo*,[190] which has been proposed as the primary failure mechanisms of these devices upon progression to full thickness cracking.

4.3.2.2 ISO 10993 In Vitro Treatment A second set of samples was subject to a mild treatment in a 3% H_2O_2 solution as per ISO standard 10993-13. The ISO treatment was expected to better resemble a more physiological concentration of hydrogen peroxide. No metal ion was included within this treatment to encourage decomposition of the hydrogen peroxide molecules.

The 12 month 3% H_2O_2 sample set of Bionate® 80A PCU, was found to only lose approximately 7.2% of its surface soft segment despite being expected to experience more physiological levels of hydrogen peroxide. In addition, it was the only PCU in this

study to show soft segment loss despite known losses in other commercially available products including CarboSil® 20 80A TSPCU.[581] Despite significant changes in the accelerated medium, Bionate® II 80A PCU was found to exhibit a substantial increase in soft segment content at the surface following 12 months of treatment in the 3% H_2O_2 system. The changes are potentially attributed to a consistent 12 month incubation causing more soft segment to migrate to the surface. While the PCUs have exhibited surface crosslinking in the accelerated medium and following explantation, no 1174 cm^{-1} peak was detected in any of the 6 materials following 12 months treatment in 3% H_2O_2. Similar to the crosslinking, no evidence of hard segment degradation was seen in any of

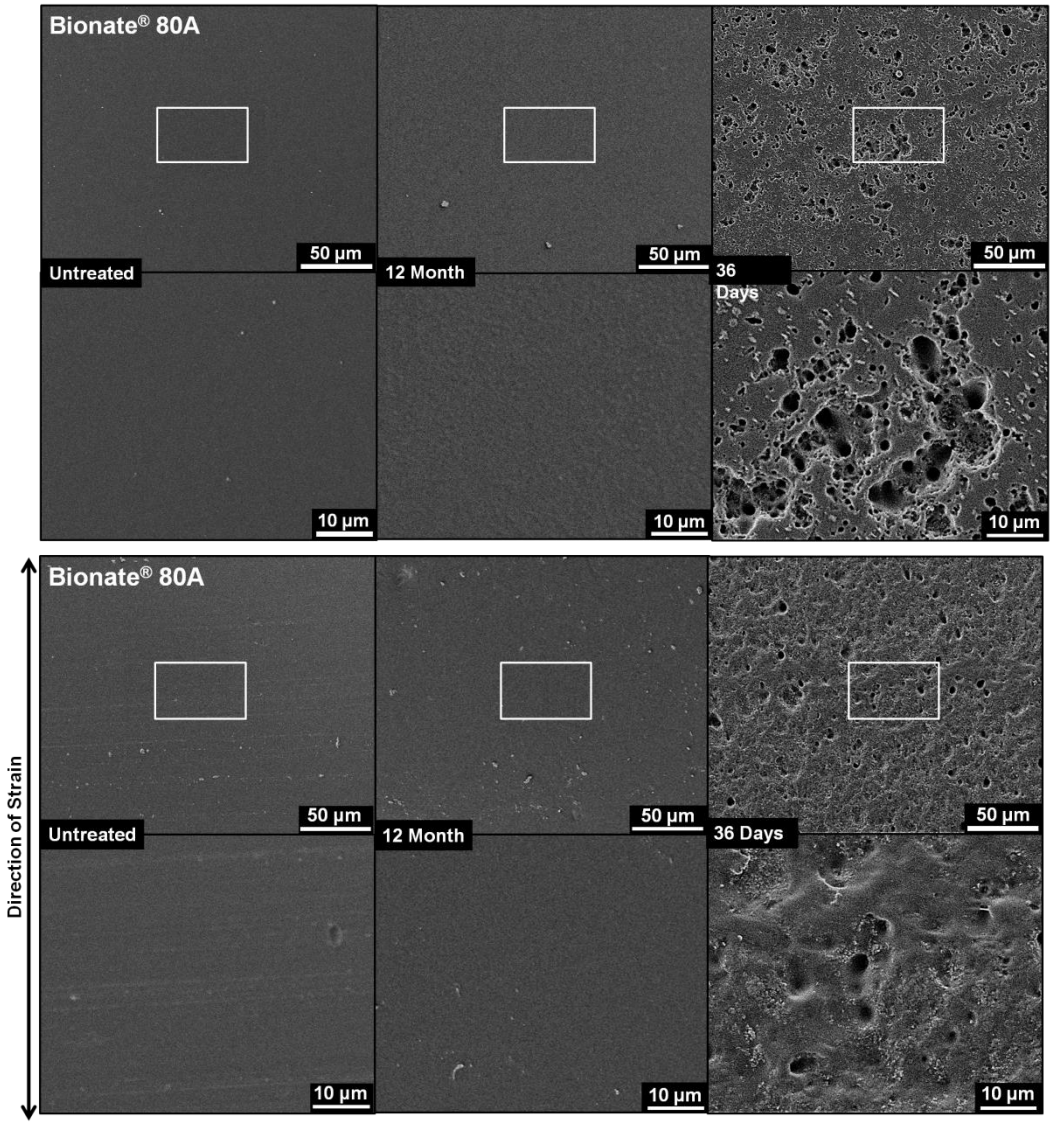

Figure 4.7. Scanning electron micrographs of unstrained and strained to failure Bionate® 80A PCU specimens showing surface damage after 12 months *in vitro* treatment (3% H_2O_2 at 37°C) and 36 days accelerated *in vitro* treatment (0.1 M $CoCl_2$/20% H_2O_2 at 37°C)

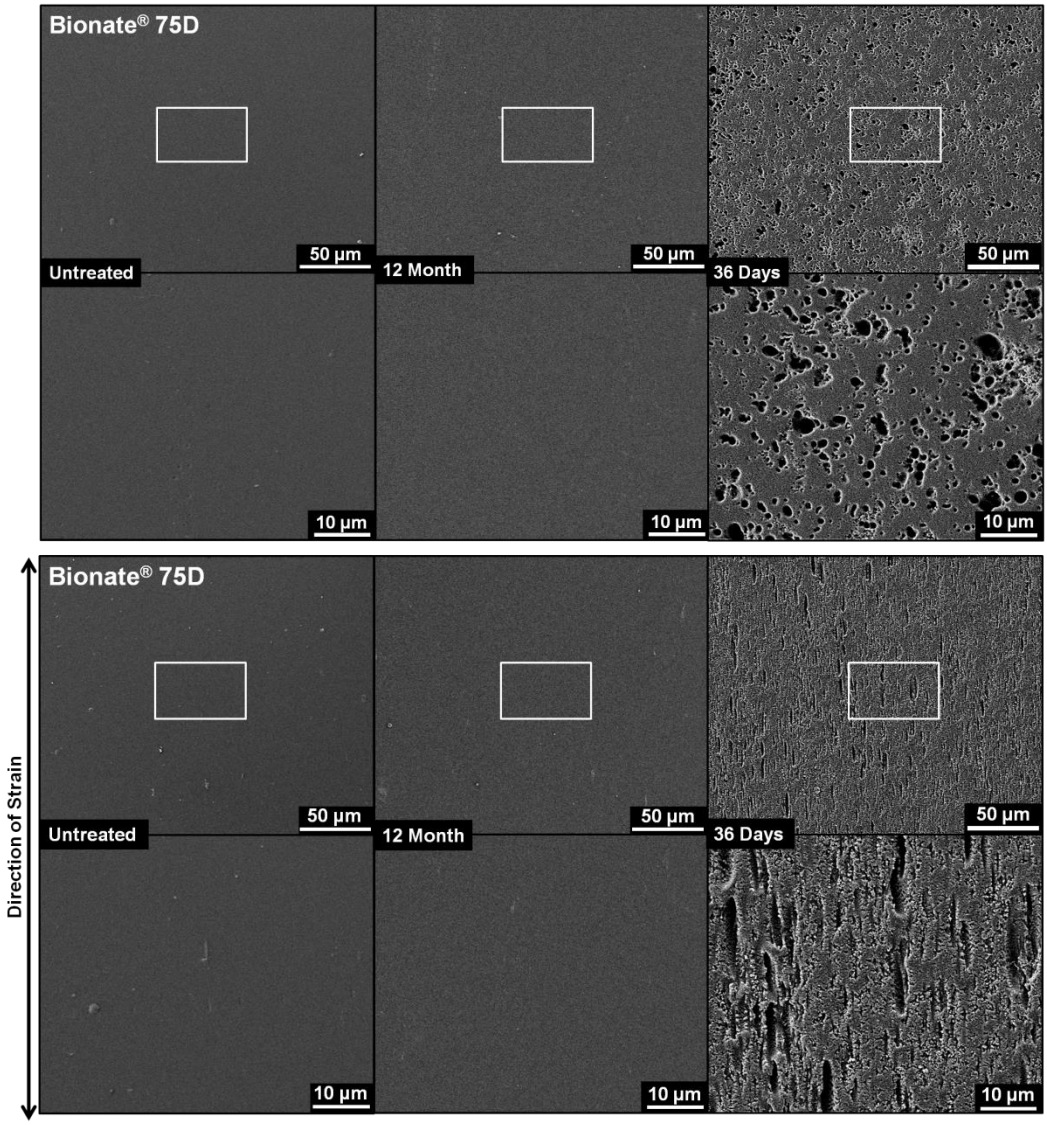

Figure 4.8. Scanning electron micrographs of unstrained and strained to failure Bionate® 75D PCU specimens showing surface damage after 12 months *in vitro* treatment (3% H_2O_2 at 37°C) and 36 days accelerated *in vitro* treatment (0.1 M $CoCl_2$/20% H_2O_2 at 37°C)

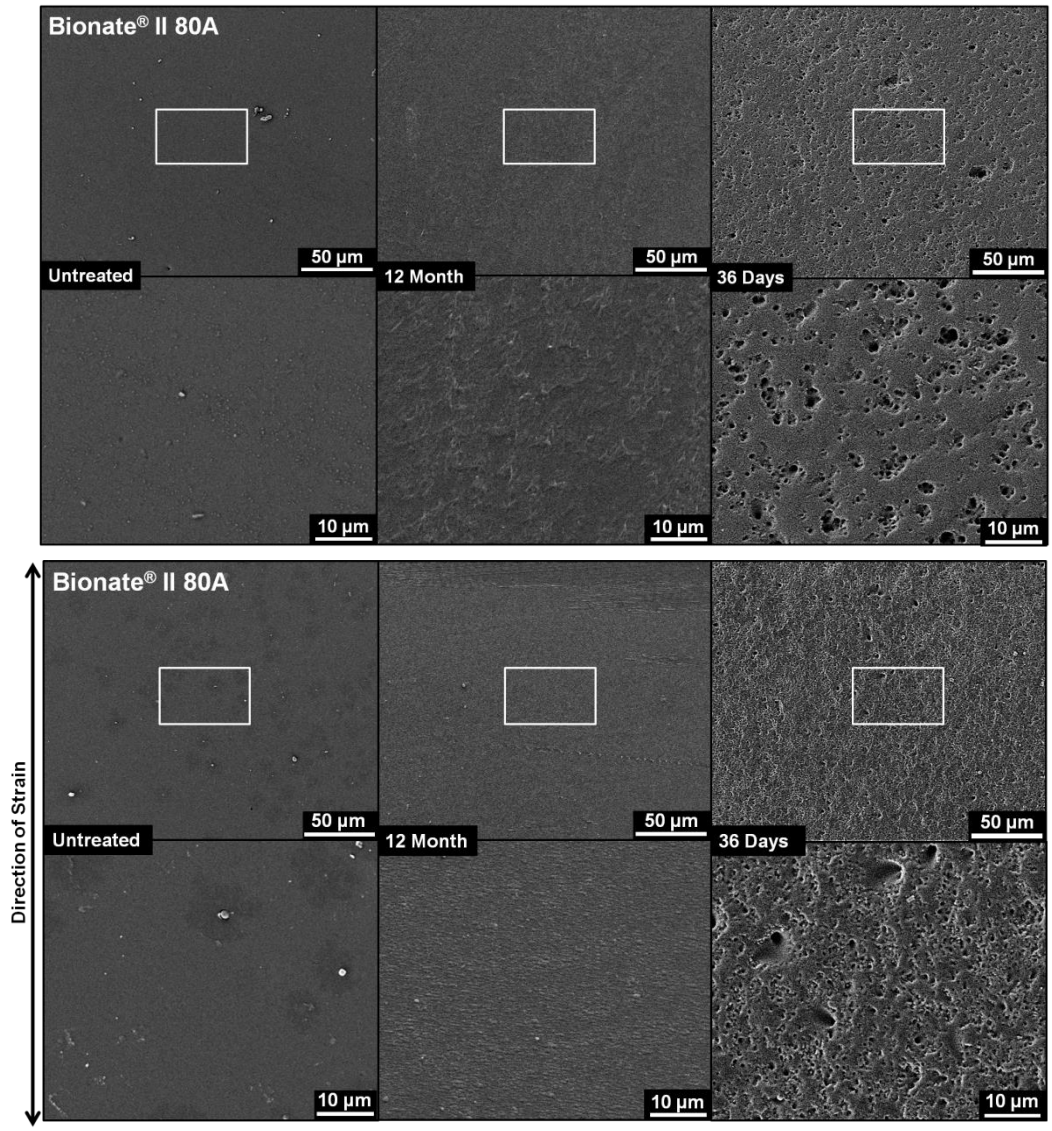

Figure 4.9. Scanning electron micrographs of unstrained and strained to failure Bionate® II 80A specimens showing surface damage after 12 months *in vitro* treatment (3% H_2O_2 at 37°C) and 36 days accelerated *in vitro* treatment (0.1 M $CoCl_2$/20% H_2O_2 at 37°C)

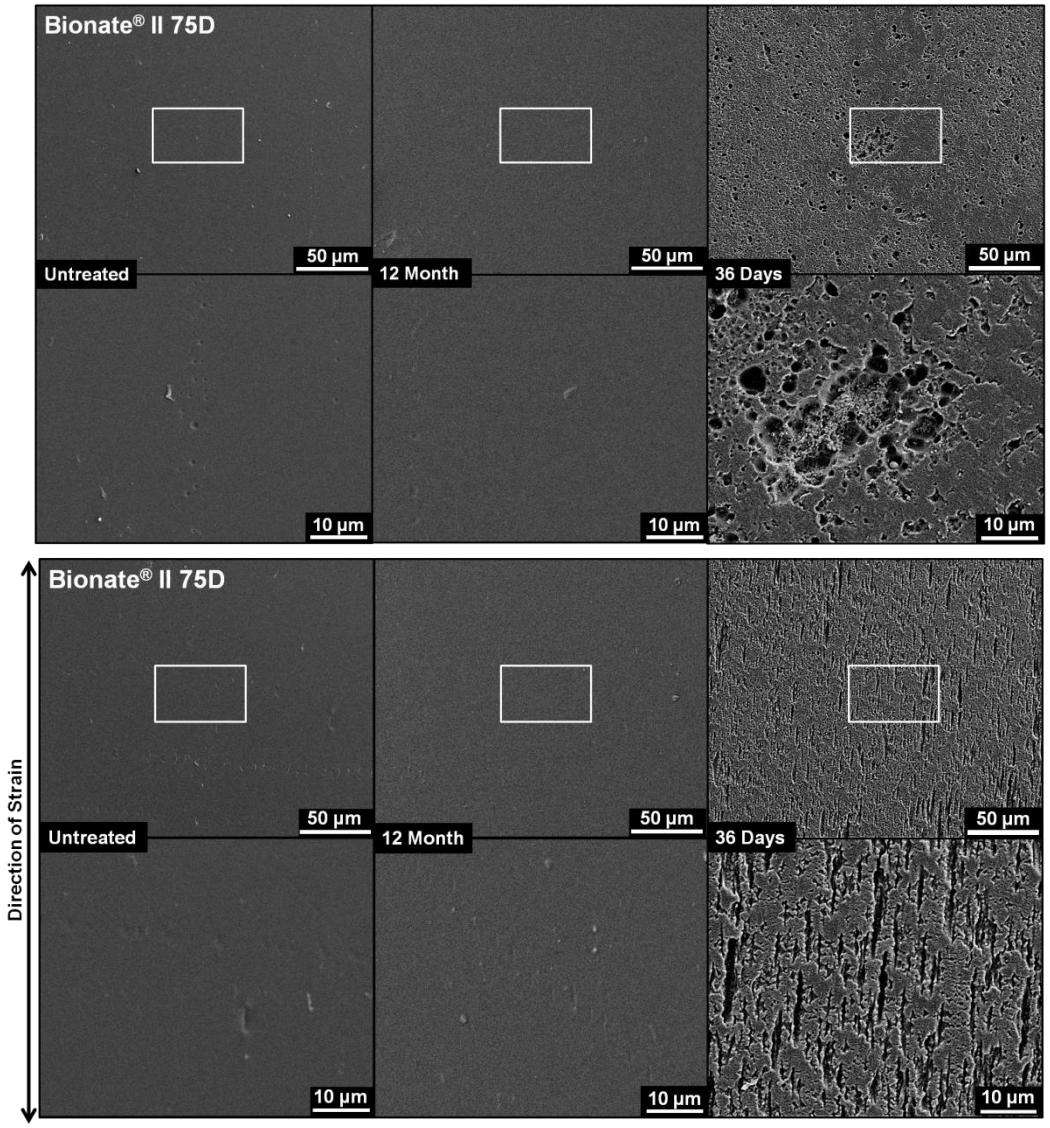

Figure 4.10. Scanning electron micrographs of unstrained and strained to failure Bionate® II 75D specimens showing surface damage after 12 months *in vitro* treatment (3% H_2O_2 at 37°C) and 36 days accelerated *in vitro* treatment (0.1 M $CoCl_2$/20% H_2O_2 at 37°C)

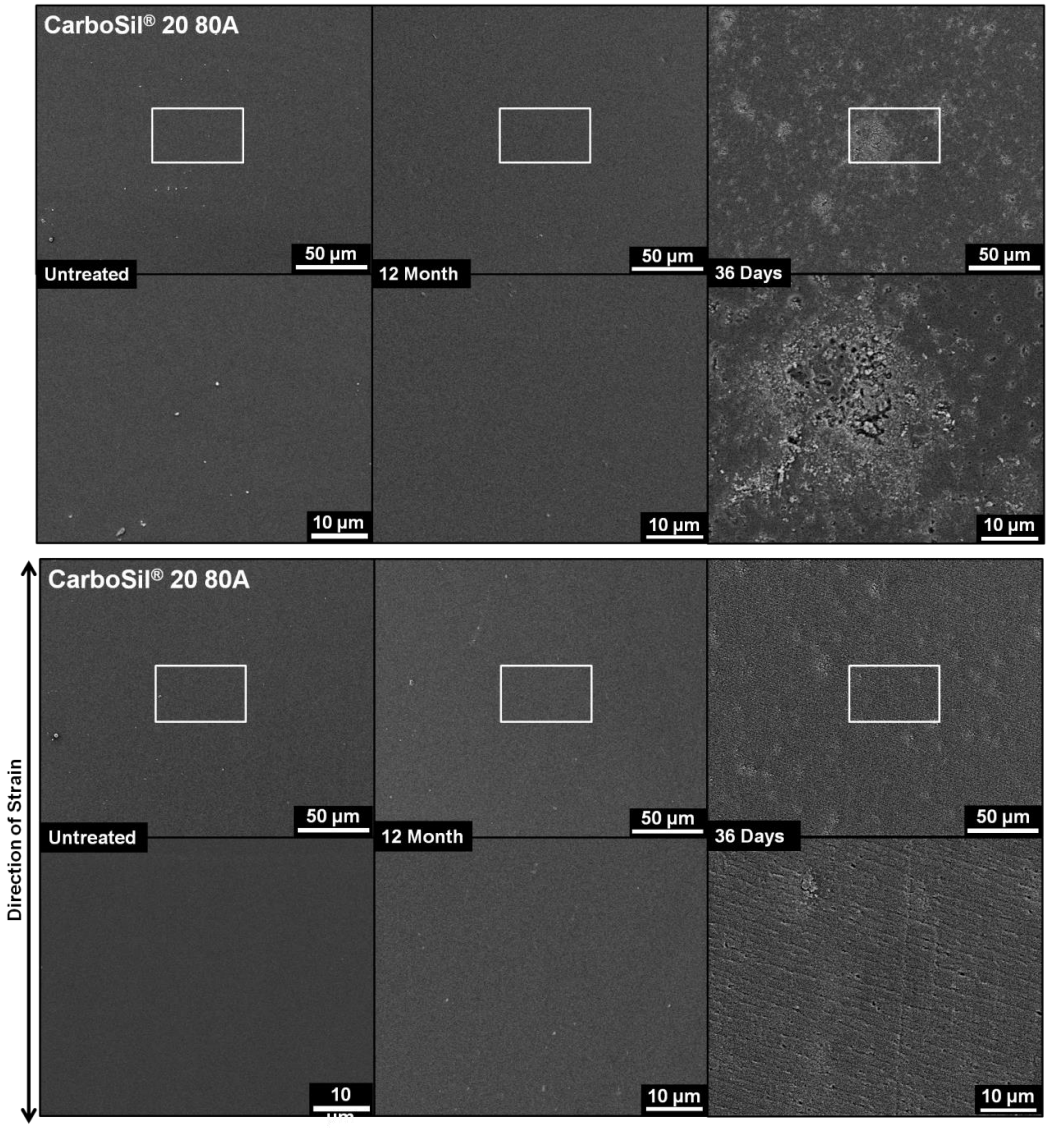

Figure 4.11. Scanning electron micrographs of unstrained and strained to failure CarboSil® 20 80A TSPCU specimens showing surface damage after 12 months *in vitro* treatment (3% H_2O_2 at 37°C) and 36 days accelerated *in vitro* treatment (0.1 M $CoCl_2$/20% H_2O_2 at 37°C)

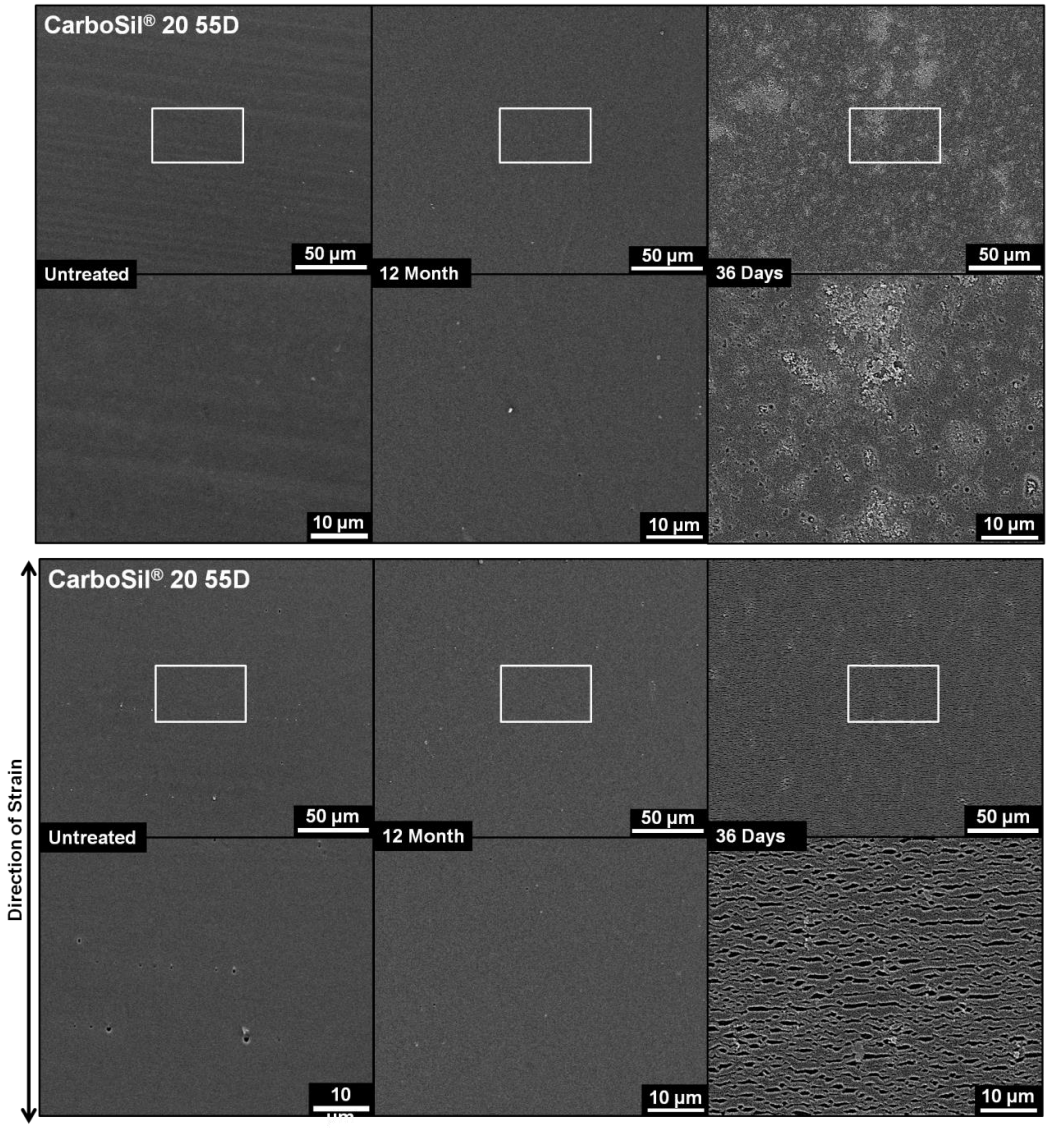

Figure 4.12. Scanning electron micrographs of unstrained and strained to failure CarboSil® 20 55D TSPCU specimens showing surface damage after 12 months *in vitro* treatment (3% H_2O_2 at 37°C) and 36 days accelerated *in vitro* treatment (0.1 M $CoCl_2$/20% H_2O_2 at 37°C)

the materials following 12 months treatment in the 3% H_2O_2 solution, which falls in line with the minor soft segment loss.

Bionate® 80A PCU exhibited a minor loss in molecular weight similar to its soft segment loss indicating an evenly distributed chain scission throughout the material, **Table 4.5**. Bionate® II 75D PCU exhibited the greatest molecular weight loss after 12 months despite its consistent molecular weight in the accelerated medium and the observed retention of surface chemistry. Though not as severe as the aforementioned PCU, CarboSil® 20 55D TSPCU also showed a greater $\overline{M_W}$ loss in the 3% H_2O_2 medium despite no change in $\overline{M_W}$ after accelerated treatment. The 80A grade TSPCU did exhibit a lower molecular weight loss though no difference was observed between CarboSil® 20 80A and Bionate® 80A grades. Finally, a consistent PDI observed within all six PCUs following 12 months 3% H_2O_2 treatment suggests that the bulk of the materials are changing at the same rate as the surface.

Materials again retained the majority of their uniaxial tensile properties. The ultimate tensile strength of the standard PCU was found to statistically decrease over 12 months which correlates with the small molecular weight changes observed. CarboSil® 20 80A TSPCU was also found to exhibit a small decrease in uniaxial tensile strength, but no changes were observed in the other material properties. Increases in initial secant modulus were observed in all 3 hard grade PCUs which suggests the materials may increase in stiffness following 12 months incubation at body temperature, not due to oxidative degradation.

No significant evidence of erosion was observed on the surface of the PCU materials following 12 months 3% H_2O_2 *in vitro* treatment. Bionate® 80A PCU exhibits no additional surface features not seen on the untreated specimens despite being the only PCU to indicate soft segment loss after exposure to the 3% H_2O_2 solution. The lack of differences in the surface morphology of the PCUs following 12 months incubation does not correlated with previously observed surface pitting after 12 months *in vivo*.

Finally, it should be noted that while these materials are subject to only a 3% H_2O_2 concentration, they are also immersed in a 97% percent water degradation medium. All 6 PCUs were demonstrated to be highly stable, both on the surface and within the bulk, in this *in vitro* testing system. Therefore, it has also been shown that these commercially available SPUs are highly resistant to hydrolytic degradation within the demonstrated time period.

4.3.3 Peroxide Content Level Iodometric titration was performed on both solutions for *in vitro* treatment to quantify any possible changes in hydrogen peroxide levels prior to scheduled solution changes. Levels of H_2O_2 in solutions of 3, 10, and 20% w/v concentration with 0, 0.025, 0.1 and 0.2 M $CoCl_2$ content were monitored after 3 and 7 days to determine ROI production, **Table 4.6**. Percent H_2O_2 lost over incubation time increased with higher ratios of $CoCl_2$ to H_2O_2 concentrations as expected given the effect of the Haber-Weiss reaction.

Table 4.6. Relative percent changes in H_2O_2 content following 3 and 7 days incubation

	3% H_2O_2		10% H_2O_2		20% H_2O_2	
	3 Days	7 Days	3 Days	7 Days	3 Days	7 Days
No $CoCl_2$	+1 ± 5%	+6 ± 3%	+7 ± 7%	+1 ± 12%	-5 ± 7%	+1 ± 3%
0.025 M $CoCl_2$	-42 ± 1%[a]	-52 ± 1%[a]	-14 ± 4%[a]	-13 ± 7%[a]	+1.9 ± 6.9%	-1 ± 1%
0.1 M $CoCl_2$	---	---	-30 ± 7%[a]	-42 ± 3%[a]	-19 ± 3%[a]	-24 ± 1%[a]
0.2 M $CoCl_2$	---	---	-29 ± 7%[a]	-49 ± 1%[a]	-20 ± 6%[a]	-26 ± 8%[a]

(average ± standard deviation; n=3; [a]$p<0.05$ from untreated)

Solutions exposed to varying levels of $CoCl_2$ exhibited significant changes in H_2O_2 content over 3 and 7 days of incubation. Rate of H_2O_2 decomposition was shown to be highly dependent on concentration of $CoCl_2$ and H_2O_2 within the solution. For all solutions with $CoCl_2$ the acceleration effect was far greater within the first 3 days than the remainder of the 7 day period where only a small percentage of additional H_2O_2, if any, was lost. This slowing of ROI production is attributed to the initial consumption of $CoCl_2$ during the first 3 days leaving a lower concentration of metal ions for the final 4 days. In addition, increasing $CoCl_2$ concentration was only found to accelerated H_2O_2 decomposition at lower levels while doubling from 0.1 to 0.2 M concentrations had no significant effect. Overall, the results from the ROI production quantification of the accelerated *in vitro* system in the current study show that relative levels of H_2O_2 concentration are kept within an acceptable steady range throughout the full 36 days.

No significant changes in H_2O_2 content were observed in all three solutions with no $CoCl_2$ in the degradation media indicating that there is no significant decomposition of the molecules during that time period. The lack of change also suggests there were no measurable levels of ROIs produced in the solution during that time period. Furthermore, no significant ROI presence in the 3% H_2O_2 solution provides an explanation for the lack of degradation evidence in all 6 PCUs following 12 months incubation.

4.3.4 In Vivo Treatment Predictability The disparity between results from the accelerated and 3% H_2O_2 *in vitro* systems highlights the need for a discussion on the predictive efficacy of each test method as it relates to biostability. Iodometric titration provided a strong explanation for the difference in the two test methods as only the $CoCl_2$ solution produces ROIs. The initiation of oxidation via hydrogen atom abstraction cannot be completed without the presence of an oxygen radical. Therefore, the 3% method, which was shown to produce no ROIs during a 7 day incubation period, did not expose any of the PCUs to a real physiological environment. The accelerated method was the only testing condition to provide results comparable to in vivo data while the 3% method could not provide a feasible correlation to physiologic degradation.

ATR-FTIR spectroscopy has been used previously to track chemical changes in PEUs, Bionate® and CarboSil® materials from *in vitro* and *in vivo* studies often providing useful comparisons between the two.[190,261,581] The calculated soft segment loss of Bionate® 80A PCU after 36 days accelerated oxidation does not exceed the 12 month data point from previous *in vivo* data,[273] but the results are far more significant than the

3% H_2O_2 system. Furthermore, the degradation rates of these materials were found to be far slower after 12 months 3% H_2O_2 treatment than typical *in vivo* data. In addition to the lack of soft segment loss seen in all of the PCUs, no additional symptoms of substantial degradation were observed including: soft segment crosslinking, hard segment degradation, and surface pitting. The difference in surface changes between the two test methods can be directly attributed to the disparity in ROI production during the incubation periods. In addition, with the exception of molecular weight, all additional materials characterization changes within the 3% H_2O_2 system were attributed more to the length of incubation time than to any oxidative degradation effects. The accelerated degradation testing was found to exhibit results more indicative of known surface oxidative degradation behavior as the media contains ROIs during incubation. It is well established that ROI-mediated degradation is limited to the surface of polyurethanes due to the high reactivity of these radicals. Specifically, more substantial changes were observed in the ATR-FTIR spectra and scanning electron micrographs, while tensile testing and GPC analysis show more subtle, if any, changes to the bulk of the materials. It is important to note the similarities between the accelerated oxidative system and previous *in vivo* data that indicate surface-specific oxidation occurs but without the ESC that caused failure of PEU-based leads. Finally, given that the 3% H_2O_2 method is an aqueous solution, the lack of degradation after 12 months also indicates the hydrolytic stability of these PCU materials.

4.4 Conclusions

All materials were found to exhibit signs of oxidative degradation following 36 days exposure to the accelerated oxidative environment. Minor changes in molecular weight, as indicated by the GPC results and mechanical properties, indicate the bulk properties of all materials were retained following accelerated or 3% H_2O_2 *in vitro* treatment. Furthermore, the lack of cracking seen in all materials following oxidative environment exposure suggests that the PCUs will be resistant to environmental stress cracking. Thus, these materials are all likely to outlast PEUs *in vivo* and should be considered as strong candidates for biostable medical devices. However; the lack of changes observed on the material surfaces in the 12 month group does not correlate with previous *in vivo* results, which suggests the test method does not simulate physiological conditions. The lack of ROI production over the 7 day incubation period raises a significant concern over the efficacy of the 3% H_2O_2 test method. Oxidation of PCUs is not expected to be initiated without the presence of an oxygen radical. Therefore, it can be concluded that the 3% H_2O_2 method does not simulate an oxidative environment previously demonstrated in other *in vitro* tests but demonstrates the hydrolytic stability of these materials after 12 months. Based on the comparison between the two tests with previous *in vivo* results, the accelerated metal ion-catalyzed method should remain the recommended choice for predicting SPU biostability.

CHAPTER V

DEVELOPMENT OF BIODEGRADABLE POLYURETHANE MATERIAL FOR REINFORCING LAYER OF TISSUE ENGINEERING VASCULAR GRAFT

5.1 Introduction

All design modifications/optimizations up to this point have focused on fabricating a long term biostable multilayer graft that properly mimics the behaviors of the surrounding tissue. The limitation with this design approach is it eliminates the potential to restore the vasoactive function of the reinforcing graft. The design of a tissue engineering vascular graft with a biodegradable polyurethane based reinforcing layer would provide a strong opportunity to set up for vasoactivity restoration. Fortunately, the high tunability of polyurethanes is especially useful in designing biodegradable materials as one can readily incorporate biodegradable components into the segmental chemistry. Some examples of biodegradable applications of SPUs include wound dressings,[248,582-588] abdominal wall replacements,[142,250,589] gene vector and vaccine delivery,[160,590-598] oroantral communication closures,[599] ophthalmological devices[197] as well as various tissue engineering applications.[487,600-602]

Linear aliphatic isocyanates such as 1,4-butane diisocyanate (BDI) and 1,6-hexane diisocyanate (HDI)[603] are most commonly used in biodegradable polyurethane formulations. Lysine diisocyanate (LDI) has also been investigated with the assumption that its lysine-based chemistry will yield safe carboxylic byproducts.[500] Unfortunately, these compounds often have lower tensile strengths (~30 MPa)[604] than aromatic SPU

products such as Biomer™ and Pellethane™ (~50 MPa).[605] Despite the promising cytocompatibility of these materials along with other linear isocyanates such as isophorone diisocyanate (IPDI)[253,606,607] and 4,4'-dicyclohexylmethane diisocyanate (H12MDI),[195,608-610] these aliphatic polyurethanes do not match the mechanical properties of their aromatic counterparts.

In order to generate a resorbable polyurethane with enhanced mechanical properties and safe degradation products, novel aromatic and biodegradable isocyanates were recently developed by Bezwada Biomedical.[611] Briefly, several aromatic isocyanates were synthesized with amino phenols, amino salicylic acids, and amino benzoic acids that are expected to degrade via hydrolysis into non-toxic byproducts.[611] DSM Biomedical, in collaboration with Bezwada Biomedical, synthesized a poly(ester urethane) (PEsU) with an aromatic hard segment based on glycolic acid and a polycaprolactone soft segment to investigate the potential of these novel aromatic PEsU for biomedical applications. In this study, we present the initial characterization of this PEsU and the accelerated hydrolytic degradation profile after four weeks *in vitro*.

5.2 Materials and Methods

5.2.1 Materials A commercially available poly(ether urethane urea) (PEUU), BioSpan® 80A, and the resorbable PEsU were synthesized by DSM Biomedical (Berkeley, CA) and supplied in 24 wt% and 20 wt% N,N'-dimethylacetamide (DMAC, Sigma Aldrich, Milwaukee, WI) solutions, respectively. PEsU and PEUU films were solvent cast from 10 wt% DMAc solutions and dried under vacuum at ambient

temperature until all solvent was removed. Specimens of dimensions 30 mm x 5.5 mm x 0.25 mm were cut from dried films and used in characterization and degradation studies.

5.2.2 In Vitro Biodegradation PEUU and PEsU specimens (n = 4) were immersed in phosphate buffer saline (PBS) or 0.1M sodium hydroxide (NaOH) solution to promote hydrolysis at an accelerated rate. Solutions were kept at a constant 37°C with mild agitation for up to four weeks. Degradation medium was changed every week and specimens removed for characterization. Specimens were rinsed with deionized water and dried overnight under vacuum to remove residual water prior to analysis.

5.2.3 Gravimetric Analysis Gravimetric analysis was performed by weighing specimens before immersion and then following cleaning and drying procedures to determine mass loss due to erosion. Percent change in mass was calculated for each specimen using the equation below:

$$\%Change = \frac{m - m_0}{m_0} x100\% ,$$

where m = mass of degraded specimen and m_0 = initial mass of specimen.

5.2.4 Chemical Analysis Changes in bulk and surface chemistry were observed using transmission and attenuated total reflectance (ATR)-Fourier transform infrared (FTIR) spectroscopy, respectively. Transmission-FTIR specimens were prepared by dissolving specimens in dilute solutions with DMAC and solution cast onto clean potassium bromide (KBr) pellets under vacuum until all solvent was removed. Spectra were recorded with a Bruker Tensor 27 FTIR spectrometer (Billerica, MA). ATR-FTIR was performed using a PikeTech multi-reflectance ATR Max II (Madison, WI) position

at a 45° incident angle and equipped with a 45° germanium crystal. All spectra were normalized to the 1602 cm^{-1} peak corresponding to the C=C bond stretch of the aromatic ring located in both hard segments.

5.2.5 Uniaxial Tensile Properties Dogbone specimens cut to ASTM D1708 standard (n=5) were used to investigate the uniaxial tensile properties before and after *in vitro* degradation. Following cleaning and drying, specimens were strained at a rate of 10 mm/min to failure using an Instron 3345 equipped with air-pneumatic tensile grips (Norwood, MA). Tensile stress values were calculated and plotted versus percent elongation. Initial (2%) secant modulus, tensile strength, and ultimate elongation were then calculated from the resulting curves. Percent recovery was measured after specimens were strained to failure. Briefly, permanent deformation, ΔL, of each fractured specimen was measured using the following equation:

$$\Delta L = L_f - L_0,$$

where L_f is the gauge length of the fractured specimen and L_0 is the original gauge length. Percent recovery was then calculated using the following equation:

$$Percent\ Recovery = \left(1 - \frac{\Delta L}{extension}\right)\ x\ 100\%$$

5.2.6 Calorimetric Analysis Differential scanning calorimetry (DSC) was used to characterize thermal transitions in the polyurethanes (melting temperature (T_m) and glass transition temperature (T_g)) as well as changes in polymer crystallinity. Polyurethane specimens of approximately 5 mg in hermetic pans were first cooled to -80°C and then heated to 80°C at a heating rate of 5°C/min using a TA Instruments Q2000 DSC (New Castle, DE). Changes in heat flow during the first scan were recorded

and plotted as a function of time. Transition temperatures were marked on the resulting DSC thermograms and enthalpy changes (ΔH) were calculated from the area of the melting peak. The percent crystallinity (% χ_c) was calculated from the equation:

$$\% \chi_c = \frac{\Delta H_m}{\Delta H_m^0} \times 100$$

where ΔH_m^0 is 139.5 J/g for 100% crystalline PCL.[612]

5.2.7 Molecular Weight Analysis Changes in molecular weight and molecular weight distribution were monitored using gel permeation chromatography (GPC). Briefly, specimens were dissolved in N,N'-dimethylformamide (DMF) with 0.1 M lithium bromide (LiBr) (Sigma Aldrich, Milwaukee, WI) at concentrations of approximately 5 mg/mL. GPC solutions were subject to vigorous stirring at 80°C for 24 hours to ensure elimination of hydrogen bonding. Specimens were put through a GPCMax (Viscotek, Malvern, PA) equipped with two Phenomenex columns with pores measuring 10^3 and 10^5 Å in diameter. DMF with 0.05 M LiBr at a flow rate of 1.0 mL/min at 60°C was used as an eluent and refractive index response was used as detection. OmniSEC software was calibrated using a set of narrow conventional calibration standards composed of polystyrene at known molecular weights of approximately 10, 50, 100, 300, 500, 800, and 1000 kDa (Agilent Technologies, Santa Clara, CA). Weight average molecular weight (M_w) and polydispersity index (PDI) were calculated and reported as average ± standard deviation.

5.2.8 Surface Damage Scanning electron microscopy (SEM) was used to analyze the surface topography of PEsU and PEUU before and after 4 weeks degradation. An Au/Pd layer of approximately 200-300 Å was deposited on all

specimens prior to imaging to increase conductivity. A JEOL 7500F field emission-SEM (FE-SEM) was used to image the specimens with a 2 kV acceleration voltage and 8mm working distance. Images were taken at magnitudes of 250X and 2000X to highlight both low and high magnification of surface topography features.

5.2.9 Cell Viability Viability analysis of 3T3 fibroblasts on solvent casted PEsU and PEUU films was conducted using the Live/Dead® Assay (Molecular Probes) to determine material cytocompatibility in comparison to tissue culture polystyrene (TCPS). NIH/3T3 Swiss mouse fibroblasts were purchased (ATCC-CCL92) and cultured with Dulbecco's Modified Eagle Medium (DMEM-high glucose, GlutaMAX) supplemented with 10% heat-inactivated fetal bovine serum (FBS), and 1% penicillin-streptomycin solution (Gibco). Prior to cell seeding, films were subjected to UV irradiation (1 hr per side), an ethanol wetting ladder to increase hydrophilicity, and overnight media incubation (37°C, 5% CO_2) supplemented with 40% v/v FBS in DMEM at 37°C. Following incubation, media was removed, specimens dried in biosafety cabinet for 30 minutes, washed with phosphate buffered saline (PBS), and pre-conditioned with growth media for 15 minutes. Cells were seeded at 5,000 cells/cm^2 and live/dead staining was performed at 24 and 72 hours. Percent cell viability was calculated from manual cell counts of images obtained through rastor patterning of 3 specimens (n = 15) with a fluorescence microscope (Nikon Eclipse TE2000-S).

5.3 Results and Discussion

5.3.1 Initial Characterization Structural features of the PEsU were first examined with infrared spectroscopy. A characteristic ATR-FTIR spectrum of the PEsU film is shown in **Figure 5.1** and was selected for analysis over transmission spectrum to enable assessment of phase morphology. ATR-FTIR peak assignments for the untreated PEsU are detailed in **Table 5.1**. Analysis of structural and morphological aspects of the PEsU revolves around analysis of the carbonyl region of the spectrum from 1800 – 1600 cm^{-1}. There are numerous carbonyls in the PEsU structure including soft segment alkyl esters, hard segment aryl esters, and hard segment urethanes. A complex ester/urethane carbonyl band envelope results from conformational differences between amorphous and ordered phases as well as free and hydrogen bonded carbonyls. Literature reports indicate that carbonyl stretching frequencies are typically lowered in ordered phases including crystalline solids and hydrogen bonding. A strong carbonyl absorbance at 1725 cm^{-1} was attributed primarily to the crystalline polycaprolactone soft segment. The peak shoulder at 1695 cm^{-1} was assigned to the hydrogen-bonded urethane carbonyl based on standard literature assignments;[544] and the peak shoulder at 1762 cm^{-1} was assigned to the aryl ester stretch of the hard segment.[613] The carbonyl band envelope also contained the absorbance band of the free urethane carbonyl at 1730 cm^{-1} and amorphous alkyl ester at 1738 cm^{-1}; however, full deconvolution of these peaks was not possible. The 1602 cm^{-1} peak in the PEsU spectrum was assigned to the C=C stretch of the aromatic ring within the hard segment based on previous assignations of

polyurethanes synthesized with MDI.[544] Similarly, peaks at 1514 cm^{-1} and 1416 cm^{-1} were assigned to C-C stretch in the aromatic ring within the hard segment.[544]

In addition to confirmation of the aromatic nature of the PEsU, assessment of phase morphology using spectral features was conducted. Phase-separated hard domains in polyurethanes are stabilized by hydrogen bonds between hard segments. Therefore, hydrogen bonding of urethanes observed in the infrared spectrum can be used as a means to assess phase morphology.[215] The N-H band at 3325 cm^{-1} observed in the spectrum of the PEsU indicates hydrogen bonding of the urethane hard segment.[544] Multiple hydrogen bonding interactions are possible between the urethane N—H groups and the various carbonyls of both the hard and soft segments. However, the presence of the hydrogen-bonded carbonyl of the urethane at 1695 cm^{-1} indicates that at least a portion of the hydrogen bonding can be attributed to hard domain formation.

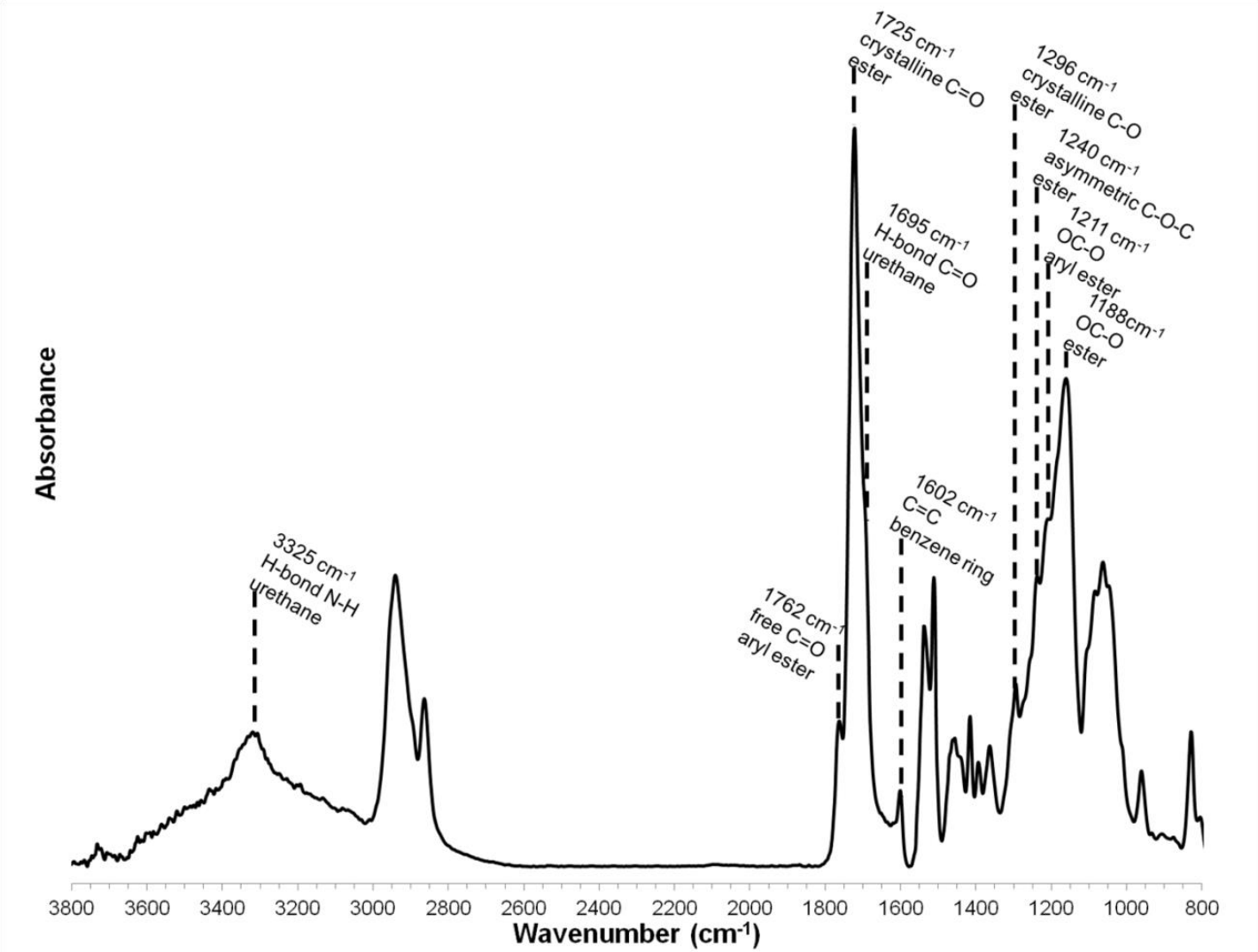

Figure 5.1 ATR-FTIR spectra of untreated PEsU film

Table 5.1. ATR-FTIR peak assignments of untreated PEsU

Wavenumber (cm^{-1})	PEsU Peak Assignment	Reference
3325	H-bonded N-H stretch, urethane	Dillon et al. [544]
2947	asymmetrical CH_2 stretch	Dillon et al. [544]
2870	symmetrical CH_2 stretch	Dillon et al. [544]
1762	C=O stretch, aryl ester	Jaffe et al. [613]
1738(sh)	free amorphous C=O, ester	Skarja et al. [215]
1730(sh)	free C=O stretch, urethane	Dillon et al. [544]
1725	crystalline C=O stretch, ester	Skarja et al. [215]
1714(sh)	H-bonded amorphous C=O stretch, ester	--
1695(sh)	H-bonded C=O stretch, urethane	Dillon et al. [544]
1602	C-C stretch, benzene ring	Dillon et al. [544]
1541	C-N stretch + N-H bend, urethane	Dillon et al. [544]
1514	C-C stretch, benzene ring	Dillon et al. [544]
1459	aliphatic CH_2 bend	Dillon et al. [544]
1416	C-C stretch, benzene ring	Dillon et al. [544]
1396	aliphatic CH_2 wag	David et al. [614]
1366	aliphatic CH_2 wag	David et al. [614]
1296	crystalline C-O and C-C stretch, ester	Elzein et al. [615]
1259(sh)	CH_2 wag	Khosroshahi et al. [616]
1240	asymmetric C-O-C stretch, ester	Elzein et al. [615]
1211	OC-O stretch, aryl ester	--
1188	OC-O stretch, ester	Elzein et al. [615]
1163	symmetric C-O-C stretch, ester	Elzein et al. [615]
1107	symmetrical C-O-C stretch	Dillon et al. [544]
1088(sh)	symmetrical C-O-C stretch, urethane	Dillon et al. [544]
1066	asymmetrical C-O-C stretch, urethane	Dillon et al. [544]
1045	symmetrical C-O-C stretch	Dillon et al. [544]
962	C-H wag, benzene ring	Dillon et al. [544]
829	C-H out of plane bending, benzene ring	Dillon et al. [544]

Thermal transitions in the PEsU were examined with differential scanning calorimetry, **Figure 5.2**. Scans of untreated PEsU indicate a melting transition (T_m) at approximately 45°C and a glass transition temperature (T_g) at -35°C.[617] These transitions are primarily due to the polycaprolactone soft segment and are shifted from commonly reported PCL values of T_g = -60ºC and T_m = 60ºC. These transition temperatures were consistent with the reported values of PCL-based polyurethanes.[215,511] The increase in Tg was attributed to the constraining effect of hard domains and a degree of phase mixing with the more rigid hard segments. The relative degree of phase mixing can be estimated by the increase in Tg from the pure soft segment. Skarja et al. reported a range of phase separation in PCL-based polyurethanes from nearly complete phase separation with a Tg only 8ºC above pure PCL (-52°C) and fully phase mixed with Tg values approaching 0ºC.[215] These reference values indicate that the PEsU in this study had a moderate level of phase separation which is also supported by the infrared spectral evidence of hydrogen bonding of hard segments described above. The depressed melting temperature as compared to PCL was attributed to reduced order of the crystalline domains due to phase mixing with the hard segment. The ability of PCL segments to crystallize in segmented polyurethanes is also impaired by the connection with hard segments and the corresponding decrease in the conformational mobility of the PCL soft segment chains.

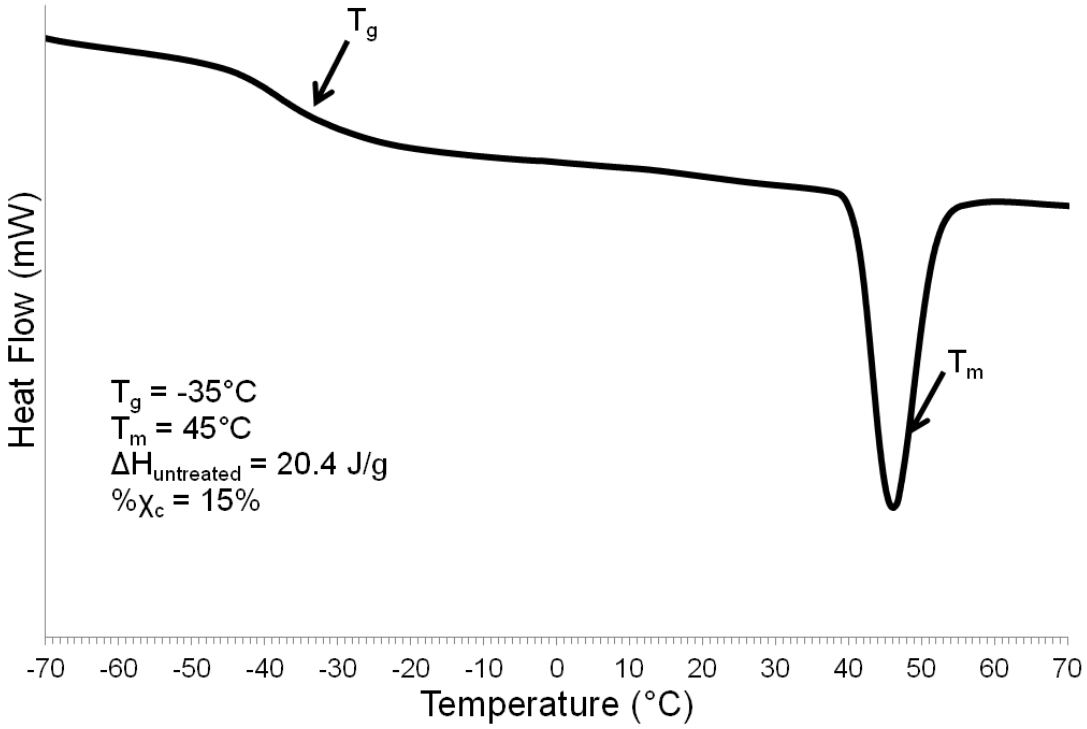

Figure 5.2. DSC thermogram (first scan) of untreated PEsU

The stress–strain behavior of PEsU is typical of a semicrystalline polymer above its T_g, in agreement with the DSC findings, **Figure 5.3**. The PEsU displayed a yield point followed by necking and drawing similar to semicrystalline PCL polyurethanes reported in the literature.[215,511,609,618,619] The PEsU were characterized by 2% secant modulus of 58 ± 5 MPa, tensile strength of 30 ± 3 MPa, and ultimate elongation of 677 ± 7%. The high modulus and tensile strength of PEsU was attributed to the semicrystalline soft segment and high cohesion hard domains. Soft segment crystalline domains are proposed to act as physical crosslinks similar to the traditional description of hard domains in segmental polyurethanes. Several studies have reported enhanced tensile

properties as a function of both increased phase separation and polyester soft segment crystallinity. PEsU outperformed BDI, HMDI and LDI-based SPUs with similar polyol and chain extender chemistries likely due to the contribution of the aromatic isocyanate, **Table 5.2**.[618,619] These enhanced properties is believed to result from the increased hard domain cohesion observed in polyurethanes with aromatic hard segments.[620] A significant amount of permanent set was also observed with percent recovery calculated to be 65 ± 4%. Given the relative high recovery of polyether-based polyurethanes, the permanent set was attributed to the deformation of soft segment crystalline domains.

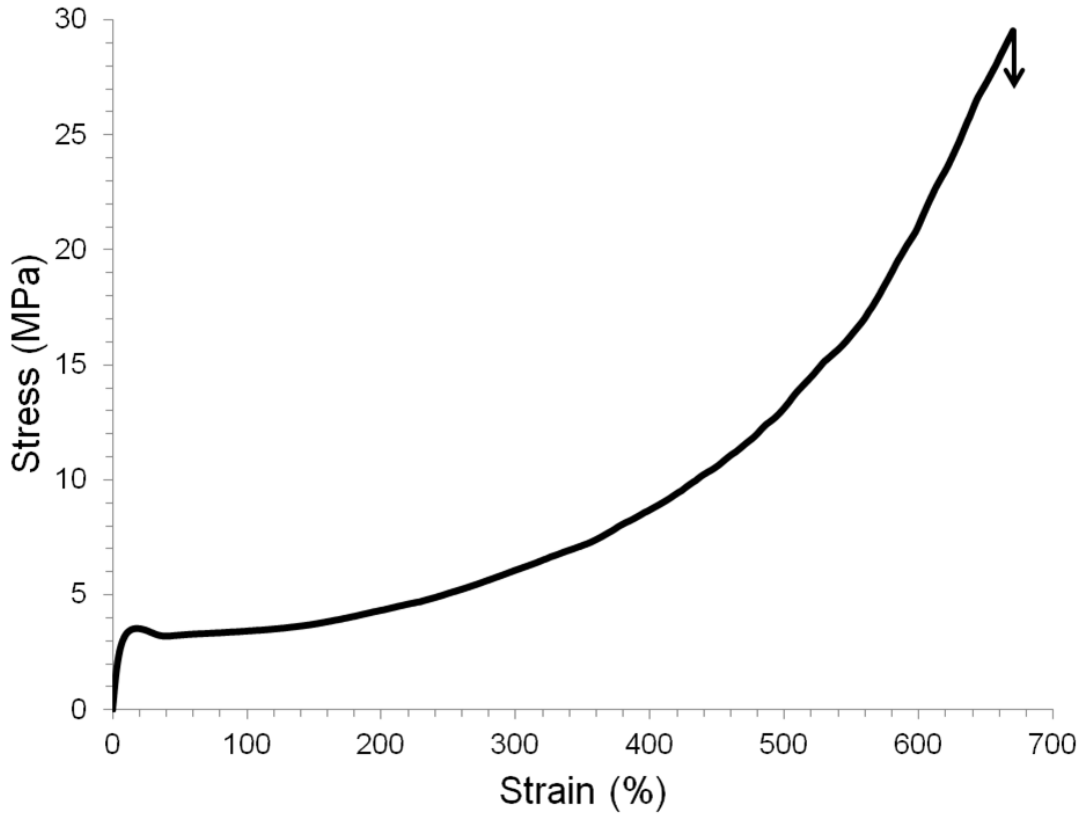

Figure 5.3. Stress-strain plot of untreated PEsU specimen uniaxially loaded at a rate of 10 mm/min to failure

Table 5.2. Comparison of effects of hard and soft segment content and chemistry on material properties poly(ester urethanes) and poly(ester urethane ureas)

Isocyanate	Polyol	Initial Modulus	Tensile Strength	T_g (°C)	T_m (°C)	ΔH_m (J/g)	Percent Crystallinity	Reference
G-E-G-G DI	PCL	58 MPa	30 MPa	-35	45	20.4	15%‡	--
BDI	PCL2000	23 MPa	23 MPa	-54	24, 69	9, 11	6, 8%‡	Spaans et al. [619]
HDI	PCL1250	38 MPa	--	-53	25, 60	16, 2	11, 1%‡	Chiono et al. [621]
HDI	PCL1250	20 MPa	28 MPa	-33	42	47*	35%	Skarja et al. [511], [215]
HDI	PCL2000	20 MPa	28 MPa	-52	45	--	--	Skarja et al. [511]
HMDI	PCL1250	3 MPa	19 MPa	-39	7	--	--	Sarkar et al. [609]

(‡value calculated using method from Zhang et al.[612]) *100% crystallization determined by melting point depression of PCL with ethyl benzoate (32.4 cal/g), ΔH_m value back-calculated

Finally, assessment of 3T3 cell viability on PEsU films after 24 and 72 hours was performed to assess the cytocompatibility of the material as compared to a commercial polyurethane control (PEUU) currently used in biomedical devices, **Figure 5.4**. PEsU cell viability results were comparable to both PEUU and the TCPS control after 24 hours. Similar levels of cell viability after 24 hours was previously reported for aliphatic polyurethanes of similar soft segment and chain extender composition.[506] After 72 hours PEsU films exhibited a small decrease in viability (86 ± 6 %) with PEUU remaining statistically similar to the TCPS control (97 ± 3 %).

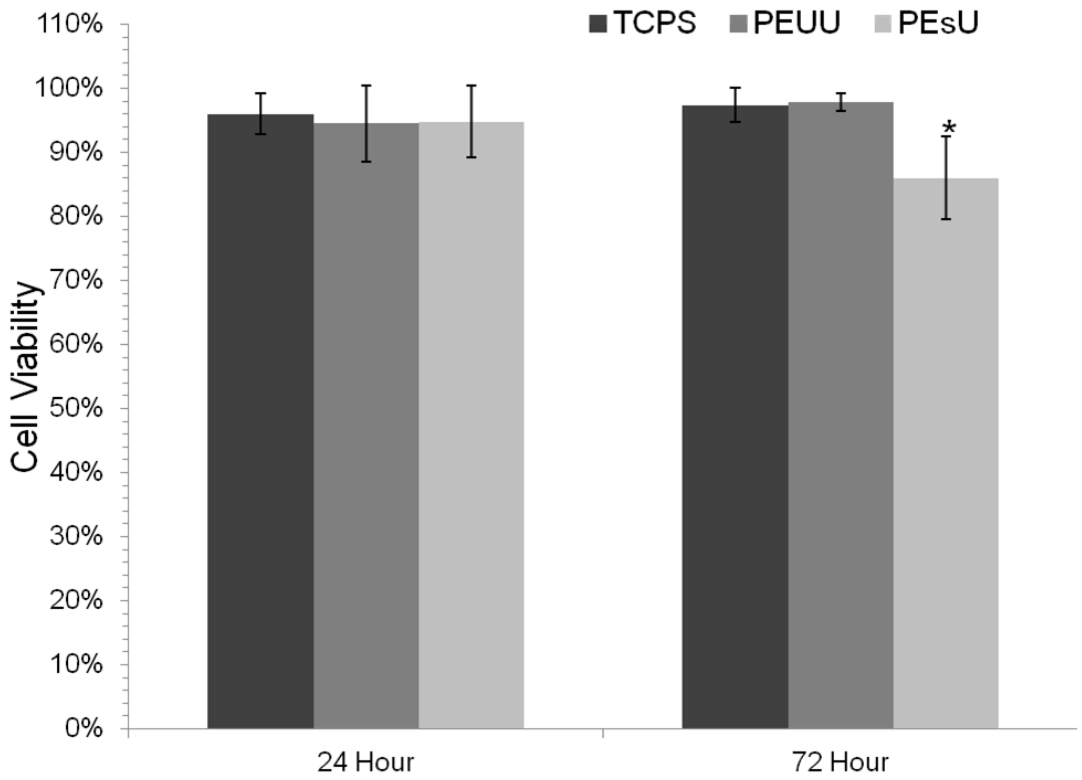

Figure 5.4. Comparison of viable 3T3 mouse fibroblasts (Live/Dead) on tissue culture polystyrene (TCPS), PEsU, and PEUU after 24 and 72 hours.

5.3.2 In Vitro Biodegradation A commercially available poly(ether urethane urea), BioSpan® 80A, was selected as a control for *in vitro* degradation studies due to its established hydrolytic stability. Infrared spectral analysis of surface and bulk chemistry was performed on untreated and treated specimens. Characteristic transmission-FTIR spectra are shown in **Figure 5.5** and indicate minimal changes in the bulk chemistry of the polyurethanes after 4 weeks of accelerated hydrolytic treatment (0.1 M NaOH). In contrast, ATR-FTIR spectra of the PEsU specimens indicated soft and hard segment loss after treatment in PBS and accelerated 0.1M NaOH solutions for 4 weeks, **Figure 5.6.** Closer examination of the carbonyl region of these spectra, **Figure 5.7**, revealed preferential loss of free urethane at 1730 cm^{-1} and reduction of peak heights corresponding to the aryl ester at 1762 cm^{-1}, the amorphous alkyl ester at 1738 cm^{-1}, and hydrogen bonded urethane at 1695 cm^{-1} after incubation in PBS. Complete loss of the aryl ester peaks at 1762 cm^{-1} and 1211 cm^{-1} was observed after accelerated hydrolytic treatment. In contrast to many PCL-based SPUs, these results indicate that the PEsU displayed significant hard segment loss while retaining the crystalline PCL soft segment, as indicated by retention of strong absorbances at 1725 cm^{-1} and 1296 cm^{-1}. [622] This preferential loss of the hard segment prior to the PCL soft segment was attributed to the more hydrolytically labile isocyanate in the PEsU. As expected, no evidence of surface chemistry changes was observed in the spectra of the PEUU specimens after treatment.

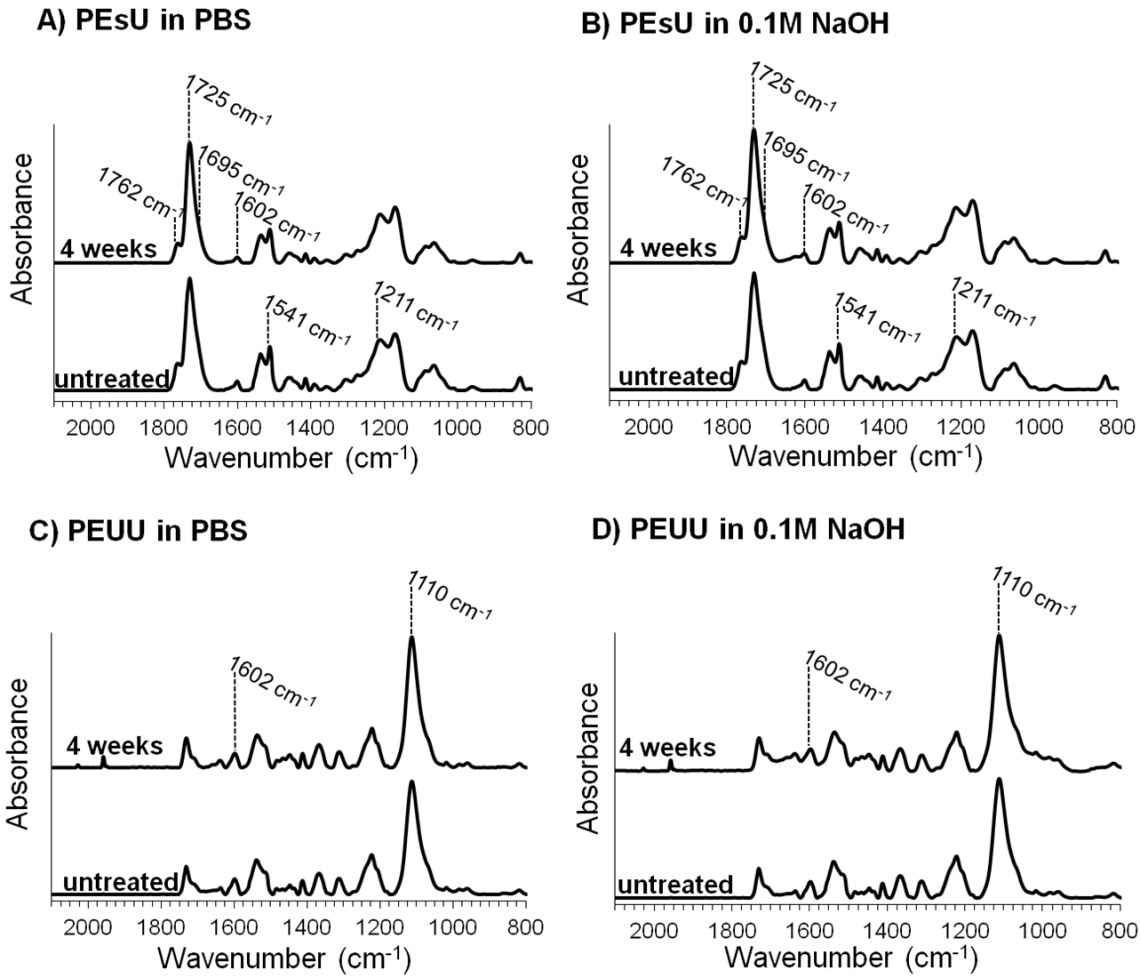

Figure 5.5 Transmission-FTIR spectra of (A) PEsU in PBS, (B) PEsU in 0.1 M NaOH, (C) PEUU in PBS, and (D) PEUU in 0.1 M NaOH before and after *in vitro* hydrolytic degradation.

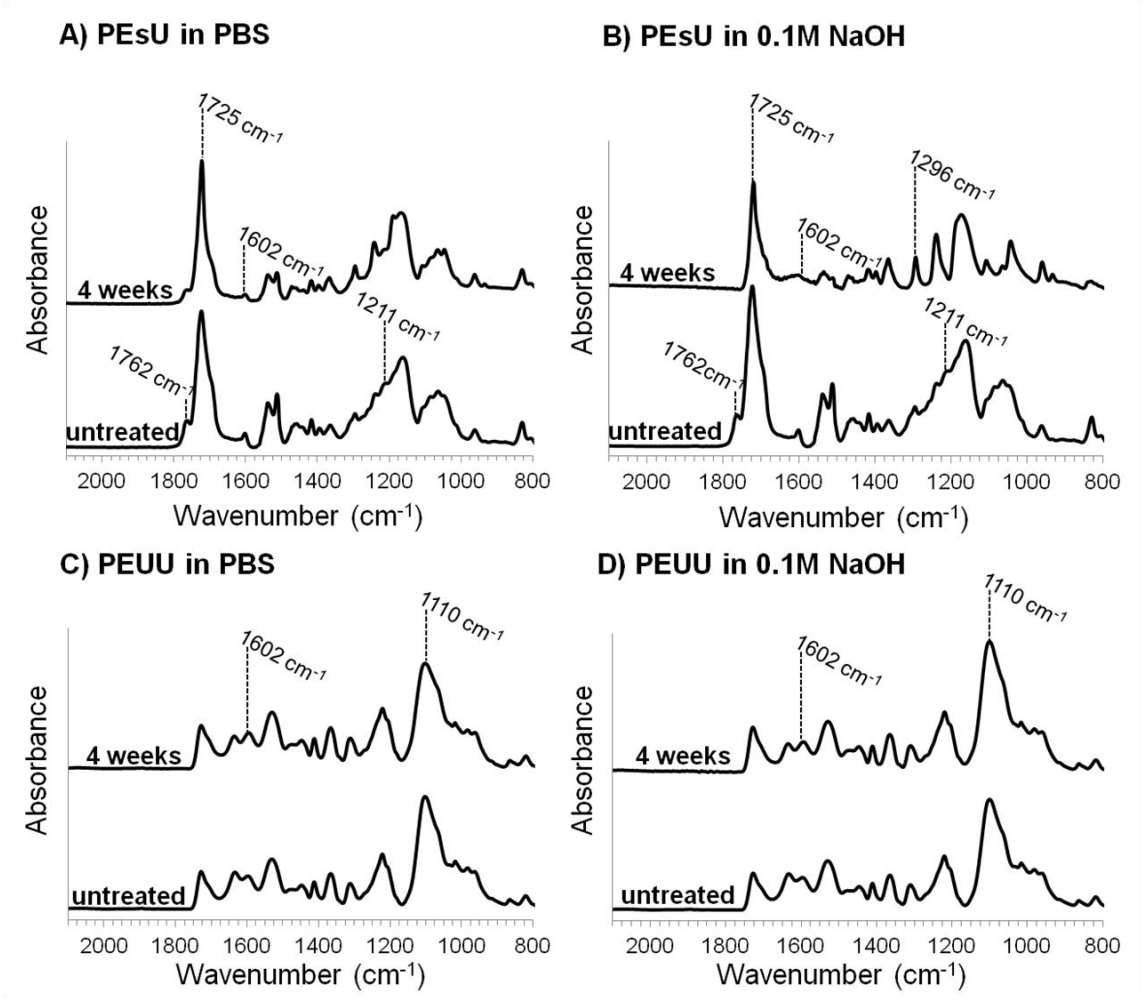

Figure 5.6 ATR-FTIR spectra of (A) PEsU in PBS, (B) PEsU in 0.1 M NaOH, (C) PEUU in PBS, and (D) PEUU in 0.1 M NaOH before and after *in vitro* hydrolytic degradation

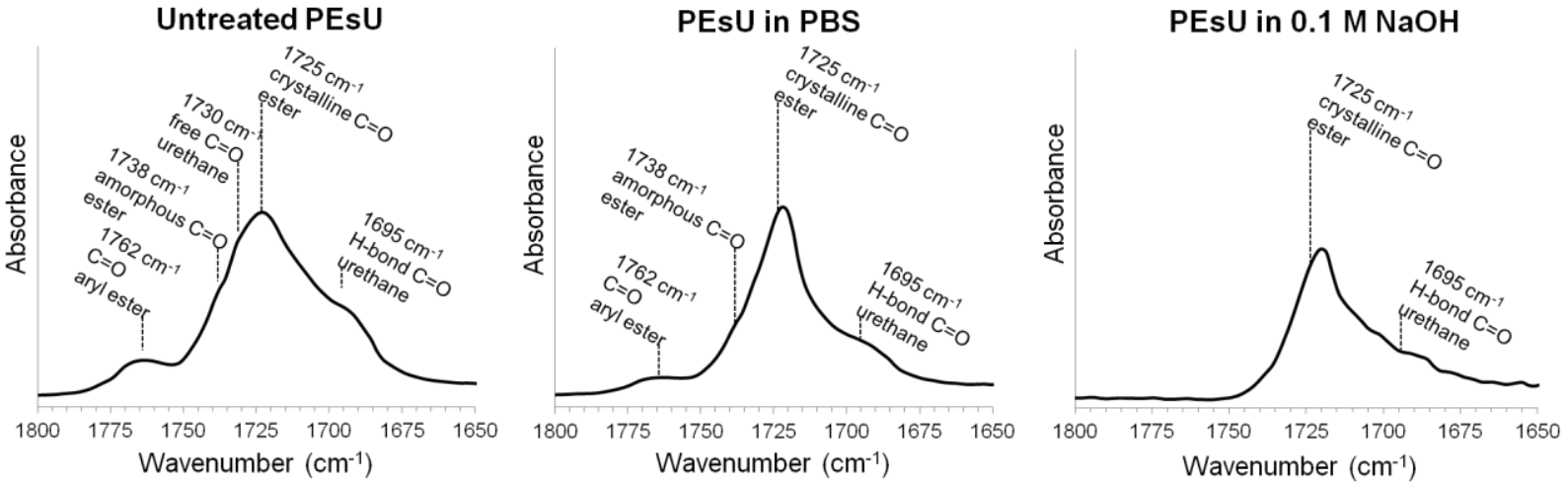

Figure 5.7. Carbonyl stretch region of ATR-FTIR spectra from PEsU specimens in PBS and 0.1 M NaOH before and after *in vitro* hydrolytic degradation.

GPC results indicate substantial loss of PEsU molecular weight (MW) after 4 weeks in both PBS and 0.1M NaOH solutions indicating substantial chain scission, **Figure 5.8**. A reduction of approximately 25% of its initial molecular weight was observed after 4 weeks in PBS, similar to results seen in aliphatic PCL-based polyurethanes.[208] Similar to the infrared findings, the 0.1 M NaOH solution accelerated molecular weight loss of the PEsU to more than double the percent molecular weight loss observed in PBS, ~54%. This result was somewhat surprising given the lack of changes observed in the transmission spectra of treated polyurethane specimens that indicates retention of bulk chemistry. In contrast, the molecular weight of PEUU specimens after 4 weeks was statistically similar to untreated control values indicating resistance to hydrolytic chain scission. Gravimetric analysis indicated that PEsU specimens experienced minor mass loss in PBS, similar to literature reports of the PCL homopolymer.[623] Substantial mass loss (31.3 ± 1.4%) was observed in the accelerated 0.1 M NaOH solution after four weeks, **Table 5.3**. The PEUU specimens showed no significant mass loss in either solution, as expected given the retention of molecular weight.

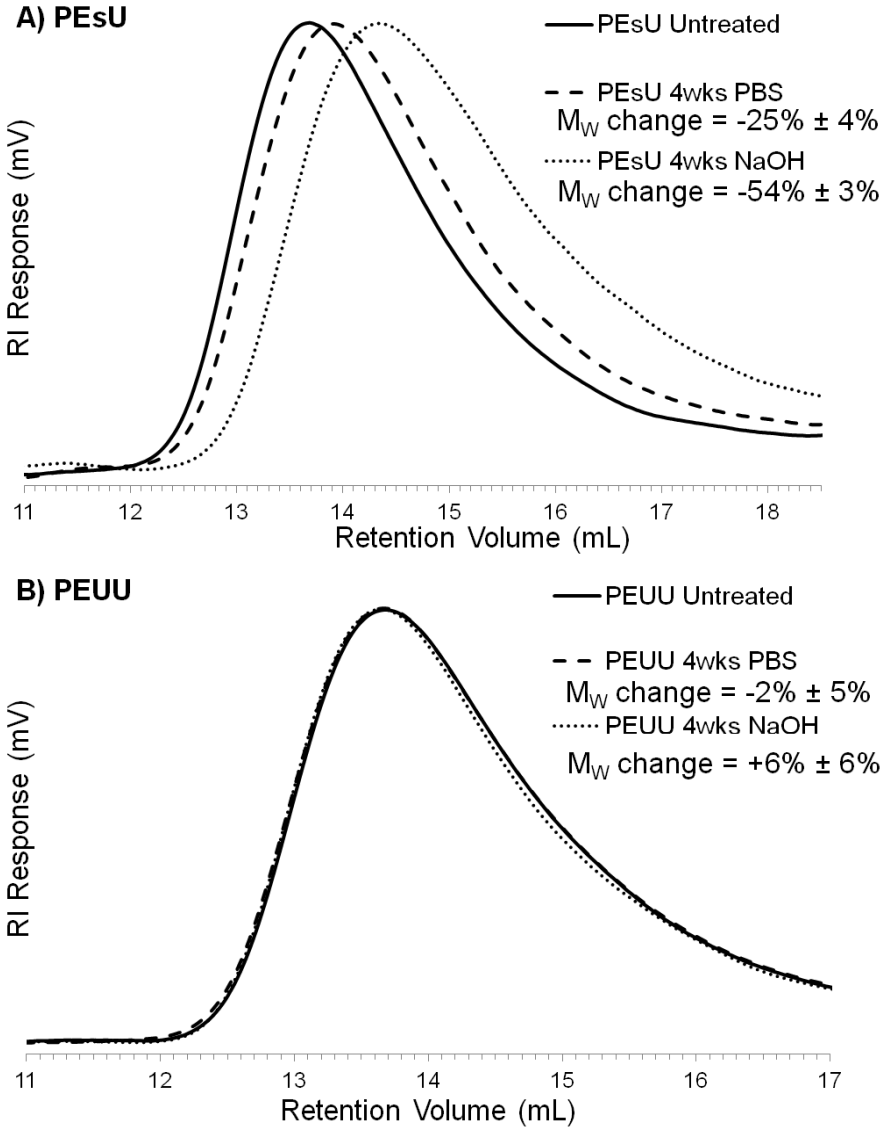

Figure 5.8 GPC Chromatograms of (A) PEsU and (B) PEUU specimens before and after *in vitro* hydrolytic degradation

Table 5.3. Percent mass loss after *in vitro* biodegradation.

	PEsU		PEUU	
	PBS	0.1 M NaOH	PBS	0.1 M NaOH
1 week	3.5 ± 0.1	9.1 ± 0.6	0.8 ± 0.1	0.8 ± 0.1
2 weeks	4.6 ± 0.3	20.7 ± 0.5	0.6 ± 0.2	1.1 ± 1.8
3 weeks	2.8 ± 0.3	25.1 ± 0.5	0.9 ± 0.2	0.8 ± 0.1
4 weeks	5.4 ± 5.3	31.3 ± 1.4	1.0 ± 0.2	0.6 ± 0.7

(average ± standard deviation; n=4)

Scanning electron micrographs revealed increased surface roughness of PEsU specimens incubated in PBS; whereas, specimens incubated in NaOH displayed substantial surface cracking after 4 weeks, **Figure 5.9**. The change in surface roughness is likely an indicator of minor erosion limited mainly to the surface of the material. Specimens immersed in 0.1 M NaOH display more substantial degradation with deep cracking similar to previously reported degradation of PCL-based polyurethanes.[622] This type of "mud-cracking" is representative of a degradation profile where the polymer undergoes chain scission (molecular weight loss) followed by extraction of low molecular weight chains (mass loss). During drying, shrinkage of the degraded surface is constrained by the bulk of the polymer specimen leading to internal stresses that cause non-directional cracking. Finally, no changes were observed in PEUU topography after 4 weeks of accelerated degradation.

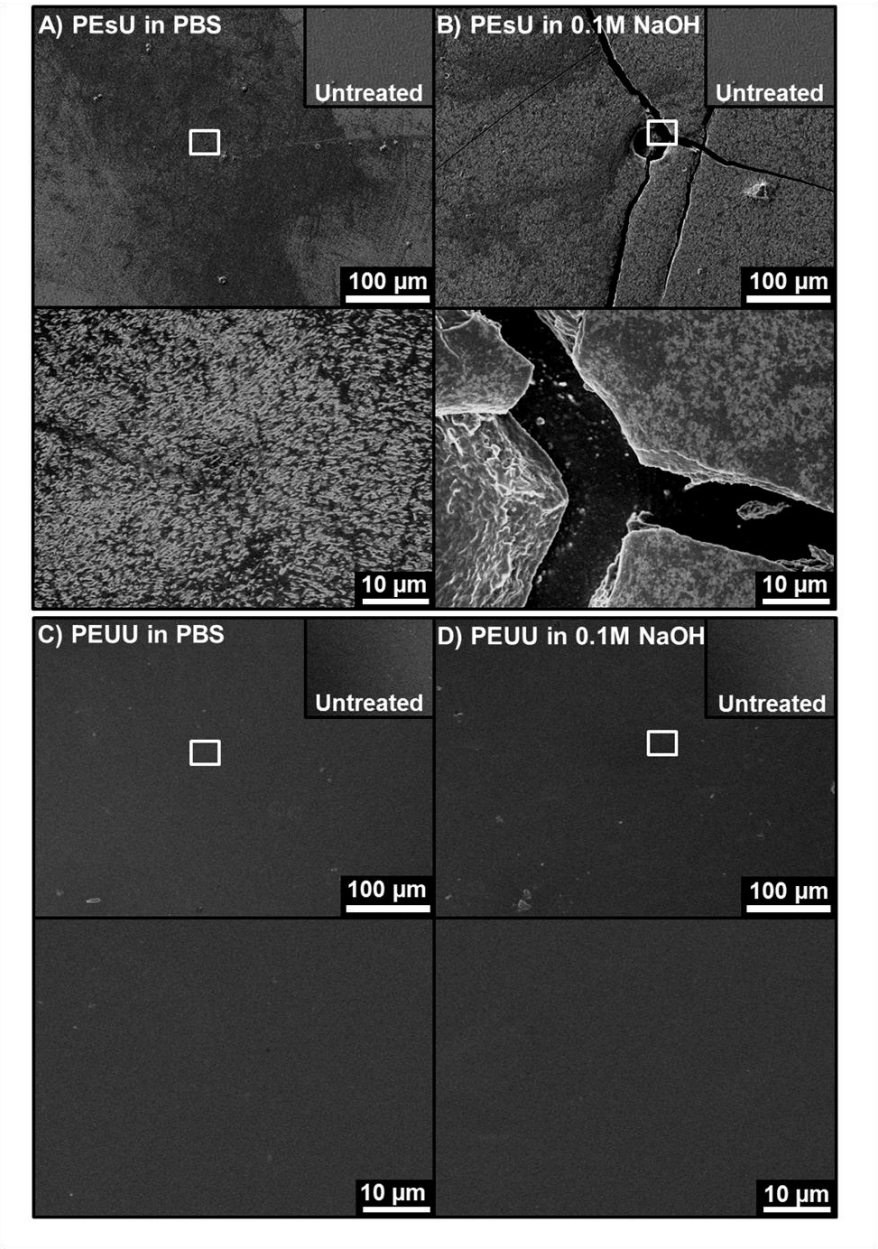

Figure 5.9. Scanning electron micrographs of (A) PEsU in PBS, (B) PEsU in 0.1 M NaOH, (C) PEUU in PBS, and (D) PEUU in 0.1 M NaOH before and after *in vitro* hydrolytic degradation

Uniaxial tensile testing of degraded PEsU specimens showed significant differences in the mechanical responses when compared to the untreated material, **Figure 5.10**. Initial modulus was the most substantial change with a drop from 57 ± 5 MPa to 11 ± 1 and 17 ± 5 MPa for PBS and NaOH specimens, respectively. Tensile strength was also reduced after degradation from 29 ± 3 MPa for untreated specimens to 17 ± 2 MPa for PBS specimens and 15 ± 4 MPa for NaOH specimens. DSC thermographic analysis of both treatment groups revealed significant changes in thermal transitions and crystallinity, **Figure 5.11**. First, a decrease in soft segment Tg was observed in NaOH specimens from -35ºC to -45°C; whereas, minimal changes in Tg were observed in specimens incubated in PBS (-35ºC versus -37ºC). More notably, changes in the soft segment crystallinity were observed in both treatment groups with more significant changes again observed after base accelerated hydrolysis treatment. Untreated specimens had a typical melting transition of 45ºC and a ΔH of 20.4 J/g that corresponded to approximately 15% crystallinity. Treatment in PBS for 4 weeks resulted in a small increase in the melting transition to 49ºC, a significant decrease in percent crystallinity to 7% (ΔH = 8.9 J/g), and a broad cold crystallization peak at 3ºC (ΔH = 1.9 J/g). The NaOH specimens exhibited two melting transitions at $T_{m,1}$ = 28ºC (ΔH_1=10.1 J/g) and $T_{m,2}$ = 58ºC (ΔH_2 = 9.9 J/g) and a more pronounced cold crystallization peak at -1ºC (ΔH = 9.5 J/g). The loss of crystallinity was attributed to soft segment chain scission that was confirmed in infrared and GPC analyses. It is also likely that this chain scission provided greater mobility to the soft segment chains allowing for enhanced order of the remaining crystallites and a corollary increase in melting temperature. These results correlate well

with the infrared findings that indicate that the remaining soft segment was highly crystalline. The cold crystallization was attributed to quenching the polymer from the treatment solution at 37ºC, which is above the melting transition, to -80 ºC in the first DSC scan. The liberated soft segment chains were then able to reorganize during the heating scan to form crystallites of reduced order and lower melting temperature. Overall, the reduced modulus of the PEsU after treatment was attributed to the loss of crystallinity of the PCL soft segment due to hydrolytic chain scission.

5.4 Conclusions

In summary, we have characterized the physical properties of a novel resorbable PEsU synthesized with biodegradable aromatic isocyanates before and after accelerated hydrolytic degradation. Infrared spectral analysis confirmed the aromatic and phase-separated nature of the PEsU. Uniaxial tensile testing displayed stress-strain behavior typical of a semicrystalline polymer above its T_g, in agreement with calorimetric findings. PEsU outperformed aliphatic PCL-based polyurethanes likely due to the enhanced cohesion of the aromatic hard domains. Accelerated degradation of the PEsU using 0.1 M sodium hydroxide resulted in hydrolysis of the polyester soft segment on the surface, reduced molecular weight, surface cracking, and a 30% mass loss after four weeks. Calorimetric studies indicated a disruption of the soft segment crystallinity after incubation which corresponded with a drop in initial modulus of the PEsU. Finally, cytocompatibility testing with 3T3 mouse fibroblasts exhibited good cell viability on PEsU films after 24 hours. Overall, this new resorbable polyurethane exhibits mechanical properties superior to current aliphatic designs along with a favorable

degradation profile making it an ideal candidate for inclusion in a future TEVG multilayer design.

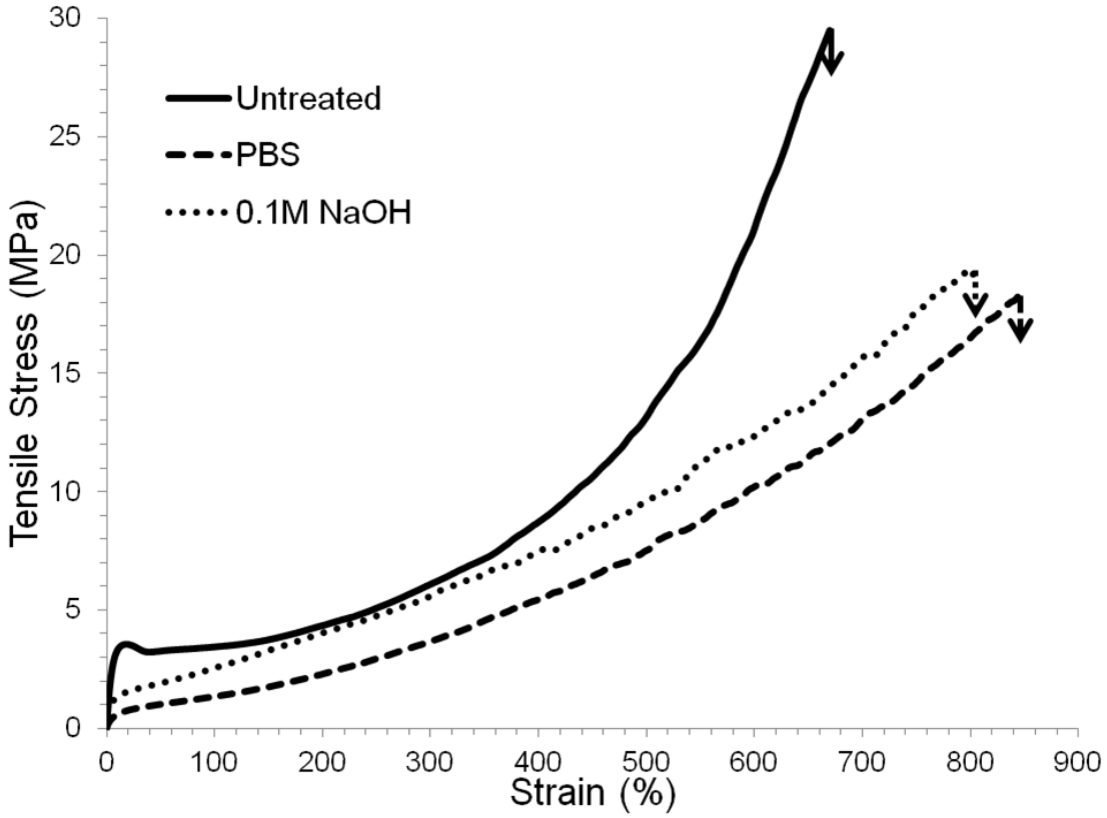

Figure 5.10. Stress-strain plots of PEsU in PBS and PEsU in 0.1 M NaOH before and after 4 weeks *in vitro* hydrolytic degradation uniaxially loaded at a rate of 10 mm/min to failure

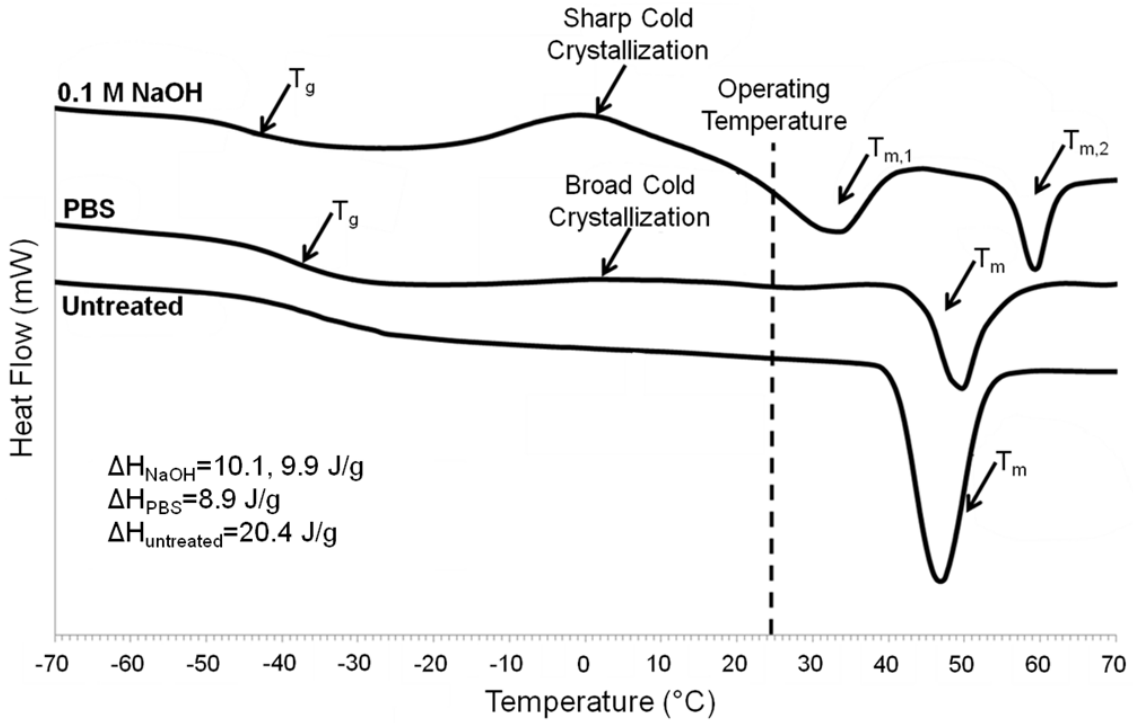

Figure 11. DSC thermograms (first scan) of PEsU in PBS and PEsU in 0.1 M NaOH before and after *in vitro* biodegradation.

CHAPTER VI

CONCLUSIONS

6.1 Summary

In this work, the material properties of various segmented polyurethanes were optimized for use as a reinforcing electrospun layer of a small-diameter multilayer vascular graft. Previous synthetic options lacked the appropriate thromboresistance and matching compliance needed for long term deployment success in small diameter ($d < 6$ mm) applications. The proposed multilayer vascular graft design in this work incorporated an intimal PEG-Scl2-2 hydrogel layer expected to provide thromboresistance and *in situ* rapid endothelialization which would prevent acute graft occlusion. An electrospun thermoplastic polyurethane reinforcing layer was then employed to provide the requisite biomechanical properties and biostability needed for ensured long term success *in vivo*. The feasibility of the multilayer vascular graft design was confirmed with successful multilayer graft integrity testing and acute *in vivo* success of early prototypes. The initial success then prompted further investigation into optimizing the material characteristics of the electrospun reinforcing layer.

Compliance matching was a key functional requirement of the reinforcing vascular graft layer to ensure high long term patency rates by preventing intimal hyperplasia. Current synthetic options and early SPU vascular graft designs often provide burst pressure exceeding the current saphenous vein properties but lack sufficient compliance to ensure long term success. Investigation into the semi-IPN

approach detailed in this work provided improved biomechanical properties of the electrospun graft. Furthermore, the required heat treatment to synthesize the silicone network within the semi-IPN chemistries had a beneficial annealing effect on grafts composed of only the PCU component. To the best of our knowledge, no synthetic small diameter graft with compliance and burst pressure values that simultaneously exceeded saphenous vein biomechanical properties had been previously reported.

In addition to compliance matching and burst pressure maintenance, the long term biostability of the reinforcing layer needed to be optimized. The *in* vitro oxidative stability of several commercially available PCUs was investigated using both the established accelerated metal ion oxidation protocol and the ISO 10993 physiological rate protocol. The demonstrated biostability of all of the PCU samples showed long term resistance to environmental stress cracking ensuring high probability of implantation success. Furthermore, the accelerated *in vitro* oxidation method was the only treatment which produced data comparable to previously reported *in vivo* studies making it the favorable protocol over the ISO 10993 method.

In addition to biostable designs, we have characterized a novel biodegradable aromatic PEsU for a new tissue engineered vascular graft design which allows for restoration of graft vasoactivity. Along with improved initial mechanical properties over previous aliphatic biodegradable SPU designs, this PEsU was expected to degrade into safe degradation byproducts. Favorable initial cytocompatibility testing and resultant degradation made it a promising choice for future tissue engineering vascular graft designs and other biomedical devices.

6.2 Significance of Work

Segmented polyurethanes already remain a prominent material selection choice for biomedical device designs due to excellent mechanical properties, fatigue strength, as well as their established bio and hemocompatibility. The high tunability of these materials stemming from their known microphase morphology allows for favorable tailoring of the reinforcing layer of our multilayered vascular graft. The added benefit of electrospinning gave further control over graft architecture which provided compliance and burst pressure values comparable to reported autologous saphenous graft properties. These resultant properties then allowed for strong initial multilayer graft integrity testing results and promising acute *in vivo* porcine model testing studies. The initial findings from these feasibility studies then prompted investigation into further optimizing the reinforcing layer of the multilayer vascular graft design.

In Chapter 3, we addressed the problem associated with the inverse relationship between compliance and burst pressure of previous synthetic options including several polyurethane-based designs. To the best of our knowledge, no prior art had presented a synthetic option capable of matching compliance while simultaneously providing sufficient burst pressure. Using our proposed semi-IPN approach, we were able to simultaneously improve the compliance and burst pressure of our electrospun grafts over reported saphenous vein properties. Additional investigation into the effect of the heating cycle for covalent network formation exposed an added beneficial annealing effect on the polyurethane component resulting in improved pure PCU biomechanical

properties. The improved compliance and burst pressures of these electrospun samples shows promise in ensuring long term patency of our multilayer grafts.

In Chapter 4, the biostability of the materials potentially used for the reinforcing layer of our vascular graft was explored to ensure long term performance of the electron meshes. The effects of modulating polycarbonate soft segment chemistry, soft segment content, and silicone modification were all limited to surface characterizations like ATR-FTIR spectroscopy and SEM, the bulk of all 6 materials were found to be unaffected. While ensuring biostability of these grafts is always important, the predictive capabilities of the *in vitro* test methods employed in this work were also evaluated. Using an iodometric titration method to quantify changes in H_2O_2 content, the accelerated method was the only *in vitro* treatment found to produce reactive oxygen intermediates. The lack of changes in H_2O_2 levels within the 3% H_2O_2 system were then found to be the root cause of no degradation evidence in any of the materials after 12 months despite previous *in vivo* data within the same time frame. Base on this work, the metal ion accelerated method should be considered as the superior treatment system for predicting oxidative stability of SPUs.

In Chapter 5, we explored the option of a biodegradable reinforcing electrospun layer as part of a tissue engineered vascular graft design intended to restore vasoactivity instead of mimicking autologous graft properties. Biodegradable SPU formulations have typically been limited to aliphatic designs due to concerns over carcinogenic aromatic degradation byproducts. The aromatic PEsU intended for use in our design contained a biodegradable hard segment expected to degrade into safe byproducts while providing

superior mechanical properties. Early cytocompatibility testing along with a strong favorable degradation profile and novel electrospun patterning techniques make this PEsU very promising for future biodegradable TEVG designs along with other biomedical devices.

Overall, the demonstrated tunability of segmented polyurethanes makes them strong candidates for the electrospun reinforcing layer of our multilayer graft design. The improved biomechanics from the heat treatment and semi-IPN approach provide strong confidence in long term patency of our grafts. In addition, the demonstrated biostability ensures long term functional capabilities of our grafts without failure due to ESC. Furthermore, the structure-property relationship knowledge gained from these studies allows for future SPU reinforcing layer component designs with superior biomechanical properties, biostability or even biodegradability.

6.3 Challenges and Future Directions

Although this work shows strong promise in the areas of matching graft properties and biostable/biodegradable graft designs, there are still several questions that need to be addressed moving forward. Given the demonstrated effect of heat treatment on electrospun grafts, prolonged exposure to temperatures higher than typical room temperatures needs to be explored. In this work, longer heat treatments of several grafts showed further improved microphase separation but more severe effects on graft architecture ultimately resulting in reduced compliance. Our grafts will be subject to a mild heat treatment throughout the entire implantation period which could potentially

affect material properties and/or graft architecture over time. Therefore long term exposures to heat under static and pulsatile flows should be investigated in future studies.

In addition to heat treatment effects, only initial mechanical properties were explored in this study. Effects of prolonged cyclic loading over an approximated implantation period should be explored to monitor potential changes in graft properties due to fatigue. Given fatigue strength is expected to stay high with a polyurethane-based reinforcing layer, this effect could be presumed to be minimal however, electrospinning has already been demonstrated to alter SPU microphase morphology. Therefore, fatigue strength of these electrospun grafts can also be changed.

The PCUs investigated in this work all demonstrated strong resistance to oxidation and low potential for failure due to ESC. The PEsU investigation was also shown to have a favorable degradation profile for tissue engineering graft designs. However all these *in vitro* tests were performed on melt-extruded or solvent cast films, not electrospun grafts. A highly porous graft such as the reinforcing fibrous mesh in our multilayer design, provides a much higher surface to volume ratio than neat films which could accelerate degradation rates further. Effects of architecture would need to be explored along with changes in material chemistry of these grafts.

Finally, all *in vitro* testing was also performed on grafts in only static conditions. Given that our multilayer grafts will be subject to a consistent pulsatile loading cycle, the reinforcing layer of our design should be tested in a bioreactor that provides both the degradation media as well as presumed cyclic loading. The designed bioreactor setup is

expected to better provide a more physiological environment than our current static degradation setups.

While this work may appear to be extensive and complex, the potential knowledge gained from these future studies could allow for more advanced insight into graft structure property relationships. Thus future multilayer vascular graft design are expected include further improved biomechanical properties, potentially enhanced biostability, and even greater control over biodegradation for vasoactivity restoration. Overall, the results from the proposed work are expected to provide a clearer path towards a greater chance of long term implantation success from the next generation of multilayer vascular grafts.

REFERENCES

1. Heart disease and stroke statistics--2011 update: a report from the American Heart Association. Circulation 2011;123:e18-e209.
2. Rosamond W, Flegal K, Furie K, Go A, greenlund K, haase N, Hailpern SM, Ho M, Howard V, Kissela B and others. Heart disease and stroke statistics -- 2008 update: a report from the American Heart Association Statistics Committee and Stroke statistics Subcommittee. Circulation 2008;117(4):e25-146.
3. Sharma PK, Vyawahare NS, Ladhha A. Preclinical screening models for hypertension in rodents: a review. Pharmacologyonline 2010;3:458-472.
4. Falk E. Pathogenesis of atherosclerosis. Journal of the American College of Cardiology 2006;47(8 Suppl C):C7-12.
5. Carter AM. Inflammation, thrombosis and acute coronary syndromes. Diabetes & Vascular Disease Research 2005;2(3):113-121.
6. Darling RC, Linton RR. Durability of femoropopliteal reconstructions: Endarterectomy versus vein bypass grafts The American Journal of Surgery 1972;123(4):472-479.
7. Williams S. Tissue engineered vascular grafts: from bench to clinical use. FASEB 2000;14(A):305.
8. Axthelm S, Porter J, Strickland S, Baur G. Antigenicity of venous allografts. Annals of Surgery 1979;189(3):290-293.
9. Carpenter J, Tomaszewski J. Human saphenous vein allograft bypass grafts: Immune response. Journal of Vascular Surgery 1998;27(3):492-499.

10. Iaffaldano RA, Lewis BE, Johnson SA, Piffare R, McKieman TL. Patency of cryopreserved saphenous vein grafts as conduits for coronary artery bypass surgery. CHEST 1995;108:725-729.

11. Dosluoglu HH, Kittredge J, Cherr GS. Use of cryopreserved femoral vein for in situ replacement of infected femorofemoral prosthetic artery bypass. Vascular and Endovascular Surgery 2008;42(1):74-78.

12. Lamm P, Juchem G, Milz S, Schuffenhauer M, Reichart B. Autologous endothelialized vein allograft: A solution in the search for small-caliber grafts in coronary artery bypass graft operations Circulation 2001;104:I108-I114.

13. Salacinski H, Goldner S, Giudiceandrea A, Hamilton G, Seifalian A. The mechanical behavior of vascular grafts: a review. Journal of Biomaterials Applications 2001;15:241-278.

14. Kinley C, Marble A. Compliance: a continuing problem with vascular grafts. J Cardiovasc Surg 1980;21:163-170.

15. Clowes A. Intimal hyperplasia and graft failure. Cardiovsac Pathol 1993;2(3):179S-186S.

16. Stewart SFC, Lyman DJ. Effects of a vascular graft/natural artery compliance mismatch on pulsatile flow Journal of Biomechanics 1992;25(3):297-310.

17. Ballyk P, Walsh C, Butany J, Ojha M. Compliance mismatch may promote graft-artery intimal hyperplasia by altering suture-line stresses. Journal of biomechanics 1998;31:229-237.

18. Weinberg CB, Bell E. A blood vessel model constructed from collagen and cultured vascular cells. Science 1986;231:397-400.

19. Niklason LE, Gao J, Abbott WM, Hirschi KK, Houser S, Marini R, Langer R. Functional arteries grown in vitro. Science 1999;284(489-493).

20. Ziegler T, Nerem RM. Tissue engineering of a blood vessel: regulation of vascular biology by mechanical stresses. Journal of Cellular Biochemistry 1994;56:204-209.

21. Kanda K, Matsuda T. In vitro reconstruction of hybrid arterial media with molecular and cellular orientations. Cell Transplantation 1994;3:537-545.

22. Seliktar D, Black RA, Vito RP, Nerem RM. Dynamic mechnical conditioning of collagen-gel blood vessel constructs induces remodeling in vitro. Annals of Biomedical Engineering 2000;28:351-362.

23. Matthews J, Wnek G, Simpson D, Bowlin G. Electrospinning of collagen nanofibers. Biomacromolecules 2002;3:232-238.

24. Yannas I. Natural Materials. In: Ratner B, Hoffman AS, Schoen FJ, Lemmons JE, editors. Biomaterials science: an introduction to materials in medicine. San Diego: Elsevier; 2004. p 127-136.

25. Boland E, Matthews J, Pawlowski K, Simpson D, Wnek G, Bowlin G. Electrospinning collagen and elastin: preliminary vascular tissue engineering. Frontiers in Bioscience 2004;9:1422-1432.

26. Venkatraman S, Boey F, Lao LL. Implanted cardiovascular polymers: natural, synthetic and bio-inspired. Progress in Polymer Science 2008;33:853-874.

27. Eiberg JP, Roder O, Stahl-Madsen M, Eldrup N, Qvarfordt P, Laursen A, Greve M, Florenes T, Nielsen OM, Seidelin C and others. Fluropolymer-coated dacron versus PTFE grafts for femorofemoral crossover bypass: randomised trial. European Journal of Vascular and Endovascular Surgery 2006;32(4):431-438.

28. Parsson H, Jundzill w, Johansson K, Jonung T, Norgren L. Healing characteristics of polymer-coated or collagen-treated Dacron grafts: an experimental porcine study. Cardiovascular Surgery 1994;2:242-248.

29. Sreerekha PR, Krishnan LK. Cultivation of endothelial progenitor cells on fibrin matrix and layering on Dacron/polytetrafluoroethylene vascular grafts. Artifical Organs 2006;30:242-249.

30. Granke K, Ochsner JL, McClugage SG, Zdrahal P. Analysis of graft healing in a new elastomer-coated vascular prosthesis. Cardiovascular Surgery 1993;1:254-261.

31. Hake U, Gabbert H, Iversen S, jakob H, Schmiedt W, Oelert H. Evaluation of the healing of precoated vascular Dacron prostheses. Landgenbeck's Archives of Surgery 1991;376:323-329.

32. Grigioni AM, Daniele C, D'Avenio G, Barbaro V. Biomechanics and hemodynamics of grafting. In: Tura A, editor. Vascular grafts: experiment and modelling. Boston, MA: WIT Press; 2003. p 41-82.

33. Lee JM, Wilson GJ. Anisotropic tensile viscoelastic properties of vascular graft materials at low strain rates. Biomaterials 1986;7:423-431.

34. Cameron BL, Suchida HT, Connall TP, Nagae T, Furukawa K, Wilson SE. High porosity PTFE improves endothelialization of arterial grafts without increasing early thrombogenicity. Journal of Cardiovascular Surgery 1993;34:281-285.

35. Akers DL, Du YH, Kempscinksi RF. The effect of carbon coating and porosity on early patency of expanded polytetrafluoroethylene grafts: an experimental study. Journal of Vascular Surgery 1993;18:10-15.

36. Kohler TR, Stratton JR, Kirkman TR, Johansen KH, Zierler BK, Cloves AW. Conventional high porosity polytetrafluoroethylene grafts: clinical evaluation. Surgery 1992;112:901-907.

37. Bacourt F. Prospective randomized study of carbon-impregnated polytetrafluroethylene grafts for below the knee popliteal and distal bypass: results at 2 years. Annals of Vascular Surgery 1997;11:596-603.

38. Kapfer X, Meichelboeck W, Groegler FM. Comparison of carbon-impregnated and standard ePTFE prostheses in extra-anatomical anterior tibial artery bypass: a proscpective randomized multicenter study. European Journal of Vascular and Endovascular Surgery 2006;32:155-168.

39. Kannan R, Salacinski H, Butler P, Hamilton G, Seifalian A. Current status of prosthetic bypass grafts: a review. Journal of Biomedical Materials Research Part B: Applied Biomaterials 2005;74B(1):570-581.

40. Greisler HP, Cziperle DJ, Kim DU, Garfield JD, Petsikas D, Murchan PM, Applegren EO, Drohan W, Burgess WH. Enhanced endothelialization of

expanded polytetrafluroethylene grafts by fibroblast growth factor type 1 pretreatment. Surgery 1992;112:244-255.

41. Walpoth BH, Zammaretti P, Cikirikcioglu M, Khabiri E, Djebaili MK, Pache J-C, Tille J-C, Aggoun Y, Morel D, Kalangos A and others. Enhanced thickening of expanded polytetrafluroethylene grafts coated with fibrin or fibrin-releasing vascular endothelial growth factor in the pig carotid artery interposition model. The Journal of Thoracic and Cardiovascular Surgery 2007;133:1163-1170.

42. Lelah MD, Cooper SL. Polyurethanes in Medicine. Boca Raton, FL: CRC Press; 1986.

43. Anderson JM, Hiltner A, Wiggins MJ, Schubert MA, Collier TO, Kao WJ, Mathur AB. Recent advances in biomedical polyurethane biostability and biodegradation. Polymer International 1998;46(3):163-171.

44. Stokes K, McVenes R, Anderson JM. Polyurethane elastomer biostability. Journal of Biomaterials Applications 1995;9(4):321-354.

45. Santerre JP, Woodhouse K, Laroche G, Labow RS. Understanding the biodegradation of polyurethanes: from classical implants to tissue engineering materials. Biomaterials 2005;26:7457-7470.

46. Lamba NMK, Woodhouse KA, Cooper SL. Polyurethanes in Biomedical Applications. Boca Raton, FL: CRC Press LLC; 1998. 277 p.

47. Tiwari A, Cheng K, Salacinski HJ, Hamilton G, Seifalian AM. Improving compliance at peripheral arterial and cardiovascular anastomosis: the effect of

suture materials and techniques. European Journal of Vascular and Endovascular Surgery 2003;25:325-329.

48. Christenson EM, Anderson JM, Baer E, Hiltner A. Relationship between nanoscale deformation process and elastic behavior of polyurethane elastomers. Polymer 2005;46(25):11744-11754.

49. Silver FH, Snowhill PB, Foran DJ. Mechanical behavior of vessel wall: a comparative study of aorta, vena cava, and carotid artery. Annals of Biomedical Engineering 2003;31:793-803.

50. Polmanteer KE. Silicone rubber, its development and technological progress. Rubber Chemistry and Technology 1988;61(3):470-502.

51. Quinn KJ, Courtney JM. Silicones as biomaterials. British Polymer Journal 1988;20(1):25-32.

52. Devanathan T, Young KA. Effect of postcuring on hemocompatibility of silicone rubber. Biomaterials, Medical Devices, and Artificial Organs 1981;9(3):225-230.

53. Arkles B, Redinger P. In: Szycher M, editor. Biocompatible Polymers, Metals, and Composites. Lancaster, PA: Technomic; 1983.

54. Abbasi F, Mirzadeh H, Katbab A-A. Modification of polysiloxane polymers for biomedical applications: a review. Polymer International 2001;50:1279-1287.

55. Yang CZ, Li C, Cooper SL. Synthesis and characterization of polydimethylsiloxane polyurea-urethanes and related zwitterionomers. Journal of Polymer Science, Part B: Polymer Physics 1991;29(1):75-86.

56. Li C, Yu X, Speckhard TA, Cooper SL. Synthesis and properties of poly(cyanoethylmethylsiloxane) polyurea urethane elastomers: a study of segmental compatibility. Journal of Polymer Science, Part B: Polymer Physics 1988;26(2):315-317.

57. Yu X, Nagarajan MR, Li C, Gibson PE, Cooper SL. Poly(chloropropylmethyl-dimethylsiloxane)-polyurthane elastomers: synthesis and properties of segmented copolymers and related zwitterionomers. Journal of Polymer Science, Part B: Polymer Physics 1986;24(12):2681-2702.

58. McMillan CR. Elastomers for biomedical applications. Rubber Chemistry and Technology 1994;67(3):417-446.

59. Karabanova LV, Mikhalovska SV, Lloyd AW, Boitex G, Sergeeva LM, Novikova TI, Lutsyk ED, Meikle S. Gradient semi-interpenetrating polymer networks based on polyurethane and poly(vinyl pyrrolidone). Journal of Materials Chemistry 2005;5(4):499-507.

60. Hsieh KH, Liao DC, Chem CY, Chiu WY. Interpenetrating polymer networks of polyurethane and maleimide-terminated polyurethane for biomedical applications. Polymers for Advanced Technologies 1996;7(4):265-272.

61. Karabanova LV, Lloyd AW, Mikhalovsky SV, Helias MPGJ, Rose SF, Mikhalovska L, Boiteux G, Sergeeva LM, Lutsyk ED, Svyatyna A. Polyurethane/poly(hydroxyethyl methacrylate) semi-interpenetrating polymer networks for biomedical applications. Journal of Materials Science: Materials in Medicine 2006;17(12):1283-1296.

62. Lu Y, Zhang L. Interfacial structure and properties of regenerated cellulose films coated with superthin polyurethane/benzoyl konjac glucomannan coating. Industrial & engineering Chemistry research 2002;41(5):1234-1241.

63. Teoh SH, Tang ZG, Ramakrishna S. Development of thin elastomeric composite membranes for biomedical applications. Journal of Materials Science 1999;10(6):343-352.

64. Zhang S, Feng Y, Zhang L, Sun J, Xu X, Xu Y. Novel interpenetrating networkswith shape-memory properties. Journal of Polymer Science, Part A: Polymer Chemistry 2007;45(5):768-775.

65. Reddy TT, Kano A, Maruyama A, Hadano M, Takahara A. Thermosensitive transparent semi-interpenetrating polymer networks for wound dressing and cell adhesion control. Biomacromolecules 2008;9(4):1313-1321.

66. Reddy TT, Kano A, Maruyama A, Hadano M, Takahara A. Synthesis and characterization of semi-interpenetrating polymer networks based on polyurethane and N-isopropylacrylamide for wound dressing. Journal of Biomedical Materials Research, Part B: Applied Biomaterials 2009;88B(1):32-40.

67. Reddy TT, Takahara A. Simultaneous and sequential micro-porous semi-interpenetrating polymer network hydrogel films for drug delivery and wound dressing applications. Polymer 2009;50(15):3537-3546.

68. Jones DS, Bonner MC, Gorman SP, Akay M, Keane PF. Sequential polyurethane-poly(methyl methacrylate) interpenetrating polymer networks as

ureteral biomaterials: mechanical properties and comparative resistance to urinary encrustation. Journal of Materials Science: Materials in Medicine 1997;8(11):713-717.

69. Nair PD, Krishnamurthy VN. Polyurethane-poly(methyl methacrylate). Journal of Applied Polymer Science 1996;60(9):1321-1327.

70. Shin YC, Han DK, Kim YH, Kim SC. Antithrombogenicity of hydrophilic polyurethane-hydrophobic polystyrene IPNs. I. Synthesis and characterization. Journal of Biomaterials Science, Polymer Edition 1994;6(2):195-210.

71. Shin YC, Han DK, Kim YH, Kim SC. Antithrombogenicity of hydrophilic polyurethane-hydrophobic polystyrene IPNs. II. In vitro and ex vivo studies. Journal of Biomaterials Science, Polymer Edition 1994;6(3):281-295.

72. Hill GA, Frisch KC, Sendijarevic V, Wong SW; Interpenetrating polymer networks for contact lens production. U.S. patent 5674942. 1997.

73. Lim D, Kulkarni CL, Repella DA; Hydrophilic polymers and contact lenses made therefrom patent 4536554. 1985.

74. Liu WL; Novel silicon-containing interpenetrating polymer networks. U.S. patent 4618644. 1986.

75. Neefe CW; Method of making a contact lens material which may be identified. U.S. patent 4632773. 1986.

76. Tighe BJ, Gee HJ; Hydrogel-forming polymeric materials. U.S. patent 4430458. 1984.

77. Arkles B; Curable silicone containing compositions and methods of making same. U.S. patent 4500688. 1985.

78. Arkles B; Curable silicone semi-interpenetrating polymer networks and methods of making same. U.S. . U.S. Patent patent 4714739. 1987.

79. Arkles B. Plastics in a qworld Economy, Proceedings of the 42nd Annual technical Conference. New Orleans: Society of Plastics Engineers; 1984. p 1080.

80. Arkles B. Plastics in a World Economy, Proceedings of the 42nd Annual Technical Conference. New Orleans: Society of Plastics Engineers; 1984. p 486.

81. Soldani G, Losi P, Bernabei M, Burchielli S, Chiappino D, Kull S, Briganti E, Spiller D. Long term performance of small-diameter vascular grafts made of a poly(ether)urethane-polydimethylsiloxane semi-interpenetrating polymeric network. Biomaterials 2010;31:2592-2605.

82. Martz H, Beaudoin G, Paynter R, King M, Marceau D, Guidoin R. Physiochemical characterization of a hydrophilic microporous polyurethane vascular graft. Journal of Biomedical Materials Research 1987;21(3):399-412.

83. Hayashi K, Takamizawa K, Saito T, Kira K, Hiramatsu K, Kondo K. Elastic properties and strength of a novel small-diameter, compliant polyurethane vascular graft. Journal of Biomedical Materials Research 1989;23(A2 Suppl):229-44.

84. Eberhart A, Zhang Z, Guidoin R, Laroche G, Guay L, De La Faye D, Batt M, King MW. A new generation of polyurethane vascular prostheses: rara avis or ignis fatuus? Journal of Biomedical Materials Research 1999;48(4):546-558.

85. Tan EPS, Ng SY, Lim CT. Tensile testing of a single ultrafine polymeric fiber. Biomaterials 2005;26(13):1453-1456.

86. McKee M, Park T, Unal S, Yilgor I, Long T. Electrospinning of linear and highly branched segmented poly(urethane urea)s. Polymer 2005;46:2011-2015.

87. Taylor G. Disintegration of water drops in an electric field. Proceedings of the Royal Society of London. Series A, Mathematical and Physical Sciences 1964;280(1382):383-397.

88. Andrews KD, Hunt JA, Black RA. Technology of electrostatic spinning for the production of polyurethane tissue engineering scaffolds. Polymer International 2008;57(2):203-210.

89. Bashur CA, Shaffer RD, Dahlgren LA, Guelcher SA, Goldstein AS. Effect of fiber diameter and alignment of electrospun polyurethane meshes on mesenchymal progenitor cells. Tissue Engineering, Part A 2009;15(9):2435-2445.

90. Borg E, Frenot A, Walkenstrom P, Gisselfalt K, Gretzer C. Electrospinning of degradable elastomeric nanofibers with various morphology and their interaction with human fibroblasts. Journal of Applied Polymer Science 2008;108(1):491-497.

91. Caracciolo PC, Thomas V, BVohra YK, Buffa F, Abraham GA. Electrospinning of novel biodegradable poly(ester urethane)s and poly(ester urethane urea)s for soft tissue-engineering applications. Journal of Materials Science: Materials in Medicine 2009;20(10):2129-2137.

92. Chen R, Ke KEQ, Mo X. Preparation and study of TPU/collagen complex nanofiber via electrospinning. American Association of Textile Chemists and Colorists 2010;10(2):59-63.

93. Chen R, Qiu L, Ke Q, He C, Mo X. Electrospinning thermoplastic polyurethane-contained collagen nanofibers for tissue-engineering applications. Journal of Biomaterials Science, Polymer Edition 2009;20(11):1513-1536.

94. Courtney T, Sacks MS, Stankus J, Guan J, Wagner WR. Design and analysis of tissue engineering scaffolds that mimic soft tissue mechanical anisotropy. 27 2006;19(3631-3638).

95. Dempsey DK, Schwartz CJ, Ward RS, Iyer AV, Parakka JP, Cosgriff-Hernandez EM. Micropatterning of electrospun polyurethane fibers through control of surface topography. Macromolecular Materials and Engineering 2010;295(11):990-994.

96. Erdodi G, Kang J, yalcin B, Cakmak M, Rosenthal kS, Grundfest-Broniatowski S, Kennedy JP. A novel macroencapsulating immunoisolatory device: the preparation and properties of nanomat-reinforced amphiphilic co-networks deposited on perforated metal scaffold. Biomedical Microdevices 2009;11(1):297-312.

97. Heldt D, Stachelek S, Levy R, Ko F. Electrospinning of segmented polyurethane-urea for use as a tissue engineered scaffold. Polymer Preprints 2003;44(2):126-127.

98. Henry JA, Simonet M, Pandit A, Neuenschwander P. Characterization of a slowly degrading biodegradable polyesterurethane for tissue engineering scaffolds. Journal of Biomedical Materials Research Part A 2007;82A(3):669-679.

99. Jeon HJ, Kim JS, Kim TG, Kim JH, Yu W-R, Youk JH. Preparation of poly(ε-caprolactone)-based polyurethane nanofibers containing silver nanoparticles. Applied Surface Science 2008;254(18):5886-5890.

100. Kang WM, Cheng BW, Li QX, Zuo FF. Novel antibacterial nanofibers of chitosan and polyurethane prepared by electrospinning. Advanced Materials Research 2011;150-151:1452-1456.

101. Liu J, Kuhn HG, Jing Y, Dahlberg J-O, Ericsson L, Nilsson A, Nyberg L, Ohady B, Svensson J, Carlberg B and others. Stem cell growth and migration on nanofibrous polymer scaffolds and micro-fluidic channels on silicon-chip. 2009. p 1080-1085.

102. Meng J, Kong H, Han Z, Wang C, Zhu G, Xie S, Xu H. Enhancement of nanofibrous scaffold of multiwalled carbon nanotubes/polyurethane composite to the fibroblasts growth and biosynthesis. Journal of Biomedical Materials Research Part A 2008;88A(1):105-116.

103. Milleret V, Simonet M, Bittermann AG, Neuenschwander P, Hall H. Cyto- and hemocompatibility of a bidoegradable 3D-scaffold material designed for medical applications. Journal of Biomedical Materials research, Part B: Applied Biomaterials 2009;91B(1):109-121.

104. Parrag IC, Woodhouse KA. Development of biodegradable polyurethane scaffolds using amino acid and dipeptide-based chain extenders for soft tissue engineering. Journal of Biomaterials Science, Polymer Edition 2010;21(6-7):843-862.

105. Rabolt JF. Electrospun polymer nanofibers and nanospheres for drug delivery and tissue engineering scaffolds. 2005; New Brunswick, NJ.

106. Raghunath J, Zhang H, Edirisinghe MJ, Darbyshire A, Butler PE, Seifalian AM. A new biodegradable nanocomposite based on polyhedral oligomeric silsequioxane nanocages: cytocompatibility and investigation into electrohydrodynamic jet fabrication techniques for tissue-engineered scaffolds. Biotechnology and Applied Biochemistry 2009;52(1):1-8.

107. Rockwood DN, Woodhouse KA, Fromstein JD, Chase DB, Rabolt JF. Characterization of biodegradable polyurethane microfibers for tissue engineering. Journal of Biomaterials Science, Polymer Edition 2007;18(6):743-758.

108. Shah PN, Manthe RL, Lopina ST, Yun YH. Electrospinning of tyrosine polyurethanes for potential biomedical applications. Polymer 2009;50(10):2281-2289.

109. Stankus JJ, Freytes DO, Badylak SF, Wagner WR. Hybrid nanofibrous scaffolds from electrospinning of a synthetic biodegradable elastomer and urinary bladder matrix. Journal of Biomaterials Science, Polymer Edition 2008;19(5):635-652.

110. Stella JA, Liao J, Hong Y, David Merryman W, Wagner WR. Tissue-to-cellular level deformation coupling in cell micro-integrated elastomeric scaffolds. Biomaterials 2008;29(22):3228-3236.

111. Stella JA, Wagner WR, Sacks MS. Scale-dependent fiber kinematics of elastomeric electrospun scaffolds for soft tissue engineering. Journal of Biomedical Materials Research Part A 2010;93A(3):1032-1042.

112. Thandavamoorthy S, Gopinath N, Ramkumar SS. Self-assembled honeycomb polyurethane nanofibers. Journal of Applied Polymer Science 2006;101(5):3121-3124.

113. Truong YB, Glattauer V, Lang G, Hands K, Kyratzis IL, Wekmeister JA, Ramshaw JAM. A comparison of the effects of fibre alignment of smooth and textured fibres in electrospun membranes on fibroblast cell adhesion. Biomedical Materials 2010;5(2):025005/1-025005/7.

114. Wagner WR, Guan J, Hong Y, Stankus JJ, Ramaswami P, Ma Z. Biodegradable thermoplastic elastomer synthesis and processing for improved biofunctionality. PMSE Preprints 2008;98:326.

115. Wang F, Li Z, Tamama K, Sen CK, Guan J. Fabrication and characterization of prosurvival growth factor releasing, anisotropic scaffolds for enhanced mesenchymal stem cell survival/growth and orientation. Biomacromolecules 2009;10(9):2609-2618.

116. Yang L, Kandel RA, Chang G, Santerre JP. Polar surface chemistry of nanofibrous polyurethane scaffold affects annulus fibrosus cell attachmet and

early matrix accumulation. Journal of Biomedical Materials Research Part A 2009;91A(4):1089-1099.

117. Yao C, Li X, Neoh KG, Shi Z, Kang ET. Surface modification and antibacterial activity of electro-spun polyurethane fibrous membranes with quaternary ammonium moieties. Journal of Membrane Science 2008;320(1+2):259-267.

118. Yeganegi M, Kandel RA, Santerre JP. Characterization of a biodegradable electrospun polyurethane nanofiber scaffold: mechanical properties and cytotoxicity. Acta Biomaterialia 2010;6(10):3847-3855.

119. Amitai G, Andersen J, Wargo S, Asche G, Chir J, Koepsel R, Russell AJ. Polyurethane-based leukocyte-inspired biocidal materials. Biomaterials 2009;30(33):6522-6529.

120. Chen J-P, Chiang Y. Bioactive electrospun silver nanoparticles-containing polyurethane nanofibers as wound dressings. Journal of Nanoscience and Nanotechnology 2010;10(11):7560-7564.

121. Chen Y, Yan L, Yuan T, Zhang Q, Fan H. Asymmetric polyurethane membrane with in situ-generated nano-TiO_2 as wound dressing. Journal of Applied Polymer Science 2011;119(3):1532-1541.

122. Kampeerapappun P. The design, characteristics, and application of polyurethane dressings using the electrospinning process. Akron, OH: University of Akron; 2008. 185 p.

123. Khil M-s, Cha D-i, Kim H-y, Kim I-s, Bhattarai N. Electrospun nanofibrous polyurethane membrane as wound dressing. Journal of Biomedical Materials research, Part B: Applied Biomaterials 2003;67B(2):675-679.

124. Kim SE, Heo DN, Lee JB, Kim JR, Park SH, Jeon SH, Kwon IK. Electrospun geltain/polyurethane blended nanofibers for wound healing. Biomedical Materials 2009;4(4):044106/1-044106/11.

125. Lakshman LR, Shalumon KT, Nair SV, Jayakumar R, Nair SV. Preparation of silver nanoparticles incorporated electrospun polyurethane nano-fibrous mat for wound dressing. Journal of Macromolecular Science, Part A: Pure and Applied Chemistry 2010;47(10):1012-1018.

126. Melaiye A, Sun Z, Hindi K, Milsted A, Ely D, Reneker DH, Tessier CA, Youngs WJ. Silver(I)-imidazole cyclophane gem-diol complexes encapsulated by electrospun tecophilic nanofibers: formation of nanosilver particles and antimicrobial activity. Journal of the American Chemical Society 2005;127(7):2285-2291.

127. Wu J, Hou S, Ren D, Mather PT. Antimicrobial properties of nanostructured hydrogel webs containing silver. Biomacromolecules 2009;10(9):2686-2693.

128. Lee CH, Shin HJ, Cho IH, kang Y-M, Kim IA, Park K-D, Shin J-W. Nanofiber alignment and direction of mechanical strain affect the ECM production of human ACL fibroblast. Biomaterials 2004;26(11):1261-1270.

129. Liao I-C, Leong KW. Efficacy of engineered FVIII-producing skeletal muscle enhanced by growth factor-releasing co-axial electrospun fibers. Biomaterials 2011;32(6):1669-1677.

130. Liao I-C, Liu JB, Bursac N, Leong KW. Effect of electrochemical stimulation on the maturation of myotubes on aligned electrospun fibers. Cellular and Molecular Bioengineering 2008;1(2-3):133-145.

131. Liu KL, Choo ESG, Wong SY, Li X, He CB, Wang J, Li J. Designing Poly[(R)]-3hydroxybutyrate]-based polyurethane block copolymers for electrospun nanofiber scaffolds with improved mechanical properties and enhanced mineralization capability. Journal of Physical Chemistry B 2010;114(22):7489-7498.

132. Nirmala R, Nam KT, Navamathavan R, Park S-J, Kim HY. Hydroxyapatite mineralization on the calcium chloride blended polyurethane nanofiber via biomimetic method. Nanoscale Research Letters 2010;6(1):1-8.

133. Riboldi SA, Sadr N, Pigini L, Neuenschwander P, Simonet M, Mognol P, Sampaolesi M, Cossue G, Mantero S. Skeletal myogenesis on highly orientated microfibrous polyesterurethane scaffolds. Journal of Biomedical Materials Research Part A 2008;84A(4):1094-1101.

134. Riboldi SA, Sampaolesi M, Neuenschwander P, Cossu G, Mantero S. Electrospun degradable polyesterurethane membranes: potential scaffolds for skeletal muscle tissue engineering. Biomaterials 2005;26(22):4606-4615.

135. Bhide M. Controlled release of nitric oxide from electrospun nanofiber transdermal matrices. 2003; Chicago, IL.

136. Coneski PN, Nash JA, Schoenfisch MH. Nitric oxide-releasing electrospun polymer microfibers. ACS Applied Materials & Interfaces 2011;3(2):426-432.

137. Kenawy E-R, Abdel-Hay FI, El-Newehy MH, Wnek GE. Processing of polymer nanofibers through electrospinning as drug delivery systems. Materials Chemistry and Physics 2009;113(1):296-302.

138. Liu C-X, Zhang S-P, Su Z-G, Wang P. Salt induced protein adsorption with extremely high loadings on electrospun nanofibers. Langmuir 2011;27(2):760-765.

139. Zhang J, Liu J, Yu H, Zhang Y, Zhu M, Chen Y. Crosslinked electrospun UPM/PHBV/PVP fibers for sustained drug release. Materials Science Forum 2009;610-613:1331-1334.

140. Carlberg B, Axell MZ, Nannmark U, Liu J, Kuhn HG. Electrospun polyurethane scaffolds for proliferation and neuronal differentiation of human embryonic stem cells. Biomedical Materials 2009;4(4):045004/1-045004/7.

141. Kuraishi K, Iwata H, Nakano S, Kubota S, Tonami H, Toda M, Toma N, Matsushima S, Hamada K, Ogawa S and others. Development of nanofiber-covered stents using electrospinning: in vitro and acute phase in vivo experiments. Journal of Biomedical Materials Research Part B: Applied Biomaterials 2008;88B(1):230-239.

142. Hashizume R, Fujimoto KL, Hoong Y, Amoroso NJ, Tobita K, Miki T, Keller BB, Sacks MS, Wagner WR. Morphological and mechanical characteristics of the reconstructed rat abdominal wall following use of a wet electrospun biodegradable polyurethane elastomer scaffold. Biomaterials 2010;31(12):3253-3265.

143. Hong Y, Fujimoto KL, Hashizume R, Guan J, Stankus JJ, Tobita K, Wagner WR. Generating elastic, biodegradable polyurethane/poly(lactide-co-glycolide) fibrous sheets with controlled antibiotic release via two-stream electrospinning. Biomacromolecules 2008;9(4):1200-1207.

144. Kang J, Erdodi G, Yalcin B, Cakmak M, Kennedy JP. Bioartificial pancreas: A novel macro-immunoisolatory device. Polymer Preprints 2008;49(1):824-825.

145. Lee KH, Kim DJ, Min BG, Lee SH. Polymeric nanofiber web-based artificial renal microfluidic chip. Biomedical Microdevices 2007;9(4):435-442.

146. Narayanan R, Wu S, Reneker DH, Wang P. Electrospun enzyme-carrying polyurethane nanofibers for use in biosensors. 2007; Boston, MA.

147. Senecal A, Magnone J, Marek P, Senecal K. Development of functional nanofibrous membrane assemblies towards biological sensing. Reactive & Functional Polymers 2008;68(10):1429-1434.

148. Senecal AG, Senecal KJ, Magnone JP, Pivarnik PE. Development of nanofibrous membranes towards biological sensing. Selected Topics in Electronics and Systems 2006;42:387-393.

149. Sheikh FA, Barakat NAM, Kanjwal MA, Chaudhari AA, Jung I-H, Lee JH, Kim HY. Electrospun antimicrobial polyurethane nanofibers containing silver nanoparticles for biotechnological applications. Macromolecular Research 2009;17(9):688-696.

150. Sheikh FA, Kanjwal MA, Saran S, Chung W-J, Kim H. Polyurethane nanofibers containing copper nanoparticles as future materials. Applied Surface Science 2011;257(7):3020-3026.

151. Zhuo H-T, Hu J-L, Chen S-J. Study of the thermal properties of shape memory polyurethane nanofibrous nonwoven. Journal of Materials Science 2011;46(10):3464-3469.

152. Baudis S, Schwarz M, Grasl C, Bergmeister H, Weigel G, Schima H, Liska R. (Bio)degradable urethane elastomers for electrospun vascular grafts. 2009. Materials Research Society.

153. Chen R, Huang C, Ke Q-F, He C-L, Wang H-S, Mo X-M. Preparation and characterization of coaxial electrospun thermoplastic polyurethane/collagen compound nanofibers for tissue engineering applications. Colloids and Surfaces, B: Biointerfaces 2010;79(2):315-325.

154. Choi WS, Bae JW, Lim HR, Joung YK, Park J-C, Kwon IK, Park KD. RGD peptide-immobilized electrospun matrix of polyurethane for enhanced endothelial cell affinity. Biomedical Materials 2008;3(4):044104/1-044104/8.

155. Detta N, Errico C, Dinucci D, Puppi D, Clarke DA, Reilly GC, Chiellini F. Novel electrospun polyurethane/gelatin composite meshes for vascular grafts. Journal of Materials Science: Materials in Medicine 2010;21(5):1761-1769.

156. El-Kurdi MS, Hong y, Stankus JJ, Soletti L, Wagner WR, Vorp DA. Transient elastic support for vein grafts using a constricting microfibrillar polymer wrap. Biomaterials 2008;29(22):3213-3220.

157. Fromstein JD, Zandstra PW, Alperin C, Rockwood D, Rabolt JF, Woodhouse KA. Seeding bioreactor-produced embryonic stem cell-derived cardiomyocytes on different porous, degradable, polyurethane scaffolds reveals the effect of scaffold architecture on cell morphology. Tissue Engineering, Part A 2008;14(3):369-378.

158. Fromstein JD, Zandstra PW, Alperin C, Rockwood DN, Rabolt JF, Woodhouse KA. Seeding bioreactor-produced embryonic stem cell-derived cardiomyocytes on different porous, degradable, polyurethane scaffolds reveals the effect of scaffold architecture on cell morphology. Tissue Engineering Part A 2008;14(3):369-378.

159. Grasl C, Bergmeister H, Stoiber M, Schima H, Weigel G. Electrospun polyurethane vascular grafts: In vitro mechanical behavior and endothelial adhesion molecule expression. Journal of Biomedical Materials Research Part A 2010;93A(2):716-723.

160. Guan J, Fujimoto KL, Sacks MS, Wagner WR. Preparation and characterization of highly porous, biodegradable polyurethane scaffolds for soft tissue applications. Biomaterials 2005;26(18):3961-3971.

161. Han J, Cao R-W, Chen B, Ye L, Zhang A-Y, Zhang J, Feng Z-G. Electrospinning and biocompatibility evaluation of biodegradable polyurethanes based on L-lysine diisocyanate and L-lysine chain extender. Journal of Biomedical materials Research, Part A 2011;96A(4):705-714.

162. Han Z, Kong H, Meng J, Wang C, Xie S, Xu H. Electrospun aligned nanofibrous scaffold of carbon nanotubes-polyurethane composite for endothelial cells. Journal of Nanoscience and Nanotechnology 2009;9(2):1400-1402.

163. Brizzola S, de Eguileor M, Brevini T, Grimaldi A, Congiu T, Neuenschwander P, Acocella F. Morphologic features of biocompatibility and neoangiogenesis onto a biodegradable tracheal prosthesis in an animal model. Interactive Cardiovascular and Thoracic Surgery 2009;8:610-614.

164. Hong Y, Ye S-H, Nieponice A, Soletti L, Vorp DA, Wagner WR. A small diameter, fibrous vascular conduit generated from a poly(ester urethane)urea and phospholipid polymer blend. Biomaterials 2009;30(13):2457-2467.

165. Huang C, Chen R, Ke Q, Morsi Y, Zhang K, Mo X. Electrospun collagen-chitosan-TPU nanofibrous scaffolds for tissue engineered tubular grafts. Colloids and Surfaces B: Biointerfaces 2011;82(2):307-315.

166. Joung YK, Hwang IK, Park KD, Lee CW. CD34 monoclonal antibody-immobilized electrospun polyurethane for the endothelialization of vascular grafts. Macromolecular Research 2010;18(9):904-912.

167. Kang YK, Park CH, Chang H, Minn K, Park CY. Development of thermoplastic polyurethane vascular prostheses. Journal of Applied Polymer Science 2008;110(5):3267-3274.

168. Kidoaki S, Kwon IK, Matsuda T. Mesoscopic spatial designs of nano- and microfiber meshes for tissue-engineering matrix and scaffold based on newly devised multilayering and mixing electrospinning. Biomaterials 2004;26(1):37-46.

169. Kidoaki S, Kwon IK, Matsuda T. Mesoscopic spatial designs of nano- and microfiber meshes for tissue-engineering matrix and scaffold based on newly devised multilayering and mixing electrospinning techniques. Biomaterials 2005;26(1):37-46.

170. Liao I-C, Liu JB, Bursac N, Leong KW. Effect of electrochemical stiumlation on the maturation of myotubes on aligned electrospun fibers. Cellular and Molecular Bioengineering 2008;1(2-3):133-145.

171. Matsuda T, Ihara M, Inoguchi H, Kwon IK, Takamizawa K, Kidoaki S. Mechano-active scaffold design of small-diameter artificial graft made of electrospun segmented polyurethane fabrics. Journal of Biomedical Materials Research Part A 2005;73A(1):125-131.

172. Meng J, Han Z, Kong H, Qi X, Wang C, Xie S, Xu H. Electrospun aligned nanofibrous composite of MWCNT/polyurethane to enhance vascular endothelium cells proliferation and function. Journal of Biomedical Materials Research, Part A 2010;95A(1):312-320.

173. Miyazu K, Kawahara D, Ohtake H, Watanabe G, Matsuda T. Luminal surface design of electrospun small-diameter graft aiming at in situ capture of endothelial progenitor cell. Journal of Biomedical Materials research, Part B: Applied Biomaterials 2010;94B(1):53-63.

174. Rockwood DN, Akins REJ, Parrag IC, Woodhouse KA, Rabolt JF. Culture on electrospun polyurethane scaffolds decreases atrial natriuretic peptide expression by cardiomyocytes *in vitro*. Biomaterials 2008;29(36):4783-4791.

175. Shin JW, Lee YJ, Heo SJ, Park, Su A., Kim S-H, Kim YJ, Kim D-H, Shin J-W. Manufacturing of multi-layered nanofibrous structures composed of polyruethane and poly(ethylene oxide) as potential blood vessel scaffolds. Journal of Biomaterials Science, Polymer Edition 2009;20(5-6):757-771.

176. Soletti L, Nieponice A, Hong Y, Ye S-H, Stankus JJ, Wagner WR, Vorp DA. In vivo performance of a phospholipid-coated bioerodable elastomeric graft for small-diameter vascular applications. Journal of Biomedical materials Research, Part A 2011;96A(2):436-448.

177. Stankus JJ, Guan J, Fujimoto K, Wagner WR. Microintegrating smooth muscle cells into a biodegradable, elastomeric fiber matrix. Biomaterials 2005;27(5):735-744.

178. Theron JP, Knoetzeb JH, Sanderson RD, Hunterd R, Mequanint K, Franz T, Zilla P, Bezuidenhout D. Modification, crosslinking and reactive electrospinning of a thermoplastic medical polyurethane for vascular graft applications. Acta Biomaterialia 2010;6(7):2434-2447.

179. Uttayarat P, Perets A, Li M, Pimton P, Stachelek SJ, Alferiev I, Composto RJ, Levy RJ, Lelkes PI. Micropatterning of three-dimensional electrospun polyurethane vascular grafts. Acta Biomaterialia 2010;6(11):4229-4237.

180. Williamson MR, Black R, Kielty C. PCL-PU composite vascular scaffold production for vascular tissue engineering: attachment, proliferation and bioactivity of human vascular endothelial cells. Biomaterials 2006;27(19):3608-3616.

181. Drilling S, Gaumer J, Lannutti. Fabrication of burst pressure competent vascular grafts via electrospinning: Effects of microstructure. J. Biomed. Mater. Res., Part A 2009;88A(4):923-934.

182. Inoguchi H, Tanaka T, Maehara Y, Matsuda T. The effect of gradually graded shear stress on the morphological integrity of a huvec-seeded compliant small-diameter vascular graft. Biomaterials 2007;28:486-495.

183. Qi H, Kong D, Hu P, Zhang J, Lin W, Song F. Biomimic tubulose scaffolds with multilayer prepared by electrospinning for tissue engineering. Mater. Sci. Forums 2006;510-511:882-885.

184. Sell S, Bowlin G. Creating small diameter bioresorbable vascular grafts through electrospinning. J. Mater. Chem. 2008;18:260-263.

185. Stitzel J, Lee S, Yoo J, Levi N, Berry J, Czerw R, Komura M, Lim G, Soker S, Atala A. Fabrication, mechanics, and biocompatibility of a nanofiber tissue engineering scaffold. Polym. Prepr. 2005;46(1).

186. Stitzel J, Liu J, Lee S, Komura M, Berry J, Soker S, Lim G, Dyke M, Czerw R, Yoo J and others. Controlled fabrication of a biological vascular substitute. Biomaterials 2006;27:1088-1094.

187. Pattamaprom C, Hongrojjanawiwat W, Koombhongse P, Supaphol P, Jarusuwannapoo T, Rangkupan R. The influence of solvent properties and functionality on the electrospinnability of polystyrene nanofibers. Macromolecular Materials and Engineering 2006;291(7):840-847.

188. Young H, Freedman R, Ford A. University Physics. San Francisco, CA: Pearson Addison Wesley; 2008. 1551 p.

189. Zhao Q, Topham N, Anderson J, Hiltner A, Lodoen G, C CP. Foreign-body giant cells and polyurethane biostability: in vivo correlation of cell adhesion and surface cracking. Journal of Biomedical Materials Research 1991;25(2):177–183.

190. Christenson EM, Hiltner A, Anderson JM. Biodegradation mechanism of polyurethane elastomers. Corrossion Engineering Science and Technology 2007;42(4):312-323.

191. Anderson J. Implant retrieval and evaluation In: Ratner B, Hoffman A, Schoen F, Lemons J, editors. Biomaterials science, an introduction to materials in medicine. New York, NY Academic; 1996. p 451–456.

192. Anderson J. Biological responses to materials. Annual Review of Materials Research 2001;31:81-110.

193. Gogolewski S. In vitro and in vivo molecular stability of medical polyurethanes: a review. Trends in Polymer Science 1991;1(1):47-61.

194. Stokes K, McVenes R. Polyurethane elastomer biostability. Journal of Biomaterials Applications 1995;9(4):321-354.

195. Sarkar D, Yang J-C, Gupta A, Lopina S. Synthesis and characterization of L-tyrosine based polyurethanes for biomaterial applications. Journal of Biomedical Materials Research Part A 2009;90A(1):263-271.

196. Ding M, Li J, Fu X, Zhou J, Tan H, Gu Q, Fu Q. Synthesis, degradation, and cytotoxicity of multiblock poly(e-caprolactone urethane)s containing gemini quaternary ammonium cationic groups. Biomacromolecules 2009;10:2857-2865.

197. da Silva G, da Silva-Cunha Jr A, Behar-Cohen F, Ayres E, Orefice R. Biodegradation of polyurethanes and nanocomposites to non-cytotoxic degradation products. Polymer Degradation and Stability 2010;95:491-499.

198. Luo Y, Zhang C, Xu F, Chen Y, Fan L, Wei Q. Synthesis and characterization of novel THTPBA/PEG-derived polyurethane scaffolds for tissue engineering. Journal of Materials Science 2010;45:1866-1877.

199. Asplund B, Aulin C, Bowden T, Eriksson N, Mathisen T, Bjursten L, Hilborn J. *In vitro* degradation and *in vivo* biocompatibility study of a new linear poly(urethane urea). Journal of Biomedical Materials Research Part B: Applied Biomaterials 2008;86B(1):45-55.

200. Zuidema J, Van Minnen B, Span M, Hissink C, Van Kooten T, Bos R. *In vitro* degradation of a biodegradable polyurethane foam, based on 1,4-butanediisocyanate: a three-year study at physiological and elevated temperature. Journal of Biomedical Materials Research Part A 2009;90A(3):920-930.

201. Liu H, Zhang L, Zuo Y, Wang L, Huang D, Shen J, Shi P, Li Y. Preparation and characterization of aliphatic polyurethane and hydroxyapatite composite scaffold. Journal of Applied Polymer Science 2009;112(5):2968-2975.

202. Pan J, Li G, Chen Z, Chen X, Zhu W, Xu K. Alternative block polyurethanes based on poly(3-hydroxybutyrate-*co*-4-hydroxybutyrate) and poly(ethylene glycol). Biomaterials 2009;30:2975-2984.

203. Knight P, Lee K, Qin H, Mather P. Biodegradable thermoplastic polyurethanes incorporating polyhedral oligosilsesquioxane. Biomacromolecules 2008;9:2458-2467.

204. Zhang C, Wen X, Vyavahare N, Boland T. Synthesis and characterization of biodegradable elastomeric polyurethane scaffolds fabricated by the inkjet technique. Biomaterials 2008;29:3781-3791.

205. Wisse E, Renken R, Roosma J, Palmans A, Meijer E. Poly(caprolactone-*co*-oxo-crown ether)-based poly(urethane)urea for soft tissue engineering applications. Biomacromolecules 2007;8:2739-2745.

206. Melnig V, Obreja L, Garlea A. In vitro degradation and erosion of degradable lactate segmented polyurethanes. Journal of Optoelectronics and Advanced Materials 2005;7(6):2803-2808.

207. Loh X, Tan K, Li X, Li J. The in vitro hydrolysis of poly(ester urethane)s consisting of poly[(R)-3-hydroxybutyrate] and poly(ethylene glycol). Biomaterials 2006;27:1841-1850.

208. Gorna K, Gogolewski S. In vitro degradation of novel medical biodegradable aliphatic polyurethanes based on e-caprolactone and Pluronics with various hydrophilics. Polymer Degradation and Stability 2002;75:113-122.

209. Skarja GA, Woodhouse KA. In vitro degradation and erosion of degradable, segmented polyurethanes containing an amino acid-based chain extender. Journal of Biomaterials Science, Polymer Edition 2001;12(8):851-873.

210. Saad B, Hirt T, Welti M, Uhlschmid GK, Neuenschwander P, Suter U. Development of degradable polyesterurethanes for medical applications: in vitro and in vivo evaluations. Journal of Biomedical Materials Research 1997;36(1):65-74.

211. Rockwood D, Woodhouse K, Fromstein J, Chase D, Rabolt J. Characterization of biodegradable polyurethane microfibers for tissue engineering. Journal of Biomaterials Science, Polymer Edition 2007;18(6):743-758.

212. Santerre J, Duguay D, Labow R, Brash J. Interactions of hydrolytic enzymes at an aqueous-polyurethane interface. Proteins at interfaces II. Journal of American Chemical Society 1995:352-70.

213. Duguay D, Labow R, Santerre J, McLean D. Developement of a mathematical model describing the enzymatic degradation of biomdeical polyurethanes. 1.

Background, rationale and model formulation. Polymer Degradation and Stability 1995;47:229-249.

214. Elliott SL, Fromstein JD, Santerre JP, Woodhouse KA. Identification of biodegradation products formed by L-phenylalanine based segmented polyurethaneureas. Journal of Biomaterials Science, Polymer Edition 2002;13(6):691–711.

215. Skarja GA, Woodhouse KA. Structure-property relationships of degradable polyurethane elastomers containing an amino acid-based chain extender. Journal of Applied Polymer Science 2000;75(12):1522-1534.

216. Ciardelli G, Rechichi A, Cerrai P, Tricoli M, Barbani N, Giusti P. Segmented polyurethanes for medical applications: synthesis, characterization and *in vitro* enzymatic degradation studies. Macromolecular Symposia 2004;218(1):261-272.

217. Sarkar D, Lopina S. Oxidative and enzymatic degradations of L-tyrosine based polyurethanes. Polymer Degradation and Stability 2007;92(11):1994-2004.

218. Yamamoto N, Nakayama A, Oshima M, Kawasaki N, Aiba S. Enzymatic hydrolysis of lysine diisocyanate based polyurethanes and segmented polyurethane ureas by various proteases. Reactive & Functional Polymers 2007;67:1338-1345.

219. Labow R, Meek E, Santerre J. The biodegradation of poly(urethane)s by the esterolytic activity of serine proteases and oxidative enzyme systems. Journal of Biomaterials Science, Polymer Edition 1999;10(7):699-713.

220. Smith R, Williams D, Oliver C. The biodegradation of poly(ether urethanes). Journal of Biomedical Materials Research 1987;21(9):1149-1165.

221. Williams D, Smith R, Oliver C. The degradation of carbon-14 labeled polymers by enzymes. Advances in Biomaterials 1986;6:239-244.

222. Phua S, Castillo E, Anderson J, Hiltner A. Biodegradation of a polyurethane in vitro. Journal of Biomedical Materials Research 1987;21(2):231-246.

223. Labow R, Tang Y, Mccloskey C, Santerre J. The effect of oxidation on the enzyme-catalyzed hydrolytic biodegradation of poly(urethane)s. Journal of Biomaterial Science Polymer Edition 2002;13(6):651-665.

224. Santerre J, Labow R, Adams G. Enzyme-biomaterial interactions: effect of biosystems on degradation of polyurethanes. Journal of Biomedical Materials Research 1993;27(1):97-109.

225. Tang Y, Labow R, Santerre J. Enzyme-induced biodegradation of polycarbonate-polyurethanes: dependence on hard-segment chemistry Journal of Biomedical Materials Research 2001;57(4):597– 611.

226. Tang Y, Labow R, Santerre J. Enzyme-induced biodegradation of polycarbonate-polyurethanes: dependence on hard-segment concentration. Journal of Biomedical Materials Research 2001;57:516-528.

227. Tang Y, Labow R, Santerre J. Enzyme induced biodegradation of polycarbonate-polyurethanes: dose dependence effect of cholesterol esterase. Biomaterials 2003;24(12):2003-2011.

228. Wang GB, Labow RS, Santerre JP. Biodegradation of a poly(ester)urea-urethane by cholesterol esterase: isolation and identification of principal biodegradation products. Journal of Biomedical Materials Research 1997;36(3):407-417.

229. Christensen EM, Patel S, Anderson JM, Hiltner A. Enzymatic degradation of poly(ether urethane) and poly(carbonate urethane) by cholesterol esterase. Biomaterials 2006;27(21):3920-3926.

230. Pkhakadze G, Grigorieva M, Gladir I, Momot G. Biodegradable polyurethanes. Journal of Materials Science: Materials in Medicine 1996;7:265-267.

231. Ratner B, Gladhill K, Horbett T. Analysis of *in vitro* enzymatic and oxidative degradation of polyurethanes. Journal of Biomedical Materials Research 1988;22(6):509-527.

232. Takahara A, Hergenrother R, Coury A, Cooper S. Effect of soft segment chemistry on the biostability of segmented polyurethanes. II. In vitro hydrolytic degradation and lipid sorption. Journal of Biomedical Materials Research 1992;26(6):801-818.

233. Thomas V, Jayabalan M. Studies on the effect of virtual crosslinking on the hydrolytic stability of novel aliphatic polyurethane ureas for blood contact applications. Journal of Biomedical Materials Research 2001;56(1):144-157.

234. Marchant R, Zhao Q, Anderson J, Hiltner A. Degradation of a poly(ether urethane urea). Polymer 1987;28(12):2032-2039.

235. Tyler B, Ratner B. Oxidative and enzymic degardation of Biomer fractions. Polymer Preprints 1990;31(1):224-225.

236. Guan J, Sacks MS, Beckman EJ, Wagner WR. Synthesis, characterization and cytocompatibility of polyurethaneurea elastomers with designed elastase sensitivity. Biomacromolecules 2005;6(5):2833-2842.

237. Guan J, Fujimoto K, Wagner W. Elastase-sensitive elastomeric scaffolds with variable anisotropy for soft tissue engineering. Pharmaceutical Research 2008;25(10):2400-2412.

238. Labow R, Erfle D, Santerre J. Elastase-induced hydrolysis of synthetic solid substrates: poly(ester-urea-urethane) and poly(ether-urea-urethane). Biomaterials 1996;17:2381-2388.

239. Bitritto M, Bell J, Brenckle G, Huang S, Knox J. Synthesis and biodeg of polymers derived from alpha-hydroxy acids. Journal of Applied Polymer Science: Applied Polymer Symposium 1979;35:405-414.

240. Wang F, Li Z, Tamama K, Sen C, Guan J. Fabrication and characterization of prosurvival growth factor releasing, anisotropic scafolds for enhanced mesenchymal stem cell survival/growth and orientation. Biomacromolecules 2009;10:2609-2618.

241. Guan J, Stankus J, Wagner W. Development of composite porous scaffolds based on collagen and biodegradable poly(ester urethane)urea. Cell Transplantation 2006;15(Supplement 1):S17-S27.

242. Sinclair T, Kerrigan C, Buntic R. Biodegradation of the polyurethane foam covering of breast implants. Plastic and Reconstructive Surgery 1993;92(6):1003-1013.

243. Sinclair T, Kerrigan C, Sampalis J. Biodegradation of polyurethane foam, revisited in the rat model. Plastic and Reconstructive Surgery 1995;96(6):1326-1335.

244. Labow R, Meek E, Matheson L, Santerre J. Human macrophage-mediated biodegradation of polyurethanes: assessment of candidate enzyme activities Biomaterials 2002;23(19):3969–3975.

245. Labow R, Sa D, Matheson L, Santerre J. Polycarbonate-urethane hard segment type influences esterase substrate specificity for human-macrophage-mediated biodegradation. Journal of BIomaterials Science, Polymer edition 2005;16(9):1167-1177.

246. Labow R, Santerre J. Effect of fibrinogen adsorption on U937-cell mediated biodegradation of polycarbonate-urethanes. In: Bloomington D, editor. New Research on Biomaterials: Nova Science Publishers, Inc.; 2007. p 145-159.

247. Pechar M, Braunova A, Ulbrich K. Poly(ethylene glycol)-based polymer carrier of doxorubicin degradable by both enzymatic and chemical hydrolyses. Czech Rep. Collection of Czechoslovak Chemical Communications 2005;70(3):327-338.

248. Bense C, Woodhouse K. Plasmin degradation of fibrin coatings on synthetic polymer substrates. Journal of Biomedical Materials Research 1999;46:305-314.

249. Wagner W, Guan J, Hong Y, Stankus J, Ramaswami P, Ma Z. Biodegradable thermoplastic elastomer synthesis and processing for improved biofunctionality. PMSE Preprints 2008;98:326.

250. Li Z, Yang X, Wu L, Chen Z, Lin Y, Xu K, Chen G-Q. Synthesis, characterization and biocompatibility of biodegradable elastomeric poly(ether-ester urethane)s based on poly(3-hydroxybutyrate-co-3-hydroxyhexanoate) and poly(ethylene glycol) via melting polymerization. Journal of Biomaterials Science, Polymer Edition 2009;20(9):1179-1202.

251. Murakami S, Aoki N, Matsumura S. Synthesis and enzymatic degradation of environmentally benign poly(carbonate-urethane). Transactions of the Materials Research Society of Japan 2007;32(4):1211-1214.

252. Gautam R, Bassi A, Yanful E. Candida rugosa lipase-catalyzed polyurethane degradation in aqueous medium. Biotechnology Letters 2007;29(7):1081-1086.

253. Jiang X, Li J, Ding M, Tan H, Ling Q, Zhong Y, Fu Q. Synthesis and degradation of nontoxic biodegradable waterborne polyurethanes elastomer with poly(e-caprolactone) and poly(ethylene glycol) as soft segment. European Polymer Journal 2007;43:1838-1846.

254. Soeda Y, Toshima K, Matsumara S. Synthesis and chemical recycling of novel poly(ester-urethane)s using an enzyme. Macromolecular Bioscience 2005;5(4):277-288.

255. Stirna U, Tupureina V, Sevastyanova I, Dzene A, Misane M. Structure and properties of biodegradable poly(ester urethanes) with side chains. Materialzinatne un Lietiska Kimija 2002;4:174-181.

256. Takamoto T, Shirasaka H, Uyama H, Kobayashi S. Lipase-catalyzed hydrolytic degradation of polyurethane in organic solvent. Chemistry Letters 2001(6):492-493.

257. Shirahama H, Hori H, Yasuda H. Synthesis, chain extension and enzymatic degradation of aliphatic-based polyesters containing an aromatic unit. Nihon Yukagakkaishi 1999;48(9):911-915.

258. Wiggins M, Wilkoff B, Anderson J, Hiltner A. Biodegradation of polyether polyurethane inner insulation in bipolar pacemaker leads. Journal of Biomedical Materials Research 2001;58(3):302–307.

259. Wu Y, Sellitti C, Anderson J, Hiltner A, Lodoen G, Payet C. An FTIR-ATR investigation of in vivo poly(ether urethane) degradation. Journal of Applied Polymer Science 1992;46:201–211.

260. Zhao Q, Agger M, Fitzpatrick M, Anderson J, Hiltner A, Stokes K, Urbanski P. Cellular interactions with biomaterials: in vivo cracking of pre-stressed Pellethane 2363-80A. Journal of Biomedical Materials Research 1990;24(5):621– 637.

261. Christenson EM, Anderson JM, Hiltner A. Oxidative mechanisms of poly(carbonate urethane) and poly(ether urethane) biodegradation: *In vivo* and *in vitro* correlations. Journal of Biomedical Materials Research Part A 2004;70A(2):245-255.

262. Christenson E, Anderson J, Hiltner A. Oxidative mechanisms of poly(carbonate urethane) and poly(ether urethane): in vivo and in vitro correlations. Journal of Biomedical Materials Research 2004;70A (2):245-255.

263. Schubert MA, Wiggins MJ, Anderson JM, Hiltner A. Role of oxygen in biodegradation of poly(etherurethane urea) elastomers. Journal of Biomedical Materials Research 1997;34(4):519-530.

264. Cozzens D, Ojha U, Kulkarni P, Faust R, Desai S. Long term in vitro biostability of segmented polyisobutylene-based thermoplastic polyurethanes. Journal of Biomedical Materials Research, Part A 2010;95A(3):774-782.

265. Erdodi G, Kang J, Kennedy JP, Yilgor E, Yilgor I. Polyisobutylene-based polyurethanes. III. Polyurethanes containing PIB/PTMO soft co-segments. Journal of Polymer Science, Part A: Polymer Chemistry 2009;47(20):5278-5290.

266. Jewrajka SK, Kang J, Erdodi G, Kennedy JP, Yilgor E, Yilgor I. Polyisobutylene-based polyurethanes. II. Polyureas containing mixed PIB/PTMO soft segments. Journal of Polymer Science, Part A: Polymer Chemistry 2009;47(11):2787-2797.

267. Kang J, Erdodi G, Brendel CM, Ely d, Kennedy JP. Polyisobutylene-based polyurethanes. V. Oxidative-hydrolytic stability and biocompatibility. Journal of Polymer Science, Part A: Polymer Chemistry 2010;48(10):2194-2203.

268. Kang J, Erdodi G, Kennedy JP. Polyisobutylene-based polyurethanes with unprecedented properties and how they came about. Journal of Polymer Science, Part A: Polymer Chemistry 2011;In Press.

269. Kang J, Erdodi G, Kennedy JP, Yilgor E, Yilgor I. PIB-based polyurethanes. IV. The morphology of polyruethanes containing soft co-segments. Journal of Polymer Science, Part A: Polymer Chemistry 2009;47(22):6180-6190.

270. Ojha U, Faust R. Synthesis, characterization and properties of biostable thermoplastic polyurethanes based on polyisobutylene and poly(tetramethylene oxide) segments. PMSE Preprints 2009;101:1228-1229.

271. Berrocal MJ, Badr IHA, Gao D, Bachas LG. Reducing the thrombogenicity of ion-selective electrode membranse through the use of a silicone-modified segmented polyurethane. Analytical Chemistry 2001;73(21):5328-5333.

272. Hernandez R, Weksler J, Padsalgikar A, Runt J. In vitro oxidation of high polydimethylsiloxane content biomedical polyurethanes: correlation with the microstructure. Journal of Biomedical Materials Research, Part A 2008;87A(2):546-556.

273. Christenson EM, Anderson JM, Hiltner A. Antioxidant inhibition of poly(carbonate urethane) in vivo biodegradation. Journal of Biomedical Materials Research 2006;76A(3):480–490.

274. Zhao QH, Anderson JM, Hiltner A, Lodoen GA, Payet CR. Theoretical analysis on cell size distribution and kinetics of foreign-body giant cell formation in vivo on polyurethane elastomers. Journal of Biomedical Materials Research 1992;26(8):1019-1038.

275. Meydani M. Vitamin E. The Lancet 1995;345:170-175.

276. Schubert MA, Wiggins MJ, Anderson JM, Hiltner A. Comparison of two antioxidants for poly(etherurethane urea) in an accelerated in vitro biodegradation system. Journal of Biomedical Materials Research 1997;34(4):493-505.

277. Green J, McHale D. Quinones related to vitamin E. In: Morton RA, editor. Biochemistry of Quinones. New York, NY: Academic Press; 1965. p 261.

278. Liebler DC. Tocopherone and epoxytocopherone products of vitamin E oxidation. Methods in Enzymology 1994;234:310-316.

279. Tanzi M, Mantovani D, Petrini P, Guidoin R, Laroche G. Chemical stability of poly(ether urethanes) versus poly(carbonate urethanes). Journal of Biomedical Materials Research 1997;36:550-559.

280. Fare S, Petrini P, Motta A, Cigada A, Tanzi M. Synergistic effects of oxidative environments and mechanical stress on *in vitro* stability of polyetherurethanes and polycarbonateurethanes. Journal of Biomedical Materials Research 1999;45:62-74.

281. Mathur A, Collier T, Kao W, Wiggins M, Schubert M, Hiltner A, Anderson J. *In vivo* biocompatibility and biostability of modified polyurethanes. Journal of Biomedical Materials Research 1997;36:246-257.

282. Salacinski H, Odlyha M, Hamilton G, Seifalian A. Thermomechanical analysis of a compliant poly(carbonate-urea) urethane after exposure to hydrolytic, oxidative, peroxidative and biological solutions. Biomaterials 2002;23(10):2231-2240.

283. Tanzi M, Mantovani D, Petrini P, Guidoin R, Laroche G. Chemical stability of poly(ether urethanes) versus poly(carbonate urethanes). Journal of Biomedical Materials Research 1997;36:550 –559.

284. Fare S, Petrini P, Motta A, Cigada A, Tanzi M. Synergistic effects of oxidative environments and mechanical stress on in vitro stability of poly(ether urethanes) and poly(carbonate urethanes). Journal of Biomedical Materials Research 1999;45(1):62–74.

285. Mathur AB, Collier TO, Kao WJ, Wiggins MJ, Schubert MA, Hiltner A, Anderson JM. In vivo biocompatibility and biostability of modified polyurethanes. Journal of Biomedical Materials Research 1997;36(2):246-257.

286. Langer R, Vacanti JP. Tissue engineering. Science 1993;260(5110):920-926.

287. Halka AT, Kielty Cw, M. G. Vascular tissue engineering. In: Gourlay T, Black RA, editors. Biomaterials and devices for the circulatory system. Oxford: Woodhead Publishing Limited; 2010. p 309-365.

288. Bhatia SN, Chen CS. Tissue engineering at the micro-scale. Biomedical Microdevices 1999;2(2):131-144.

289. Ravi S, Qu Z, Chaikof EL. Polymeric materials for tissue engineering of arterial substitutes. Vascular 2009;17(Suppl 1):S45-S54.

290. Stegemann JP, Kaszuba SN, Rowe SL. Review: advances in vascular tissue engineering using protein-based biomaterials. Tissue Engineering 2007;13:2601-2613.

291. Xue L, Greisler H. Biomaterials in the development and future of vascular grafts. Journal of vascular surgery 2003;37(472-80).

292. Bajaj P, Khang D, Webster TJ. Control of spatial cell attachment on carbon nanofiber patterns on polycarbonate urethane. International Journal of Nanomedicine 2006;1(3):361-365.

293. Bezuidenhout D, Davies N, Black M, Schmidt C, Oosthuysen A, Zilla P. Covalent surface heparinization potentiates porous polyurethane scaffold vascularization. Journal of Biomaterials Applications 2010;24(5):401-418.

294. Blit PH, Shen YH, Ernsting MJ, Woodhouse KA, Santerre JP. Bioactivation of porous polyurethane scaffolds using fluorinated RGD surface modifiers. Journal of Biomedical Materials Research, Part A 2010;94A(4):1226-1235.

295. Danielsson C, Adelow C, U. H, Neuenschwander P, Frey P. In-vitro engineering of implantable human urinary tract tissue matrices. Swiss medical weekly 2007;137(Suppl 155):93S-98S.

296. Ganta SR, Piesco NP, Long P, Gassner R, Motta LF, Papworth GD, Stolz DB, Watkins SC, Agarwal S. Vascularization and tissue infiltration of a biodegradable polyurethane matrix. Journal of Biomedical Materials Research, Part A 2003;64A(2):242-248.

297. Guan J, Fujimoto KL, Wagner WR. Elastase-sensitive elastomeric scaffolds with variable anisotropy for soft tissue engineering. Pharmaceutical Research 2008;25(10):2400-2412.

298. Guan J, Sacks MS, Beckman EJ, Wagner WR. Synthesis, characterization, and cytocompatibility of elastomeric, biodegradable poly(ester-urethane)ureas based on poly(caprolactone) and putrescine. Journal of Biomedical Materials Research 2002;61(3):493-503.

299. Guan J, Stankus JJ, Wagner WR. Biodegradable elastomeric scaffolds with basic fibroblast growth factor release. Journal of Controlled Release 2007;120(1-2):70-78.

300. Hong Y, Guan J, Fujimoto KL, Hashizume R, Pelinescu AL, Wagner WR. Tailoring the degradation kinetics of poly(ester carbonate urethane)urea thermoplastic elastomers for tissue engineering scaffolds. Biomaterials 2010;31(15):4249-4258.

301. Jell G, Verdejo R, Safinia L, Shaffer MSP, Stevens MM, Bismarck A. Carbon nanotube-enhanced polyuretha scaffolds fabricated by thermally induced phase separation. Journal of Materials Chemistry 2008;18(16):1865-1872.

302. Kannan RY, Salacinski HJ, Edirisinghe M, J., Hamilton G, Seifalian AM. Polyhedral oligomeric silsequioxane-polyurethane nanocomposite microvessels for an artificial capillary bed. Biomaterials 2006;27(26):4618-4626.

303. Park D, Wu W, Wang Y. A functionalizable reverse thermal gel based on a polyurethane/PEG block copolymer. Biomaterials 2010;32(3):777-786.

304. Pattison M, Webster TJ, Leslie J, Kaefer M, Haberstroh KM. Evaluating the in vitro and in vivo efficacy of nano-structured polymers for bladder tissue replacement applications. Macromolecular Bioscience 2007;7(5):690-700.

305. Pattison MA, Webster TJ, Haberstroh KM. Select bladder smooth muscle cell functions were enhanced on three-dimensional nano-structured poly(ether urethane) scaffolds. Journal of Biomaterials Science, Polymer Edition 2006;17(11):1317-1332.

306. Ritchie AC, Wijaya S, Ong WF, Zhong SP, Chian KS. Dependence of alignment direciton on magnitude of strain in esophageal smooth muscle cells. Biotechnology and Bioengineering 2009;102(6):1703-1711.

307. van Minnen B, van Leeuwen MBM, Stegenga B, Zuidema J, Hissink CE, van Kooten TG, Bos RRM. Short-term in vitro and in vivo biocompatibility of a biodegradable polyurethane foam based on 1,4-butanediisocyanate. Journal of Materials Science: Materials in Medicine 2005;16(3):221-227.

308. Wang F, Li Z, Lannutti JL, Wagner WR, Guan J. Synthesis, characterization and surface modification of low moduli poly(ether carbonate urethane)ureas for soft tissue engineering. Acta Biomaterialia 2009;5(8):2901-2912.

309. Wang F, Li Z, Lannutti JL, Wagner WR, Guan J. Synthesis, characterization and surface modification of low moduli poly(ether carbonate urethane)ureas for soft tissue engineering. Acta Biomaterialia 2010;5(8):2901-2912.

310. Zhang JY, Beckman EJ, Piesco NP, Agarwal S. A new peptide-based urethane polymer: synthesis, biodegradation, and potential to support cell growth in vitro. Biomaterials 2000;21(12):1247-1258.

311. Adhikari R, Gunatillake PA, Griffiths I, Tatai L, Wickramaratna M, Houshyar S, Moore T, Mayadunne RTM, Field J, McGee M and others. Biodegradable

injectable polyurethanes: synthesis and evaluation for orthopedic applications. Biomaterials 2008;29(28):3762-3770.

312. Asefnejad A, Behnamghader A, Khorasani MT, Farsadzadeh B. Polyurethane/fluor-hydroxyapatite nanocomposite scaffolds for bone tissue engineering. Part I: morphological, physical, and mechanical characterization. International Journal of Nanomedicine 2011;6:93-100.

313. Baino F, Verne E, Vitale-Brovarone C. Feasibility, tailoring and properties of polyurethane/bioactive glass composite scaffolds for tissue engineering. Journal of Materials Science: Materials in Medicine 2009;20(11):2189-2195.

314. Bakunova NV, Komlev VS, Fedotov AY, Fadeeva IV, Smirnov VV, Shvorneva LI, Gurin AN, Barinov SM. A method of fabrication of porous carbonated hydroxyapatite scaffolds for bone tissue engineering. Powder Metallurgy Progress 2008;8(4):336-342.

315. Bertoldi S, Fare S, Denegri M, Rossi D, Haugen HJ, Parolini O, Tanzi MC. Ability of polyurethane foams to support placenta-derived cell adhesion and osteogenic differentiation: preliminary results. Journal of Materials Science: Materials in Medicine 2010;21(3):1005-1011.

316. Bil M, Ryszkowska J, Roether JA, Bretcanu O, Boccaccini AR. Bioactivity of polyurethane-based scaffolds coated with Bioglass. Biomedical Materials 2007;2(2):93-101.

317. Bil M, Ryszkowska J, Wozniak P, Kurzydlowski KJ, Lewandowska-Szumiel M. Optimization of the structure of polyurethanes for bone tissue engineering applications. Acta Biomaterialia 2010;6(7):2501-2510.

318. Boccaccini AR, Chicatun F, Cho J, Bretcanu O, Roether JA, Novak S, Chen Q. Carbon nanotube coatings on Bioglass-based tissue engineering scaffolds. Advanced Functional Materials 2007;17(15):2815-2822.

319. Boissard CIR, Bourban P-E, Tami AE, Alini M, Eglin D. Nanohydroxyapatite/poly(ester urethane) scaffold for bone tissue engineering. Acta Biomaterialia 2009;5(9):3316-3327.

320. Bonzani IC, Adhikari R, Houshyar S, Mayadunne R, Gunatillake PA, Stevens MM. Synthesis of two-component injectable polyurethanes for bone tissue engineering. Biomaterials 2007;28(3):423-433.

321. Bretcanu O, Samaille C, Boccaccini AR. Simple methods to fabricate Bioglass-derived glass-ceramic scaffolds exhibiting porosity gradient. Journal of Materials Science 2008;43(12):4127-4134.

322. Cai S, Xu GH, Yu XZ, Zhang WJ, Xiao ZY, Yao KD. Fabrication and biological characteristics of β-tricalcium phosphate porous ceramic scaffolds reinforced with calcium phosphate glass. Journal of Materials Science: Materials in Medicine 2009;20(1):351-358.

323. Chavarria-Gaytan mC, Olivas-Armendariz I, Garcia-Casillas PE, Martinez-Villafane A, Martinez-Perez CA. Synthesis and characterization of polyurethane scaffolds for biomedical applications. 2010.

324. Chen QZ, Boccaccini AR, Zhang HB, Wang DZ, Edirisinghe MJ. Improved mechanical stability of bone tissue engineering (zirconia) scaffolds by electrospraying. Journal of the American Ceramic Society 2006;89(5):1534-1539.

325. Chowdhury S, Thomas V, Dean D, Catledge SA, Vohra YK. Nanoindentation on porous bioceramic scaffolds for bone tissue engineering. Journal of Nanoscience and Nanotechnology 2005;5(11):1816-1820.

326. Costa HS, mansur AAP, Barbosa-Stancioli EF, Pereira MM, Mansur HS. Morphological, mechanical, and biocompatibility characterization of macroporous alumina scaffolds coated with calcium phosphate/PVA. Journal of Materials Science 2008;43(2):510-524.

327. Detsch R, Uhl F, Deisinger U, Ziegler G. In vitro-studies of cell growth on three differently fabricated hydroxyapatite ceramic scaffolds for bone tissue engineering. Key Engineering Materials 2008;361-363(Pt. 2, Bioceramics):1181-1184.

328. Dong YS, Liu B, Lin PH, Zhang QG, Pu YP. Macroporous hydroxyapatite scaffold fabricated by foam impregnation. Key Engineering Materials 2005;288-289(Advanced Biomaterials VI):565-568.

329. Dong Z, Li Y, Zou Q. Degradation and biocompatibility of porous nano-hydroxyapatite/polyurethane composite scaffold for bone tissue engineering. Applied Surface Science 2009;255(12):6087-6091.

330. Dumas JE, Davis T, Holt GE, Yoshii T, Perrien DS, Nyman JS, Boyce T, Guelcher SA. Synthesis, characterization, and remodeling of weight-bearing allograft bone/polyurethane composites in the rabbit. Acta Biomaterialia 2010;6(7):2394-2406.

331. Eglin D, Griffon S, Alini M. Thiol-containing degradable poly(thiourethane-urethane)s for tissue engineering. Journal of Biomaterials Science, Polymer Edition 2010;21(4):477-491.

332. Eglin D, Mortisen D, Alini M. Degradation of synthetic polymeric scaffolds for bone and cartilage tissue repairs. Soft Matter 2009;5(5):938-947.

333. Fassina L, Visai L, Asti L, Benazzo F, Speziale P, Tanzi MC, Magenes G. Calcified matrix production by SAOS-2 cells inside a polyurethane porous scaffold, using a perfusion bioreactor. Tissue Engineering 2005;11(5/6):685-700.

334. Fassina L, Visai L, Benazzo F, Benedetti L, Calligaro A, De Angelis MGC, Farina A, Maliardi V, Magenes G. Effects of electromagnetic stimulation on calcified matrix production by SAOS-2 cells over a polyurethane porous scaffold. Tissue Engineering 2006;12(7):1985-1999.

335. Fu Q, Rahaman MN, Bal BS, Brown RF, Day DE. Mechanical and in vitro performance of 13-93 bioactive glass scaffolds prepared by a polymer foam replication technique. Acta Biomaterialia 2008;4(6):1854-1864.

336. Fu S, Guo G, Wang X, Zhou L, Liu T, Dong P, Luo f, Gu Y, Shi X, Zhao X and others. Preparation and characterization of n-hydroxyapatite/PCL-pluronic-PCL

nanocomposites for tissue engineering. Journal of Nanoscience and Nanotechnology 2010;10(2):711-718.

337. Geckeler K, Wacker R, Martini F, Hack A, Aicher W. Enhanced biocompatibility for SAOS-2 osteosarcoma cells by surface coating with hydrophobic epoxy resins. Cellular Physiology and Biochemistry 2003;13(3):155-164.

338. Hafeman AE, Davidson JM, Guelcher SA. Effects of polyol, isocyanate, and additives on poly(ester urethane)urea scaffolds: material and in vivo histological properties. PMSE Preprints 2007;97:546.

339. Hafeman AE, Li B, Yoshii T, Zienkiewicz KJ, Davidson JM, Guelcher SA. Injectable biodegradable polyurethane scaffolds with release of platelet-derived growth factor for tissue repair and regeneration. Pharmaceutical Research 2008;25(10):2387-2399.

340. Hafeman AE, Zienkiewicz KJ, Carney E, Litzner B, Stratton C, Wenke JC, Guelcher SA. Local delivery of tobramycin from injectable biodegradable polyurethane scaffolds. Journal of Biomaterials Science, Polymer Edition 2010;21(1):95-112.

341. Hariraksapitak P, Suwantong O, Pavasant P, Supaphol P. Effectual drug-releasing porous scaffolds from 1,6-diisocyanatohexane-extended poly(1,4-butylene succinate) for bone tissue regeneration. Polymer 2008;49(11):2678-2685.

342. Heilmann F, Standard OC, Mueller FA, Hoffman M. Development of graded hydroxyapatite/$CaCO_3$ composite structures for bone ingrowth. Journal of Materials Science: Materials in Medicine 2007;18(9):1817-1824.

343. Hill CM, An YH, kang QK, Hartsock LA, Gogolewski S, Gorna K. Osteogenesis of osteoblast seeded polyurethane-hydroxyapatite scaffolds in nude mice. Macromolecular Symposia 2007;253:94-97.

344. Hofmann A, Ritz U, Verrier S, Eglin D, Alini M, Fuchs S, Kirkpatrick CJ, Rommens PM. The effect of human osteoblasts on proliferation and neo-vessel formation of human umbilical vein endothelial cells in a long-term 3D co-culture on polyurethane scaffolds. Biomaterials 2008;29(31):4217-4226.

345. Huang X, Miao X. Novel porous hydroxyapatite prepared by combining H_2O_2 foaming with PU sponge and modified with PLGA and bioactive glass. Journal of Biomaterials Applications 2007;21(4):351-374.

346. Ishikawa K, Karashima S, Takeuchi A, Matsuya S. Apatite foam fabrication based on hydrothermal reaction of α-tricalcium phosphate foam. Key Engineering Materials 2008;361-363(Pt. 1, Bioceramics):319-322.

347. Jo I-H, Shin K-H, Soon Y-M, Koh Y-H, Lee J-H, Kim H-E. Highly porous hydroxyapatite scaffolds with elongated pores using stretched polymeric sponges as novel template. Materials Letters 2009;63(20):1702-1704.

348. Kavlock KD, Pechar TW, Hollinger JO, Guelcher SA, Goldstein AS. Synthesis and characterization of segmented poly(esterurethane urea) elastomers for bone tissue engineering. Acta Biomaterialia 2007;3(4):475-484.

349. Kommareddy KP, Lange C, Rumpler M, Dunlop JWC, Manjubala I, Cui J, Kratz K, Lendlein A, Fratzl P. Two stages in three-dimensional in vitro growth of tissue generated by osteoblastlike cells. Biointerphases 2010;5(2):45-52.

350. Laschke MW, Strohe A, menger MD, Alini M, Eglin D. In vitro and in vivo evaluation of anovel nanosize hydroxyapatite particles/poly(ester-urethane) composite scaffold for bone tissue engineering. Acta Biomaterialia 2010;6(6):2020-2027.

351. Laska J, Blazewicz S. Processing of biodegradable linear polyurethane for different medical applications. Polish Journal of Applied Chemistry 2009;53(1):43-49.

352. Li B, Yoshii T, Hafeman AE, Nyman JS, Wenke JC, Guelcher SA. The effects of rhBMP-2 released from biodegradable polyurethane/microsphere composite scaffolds on new bone formation in rat femora. Biomaterials 2009;30(35):6768-6779.

353. Li YF, Peng Q, Bao CY, Qiu YL, Wei X, Weng J. Preliminary study on novel bone tissue engineering scaffold with stacking hollow hydroxyapatite microspheres. Key Engineering Materials 2008;361-363(Pt. 2, Bioceramics):951-954.

354. Liu H, Zhang L, Shi P, Zou Q, Zuo Y, Li Y. Hydroxyapatite/polyurethane scaffold incorporated with drug-loaded ethyl cellulose microspheres for bone regeneration. Journal of Biomedical Materials Research, Part B: Applied Biomaterials 2010;95B(1):36-46.

355. Liu KL, Choo ESG, Wong Sy, li X, He cB, Wang J, Li J. Designing poly[(R)-3-hydroxybutyrate]-based polyurethane block copolymers for electrospun nanofiber scaffolds with improved mechanical properties and enhanced mineralization capability. Journal of Physical Chemistry B 2010;114(22):7489-7498.

356. Martinez-Perez CA, Garcia-Casillas PE, Romero P, Juarez C, Martinez-Villafane CA, Moller AD, Romero-Garcia J. Porous biodegradable polyurethane scaffolds prepared by thermally induced phase separation. Journal of Advanced Materials 2006;Spec. Iss 1:5-11.

357. Miao X, Hu Y, Lu J, Wong AP. Porous calcium phosphate ceramics prepared by coating polyurethane foams with calcium phosphate cements. Materials Letters 2003;58(3-4):397-402.

358. Miao X, Tan DM, Li J, Xiao Y, Crawford R. Mechanical and biological properties of hydroxyapatite/tricalcium phosphate scaffolds coated with poly(lactic-co-glycolic acid). Acta Biomaterialia 2008;4(3):638-645.

359. Miao X, Tan L-P, Tan L-S, Huang X. Porous calcium phosphate ceramics modified with PLGA-bioactive glass. Materials Science & Engineering, C: Biomimetic and Supramolecular Systems 2007;27(2):274-279.

360. Oliveira JM, Silva SS, Malafaya PB, Rodrigues MT, Kotobuki N, Hirose M, Gomes ME, Mano JF, Ohgushi H, Reis RL. Macroporous hydroxyapatite scaffolds for bone tissue engineering applications: physicochemical

characterization and assessment of rat bone marrow stromal cell viability. Journal of Biomedical Materials Research, Part A 2009;91A(1):175-186.

361. Park Y-S, Kim K-N, Kim K-M, Choi S-H, Kim C-K, Legeros RZ, Lee Y-K. Feasibility of three-dimensional macroporous scaffold using calcium phosphate glass and polyurethane sponge. Journal of Materials Science 2006;41(13):4357-4364.

362. Rabiee SM, Moztarzadeh F, Solati-Hashjin M, Salimi-Kenari H. Porous tricalcium phosphate as a bone substitute. American Ceramic Society Bulletin 2008;87(2):43-45.

363. Rainer A, Giannitelli SM, Abbruzzese F, Traversa E, Licoccia S, Trombetta M. Fabrication of bioactive glass-ceramic foams mimicking human bone portions for regenerative medicine. Acta Biomaterialia 2008;4(2):362-369.

364. Ryszkowska JL, Auguscik M, Sheikh A, Boccaccini AR. Biodegradable polyurethane composite scaffolds containing Bioglass for bone tissue engineering. Composites Science and Technology 2010;70(13):1894-1908.

365. Sailon AM, Allori AC, Davidson EH, Reformat DD, Allen RJ, Jr., Warren SM. A novel flow-perfusion bioreactor supports 3D dynamic cell culture. Journal of Biomedicine and Biotechnology 2009.

366. Saki M, Narbat MK, Samadikuchakaksaraei A, Ghafouri HB, Gorjipour F. Biocompatibility study of a hydroxyapatite-alumina and silicon carbide composite scaffold for bone tissue engineering. Yakhteh 2009;11(41):55-60.

367. Schlickewei C, Verrier S, Lippross S, Pearce S, Alini M, Gogolewski S. Interaction of sheep bone marrow stromal cells with biodegradable polyurethane bone substitutes. Macromolecular Symposia 2007;253:162-171.

368. Shih CJ, Chen HT, Huang LF, Lu PS, Chang HF, Chang IL. Synthesis and in vitro bioactivity of mesoporous bioactive glass scaffolds. Materials Science & Engineering, C: Materials for Biological Applications 2010;30(5):657-663.

369. Shu C, Zhang W, Xu G, Wei Z, Wei J, Wang D. Dissolution behavior and bioactivity study of glass ceramic scaffolds in the system of CaO-P_2O_5-Na_2O-ZnO prepared by sol-gel technique. Materials Science & Engineering, C: Materials for Biological Applications 2010;30(1):105-111.

370. Tare RS, Khan F, Tourniaire G, Morgan SM, Bradley M, Oreffo ROC. A microarray approach to the identification of polyurethanes for the isolation of human skeletal progenitor cells and augmentation of skeletal cell growth. Biomaterials 2009;30(6):1045-1055.

371. Teixeira S, Fernandes H, Leusink A, van Blitterswijk C, Ferraz MP, Monteiro FJ, de Boer J. In vivo evaluation of highly macroporous ceramic scaffolds for bone tissue engineering. Journal of biomedical Materials Research, Part A 2010;93A(2):567-575.

372. Teixeira S, Ferraz MP, Monteiro FJ. Biocompatibility of highly macroporous ceramic scaffolds: cell adhesion and morphology studies. Journal of Materials Science: Materials in Medicine 2008;19(2):855-859.

373. Teixeira S, Ferraz MP, Monteiro FJ. Three dimensional macroporous calcium phosphates scaffolds for bone tissue engineering. Microscopy and Microanalysis 2009;15(Suppl. 3):61-62.

374. Teixeira S, Rodriguez MA, Pena P, De Aza AH, De Aza S, Ferraz MP, Monteiro FJ. Physical characterization of hydroxyapatite porous scaffolds for tissue engineering. Materials Science & Engineering, C: Materials for Biological Applications 2009;29(5):1510-1514.

375. Tsui YK, Gogolewski S. Microporous biodegradable polyurethane membranes for tissue engineering. Journal of Materials Science: Materials in Medicine 2009;20(8):1729-1741.

376. Verdejo R, jell G, Safinia L, Bismarck A, Stevens MM, Shaffer MSP. Reactive polyurethane carbon nanotube foams and their interactions with osteoblasts. Journal of biomedical Materials Research, Part A 2008;88A(1):65-73.

377. Vitale-Brovarone C, Baino F, Bretcanu O, Verne E. Foam-like scaffolds for bone tissue engineering based on a novel couple of silicate-phosphate specular glasses: synthesis and properties. Journal of Materials Science: Materials in Medicine 2009;20(11):2197-2205.

378. Vitale-Brovarone C, Baino F, Verne E. High strength bioactive glass-ceramic scaffolds for bone regeneration. Journal of Materials Science: Materials in Medicine 2009;20(2):643-653.

379. Vitale-Brovarone C, Verne E, Robiglio L, Appendino P, Bassi F, Martinasso G, Muzio G, Canuto R. Development of glass-ceramic scaffolds for bone tissue

engineering: characterisation, proliferation of human osteoblasts and nodule formation. Acta Biomaterialia 2007;3(2):199-208.

380. Wakae H, Takeuchi A, Udoh K, Matsuya S, Munar ML, LeGeros RZ, Nakasima A, Ishikawa K. Fabrication of macroporous carbonate apatite foam by hydrothermal conversion of α-tricalcium phosphate in carbonate solutions. Journal of Biomedical Materials Research, Part A 2008;87A(4):957-963.

381. Wang L, Li Y, Zuo Y, Zhang L, Zou Q, Cheng L, Jiang H. Porous bioactive scaffold of aliphatic polyurethane and hydroxyapatite for tissue regeneration. Biomedical Materials 2009;4(2):025003/1-025003/7.

382. Wang S, Jain H. High surface area nanomacroporous bioactive glass scaffold for hard tissue engineering. Journal of the American Ceramic Society 2010;93(10):3002-3005.

383. Wozniak P, Bil M, Ryszkowska J, Wychowanski P, Wrobel E, Ratajska A, Hoser G, Przybylski J, Kurzydlowski KJ. Candidate bone-tissue-engineered product based on human-bone-derived cells and polyurethane scaffold. Acta Biomaterialia 2010;6(7):2484-2493.

384. Xiao Z, Cai S, Yu X. Preparation of unsintering calcium phosphate macroporous materials with hydroxyapatite nanowhisker in-situ growth. Key Engineering Materials 2007;336-338(Pt. 2, High-Performance Ceramics IV):1609-1611.

385. Xu G, Cai S, Ye X, Yuan W, Yu X, Shi J, Li J. Preparation and physics characteristic of bone scaffold with calcium phosphate nanocomposite. Nanoscience 2006;11(3):183-188.

386. Yang TY, Lee JM, Yoon SY, Park HC. Hydroxyapatite scaffolds processed using a TBA-based freeze-gel casting/polymer sponge technique. Journal of Materials Science: Materials in Medicine 2010;21(5):1495-1502.

387. Yoshii T, Hafeman AE, Nyman JS, Esparza JM, Shinomiya K, Spengler DM, R. MG, Gutierrez GE, Guelcher SA. A sustained release of lovastatin from biodegradable, elastomeric polyurethane scaffolds for enhanced bone regeneration. Tissue Engineering, Part A 2010;16(7):2369-2379.

388. You M-H, Kwak MK, Kim D-H, Kim K, Levchenko A, Kim D-Y, Suh K-Y. Synergistically enhanced osteogenic differentiation of human mesenchymal stem cells by culture on nanostructured surfaces with induction media. Biomacromolecules 2010;11(7):1856-1862.

389. Yu X, Cai S, Xu G, Zhou W, Wang D. Low temperature fabrication of high strength porous calcium phosphate and the evaluation of the osteoconductivity. Journal of Materials Science: Materials in Medicine 2009;20(10):2025-2034.

390. Yun H-s, Kim S-E, Hyun Y-t. Fabrication of hierarchically porous bioactive glass ceramics. Key Engineering Materials 2008;361-363(Pt. 1, Bioceramics):285-288.

391. Zanetta M, Quirici N, Demarosi F, Tanzi MC, Rimondini L, Fare S. Ability of polyurethane foams to support cell proliferation and the differentiation of MSCs into osteoblasts. Acta Biomaterialia 2009;5(4):1126-1136.

392. Zawadzak E, Bil M, Ryszkowska J, Nazhat SN, Cho J, Bretcanu O, Roether JA, Boccaccini AR. Polyurethane foams electrophoretically coated with carbon

nanotubes for tissue engineering scaffolds. Biomedical Materials 2009;4(1):015008/1-015008/9.

393. Zhang J, Doll BA, Beckman EJ, Hollinger JO. A biodegradable polyurethane-ascorbic acid scaffold for bone tissue engineering. Journal of Biomedical Materials Research, Part A 2003;67A(2):389-400.

394. Zhang J-Y, Doll BA, Beckman EJ, Hollinger JO. Three-dimensional biocompatible ascorbic acid-containing scaffold for bone tissue engineering. Tissue Engineering 2003;9(6):1143-1157.

395. Zhang X, Takahashi T, Vecchio KS. Development of bioresorbable Mg-substituted tricalcium phosphate scaffolds for bone tissue engineering. Materials Science & Engineering, C: Materials for Biological Applications 2009;29(6):2003-2010.

396. Zhao J, Guo LY, Yang XB, Weng J. Preparation of bioactive porous HA/PCL composite scaffolds. Applied Surface Science 2008;255(5, Pt. 2):2942-2946.

397. Zhao J, Lu X, Duan K, Guo LY, Zhou BS, Weng J. Improving mechanical and biological properties of macroporous HA scaffolds through composite coatings. Colloids and Surfaces, B: Biointerfaces 2009;74(1):159-166.

398. Zhao J, Lu X, Weng J. Macroporous Ti-based composite scaffold prepared by polymer impregnating method with calcium phosphate coatings. Materials Letters 2008;62(17-18):2921-2924.

399. Zhao J, Xiao S, Lu X, Wang J, Weng J. A study on improving mechanical properties of porous HA tissue engineering scaffolds by hot isostatic pressing. Biomedical Materials 2006;1(4):188-192.

400. Zhu Y, Kaskel S. Comparison of the in vitro bioactivity and drug release property of mesoporous bioactive glasses (MBGs) and bioactive glasses (BGs) scaffolds. Microporous and Mesoporous Materials 2009;118(1-3):176-182.

401. Zhu Y, Wu C, Ramaswamy Y, Kockrick E, Simon P, Kaskel S, Zreiqat H. Preparation, characterization and in vitro bioactivity of mesoporous bioactive glasses (MBGs) scaffolds for bone tissue engineering. Microporous and Mesoporous Materials 2008;112(1-3):494-503.

402. Mulder MM, Hitchcock RW, Tresco PA. Skeletal myogenesis on elastomeric substrates: implications for tissue engineering. Journal of Biomaterials Science, Polymer Edition 1998;9(7):731-748.

403. Riboldi SA, Sadr N, Pigini L, Neuenschwander P, Simonet M, Mognol P, Sampaolesi M, Cossu G, Mantero S. Skeletal myogenesis on highly orientated microfibrous polyesterurethane scaffolds. Journal of Biomedical Materials Research, Part A 2008;84A(4):1094-1101.

404. Riboldi SA, Sampaolesi M, Neuenschwander P, Cossue G, Mantero S. Electrospun degradable polyesterurethane membrnaes: potential scaffolds for skeletal muscle tissue engineering. Biomaterials 2005;26(22):4606-4615.

405. Amanpour S, Solouk A, Mirzadeh H, Mohagheghi M-A, Rabbani S, Tirgari F. In vitro and in vivo assays of cartilage repair by perforated polyurethane scaffold. Iranian Polymer Journal 2010;19(6):403-415.

406. Bonakdar S, Emami SH, Shokrgozar MA, Farhadi A, Ahmadi SAH, Amanzadeh A. Preparation and characterization of polyvinyl alcohol hydrogels crosslinked by biodegradable polyurethane for tissue engineering of cartilage. Materials Science & Engineering, C: Materials for Biological Applications 2010;30(4):636-643.

407. Brophy RH, Cottrell J, Rodeo SA, Wright TM, Warren RF, Maher SA. Implantation of a synthetic meniscal scaffold improves joint contact mechanics in a partial meniscectomy cadaver model. Journal of Biomedical Materials Research, Part A 2010;92A(3):1154-1161.

408. Chetty A, Steynberg T, Moolman S, Nilen R, Joubert A, Richter W. Hydroxyapatite-coated polyurethane for auricular cartilage replacement: an in vitro study. Journal of Biomedical Materials Research, Part A 2007;84A(2):475-482.

409. Chia S-L, Gorna K, Gogolewski S, Alini M. Biodegradable elastomeric polyurethane membranes as chondrocyte carriers for cartilage repair. Tissue Engineering 2006;12(7):1945-1953.

410. De Groot JH, Spaans CJ, Dekens FG, Pennings AJ. On the role of aminolysis and transesterification in the synthesis of ε-caprolactone and L-lactide-baed polyurethanes. Polymer Bulletin (Berlin) 1998;41(3):299-306.

411. Eglin D, Grad S, Gogolewski S, Alini M. Farsenol-modified biodegradable polyurethanes for cartilage tissue engineering. Journal of BIomedical Materials Research, Part A 2010;92A(1):393-408.

412. Eyrich D, Wiese H, Maier G, Skodacek D, Appel B, Sarhan H, Tessmar J, Staudenmaier R, Wenzel MM, Goepferich A and others. In vitro and in vivo cartilage engineering using a combination of chrondrocyte-seeded long-term stable fibrin gels and polycaprolactone-based polyurethane scaffolds. Tissue Engineering 2007;13(9):2207-2218.

413. Grad S, Kupcsik L, Gorna K, Gogolewski S, Alini M. The use of biodegradable polyurethane scaffolds for cartilage tissue engineering. Biomaterials 2003;24(28):5163-5171.

414. Havla JB, Lotz AS, Richter E, Roelich K, Hagen R, Staudenmaier R, Kleinsasser NH. Cartilage tissue engineering for auricular reconstruction: in vitro evaluation of potential genotoxic and cytotoxic effects of scaffold materials. Toxicology in Vitro 2010;24(3):849-853.

415. Lee CR, Grad S, Gorna K, Gogolewski S, Goessl A, Alini M. Fibrin-polyurethane composites for articular cartilage tissue engineering: a preliminary analysis. Tissue Engineering 2005;11(9/10):1562-1573.

416. Li Z, Kupcsik L, Yao S-J, Alini M, Stoddart MJ. Chondrogenesis of human bone marrow mesenchymal stem cells in fibrin-polyurethane composites. Tissue Engineering, Part A 2009;15(7):1729-1737.

417. Li Z, Yao S-J, Alini M, Stoddart MJ. Chondrogenesis of human bone marrow mesenchymal stem cells in fibrin-polyurethane composites is modulated by frequency and amplitude of dynamic compression and shear stress. Tissue Engineering, Part A 2010;16(2):575-584.

418. Liu y, Webb K, Kirker KR, Bernshaw NJ, Tresco PA, Gray SD, Prestwich GD. Composite articular cartilage engineered on a chondrocyte-seeded aliphatic polyurethane sponge. Tissue Engineering 2004;10(7/8):1084-1092.

419. Lotz AS, Havla JB, Richter E, Roelich K, Staudenmaier R, Hagen R, Kleinsasser NH. Cytotoxic and genotoxic effects of matrices for cartilage tissue engineering. Toxicology Letters 2009;190(2):128-133.

420. Mirzadeh H, Mohagheghi M-A, Ahmadi H, Mirkhani H, Amanpour S, Salehian P. Cartilage tissue engineering for ear as in rabbit model with perforated polyurethane prosthesis: in vivo assay. Iranian Polymer Journal 2000;9(2):73-80.

421. Raghunath J, Georgiou G, Armitage D, Nazhat SN, Sales KM, Butler PE, Seifalian AM. Degradation studies on biodegradable nanocomposite based on polycaprolactone/polycarbonate (80:20%) polyhedral oligomeric silsesquioxane. Journal of Biomedical Materials Research, Part A 2009;91A(3):834-844.

422. Salzmann GM, Nuernberger B, Schmitz P, Anton M, Stoddart mJ, Grad S, Milz S, Tischer T, Vogt S, Gansbacher B and others. Physicobiochemical synergism through gene therapy and functional tissue engineering for in vitro chondrogenesis. Tissue Engineering, Part A 2009;15(9):2513-2524.

423. Walinska K, Iwan A, Gorna K, Gogolewski S. The use of long-chain plant polyprenols as a means to modify the biological properties of new biodegradable polyurethane scaffolds for tissue engineering. A pilot study. Journal of Materials Science: Materials in Medicine 2008;19(1):129-135.

424. Wang P-Y, Chow H-H, Wei-Bor F, Hsu-Wei. Modulation of gene expression of rabbit chondrocytes by dynamic compression of polyurethane scaffolds with collagen gel encapsulation. Journal of Biomaterials Applications 2009;23(4):347-366.

425. Werkmeister JA, Adhikari R, White JF, Tebb TA, Le TPT, Taing HC, Mayadunne R, Gunatillake PA, Danon SJ, Ramshaw JAM. Biodegradable and injectable cure-on-demand polyurethane scaffolds for regeneration of articular cartilage. Acta Biomaterialia 2010;6(9):3471-3481.

426. Wernike E, Li Z, Alini M, Grad S. Effect of reduced oxygen tension and long-term mechanical stimulation on chondrocyte-polymer constructs. Cell & Tissue Research 2008;331(2):473-483.

427. Seil JT, Webster TJ. Decreased astroglial cell adhesion and proliferation on zinc oxide nanoparticle polyurethane composites. International Journal of Nanomedicine 2008;3(4):523-531.

428. Li B, Davidson JM, Guelcher SA. The effect of the local delivery of platelet-derived growth factor from reactive two-component polyurethane scaffolds on the healing in rat skin excisional wounds. Biomaterials 2009;30(20):3486-3494.

429. Phan TT, Lim IJ, Tan EK, Bay BH, Lee ST. Evaluation of cell culture on the polyurethane-based membrane (Tegaderm): implication for tissue engineering of skin. Cell and Tissue Banking 2005;6(2):91-97.

430. Price RD, Das-Gupta V, Frame JD, Navsaria HA. A study to evaluate primary dressings for the application of cultured keratinocytes. British journal of plastic surgery 2001;54(8):687-696.

431. Sarkar S, Chourasia A, Maji S, Sadhukhan S, Kumar S, Adhikari B. Synthesis and characterization of gelatin based polyester urethane scaffold. Bulletin of Materials Science 2006;29(5):475-484.

432. Wang W, Peng P, Yu H, Chen X, Jing X. Synthesis and characterization of a novel biodegradable, thermoplastic polyurethane elastomer. Journal of Polymer Science, Part A: Polymer Chemistry 2006;44(19):5505-5512.

433. Ijima H, Hou Y-T, Takei T. Development of hepatocyte-embedded hydrogel-filled macroporous scaffold cultures using transglutaminase. Biochemical Engineering Journal 2010;52(2-3):276-281.

434. Ijima H, Mizumoto H, Nakazawa K, Kajiwara T, Matsushita T, Funatsu K. Hepatocyte growth factor and epidermal growth factor promote spheroid formation in polyurethane foam/hepatocyte culture and improve expression and maintenance of albumin production. Biochemical Engineering Journal 2009;47(1-3):19-26.

435. Mizumoto H, Funatsu K. Liver regeneration using a hybrid artificial liver support system. Artificial Organs 2004;28(1):53-57.

436. Pavlica S, Piscioneri A, Penemann F, Keller M, Milosevic J, Staeudte A, Heilmann A, Schulz-Siegmund M, Laera S, Favia P and others. Rat embryonic liver cell expansion and differentiation on NH_3 plasma-grafted PEEK-WC-PU membranes. Biomaterials 2009;30(33):6514-6521.

437. Soto-Gutierrez A, Navarro-Alvarez N, Rivas-Carrillo JD, Tanaka K, Chen Y, Misawa H, Okitsu T, Noguchi H, Tanaka N, Kobayashi N. Construction and transplantation of an engineered hepatic tissue using a polyaminourethane-coated nonwoven polytetrafuloroethylene fabric. Transplantation 2007;83(2):129-137.

438. Xu W, Wang X, Yan Y, Zhang R. A polyurethane-gelatin hybrid construct for manufacturing implantable bioartificial livers. Journal of Bioactive and Compatible Polymers 2008;23(5):409-422.

439. Cho EH, Yang YI, Mun C-W, Kim JK. Tissue-engineered semi-microporous segmented polyetherurethane vascular prostheses. Journal of Biomaterials Science, Polymer Edition 2005;16(6):775-790.

440. Danielsson C, Ruault S, Simonet M, Neuenschwander P, Frey P. Polyesterurethane foam scaffold for smooth muscle cell tissue engineering. Biomaterials 2006;27(8):1410-1415.

441. de Mel A, Punshon G, Ramesh B, Sarkar S, Darbyshire A, Hamilton G, Seifalian AM. In situ endothelialization potential of a biofunctionalised nanocomposite biomaterial-based small diameter bypass graft. Bio-medical materials and engineering 2009;19(4-5):317-331.

442. Dey J, Xu H, Nguyen KT, Yang J. Crosslinked urethane doped polyester biphasic scaffolds: potential for in vivo vascular tissue engineering. Journal of Biomedical Materials Research, Part A 2010;95A(2):361-370.

443. Gao C, Guan J, Zhu Y, Shen J. Surface immobilization of bioactive molecules on polyurethane for promotion of cytocompatibility to human endothelial cells. Macromolecular Bioscience 2003;3(3/4):157-162.

444. Grenier S. Vascular smooth muscle cell responses to 3D polyurethane scaffolds for tissue engineering applications. London, ON: University of Western Ontario; 2009. 177 p.

445. Grenier S, Sandig M, Holdsworth DW, Mequanint K. Interactions of coronary artery smooth muscle cells with 3D porous polyurethane scaffolds. Journal of Biomedical Materials Research, Part A 2009;89A(2):293-303.

446. Grenier S, Sandig M, Mequanint K. Polyurethane biomaterials for fabricating 3D porous scaffolds and supporting vascular cells. Journal of Biomedical Materials Research, Part A 2007;82A(4):802-809.

447. Grenier S, Sandig M, Mequanint K. Smooth muscle α-actin and calponin expression and extracellular matrix production of human coronary artery smooth muscle cells in 3D scaffolds. Tissue Engineering, Part A 2009;15(10):3001-3011.

448. He C, Zhang L, Wang H, Zhang F, Mo X. Physical-chemical properties and in vitro biocompatibility assessment of spider silk, collagen and polyurethane nanofiber scaffolds for vascular tissue engineering. Nano Biomedicine and Engineering 2009;1:119-129.

449. He H, Matsuda T. Arterial replacement with compliant hierarchic hybrid vascular graft: biomechanical adaptation and failure. Tissue Engineering 2002;8(2):213-224.

450. He H, Shirota T, Yasui H, Matsuda T. Canine endothelial progenitor cell-lined hybrid vascular graft with nonthrombogenic potential. The Journal of thoracic and cardiovascular surgery 2003;126(2):455-464.

451. Hsu S-H, Sun S-H, Chen DC. Improved retention of endothelial cells seeded on polyurethane small-diamter vascular grafts modified by a recombinant RGD-containing protein. Artificial Organs 2003;27(12):1068-1078.

452. Jiang X, Yu F, Wang Z, Li J, Tan H, Ding M, Fu Q. Fabrication and characterization of waterborne biodegradable polyurethanes 3-dimensional porous scaffolds for vascular tissue engineering. Journal of Biomaterials Science, Polymer Edition 2010;21(12):1637-1652.

453. Jovanovic D, Engels GE, Plantinga JA, Bruinsma M, van Oeveren W, Schouten AJ, van Luyn MJA, Harmsen MC. Novel polyurethanes with interconnected porous structure induce in vivo tissue remodeling and accompanied vascularization. Journal of Biomedical Materials Research, Part A 2010;95A(1):198-208.

454. Jun H-W, West JL. Endothelialization of microporous YIGSR/PEG-modified polyurethaneurea. Tissue Engineering 2005;11(7-8):1133-1140.

455. Kidane AG, Punshon G, Salacinski HJ, Ramesh B, Dooley A, Olbrich M, Heitz J, Hamilton G, Seifalian AM. Incorporation of a lauric acid-conjugated GRGDS

peptide directly into the matrix of a poly(carbonate-urea)urethane polyme rfor use in cardiovascular bypass graft applications. Journal of Biomedical Materials Research, Part A 2006;79A(3):606-617.

456. Li J, Ding M, Fu Q, Tan H, Xie X, Zhong Y. A novel strategy to graft RGD peptide on biomaterials surfaces for endothelialization of small-diameter vascular grafts and tissue engineering blood vessel. Journal of Materials Science: Materials in Medicine 2008;19(7):2595-2603.

457. Liliensiek SJ, Wood JA, Yong J, Auerbach R, Nealey PF, Murphy CJ. Modulation of human vascular endothelial cell behaviors by nanotopographic cues. Biomaterials 2010;31(20):5418-5426.

458. Lim HR, Baek HS, Lee MH, Woo yI, Han D-W, Han MH, Baik HK, Choi WS, Park KD, Chung K-H and others. Surface modification for enhancing behaviors of vascular endothelial cells onto polyurethane films by microwave-induced argon plasma. Surface and Coatings Technology 2008;202(22-23):5768-5772.

459. McBane JE, Battiston KG, Wadhwani A, Sharifpoor S, Labow RS, Santerre JP. The effect of degradable polymer surfaces on co-cultures of monocytes and smooth muscle cells. Biomaterials 2011;32(14):3584-3595.

460. McBane JE, Matheson LA, Sharifpoor S, Santerre JP, Labow RS. Effect of polyurethane chemistry and protein coating on monocyte differentiation towards a wound healing phenotype macrophage. Biomaterials 2009;30(29):5497-5504.

461. McMahon RE, Qu X, Jimenez-Vergara AC, Bashur CA, Guelcher SA, Goldstein AS, Hahn MS. Hydrogel-electrospun mesh composite for coronary artery bypass grafts. Tissue Engineering, Part C: Methods 2011;17(4):451-461.

462. Milleret V, Simonet M, Bittermann AG, Neuenschwander P, Hall H. Cyto- and hemocompatibility of a biodegradable 3D-scaffold material designed for medical applications. Journal of Biomedical Materials Research, Part B: Applied Biomaterials 2009;91B(1):109-121.

463. Nakayama Y, Nishi S, Ishibashi-Ueda H, Matsuda T. Surface microarchitectural design in biomedical applications: in vivo analysis of tissue ingrowth in excimer laser-directed micropored scaffold for cardiovascular tissue engineering. Journal of Biomedical Materials Research 2000;51(3):520-528.

464. Nelson DM, Baraniak PR, Ma Z, Guan J, Mason NS, Wagner WR. Controlled release of IGF-1 and HGF from a biodegradable polyurethane scaffold. Pharmaceutical Research **In Press**.

465. Nieponice A, Soletti L, Guan J, Deasy BM, Huard J, Wagner WR, Vorp DA. Development of a tissue-engineered vascular graft combining a biodegradable scaffolds, muscle-derived stem cells and a rotational vacuum seeding technique. Biomaterials 2008;29(7):825-833.

466. Ouyang C, Xu H, Wang W, Yang H, Xu W. In vivo histocompatibility evaluation of polyurethane membrane modified by superfine silk-fibroin powder. Journal of Huazhong University of Science and Technology, Medical Sciences 2009;29(4):508-511.

467. Patel A, Mequanint K. Novel physically crosslinked polyurethane-block-poly(vinyl pyrrolidone) hydrogel biomaterials. Macromolecular Bioscience 2007;7(5):727-737.

468. Patel S, Wong C, Morsi Y, Mo X, Rui C. Endothelialisation and cell retention on gelatin chitosan-coated electrospun polyurethane, poly(lactide-co-glycolide) and collagen-coated pericardium. Advanced Materials Research (Zuerich, Switzerland) 2008;32(Frontiers in Materials Science and Technology):233-236.

469. Punshon G, Vara DS, Sales KM, Kidane AG, Salacinski HJ, Seifalian AM. Interactions between endothelial cells and a poly(carbonate-silsesquioxane-bridge-urea)urethane. Biomaterials 2005;26(32):6271-6279.

470. Rashid ST, Fuller B, Hamilton G, Seifalian AM. Tissue engineering of a hybrid bypass graft for coronary and lower limb bypass surgery. FASEB Journal 2008;22(6):2084-2089.

471. Rashid ST, Salacinski HJ, Button MJC, Fuller B, Hamilton G, Seifalian AM. Cellular engineering of conduits for coronary and lower limb bypass surgery: role of cell attachment peptides and pre-conditioning in optimising smooth muscle cells (SMC) adherence to compliant poly(carbonate-urea)urethane (MyoLink) scaffolds. European journal of vascular and endovascular surgery: the official journal of the European Society for Vascular Surgery 2004;27(6):608-616.

472. Salacinski HJ, Punshon G, Krijgsman B, Hamilton G, Seifalian AM. A hybrid compliant vascular graft seeded with microvacular endothelial cells extracted from human omentum. Artificial Organs 2001;25(12):974-982.

473. Sharifpoor S, Labow RS, Santerre JP. Synthesis and characterization of degradable polar hydrophobic ionic polyurethane scaffolds for vascular tissue engineering applications. Biomacromolecules 2009;10(10):2729-2739.

474. Sharifpoor S, Simmons CA, Labow RS, Santerre JP. A study of vascular smooth muscle cell funciton under cyclic mechanical loading in a polyurethane scaffold with optimized porosity. Acta Biomaterialia 2010;6(11):4218-4228.

475. Sharifpoor S, Simmons CA, Labow RS, Santerre JP. Functional characterization of human coronary artery smooth muscle cells under cyclic mechanical strain in a degradable polyurethane scaffold. Biomaterials 2011;32(21):4816-4829.

476. Shin JW, Lee YJ, Heo SJ, Park SA, Kim S-H, Kim YJ, Kim D-H, Shin J-W. Manufacturing of multi-layered nanofibrous structures composed of polyurethane and poly(ethylene oxide) as potential blood vessel scaffolds. Journal of Biomaterials Science, Polymer Edition 2009;20(5-6):757-771.

477. Shirota T, He H, Yasui H, Matsuda T. Human endothelial progenitor cell-seeded hybrid graft: proliferative and antithrombogenic potentials in vitro and fabrication processing. Tissue Engineering 2003;9(1):127-136.

478. Sin DC, Miao X, Liu G, Wei F, Chadwick G, Yan C, Friis T. Polyurethane (PU) scaffolds prepared by solvent casting/particulate leaching (SCPL) combined with

centrifugation. Materials Science & Engineering, C: Materials for Biological Applications 2010;30(1):78-85.

479. Stephan S, Ball SG, Williamson M, Bax DV, Lomas A, Shuttleworth CA, Kielty CM. Cell-matrix biology in vascular tissue engineering. Journal of Anatomy 2006;209(4):495-502.

480. Theron JP, Knoetzeb JH, Sanderson RD, Hunterd R, Mequanint K, Franz T, Zilla P. Modification, crosslinking and reactive electrospinning of a thermoplastic medical polyurethane for vascular graft applications. Acta Biomaterialia 2010;6(7):2434-2447.

481. Tiwari A, Salacinski HJ, Punshon G, Hamilton G, Seifalian AM. Development of a hybrid cardiovascular graft using a tissue engineering approach. The FASEB journal 2002;16(8):791-796.

482. Xu W, Wang X, Yan Y, Zhang R. Rapid prototyping of polyurethane for the creation of vascular systems. Journal of Bioactive and Compatible Polymers 2008;23(2):103-114.

483. Yoon SS, Kim JH, Yoon JJ, Kim YJ, Park TG, Kim SC. Adhesion and growth of human umbilical vein endothelial cells on collagen-treated polyurethane/polyethylene diethacrylate interpenetrating polymer networks. Journal of Biomaterials Science, Polymer Edition 2006;17(7):765-780.

484. Zhang L, Zhou J, Lu Q, Wei Y, Hu S. A novel small-diameter vascular graft: in vivo behavior of biodegradable three-layered tubular scaffolds. Biotechnology and Bioengineering 2008;99(4):1007-1015.

485. Zhu Y, Gao C, Guan J, Shen J. Engineering porous polyurethane scaffolds by photografting polymerization of methacrylic acid for improved endothelial cell compatibility. Journal of biomedical Materials Research, Part A 2003;67A(4):1367-1373.

486. Zhu Y, Gao C, He T, Shen J. Endothelium regeneration on luminal surface of polyurethane vascular scaffold modified with diamine and covalently grafted with gelatin. Biomaterials 2003;25(3):423-430.

487. Alperin C, Zandstra PW, Woodhouse KA. Polyurethane films seeded with embryonic stem cell-derived cardiomyocytes for use in cardiac tissue engineering applications. Biomaterials 2005;26(35):7377-7386.

488. Ashton JH, Mertz JAM, Harper JL, Slepian MJ, Mills JL, McGrath DV, Vande Geest JP. Polymeric endoaortic paving: mechanical, thermoforming, and degradation properties of polycaprolactone/polyurethane blends for cardiovascular applications. Acta Biomaterialia 2011;7(1):287-294.

489. Blumenthal B, Golsong P, Poppe A, Heilmann C, Schlensak C, Beyersdorf F, Siepe M. Polyurethane scaffolds seeded with genetically engineered skeletal myoblasts: a promising tool regenerate myocardial function. Artificial Organs 2010;34(2):E46-E54.

490. Kim D-H, Lipke EA, Kim P, Cheong R, Thompson S, Delannoy M, Suh K-Y, Tung L, Levchenko A. Nanoscale cues regulate the structure and function of macroscopic cardiac tissue constructs. Proceedings of the National Academy of Sciences of the United States of America 2010;107(2):565-570.

491. McDevitt TC, Woodhouse KA, Hauschka SD, Murry CE, Stayton PS. Spatially organized layers of cardiomyocytes on biodegradable polyurethane films for myocardial repair. Journal of Biomedical Materials Research, Part A 2003;66A(3):586-595.

492. Rockwood D, Fromstein J, Woodhouse K, Chase B, Rabolt JF. Electrospinning of a biodegradable polyurethane for use in tissue engineering. Polymer Preprints 2004;45(2):406.

493. Siepe M, Giraud M-N, Liljensten E, Nydegger U, Mesche P, Carrel T, Tevaearai HT. Construction of skeletal myoblast-based polyurethane scaffolds for myocardial repair. Artificial Organs 2007;31(6):425-433.

494. Stachelek SJ, Alferiev I, Connolly JM, Sacks M, Hebbel RP, Bianco R, Levy RJ. Cholesterol-modified polyurethane valve cusps demonstrate blood outgrowth endothelial cell adhesion post-seeding in vitro and in vivo. The Annals of thoracic surgery 2006;81(1):47-55.

495. Hafeman A, Davidson J, Guelcher S. Effects of polyol, isocyanate, and additives on poly(ester urethane)urea scaffolds: material and in vivo histological properties. PMSE Preprints 2007;97:546.

496. Kim Y, Kim S. Effect of chemical structure on the biodegradation of polyurethanes under composting conditions. Polymer Degradation and Stability 1998;62:343-352.

497. Zhang JY, Beckman EJ, Hu J, Yang GG, Agarwal S, Hollinger JO. Synthesis, biodegradability, and biocompatibility of lysine diisocyanate-glucose polymers. Tissue Engineering 2002;8(5):771-785.

498. Taylor M, Daniels A, Andriano K, Heller J. Six bioabsorbable polymers: *in vitro* acute toxicity of accumulated degradation products. Journal of Applied Biomaterials 1994;5(2):151-157.

499. van Och F, Slob W, de Jong W, Vandebriel R, van Loveren H. A quantitative method for assessing the sensitizing potency of low molecular weight chemicals using a local lymph node assay: employment of a regression method that includes determination of uncertainty margins. Toxicology 2000;146:49-59.

500. Bruin P, Veenstra GJ, Nijenhuis AJ, Pennings AJ. Design and synthesis of biodegradable poly(ester-urethane) elastomer networks composed of non-toxic building blocks. Makromolekulare Chemie, Rapid Communcations 1988;9(8):589 -594.

501. Tatai L, Moore T, Adhikari R, Malherbe F, Jayasekara R, Griffiths I, Gunatillake P. Thermoplastic biodegradable polyurethanes: the effect of chain extender structure on properties and *in-vitro* degradation. Biomaterials 2007;28:5407-5417.

502. Guelcher SA. Biodegradable Polyurethanes: Synthesis and Applications in Regenerative Medicine. Tissue Engineering 2008;14.

503. Gorna K, Gogolewski S. Preparation, degradation, and calcification of biodegradable polyurethane foams for bone graft substitutes. Journal of Biomedical Materials Research 2003;67A(3):813–827.

504. Guan J, Sacks M, Beckman E, Wagner W. Biodegradable poly(ether ester urethane urea) triblock copolymers and purtrescine: synthesis, characterisation and cytocompatibility. Biomaterials 2004;25(1):85-96.

505. Storey RF, Wiggins JS, Mauritz KA, Puckett AD. Bioabsorbable composites: II. nontoxic, L-lysine based poly(ester urethane) matrix composites. Polymer Composites 1993;14(1):17-25.

506. Guelcher S, Srinivasan A, Hafeman A, Gallagher KM, Doctor JS, Khetan S, Mcbride S, Hollinger JO. Synthesis, in vitro degradation, and mechanical properties of two-component poly(ester urethane) urea scaffolds: effects of water and polyol composition. Tissue Engineering 2007;13(9):2321-2333.

507. Sawhney A, Hubbell J. Rapidly degraded terpolymers of dl-lactide, glycolide, and e-caprolactone with increased hydrophilicity by copolymerization with polyethers. Journal of Biomedical Materials Research 1990;24(10):1397-1411.

508. Cohn D, Stern T, Gonzalez M, Epstein J. Biodegradable poly(ethylene oxide)/poly(e-caprolactone) multiblock copolymers. Journal of Biomedical Materials Research 2002;59(2):273-281.

509. Fromstein J, Woodhouse K. Elastomeric biodegradable polyurethane blends for soft tissue applications. Journal of BIomaterials Science. Polymer edition 2002;13(4):391-406.

510. Guan J, Sacks M, Beckman E, Wagner W. Synthesis, characterization, and cytocompatibility of elastomeric, biodegradable poly(ester-urethane)ureas based on poly(caprolactone) and putrescine. Journal of Biomedical Materials Research 2002;61(3):493-503.

511. Skarja G, Woodhouse K. Synthesis and characterization of degradable polyurethane elastomers containing an amino acid-based chain extender. Journal of Biomaterial Science, Polymer Edition 1998;9(3):271-295.

512. Salacinski H, Goldner S, Giudiceandrea A, Hamilton G, Seifalian A. The mechanical behavior of vascular grafts: a review. Journal of Biomaterials Applications 2001;15(3):241-278.

513. Solan A, Mitchell S, Moses M, Niklason L. Effect of pulse rate on collagen deposition in the tissue-engineered blood vessel. Tissue Engineering 2003;9(4):579-586.

514. Hahn M, McHale M, Wang E, Schmedlen R, West J. Physiologic Pulsatile Flow Bioreactor Conditioning of Poly(ethylene glycol)-based Tissue Engineered Vascular Grafts. Annals of Biomedical Engineering 2007;35(2):190-200.

515. Jeong SI, Kwon JH, Lim JI, Cho S-W, Jung Y, Sung WJ, Kim SH, Kim YH, Lee YM, Kim B-S and others. Mechano-active tissue engineering of vascular smooth muscle using pulsatile perfusion bioreactors and elastic PLCL scaffolds. Biomaterials 2005;26:1405-1411.

516. L'Heureux N, Paquet S, Labbe R, Germain L, Auger F. A completely biological tissue-engineered human blood vessel. The FASEB Journal 1998;12:47-56.

517. Burkel WE. The challenge of small diameter vascular grafts. Med Prog Technol 1989;14(3-4):165-175.

518. Schmedlen RH, Elbjeirami WM, Gobin AS, West JL. Tissue engineered small-diameter vascular grafts. Clinics in Plastic Surgery 2003;30:507-517.

519. Cosgriff-Hernandez E, Hahn M, Wilems T, Munoz-Pinto DJ, Browning MB, Rivera J, Russell B, Höök M. Bioactive hydrogels based on designer collagens. Acta Biomaterialia 2010;6(10):3969-3977.

520. Gray DS, Tien J, Chen CS. Repositioning of cells by mechanotaxis on surfaces with micropatterned Young's modulus. Journal of Biomedical Material Res 2003;66A:605–614.

521. Reinhart-King CA, Dembo M, Hammer DA. Cell-cell mechanical communication through compliant substrates. Biophysical Journal 2008;Volume 95 (December 2008):6044–6051.

522. Pelham Jr. RJ, Wang Y. Cell locomotion and focal adhesions are regulated by substrate flexibility. . Proc. Natl. Acad. Sci. USA 1997;94(25):13661–13665.

523. Peyton S, Putnam A. Extracellular matrix rigidity governs smooth muscle cell motility in a biphasic fashion. Journal of Cell Physiology 2005;204:198-209.

524. Pham QP, Sharma U, Mikos AG. Electrospinning of polymeric nanofibers for tissue engineering applications: a review. Tissue Engineering 2006;12(5):1197-1211.

525. Sarkar S, Hillery C, Scifalian A, Hamilton G. Critical parameter of burst pressure measurement in development of bypass grafts is highly dependent on methodology used. Journal of Vascular Surgery 2006;44(4):846-852.

526. Stankus J, Soletti L, Fujimoto K, Hong Y, Vorp D, Wagner W. Fabrication of cell microintegrated blood vessel constructs through electrohydrodynamic atomization. Biomaterials 2007;28:2738-2746.

527. Schwartz RS, Edelman ER. Preclinical evaluation of drug-eluting stents for peripheral applications. Circulation 2004;110:2498-2505.

528. Browning MB, Dempsey D, Guiza V, Becerra S, Rivera J, Russell B, Höök M, Clubb F, Miller M, Fossum T and others. Multilayer vascular grafts based on collagen-mimetic proteins. Acta Biomaterialia 2012;8(3):1010-1021.

529. Sarkar S, Burriesci G, Wojcik A, Aresti N, Hamilton G, Seifalian AM. Manufacture of small calibre quadruple lamina vascular bypass grafts using a novel automated extrusion-phase-inverison method and nanocomposite polymer. Journal of Biomechanics 2009;42:722-730.

530. Tiwari A, Salacinski H, Seifalian AM, Hamilton G. New prostheses for use in bypass grafts with special emphasis on polyurethanes. Cardiovascular Surgery 2002;10(3):191-197.

531. Roach M, Burton A. The reason for the shape of the distensibility curves of arteries. Can J Biochem Physiol 1957;35.

532. Christenson EM, Anderson JM, Hiltner A, Baer E. Relationship between nanoscale deformation processes and elastic behavior of polyurethane elastomers. Polymer 2005;46(25):11744-11754.

533. Nezarati RM, Eifert MB, Dempsey DK, Cosgriff-Hernandez EM. Electrospun vascular grafts with improved compliance matching to native vessels. Submitted 2013.

534. Nair PD, Jayabalan M, Krishnamurthy VN. Polyurethane-polyacrylamide IPNS. I. Synthesis and characterization. Journal of Polymer Science Part A: Polymer Chemistry 1990;28(13):3775-3786.

535. Kim SR, Yuk SH, Jhon MS. A semi-interpenetrating network system for a polymer membrane. European Polymer Journal 1997;33(7):1009-1014.

536. Oh B, Hyung Y-E, Vissers DR, Amine K. New interpenetrating network-type siloxane polymer electrolyte. Electrochemical and Solid-State Letters 2002;5(11):E59-E61.

537. Xin X, Borzacchiello A, Netti PA, Ambrosio L, Nicolais L. Hyaluronic-acid-based semi-interpenetrating materials. Journal of Biomaterials Science, Polymer Edition 2004;15(9):1223-1236.

538. Karabanova LV, Lloyd AW, Mikhalovsky SV, Helias M, Phillips GJ, Rose SF, Mikhalovska L, Boiteux G, Sergeeva LM, Lutsyk ED and others. Polyurethane/poly(hydroxyethyl methacrylate) semi-interpenetrating polymer networks for biomedical applications. Journal of Materials Science: Materials in Medicine 2006;17(12):1283-1296.

539. Ashton F, Geddes R, Fejfar J. Woven silicone rubber as a venous prosthesis. British Medical Journal 1969;3:409-410.

540. McCaughan JS. Evaluation of Silastic-reinforced Dacron for replacement of inferior vena cava. Surgery 1969;66(2):375-376.

541. Jewell ML. Silicone gel breast implants at 50: the state of the science. Aesthetic Surgery Journal 2012;32(8):1031-1034.

542. Christenson EM, Dadsetan M, Anderson JM, Hiltner A. Biostability and macrophage-mediated foreign body reaction of silicone-modified polyurethanes. Journal of Biomedical Materials Research Part A 2005;74A:141-155.

543. Nezarati RM, Eifert MB, Cosgriff-Hernandez E. Effects of humidity and solution viscosity on electrospun fiber morphology. Tissue Engineering Part C: Methods 2013;19(10):In press.

544. Dillon J. Infared spectroscopic atlas of polyurethanes. Lancaster, PA: Technomic Publication 1989.

545. Engelmayr JGC, Sacks MS. A structural model for the flexural mechanics of nonwoven tissue engineering scaffolds. J Biomech Eng 2006;128(4):610-622.

546. Amoroso NJ, D'Amore A, Hong Y, Rivera CP, Sacks MS, Wagner WR. Microstructural manipulation of electrospun scaffolds for specific bending stiffness for heart valve tissue engineering. Acta Biomater 2012;8(12):4268-77.

547. Amoroso NJ, D'Amore A, Hong Y, Wagner WR, Sacks MS. Elastomeric electrospun polyurethane scaffolds: the interrelationship between fabrication

conditions, fiber topology, and mechanical properties. Adv Mater 2011;23(1):106-111.

548. Brandrup J, Immergut EH, Grulke EA. Polymer Handbook. Hoboken, NJ: John Wiley & Sons, Inc.; 1999.

549. Anseth KS, Wang CM, Bowman CN. Reaction behaviour and kinetic constants for photopolymerizations of multi(meth)acrylate monomers. Polymer 1994;35(15):3243-3250.

550. Matinlinna JP, Dahl JE, Karlsson S, Lassila LVJ, Vallittu PK. The effect of the novel silane system on the flexural properties of E-glass fiber-reinforced composites for dental use. In: Mittal KL, editor. Silanes and Other Coupling Agents. Boca Raton, FL: CRC Press; 2009. p 107-121.

551. Eceiza A, Martin KdlC, G. Kortaberria, N. Gabilondo, M.A. Corcuera, Mondragon I. Thermoplastic polyurethane elastomers based on polycarbonate diols with different soft segment molecular weight and chemical structure: Mechanical and thermal properties. Polymer Engineering and Science 2008;48:297-306.

552. Zhuo H, Hu J, Chen S. Electrospun polyurethane nanofibres having shape memory effect. Materials Letters 2008;62:2074-2076.

553. Leung LM, Koberstein JT. DSC annealing study of microphase separation and multiple endothermic behavior in polyether-based polyurethane block copolymers. Macromolecules 1986;19:706-713.

554. Seymour RW, Cooper SL. Thermal analysis of polyurethane block polymers. Macromolecules 1973;6(1):48-53.

555. Cipriani E, Zanetti M, Brunella V, Costa L, Bracco P. Thermoplastic polyurethanes with polycarboante soft phase: effect of thermal treatment on phase morphology. Polymer Degradation and Stability 2012;97(9):1794-1800.

556. Nallicheri RA, Rubner MF. Thermal and mechanical properties of polyurethane-diacetylene segmented copolymers. 1. Molecular weight and annealing effects. Macromolecules 1990;23:1005-1016.

557. Salacinski H, Goldner S, Giudiceandrea A, Hamilton G, Seifalian A. The mechanical behavior of vascular grafts: a review. J Biomater Appl 2001;15:241-278.

558. L'Heureux N, Stoclet J-C, Auger FA, Lagaud GJ-L, Germain L, Andriantsitohaina R. A human tissue-engineered vascular media: a new model for pharmacological studies of contractile responses. The FASEB Journal 2001;15(2):515-524.

559. Mirkovitch V, Akutsu T, Kolff WJ. Polyurethane aortas in dogs. Three-year results. Transactions of the American Society for Artificial Internal Organs 1962;8(1):79-83.

560. Stokes KB. Polyether polyurethanes: biostable or not? Journal of Biomaterials Applications 1988;3(2):228-259.

561. Christenson E, Wiggins M, Dadsetan M, Anderson J, Hiltner A. Poly(carbonate urethane) and poly(ether urethane) biodegradation: in vivo studies. Journal of Biomedical Materials Research 2004;69A(3):407-416.

562. Anderson JM, Rodriguez A, Chang DT. Foreign body reaction to biomaterials. Seminars in Immunology 2008;20:86-100.

563. Stokes K, Urbanski P, Upton J. The in vivo auto-oxidation of polyether polyurethane by metal ions. Journal of Biomaterials Science, Polymer Edition 1990;1:207-230.

564. Henson PM. The immunologic release of constituents from neutrophil leukocytes I. The role of antibody and complement on nonphagocytosable usrfaces or phagocytosable particles. The Journal of Immunology 1971;107(6):1535-1546.

565. Henson PM. The immunologic release of constituents from neutrophil leukocytes II. Mechanisms of release during phagocytosis, and adherence to nonphagocytosable surfaces. The Journal of Immunology 1971;107(6):1547-1557.

566. Christenson EM, Patel S, Anderson JM, Hiltner A. Enzymatic degradation of poly(ether urethane) and poly(carbonate urethane) by cholesterol esterase. Biomaterials 2006;27(21):3920-3926.

567. Pawlowski P, Rockicki G. Synthesis of oligocarbonate diols from ethylene carbonate and aliphatic diols catalyzed by alkali metal salts. Polymer 2004;45(10):3125-3137.

568. Ward RS, Jones RL. Polyurethanes and silicone polyurethane copolymers. In: Ducheyne P, Healy KE, Hutmacher DW, Grainger DW, Kirkpatrick CJ, editors. Comprehensive Biomaterials; 2011. p 431-477.

569. Dadsetan M, Christensen E, Unger F, Ausborn M, Kissel T, Hiltner A, Anderson J. In vivo biocompatibility and biodegradation of poly(ethylene carbonate). Journal of Controlled Release 2003;93:259-270.

570. Ward R. Biomedical polyjmers with controlled surface properties: syntehsis, characterization and device fabrication. 2006 PSE Symposium Polymers in Biomedicine & Pharmaceuticals. Amherst, MA; 2006.

571. Kreipe H, Radzun HJ, Rudolph P, Barth J, Hansmann M-L, Heidorn K, Parwaresch MR. Multinucleated giant cells generated in vitro: terminally differentiated macrophages with down-regulated c-fms expression. American Journal of Pathology 1988;130(2):232-243.

572. Salacinski H, Tai N, Carson R, Edwards A, Hamilton G, Seifalian A. In vitro stability of a novel compliant poly(carbonate urea) urethane to oxidative and hydrolytic stress Journal of Biomedical Materials Research 2002;59(2):207-218.

573. Li Y, Ren Z, Zhao M, Yang H, Chu B. Multiphase structure of segmented polyurethanes: effects of hard-segment flexibility. Macromolecules 1993;26:612-622.

574. Meijs GF, McCarthy SJ, Rizzardo E, Chen Y-C, Chatelier RC, Brandwood A, Schindhelm K. Degradation of medical-grade polyurethane elastomers: the effect

of hydrogen peroxide *in vitro*. Journal of Biomedical Materials Research 1993;27:345-356.

575. Schubert M, Wiggins M, Hiltner A, Anderson J. Role of oxygen in biodegradation of poly(ether urethane urea) elastomers. Journal of Biomedical Materials Research 1997;34(4):519 –530.

576. Stokes KB, Berthelson WA, Davis MW. Metal catalyzed oxidative degradation of implanted polyurethane devices. In: Gebelein CG, editor. Advances in Biomedical Polymers. New York, NY: Plenum Press; 1987. p 159-169.

577. Thoma RJ, Phillips RE. Studies of poly(ether) urethane pacemaker lead insulation oxidation. Journal of Biomedical Materials Research 1987;21:525-530.

578. Takahara A, Coury AJ, Hergenrother RW, Cooper SL. Effect of soft segment chemistry on the biostability of segmented polyurethanes I. *In vitro* oxidation. Journal of Biomedical Materials Research 1991;25:341-356.

579. Ward B, Anderson J, Ebert M, McVenes R, Stokes K. *In vivo* biostability of polysiloxane polyether polyurethanes: resistance to metal ion oxidation. Journal of Biomedical Materials Research Part A 2006;77A(2):380-389.

580. LeBaron PC, Pinnavaia TJ. Clay nanolayer reinforcement of a silicone elastomer. Chemistry of Materials 2001;13(10):3760-3765.

581. Christenson EM, Dadsetan M, Anderson JM, Hiltner A. Biostability and macrophage-mediated foreign body reaction of silicone-modified polyurethanes. Journal of Biomedical Materials Research, Part A 2005;74A(2):141-155.

582. Yucedag F, Atalay-Oral C, Erkal S, Sirkecioglu A, Karasartova D, Sahin F, Tantekin-Ersolmaz SB, Guner FS. Antibacterial oil-based polyurethane films for wound dressing applications. Journal of Applied Polymer Science 2010;115(3):1347-1357.

583. Lamba NMK, Woodhouse KA, Cooper SL. Polyurethanes in Biomedical Applications. Boca Raton, FL: CRC Press LLC; 1998.

584. Madra H, Tantekin-Ersolmaz S, Guner F. Monitoring of oil-based polyurethane synthesis by FTIR-ATR. Polymer Testing 2009;28(7):773-779.

585. Gultekin G, Atalay-Oral C, Erkal S, Sahin F, karastova D, Tantekin-Ersolmaz S, Guner F. Fatty acid-based polyurethane films for wound dressing applications. Journal of Materials Science: Materials in Medicine 2009;20(1):421-431.

586. Pavlova M, Draganova M. Biocompatible and biodegradable polyurethane polymers. Biomaterials 1993;14(13):1024-1029.

587. Ulubayram K, Hasirci N. Polyurethanes: effect of chemical composition on mechanical properties and oxygen permeability. Polymer 1992;33(10):2084-2088.

588. Kim S, Heo D, Lee J, Kim J, Park S, Jeon S, Kwon I. Electrospun gelatin/polyurethane blended nanofibers for wound healing. Biomedical Materials 2010;4(4):044106.

589. Walpoth B, Rheiner P, Cox J, Rothen R, Faidutti B, Megevand R, Gogolewski S. Biocompatibility of new biodegradable and nondegradable polymeric membranes. Life Support Systems 1986;4(Suppl. 2):82-84.

590. Shau M, Tseng S, Yang T, Cherng J, Chin W. Effect of molecular weight on the transfection efficiency of novel polyurethane as a biodegradable gene vector. Journal of Biomedical Materials Research, Part A 2006;77A:736-746.

591. Nathan A, Bolikal D, Vyavahare N, Zalipsky S, Kohn J. Hydrogels based on water-soluble poly(ether urethanes) derived from L-lysine and poly(ethylene glycol). Macromolecules 1992;25:4476-4484.

592. Zhou C, Yi Z. Blood-compatibility of polyurethane/liquid crystal composite membranes. Biomaterials 1999;20:2093-2099.

593. Yang T, Chin W, Cherng J, Shau M. Synthesis of novel biodegradable cationic polymer: *N*,*N*-diethylethylenediamine polyurethane as a gene carrier. Biomacromolecules 2004;5:1926-1932.

594. Tseng S-j, Tang S-c, Shau M-d, Zeng Y-f, Cherng J-y, Shih M-f. Structural characterization and buffering capacity in relation to the transfection efficiency of biodegradable polyurethane. Bioconjugate Chemistry 2005;16(6):1375-1381.

595. Hung W, Shau M, Kao H, Shih M, Cherng J. The synthesis of cationic polyurethanes to study the effect of amines and structures on their DNA transfection potential. Journal of Controlled Release 2009;133:68-76.

596. Liu X-Y, Ho W-Y, Hung W, Shau M-D. The characteristics and transfection efficiency of cationic poly(ester-co-urethane) - short chain PEI conjugates self-assembled with DNA. Biomaterials 2009;30:6665-6673.

597. Zhang S, Xu Y, Wang B, Qiao W, Liu D, Li Z. Cationic compounds used in lipoplexes and polyplexes for gene delivery. Journal of Controlled Release 2004;100:165-180.

598. Bachelder E, Beaudette T, Broaders K, Paramonov S, Dashe J, Frechet J. Acid-degradable polyurethane particles for protein-based vaccines: biological evaluation and in vitro analysis of particle degradation products. Molecular Pharmaceutics 2008;5(5):876-884.

599. Visscher S, van Minnen B, van Leeuwen M, van Kooten T, Bos R. Closure of oroantral communications using biodegradable polyurethane foam: a long term study in rabbits. Journal of Biomedical Materials Research Part B: Applied Biomaterials 2009;91B(2):957-963.

600. Spaans C, de Groot J, Dekens F, Veth R, Pennings A. Development of new poly(urethane)s for repair and replacement of the knee joint meniscus. Polymer Preprints 1999;40(2):589-590.

601. de Groot J, de Vrijer R, Pennings A, Klompmaker J, Veth R, Jansen H. Use of porous polyurethanes for meniscal reconstruction and meniscal prostheses. Biomaterials 1996;17:163-173.

602. Adhikari R, Danon S, Bean P, Le T, Gunatillake P, Ramshaw J, Werkmeister J. Evaluation of in situ curable biodegradable polyurethanes containing zwitterion components. Journal of Materials Science: Materials in Medicine 2010;21:1081-1089.

603. Dempsey D, Benhardt H, Cosgriff-Hernandez E. Resorbably Polyurethanes. In: Szycher M, editor. Szycher's Handbook of Polyurethanes. Boca Raton, FL: CRC Press; 2012. p 671-710.

604. Reddy T, Hadano M, Takahara A. Controlled release of model drug from biodegradable segmented polyurethane ureas: morphological and structural features. Macromolecular Symposia 2006;242(1):241-249.

605. Hergenrother RW, Wabers HD, Cooper SL. Effect of hard segment chemistry and strain on the stability of polyurethanes: in vivo biostability. Biomaterials 1993;14(6):449-458.

606. Ayres E, Orefice R, Yoshida M. Phase morphology of hydrolysable polyurethanes derived from aqueous dispersions. European Polymer Journal 2007;43(8):3510-3521.

607. Gong C, Fu S, Gu Y, Liu C, Kan B, Deng H, Luo F, Qian Z. Synthesis, characterization, and hydrolytic degradation of biodegradable poly(ether ester)-urethane copolymers based on ε-caprolactone and poly(ethylene glycol). Journal of Applied Polymer Science 2009;113(2):1111-9.

608. Moravek S, Cooper T, Hassan M, Wiggins J, Mauritz K, Storey R. Degradable thermoplastic polyurethanes based on 4,4'-dicyclohexylmethane diisocyanate. Polymer Preprints 2007;48(1):568-569.

609. Sarkar D, Yang J-C, Lopina S. Structure-property relationship of L-tyrosine-based polyurethanes for biomaterial applications. Journal of Applied Polymer Science 2008;108(4):2345-2355.

610. Tang Y, Labow R, Revenko I, Santerre J. Influence of surface morphology and chemistry on the enzyme catalyzed biodegradation of polycarbonate-urethanes. Journal of Biomaterial Science, Polymer Edition 2002;13(4):463-483.

611. Bezwada R; Bioabsorbable and biocompatible polyurethanes and polyamides for medical devices. US patent 20060188547 A1. 2006.

612. Zhang D, Giese ML, Prukop SL, Grunlan MA. Poly(ε-caprolactone)-based shape memory polymers with variable polydimethylsiloxane soft segment lengths. Journal of Polymer Science Part A: Polymer Chemistry 2011;49(3):754-761.

613. Jaffe M, Ophir Z, Collins G, Recber A, Yoo S-u, Rafalko JJ. Process-structure-property relationships of erodable polymeric biomaterials: II-long range orer in poly(desaminotyrosyl arylates). Polymer 2003;44:6033-6042.

614. David G, Simionescu BC, Maier S, Balhut C. Micro-/nanostructured polymeric materials: poly(ε-caprolactone) crosslinked collagen sponges. Digest Journal of Nanomaterials and Biostructures 2011;6(4):1575-1585.

615. Elzein T, Nasser-Eddine M, Delaite C, Bistac S, Dumas P. FTIR study of polycaprolactone chain organization at interfaces. Journal of Colloid and Interface Science 2004;273:381-387.

616. Khosroshahi ME, Karkhaneh A, Orang F. A comparative study of chop-wave and superpulse CO_2 laser surface modification of polyurethane. Iranian Polymer Journal 2004;13(6):503-511.

617. Schaw JEK, Bergman E, Winter W. A method for analysis of the measured curves of TMDSC investigation in the melting region of polymers. Journal of Thermal Analysis 1998;54:565-576.

618. Han J, Chen B, Ye L, Zhang A-Y, Zhang J, Feng Z-G. Synthesis and characterization of biodegradable polyurethane based on poly(ε-caprolactone) and L-lysine ethyl ester diisocyanate. Frontiers of Materials Science in China 2009;3(1):25-32.

619. Spaans C, de Groot J, Dekens F, Pennings A. High molecular weight polyurethanes and a polyurethane urea based on 1,4-butanediisocyanate. Polymer Bulletin 1998;41:131-138.

620. Dawlee S, Jayabalan M. Development of segmented polyurethane elastomers with low iodine content exhibiting radiopacity and blood compatibility. Biomedical Materials 2011;6:1-12.

621. Chiono V, Sartori S, Rechichi A, Tonda-Turo C, Vozzi G, Vozzi F, D'Acunto M, Salvadori C, Dini F, Barsotti G and others. Poly(ester urethane) guides for peripheral nerve regeneration. Macromolecular Bioscience 2011;11(2):245-256.

622. Chan-Chan LH, Solis-Correa R, Vargas-Coronado RF, Cervantes-Uc JM, Cauich-Rodríguez JV, Quintana P, Bartolo-Pérez P. Degradation studies on segmented polyurethanes prepared with HMDI, PCL and different chain extenders. Acta Biomaterialia 2010;6:2035-2044.

623. D. G. A review of the biodegradability and utility of poly(caprolactone). Journal of Polymers and the Environment 1995;3(2):61-67.

624. Drilling S, Gaumer J, Lannutti. Fabrication of burst pressure competent vascular grafts via electrospinning: Effects of microstructure. Journal of Biomedical Materials Research Part A 2009;88A(4):923-934.

625. Qi H, Kong D, Hu P, Zhang J, Lin W, Song F. Biomimic tubulose scaffolds with multilayer prepared by electrospinning for tissue engineering. Materials Science Forums 2006;510-511:882-885.

626. Sell S, Bowlin G. Creating small diameter bioresorbable vascular grafts through electrospinning. Journal of Material Chemistry 2008;18:260-263.

627. Stitzel J, Lee S, Yoo J, Levi N, Berry J, Czerw R, Komura M, Lim G, Soker S, Atala A. Fabrication, mechanics, and biocompatibility of a nanofiber tissue engineering scaffold. Polymer Preprints 2005;46(1).

628. Stitzel J, Liu J, Lee SJ, Komura M, Berry J, Soker S, Lim G, Van Dyke M, Czerw R, Yoo JJ and others. Controlled fabrication of a biological vascular substitute. Biomaterials 2006;27(7):1088-1094.

629. Kameoka J, Ilic R, Czaplewski D, Mathers R, Coates G, Craighead H. Fabrication of blended polyphenylenevinylene nanowires by scanned electrospinning. Journal of Photopolymer Science and Technology 2004;17(3):421-426.

630. Li D, Wang Y, Xia Y. Electrospinning of polymeric and ceramic nanofibers as uniaxially aligned arrays. Nano Letters 2003;3(8):1167-1171.

631. Li D, Wang Y, Xia Y. Electrospinning nanofibers as uniaxially aligned arrays and layer-by-layer stacked films. Advanced Materials 2004;16(4):361-366.

632. Singh G, Bittner A, Loscher S, Malinowski N, Kern K. Electrospinning of diphenylalanine nanotubes. Advanced Materials 2008;20(12):2332-2336.

633. Dalton P, Grafahrend D, Klinkhammer K, Klee D, Moller M. Electrospinning of polymer melts: phenomenological observations. Polymer 2007;48:6823-6833.

634. Dalton P, Joergensen N, Groll J, Moeller M. Patterned melt electrospun substrates for tissue engineering. Biomedical Materials 2008;3:1-11.

635. Czaplewski D, Kameoka J, Craighead H. Nonlithographic approach to nanostructure fabrication using a scanned electrospinning source. Journal of Vacuum Science and Technology B 2003;21(6):2994-2997.

636. Liu Y, Ji Y, Ghosh K, Clark R, Huang L, Rafailovich M. Effects of fiber orientation and diameter on the behavior of human dermal fibroblasts on electrospun PMMA scaffolds. Journal of Biomedical Materials Research Part A 2009;90A(4):1092-1106.

637. Wu H, Zhang R, Sun Y, Lin D, Sun Z, Pan W, Downs P. Biomimetic nanofiber patterns with controlled wettability. Soft Matter 2008;4:2429-2433.

638. Xie J, MacEwan M, Li X, Sakiyama-Elbert S, Xia Y. Neurite outgrowth on nanofiber scaffolds with different orders, structures, and surface properties. ACS Nano 2009;3(5):1151-1159.

639. Dalton P, Klee D, Moller M. Electrospinning with dual collection rings. Polymer 2005;46:611-614.

640. Gibson P, Schreuder-Gibson H. Patterned electrospray fiber structures. International Nonwovens Journal 2004;13(2):34-41.

641. Neves N, Campos R, Pedro A, Cunha J, Macedo F, Reis R. Patterning of polymer nanofiber meshes by electrospinning for biomedical applications. International Journal of Nanomedicine 2007;2(3):433-448.

642. Pan C, Han Y, Dong L, Wang J, Gu Z. Electrospinning of continuous, large area, latticework fiber onto two-dimensional pin-array collectors. Journal of Macromolecular Science, Part B: Physics 2008;47:735-742.

643. Zhang D, Chang J. Electrospinning of three-dimensional nanofibrous tubes with controllable architectures. Nano Letters 2008;8(10):3283-3287.

644. Ding Z, Salim A, Ziaie B. Selective nanofiber deposition through field-enhanced electrospinning. Langmuir 2009;25(17):9648-9652.

645. Zhang D, Chang J. Patterning of electrospun fibers using electroconductive templates. Advanced Materials 2007;19(21):3664-3667.

646. Deitzel J, Kleinmeyer J, Hirvonen J, Tan N. Controlled deposition of electrospun poly(ethylene oxide) fibers. Polymer 2001;42:8163-8170.

APPENDIX A

MICROPATTERNING OF ELECTROSPUN POLYURETHANE FIBERS THROUGH CONTROL OF SURFACE TOPOGRAPHY

A.1 Introduction

Electrospinning has gained increasing popularity in tissue engineering as a facile and tunable process to generate high porosity scaffolds. Current research has expanded the versatility of electrospinning through controlled fiber alignment and assembly. Fiber alignment is of particular interest in tissue engineering because topographical features have been shown to strongly influence cellular alignment on a substrate. Thus, control of electrospun fiber alignment can be used to generate desired cellular distributions and orientations within the tissue engineered construct. Fiber alignment and patterning can also be used to enhance mechanical properties and mimic the native orientation and anisotropic properties of native tissues. Common methods to control the fiber alignment and patterning include setups that utilize a spooling collector rather than a stationary target[182,624-628] and setups that modulate the electric field.[629-632] Spooling setups induce specific fiber orientations by physical manipulation of the resulting fibers using a moving collector stage,[633,634] revolving disk,[635] or rotating mandrel.[636] Modulation of the electric field with different setups has been used to create a range of fiber geometries

*Reprinted with permission from "Micropatterning of electrospun polyurethane fibers through control of surface topography," by D. K. Dempsey, C. J. Schwartz, R. S. Ward, A. Iyer, J. Parakka, and E. Cosgriff-Hernandez, Macrmolecular Materials and Engineering 2010, 295, 990-994. Copyright (2010) Wiley.

including leaf patterns,[637] aligned fibers stacks,[638] and fiber arrays with grounded rings to wind into yarn.[639] Recently, modification of the collector's surface topography has shown great promise in controlling fiber deposition. Selective deposition was observed on electroconductive templates (woven wire meshes) and resulted in improved mechanical properties of the resultant fiber mats.[640] Alternative collectors with different surface topographical features have also affected cell adhesion patterns on electrospun fiber mats.[641] Pan et al. showed that fibers align themselves creating grid patterns between adjacent conducting pins inserted within an insulating surface.[642] Zhang et al. demonstrated that electrospun fibers are attracted to raised topographical features of conducting substrates with raised patterns.[643] In contrast, Ding et al. utilized field-enhanced electrospinning on an elastomeric substrate with gold-coated pyramidal protrusions to increase the population of fibers at raised points.[644] Similar to the works by Pan and Zhang, the effect was attributed to a redistribution of the electric field in close proximity to the collector as a result of the change in surface topography of the substrate.[642-645] Although these studies have laid the foundation for the mechanistic understanding of the selective fiber deposition process, great strides are still needed enable the practical application of patterning techniques in the fabrication of improved tissue engineering constructs.

In this communication we present a simple method of manipulating the morphology and arrangement of electrospun polyurethane fibers by controlling the surface topography of an insulating collector substrate. Two polyurethanes, poly(ester urethane) (PEsU) and poly(ether urethane urea) (PEUU), were electrospun onto

patterned silicone substrates generated with standard soft lithography techniques. The effect of surface topography on selective fiber deposition and bundling was investigated. Particular attention was given to material-specific effects on fiber deposition patterns which were previously unexplored in the literature. Our results showed patterned PEsU fibers and randomized PEUU fibers indicating that this effect is material specific. Specifically, alignment of the polar carbonyls of the polyester soft segment in the electric field was hypothesized to result in fiber attraction and increased patterning throughout the deposition period. Overall, the combination of low cost, ease of use, tunability, and generation of relatively large fiber mats available with this technique greatly expands the utility of patterned electrospun scaffolds in tissue engineering and other biomedical applications.

A.2 Materials and Methods

A.2.1 Materials BioSpan®, a commercially available poly(ether urethane urea) (PEUU), and an experimental bioresorbable poly(ester urethane) (PEsU) were synthesized by DSM-Polymer Technology Group (Berkeley, CA, USA). Transmission FTIR spectra of neat polyurethanes were recorded using a Bruker TENSOR 27 Fourier transform infrared spectrometer by solution casting directly onto KBr pellets to elucidate key structural features, **Figure A.1**. The dominant peak in the PEsU spectra is located at 1730 cm^{-1} and corresponds to the stretching of the free carbonyl group (C=O) of the ester linkage in the soft segment. For PEUU, the major peak is found at 1110cm^{-1} and

corresponds to the stretching of the ether group (C-O-C) in the soft segment of the polymer.

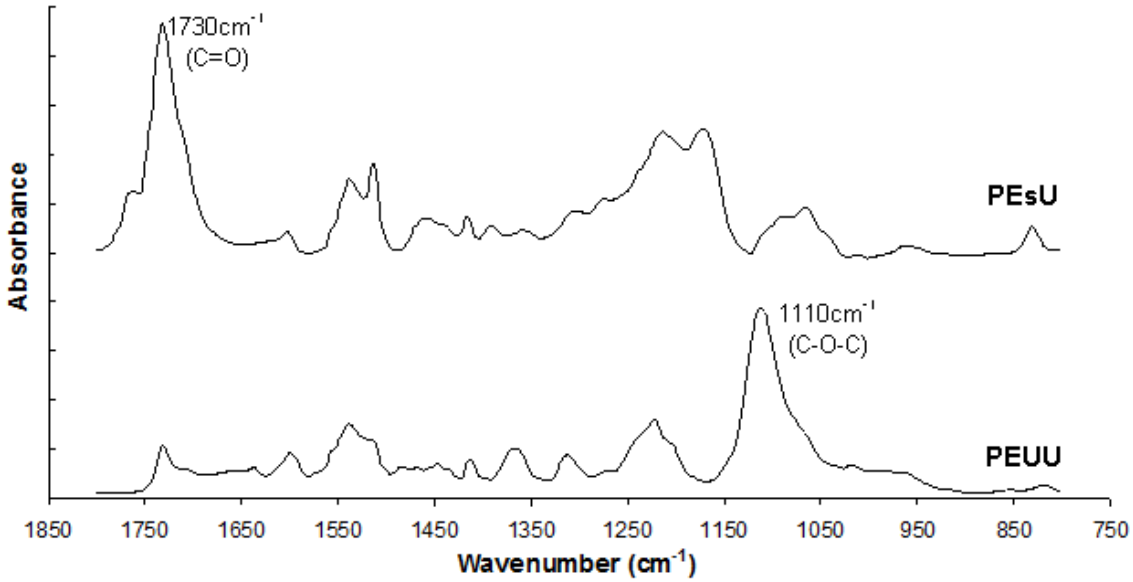

Figure A.1. FTIR spectra of PEsU and PEUU.

A.2.2 Soft Lithography Standard photolithography processes were used to prepare epoxy-based master molds (SU-8, MicroChem) with raised square patterns approximately 12µm high and lengths of 50, 100, 200, and 500 µm. These molds were then used to create negative PDMS replica of these patterns via soft lithography to generate PDMS collector substrates with raised grid patterns. Briefly, a PDMS elastomer kit (Sylgard 184, Dow Corning) was first mixed at a standard 10:1 base to curing agent ratio. The master mold was treated with a chemical release agent, (Tridecafluoro-1,1,2,2-Tetrahydrooctyl)-1-Trichlorosilane and the mixed elastomer spin-coated (Laurell Technologies Corporation) onto the mold at 500 rpm for 25 seconds to ensure that a uniform, thin layer of PDMS (~300 µm) was applied. The PDMS/mold assembly was

then cured in an oven at 85°C for 20 minutes. A 200 Å-thick gold/palladium layer was deposited on the PDMS collector sheets by sputter coating to prevent PDMS swelling from contact with solvent during electrospinning. The layer of gold/palladium was not expected to affect the conductivity of the collector as there was no contact of the sputter coated material with the plate behind the PDMS substrates. Indeed, fiber patterning and bundling was observed without substrate coating; however, solvent swelling of the PDMS substrate prevented removal of the fiber mesh and full characterization (data not shown).

A.2.3 Electrospinning PEUU and PEsU solutions (15 wt%) were prepared in N,N‘ dimethylacetamide (DMAC) (Sigma Aldrich) and dispensed from 10 mL glass syringes at a rate of 0.2 mL/hr, as controlled by a syringe pump (KDS100, KD Scientific). A high voltage source (Gamma High Voltage) was used to apply 8.5kV to the tip of a blunted 23g1 needle attached to the glass syringe. Electrospun fibers were collected on both patterned and flat PDMS sheets attached to the front face of a copper plate which was grounded and positioned 20 cm from the tip of the needle. Electrospun fibers were collected for 2 hours and fiber mats removed from the collector sheets prior to characterization.

A.2.4 Characterization Surface topography images of the patterned, silicone collector sheets were obtained using an optical profilometer (Zygo Corporation) equipped with a 10x objective. Five scans of 40 μm lengths were average to minimize noise. High resolution images of electrospun fiber mats were captured using a field emission – scanning electron microscope (JSM-7500F, JEOL) operated at 2kV.

Quantification of grid dimensions and electrospun fiber diameters were determined using pixel to length ratios of dimensions measured in SEM and profilometer images. Briefly, 15 edge-to-edge measurements of each silicone and electrospun fiber grid were obtained on three specimens for a total of 45 measurements. For quantification of fiber diameter, measurements were made on the first fifteen fibers that intersected a line drawn across the middle of an image. Images from three specimens were used for a total of 45 measurements. Average dimensions and standard deviations were reported.

A.3 Results and Discussion

The selected surface topography designs were raised grid patterns 20 μm wide with approximate heights of 12 μm and spacing of 50, 100, 200, and 500 μm. The results from the optical profilometer indicated successful fabrication of the anticipated surface topography of the PDMS replica, **Figure A.2** with minimal deviation from the intended dimensions, **Table A.1**. In order to isolate the effect of the patterned surface topography from other electrospinning variables, the polymer concentration (15 wt%), solution flow rate (0.2 mL/hr), output voltage (8.5 kV), distance to collector (20 cm), and spinning time (2 hours) were kept constant. PEsU and PEUU were both electrospun onto flat and patterned PDMS substrates and the resulting morphologies observed with scanning electron microscopy. **Figure A.2** shows the successful patterning of PEsU fibers which reproduced the grid pattern of the PDMS collector substrate, **Table A.1**. Quantitative analysis of fiber diameter revealed a bimodal distribution with random fibers ranging from 1.4-1.9 microns in diameter and what appear to be fused fiber bundles that were an

order of magnitude larger than the random fibers (16-22 microns), **Table A.1**. The high magnification image of these fiber bundles, **Figure A.3** appears to indicate that the overlay of fibers and subsequent fusion resulted in the observed bimodal distribution. **Figure A.3C** shows the comparison between PEUU and PEsU fibers electrospun onto flat PDMS substrates which served as a negative control for topographical effects on fiber deposition. As expected, neither the PEsU nor the PEUU fibers showed any patterning on the flat substrate though the PEsU fibers did still exhibit random fiber bundling.

Table A.1. Dimensions of resultant PDMS collectors and electrospun PEsU fiber mats

	PDMS Grid Size	Fiber Pattern Grid Size	PEsU Bundled Fibers	PEsU Random Fibers	PEUU Random Fibers
50 µm Grid	54 ± 2 µm	45 ± 3 µm	20 ± 2 µm	1.4 ± 0.2 µm	0.8 ± 0.3 µm
100 µm Grid	103 ± 1 µm	85 ± 7 µm	22 ± 4 µm	1.9 ± 0.5 µm	0.8 ± 0.2 µm
200 µm Grid	202 ± 1 µm	193 ± 14 µm	17 ± 6 µm	1.4 ± 0.3 µm	0.9 ± 0.2 µm
500 µm Grid	500 ± 2 µm	400 ± 20 µm	22 ± 7 µm	1.5 ± 0.3 µm	0.9 ± 0.2 µm
Flat PDMS	--	--	16 ± 4 µm	1.5 ± 0.4 µm	0.8 ± 0.2 µm

(n = 45; average ± standard deviation)

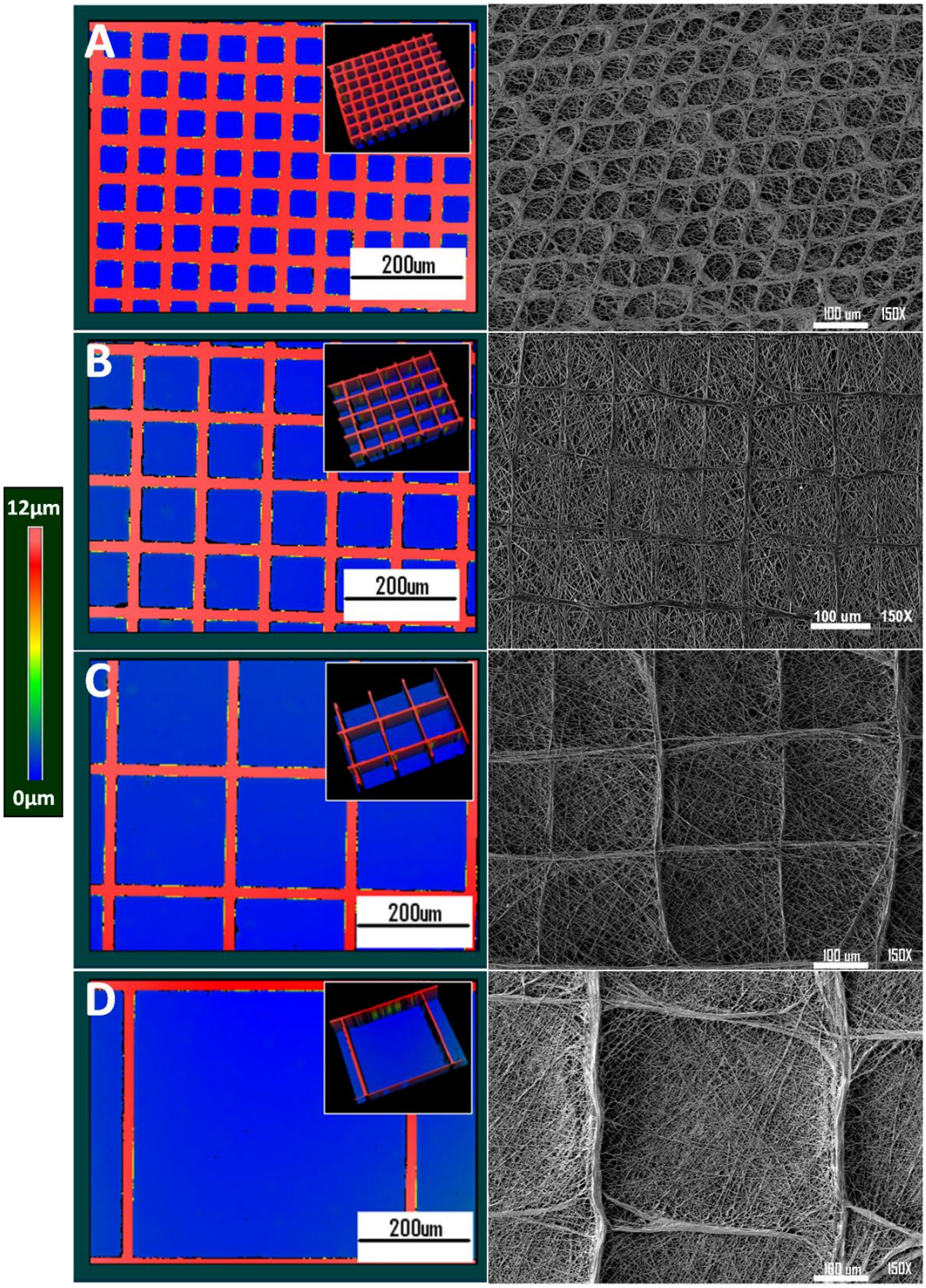

Figure A.2. Optical profilometer scans of patterned PDMS collector substrates (left) and scanning electron micrographs of the resultant electrospun PEsU fibers (right) for (A) 50 µm, (B) 100 µm, (C) 200 µm, and (D) 500 µm

During the electrospinning process, the initial movement of the charged fibers is randomized.[646] However, the motion after ejection is controlled by electrostatic forces exerted by the external field, collector, and any adjacent charged fibers.[629-632,640-643] In the flat collector plate setup, there is no preferential direction in the plane of the collector resulting in a random fiber mesh. Whereas, a patterned collector substrate results in selective fiber deposition and arrangement due to an increase in Coulomb interactions with the raised topographical features of the collector.[645] When this theory is applied to the patterned PDMS substrates used in the current study, two effects are in competition. The increased thickness of the insulator at the raised features results in increased charge dissipation; however, there is also a shorter distance between the raised features and the charged needle thus creating stronger electric fields. The effect of a shortened distance between charges is dominant and resulted in the observed fiber patterning.[188] This was found to be true only at relatively thin insulating substrate thicknesses (~300 μm) achieved by spin-coating the PDMS onto the SU-8 mold. Thicker PDMS substrates were initially used (results not shown) and it was observed that very few fibers were attracted to the collector because of the weakened electric field.

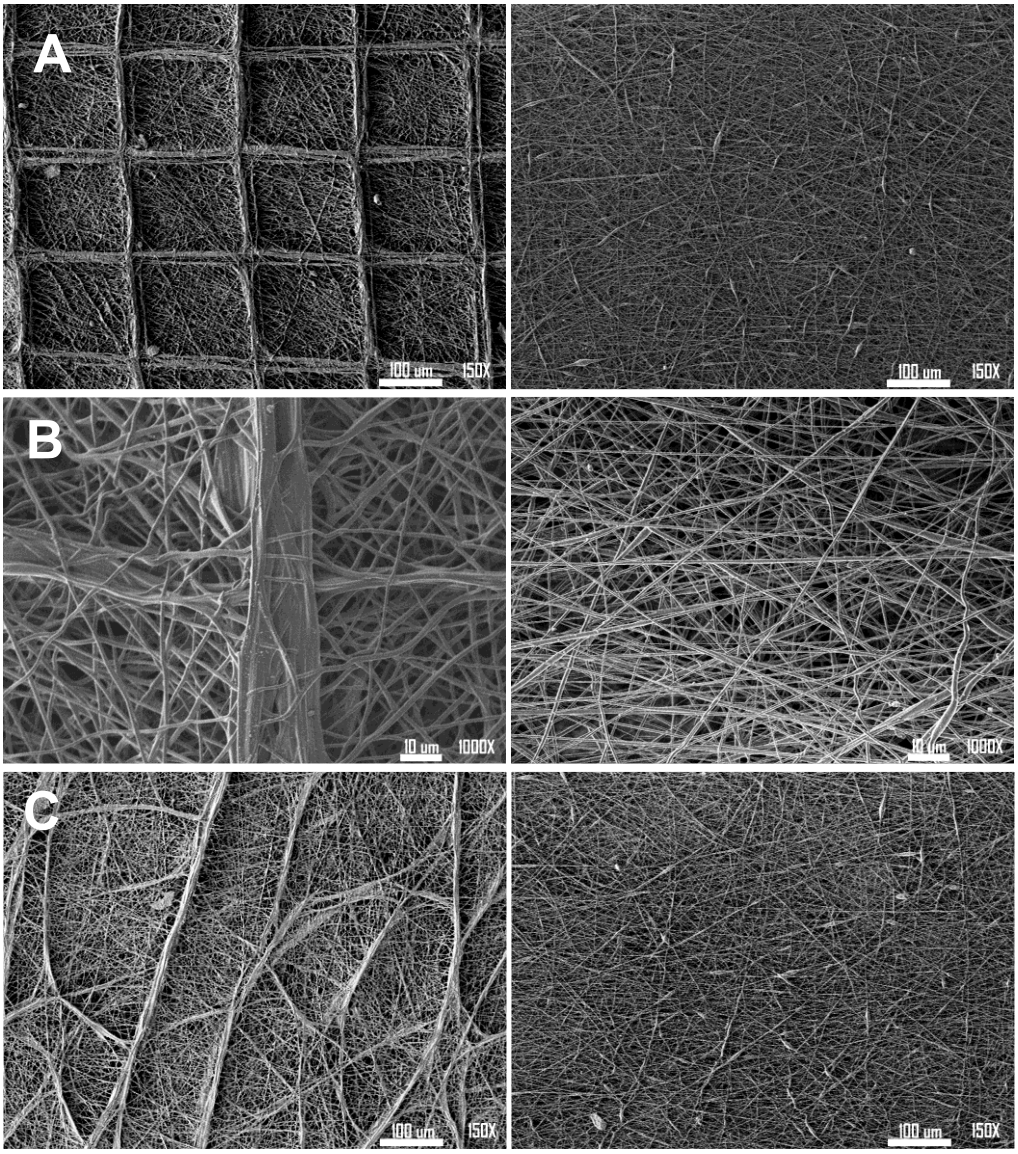

Figure A.3. Scanning electron micrographs of PEsU (left) and PEUU fibers (right) electrospun on (A) patterned PDMS; (B) high magnification on patterned PDMS; (C) flat PDMS.

The theory described above is consistent with the current literature of electrospinning on patterned conducting substrates; however, it does not address the material specificity of patterning observed in the current study. Typically in electrospinning, the solvent reduces the viscosity of the polymer to enable fiber drawing

and provides sufficient conductivity for the polymer solution to be electrospun. Thus, solvents with higher dipole moments are subject to greater electrical forces which impacts the 'electrospinnability' of the polymer solution.[187] The comparisons between the PEsU fibers and the PEUU fibers seen in **Figure A.3** show a distinct difference in the effect of the patterned PDMS despite having the same conductive solvent, dimethylacetamide. Therefore, the difference in patterning was attributed to differences in contribution to the total dipole moment from the polymers themselves, specifically, the carbonyl of the ester linkages in the soft segment of the PEsU that are absent in the PEUU. It should be noted that urethanes also contain carbonyl groups; however, the two polyurethanes have similar and relatively low hard segment content which appears to have mitigated their effect on fiber deposition.

Fused fiber bundles were observed in the micrographs of PEsU fibers electrospun onto the flat or patterned silicone substrates. To the best of our knowledge this level of fusion was not previously reported in the literature. Initial fiber-fiber contact during electrospinning can result in fusion due to residual solvent in the polymer fibers that permits chain entanglement. Therefore, the fiber bundling was attributed to PEsU fiber attraction which resulted in fiber contact along the full length of the fiber and subsequent fusion. In contrast, the PEUU fibers exhibited no discernable pattern or fiber bundling when electrospun onto patterned silicone substrates, **Figure A.3A**, and indicates a previously unobserved material-specific effect on fiber deposition. The PEsU has numerous polar carbonyls in its structure, **Figure A.1**, thus creating multiple dipoles within the polymer chain. When in the presence of an electric field, polar molecules

align in the direction of the field leading with the positive ends.[188] It may then be extrapolated that while traveling to the collector, PEsU fibers align based on the direction of the applied electric field. Upon reaching the collector, the dipoles within the PEsU molecules will have their positive ends towards the face of the collector and the negative ends away from the collector thus giving the collector a partial negative charge. This effect is heightened at the raised features of the silicone substrate due to the enhanced electric field at these points, as described above. New fibers are then attracted to these fibers because the partial negative ends of the carbonyl groups in the deposited fibers attract the partial positive ends in the new fibers. Electrospun fiber deposition over time (1, 5, 10, 20, 40 and 60 minutes) was characterized to investigate the effect of charge accumulation on fiber patterning. Fiber patterning and fusion occurred as early as 1 minute and continued without observable difference throughout the 2 hour spinning process (data not shown). We hypothesize that initially the topography dictates fiber alignment and fiber attraction resulted in continued fiber patterning and fusion. It is necessary here to address the fact that non-polar and low polarity molecules will also slightly align themselves along the direction of the electric field;[188] however, this was insufficient to yield patterning of the PEUU under the conditions used in this study. Generation of a bimodal distribution of fiber diameters may be of great utility in the fabrication of tissue engineered scaffolds to modulate mechanical properties, degradation rates, and pore sizes. For example, large fibers would be expected to degrade slower and thus maintain structural support of the scaffold while rapid degradation of the smaller fibers would increase pore size and enhance cell infiltration.

A.4 Conclusions

In summary, we have demonstrated a novel technique to control the deposition pattern of electrospun PEsU fibers. The results from this study indicate that a patterned insulating collector substrate can be used to control the selective deposition of electrospun fibers, this patterning effect is material specific, and that fusion due to fiber attraction results in a bimodal distribution of fiber diameters. This method can be used to control selective fiber deposition with broad pattern dimensions (50-500 μm) over a large area. Patterning was observed as early as 5 minutes and continued throughout fiber deposition (up to 2 hours) indicating that thick mats that retain the desired pattern are feasible. The combination of ease of use, low cost, tunability, and generation of relatively large fiber mats available with this technique greatly expands the utility of patterned electrospun scaffolds in tissue engineering. Further investigation of the effect of fiber patterning on mechanical properties, degradation rate, and cellular alignment is currently in progress.